

**STUDY OF FOUR WAVE MIXING IN A HIGHLY NONLINEAR
MEDIA AND THEIR APPLICATIONS**

NOOR AZURA BINTI AWANG

**THESIS SUBMITTED IN FULFILLMENT OF
THE REQUIREMENT FOR THE DEGREE
OF DOCTOR OF PHILOSOPHY**

**DEPARTMENT OF PHYSICS
FACULTY OF SCIENCE
UNIVERSITY OF MALAYA
KUALA LUMPUR**

2012

UNIVERSITI MALAYA
ORIGINAL LITERARY WORK DECLARATION

Name of Candidate: **NOOR AZURA BINTI AWANG** (I.C/Passport No: **820314-03-5016**)

Registration/Matric No: **SHC080038**

Name of Degree: **DOCTOR OF PHILOSOPHY**

Title of Project Paper/Research Report/Dissertation/Thesis ("this Work"):

STUDY OF FOUR WAVE MIXING IN A HIGHLY NONLINEAR MEDIA AND THEIR APPLICATIONS

Field of Study: **FIBRE OPTICS**

I do solemnly and sincerely declare that:

- (1) I am the sole author/writer of this Work;
- (2) This Work is original;
- (3) Any use of any work in which copyright exists was done by way of fair dealing and for permitted purposes and any excerpt or extract from, or reference to or reproduction of any copyright work has been disclosed expressly and sufficiently and the title of the Work and its authorship have been acknowledged in this Work;
- (4) I do not have any actual knowledge nor do I ought reasonably to know that the making of this work constitutes an infringement of any copyright work;
- (5) I hereby assign all and every rights in the copyright to this Work to the University of Malaya ("UM"), who henceforth shall be owner of the copyright in this Work and that any reproduction or use in any form or by any means whatsoever is prohibited without the written consent of UM having been first had and obtained;
- (6) I am fully aware that if in the course of making this Work I have infringed any copyright whether intentionally or otherwise, I may be subject to legal action or any other action as may be determined by UM.

Candidate's Signature

Date

Subscribed and solemnly declared before,

Witness's Signature

Date

Name:

Designation:

ABSTRACT

This thesis presents a comprehensive study of the four wave mixing (FWM) effect in the highly nonlinear fibre (HNLF) and semiconductor optical amplifier (SOA); and their applications. The nonlinearity parameters such as zero-dispersion wavelength (ZDW), chromatic dispersion (CD) and nonlinear coefficient of HNLF has successfully investigated by using several FWM techniques. Results from all techniques have been achieved approximately similar to the manufacturer specification. This technique is then employed for the measurement of the FWM power and FWM efficiency in a SOA, in addition to the gain performance, which is measured using conventional methods. Based on these parameters, a good agreement between experiments and numerical has been obtained. This characterization is important for nonlinear application such as wavelength conversion, fibre optic parametric amplifier (FOPA) and multiwavelength fibre laser. Wavelength conversion is a key for wavelength division multiplexed (WDM) networks. Wavelength converter based on HNLF and SOA are promising candidates for implementing wavelength conversion. This thesis presents a thorough investigation of new configurations of the wavelength converter generation by using degenerate case and non-degenerate case of FWM effect in nonlinear media. Most of wavelength conversion configuration used self-constructed dual-wavelength fibre laser as a signal and pump sources due to compact size as well as compatible with current telecommunications system. The dual-wavelength fibre laser used in this thesis is more cost effective and inexpensive as compared to the tunable laser sources (TLS). It allows for a smooth wavelength tuning over a wide range and has high performance stability. In the case of a two independent laser sources from TLS, an effective wavelength conversion is achieved by using a lower pump power and signal in HNLF

via the FWM effect. This configuration obtained a higher and flat of conversion efficiency and a Signal-to-Noise Ratio (SNR) over 20 nm and can provide an effective means of wavelength conversion for telecommunication applications. However, despite the high conversion efficiency, this configuration suffers from both higher cost as well as a smaller wavelength conversion band. The other application reported in this thesis is fibre optical based parametric amplifier (FOPA). The novelty of this configuration used is a ring cavity as opposed to the commonly used method of linear cavity. This configuration reduces the required pump power for the amplifications of the signal and also the generation of the idlers. The last application reported in this thesis is a stable multiwavelength fibre laser utilizing the FWM effect in HNLF is proposed and demonstrated. The multi-wavelength fibre is based on the ring cavity configuration, and utilizes a low power erbium doped fibre amplifier (EDFA) as a gain medium to generate 11 lines in the range of 1582 nm to 1600 nm and a SNR of 43 dB.

ABSTRAK

Tesis ini membentangkan satu kajian menyeluruh kesan empat gelombang (FWM) dalam serat yang tinggi ketaklinearannya (HNLF) dan semikonduktor pengganda optik (SOA) dan aplikasinya. Parameter ketaklinearan seperti panjang gelombang pada penyerakan kosong (ZDW), penyerakan kromatik (CD) dan pekali tak linear bagi HNLF telah dengan jayanya diselidiki dengan menggunakan beberapa teknik FWM. Keputusan daripada semua teknik yang telah dijalankan mendapati bahawa parameter yang diperolehi menghampiri nilai spesifikasi pengeluar. Teknik ini kemudian digunakan untuk mengukur kuasa dan kecekapan FWM dalam SOA, manakala prestasi gandaan SOA diukur menggunakan kaedah biasa. Berdasarkan parameter-parameter ini, satu persamaan telah diperolehi antara eksperimen dan pengiraan. Sifat-sifat dalam medium tak linear adalah penting dalam aplikasi penukar panjang gelombang, pengganda berparameter gentian optik (FOPA) dan laser gentian pelbagai panjang gelombang. Penukaran panjang gelombang ialah satu penyelesaian untuk bahagian panjang gelombang jaringan multiplex (WDM). Penukar panjang gelombang berdasarkan HNLF dan SOA adalah medium yang paling sesuai untuk melaksanakan penukaran panjang gelombang. Tesis ini menerangkan satu penyelidikan yang menyeluruh tentang konfigurasi-konfigurasi baru bagi penghasilan penukaran panjang gelombang dengan menggunakan kes merosot dan kes tak merosot bagi kesan FWM dalam medium-medium tak linear. Kebanyakan konfigurasi penukaran panjang gelombang menggunakan laser gentian dual panjang gelombang buatan sendiri sebagai sumber isyarat dan pam disebabkan saiz padatnya dan keserasiannya dengan sistem telekomunikasi. Laser gentian dual panjang gelombang yang digunakan di dalam kajian ini lebih murah kosnya berbanding dengan sumber laser boleh tala (TLS). Tambahan pula, ia

memberikan penalaan panjang gelombang yang besar disamping kestabilan prestasi yang tinggi. Dalam kes laser boleh tala pula, penukaran panjang gelombang dicapai dengan menggunakan kuasa pam dan isyarat yang rendah dalam HNLF melalui kesan FWM. Dalam konfigurasi ini, diperolehi kecekapan penukaran dan nisbah isyarat hingar (SNR) yang lebih tinggi dan rata sepanjang 20 nm dan ia merupakan penukaran panjang gelombang yang efektif untuk aplikasi telekomunikasi. Bagaimanapun, walaupun dengan kecekapan penukaran yang tinggi ini, tatarajah ini menderita akibat kos-kos yang tinggi serta jarak penalaan penukar panjang gelombang yang kecil. Selain itu, aplikasi yang dilaporkan dalam tesis ini ialah FOPA. Konfigurasi novel ini menggunakan kaviti bulatan berbanding dengan kaedah biasa menggunakan kaviti linear. Konfigurasi ini menggunakan kuasa pam yang rendah untuk digandakan kuasa isyarat dan juga penghasilan panjang gelombang baru. Aplikasi terakhir yang dilaporkan dalam tesis ini adalah laser gentian pelbagai panjang gelombang yang stabil menggunakan kesan FWM dalam HNLF. Laser gentian panjang gelombang ini juga berdasarkan konfigurasi bulatan yang menggunakan kuasa pengganda cahaya gentian optik berdop erbium (EDFA) yang rendah sebagai medium gandaan bagi penghasilan 11 panjang gelombang dalam lingkungan 1582 nm sehingga 1600 nm dengan SNR adalah 43 dB.

ACKNOWLEDGEMENTS

First and foremost, I wish to express deep thanks to my advisor, Professor Dr. Harith Ahmad. I have thoroughly enjoyed working with him and learning from him. His keen physical insight has continually provided invaluable guidance. His dedication and enthusiasm has set an example for me of how to do science, and any professional work. I will always look back with pride what I have accomplished with him at University of Malaya in the past four years. I am also grateful to my co-supervisor, Professor Dr. Sulaiman Wadi Harun for the continuous support of my research, for encouraging independent thinking and for his guidance throughout this study.

I owe my deepest gratitude to my parents, Hj. Awang Salleh, Hjh. Mek Yah Latif and Hjh. Cik Bidah Cik Him. They have constantly provided me with love and support and I hope I will be able to make them proud. I would also like to thank my brothers and sisters for their unwavering support throughout the years of my education. They are not only my siblings but also my lifetime friends.

A special thanks you to my beloved husband, Hamdan Omar, for always understanding, support, encouragement and love during these past four years. These special thanks also to my daughters Ayu Zharifa, Ain Zahra and Afia Zarin for encourage me in difficult time and share my joy in good time. Mama loves you all.

In closing, I would like to thank various friends from PRC, Amirah Abdul Latif, Muhd Imran Mustafa Abdul Kudus, Siti Fatimah Norizan, Zamani Zulkifli, Mohd. Hafizin Jemangin, Farah Diana Muhammad, Ruhaida Bahru and all photonics member. They not only gave me research advice, but also helped me to cultivate my attitude toward research.

Last but not least, my entire study at University of Malaya has been sponsored by the “Skim Latihan Akademik Bumiputera (SLAB)” from Ministry of Tertiary Education and University of Tun Hussein Onn Malaysia (UTHM). I thank them for their generosity, which helped me to achieve my PhD.

LIST OF ISI PUBLICATIONS

1. N. S. Shahabuddin, **N. A. Awang**, H. Ahmad, H. Arof, K. Dimyati, Z. Yusoff and S. W. Harun, "Supercontinuum generation using a passive mode-locked stretched-pulse bismuth-based erbium-doped fibre laser," *Optics and Laser Technology*, vol. 22, pp. 741-743, 2012.
2. H. Ahmad, **N. A. Awang**, A. A. Latif and S. W. Harun, "Generation of high power pulse of Bi-EDF and octave spanning supercontinuum using highly nonlinear fibre," *Microwave and Optical Technology Letters*, vol. 54, pp. 983-987, 2012.
3. H. Ahmad, **N. A. Awang**, M. C. Paul, M. Pal, A. A. Latif and S. W. Harun, "All fibre passively mode locked zirconium-based erbium-doped fibre laser," *Optics and Laser Technology*, vol. 44, pp. 534-537, 2012.
4. H. Ahmad, A. A. Latif, M. Z. Zulkifli, **N. A. Awang** and S. W. Harun, "High power dual-wavelength tunable fibre laser in linear and ring cavity configurations," *Chinese Optics Letters*, vol. 10, article no. 010603, 2012.
5. H. Ahmad, **N. A. Awang**, M. Z. Zulkifli, K. Thambiratnam, M. C. Paul, S. Das and S. W. Harun, "Supercontinuum from Zr-EDF using Zr-EDF mode-locked fibre laser," *Laser Physics Letters*, vol. 9, pp. 44-49, 2012.
6. H. Ahmad, **N. A. Awang**, A. A. Latif, M. Z. Zulkifli, Z. A. Ghani and S. W. Harun, "Wavelength conversion based on four-wave mixing in a highly nonlinear fibre in ring configuration," *Laser Physics Letters*, vol. 8, pp. 742-746, 2011.

7. H. Ahmad, S. F. Norizan, **N. A. Awang**, M. Z. Zulkifli, Z. A. Ghani and S. W. Harun, "Tunable Microwave Photonic Frequencies Generation based on Stimulated Brillouin Scattering Operating in The L-Band Region," *Microwave and Optical Technology Letters*, vol. 53, pp. 1710-1713, 2011.
8. **N. A. Awang**, M. Z. Zulkifli, A. A. Latif, S. W. Harun and H. Ahmad, "Stable power multi-wavelength fibre laser based on four-wave mixing in a short length of highly non-linear fibre," *Journal of Optics*, vol. 13, article no. 075401, 2011.
9. A. A. Latif, H. Ahmad, **N. A. Awang**, M. Z. Zulkifli, C. H. Pua, Z. A. Ghani and S. W. Harun, "Tunable high power fibre laser using an AWG as the tuning element," *Laser Physics*, vol. 21, pp. 712-717, 2011.
10. H. Ahmad, **N. A. Awang** and S. W. Harun, "Fibre optical based parametric amplifier in a highly nonlinear fibre (HNLF) by using a ring configuration" *Journal of Modern Optics*, vol. 58, pp. 1065-1069, 2011.
11. A. A. Latif, **N. A. Awang**, M. Z. Zulkifli, S. W. Harun, Z. A. Ghani and H. Ahmad, "Dual-wavelength tunable fibre laser with a 15-dBm peak power," *Quantum Electronics*, vol. 41, pp. 709-714, 2011.
12. **N. A. Awang**, H. Ahmad, A. A. Latif, M. Z. Zulkifli and S. W. Harun, "Four-wave mixing in dual wavelength fibre laser utilizing SOA for wavelength conversion," *Optik*, vol. 122, pp. 754-757, 2011.
13. **N. A. Awang**, H. Ahmad, A. A. Latif, M. Z. Zulkifli, Z. A. Ghani and S. W. Harun, "Wavelength conversion based on FWM in a HNLF by using a tunable dual-wavelength erbium doped fibre laser source," *Journal of Modern Optics*, vol. 58, pp. 566-572, 2011.

14. A. A. Latif, M. Z. Zulkifli, **N. A. Awang**, S. W. Harun and H. Ahmad, "A simple linear cavity dual-wavelength fibre laser using AWG as wavelength selective mechanism," *Laser Physics*, vol. 20, pp. 2006-2010, 2010.
15. **N. A. Awang**, M. Z. Zulkifli, S. F. Norizan, S. W. Harun, Z. A. Ghani, H. Ahmad, "Highly Efficient and High Output Power of Erbium Doped Fibre Laser in a Linear Cavity Configuration," *Laser Physics*, vol. 20, pp. 1894-1898, 2010.
16. M. Z. Zulkifli, N. A. Hassan, **N. A. Awang**, Z. A. Ghani, S. W. Harun and H. Ahmad, "Multi-wavelength fibre laser in the S-band region using a Sagnac loop mirror as a comb generator in an SOA gain medium," *Laser Physics Letters*, vol. 7, pp. 673-676, 2010.
17. **N. A. Awang**, H. Ahmad, A. A. Latif, M. Z. Zulkifli, Z. A. Ghani and S. W. Harun, "O-band to C-band wavelength converter by using four-wave mixing effect in 1310 nm SOA," *Journal of Modern Optics*, vol. 57, pp. 2147-2153, 2010.
18. **N. A. Awang**, H. Ahmad, S. F. Norizan, M. Z. Zulkifli, Z. A. Ghani and S. W. Harun, "An all-optical frequency up/down converter utilizing stimulated brillouin scattering in a TRF and DCF for ROF application," *Journal of Science and Technology*, pp. 35-45, 2010.

LIST OF CONFERENCES

1. **N. A. Awang**, M. Z. Zulkifli, S. F. Norizan, S. W. Harun, Z. A. Ghani and H. Ahmad, “Highly Efficient and High Output Power of Erbium Doped Fibre Laser in a Linear Cavity Configuration,” Seminar Kebangsaan Aplikasi Sains dan Matematik 2010 (SKASM2010), The Zone Hotel, Johor Bahru, Johor, 8th – 10th Disember 2010.
2. **N. A. Awang**, S. F. Norizan, S. W. Harun and H. Ahmad, “Frequency Conversion of Brillouin Fibre Laser,” 2nd Topical Meeting on Laser and Optoelectronics 2010 (TMLO), Berjaya Redang Resort, Kuala Terengganu, 13th – 15th March 2010.
3. **N. A. Awang**, S. W. Harun and H. Ahmad, “Four-Wave Mixing Pump Suppression Using Loop Mirror,” 5th Mathematics and Physical Sciences Graduate Congress 2009, Faculty of Science, Chulalongkorn University, Bangkok, Thailand, 7th – 9th December 2009.
4. Y. S. Hussein, S. W. Harun, **N. A. Awang** and H. Ahmad, “Enhancement of Four Wave Mixing Characteristic in Semiconductor Optical Amplifier Using Fibre Loop Mirror,” International Conference for Technical Postgraduates (TECHPOS 2009), pp. 257-259, Faculty Engineering, University of Malaya, Kuala Lumpur, 14-15 May 2009.

LIST OF AWARDS

1. **N. A. Awang**, S. F. Norizan, A.A.Latif, N.A.Hassan, M.Z.Zulkifli, S.W.Harun and H.Ahmad An All-Optical Frequency Up/Down-Converter Utilizing Stimulated Brillouin and Raman Scattering in a Truewave Reach Fibre and Dispersion Compensating Fibre for Radio Over Fibre Application, Gold Medal in Innovation & Creativity Expo University Of Malaya 2010 at 1st – 3rd April 2010.
2. A.A.Latif, N.A.Hassan, M.Z.Zulkifli, **N. A. Awang**, S. F. Norizan, S.W.Harun and H.Ahmad Novel O-band Tunable fibre laser using an AWG, Gold Medal in Innovation & Creativity Expo University Of Malaya 2010 at 1st – 3rd April 2010.

CONTENT

ORIGINAL LITERARY WORK DECLARATION	i
ABSTRACT	ii
ABSTRAK	iv
ACKNOWLEDGEMENTS	vi
LIST OF PUBLICATIONS	viii
LIST OF CONFERENCES	xi
LIST OF AWARDS	xii
CONTENTS	xiii
LIST OF FIGURES	xvii
LIST OF TABLES	xviii
ACRONYMS	xix
NOMENCLATURE	xxi

1. INTRODUCTION

1.1	Fibre Optical Communication System	1
1.2	History of Nonlinear Optics	3
1.3	Fibre Nonlinearity Effect	5
1.3.1	Stimulated Raman Scattering (SRS)	6
1.3.2	Stimulated Brillouin Scattering (SBS)	6
1.3.3	Self-Phase Modulation (SPM)	7
1.3.2	Cross Phase Modulation (XPM)	8
1.3.3	Four Wave Mixing (FWM)	8
1.4	Wavelength Conversion	9
1.5	Fibre Optic Parametric Amplifier (FOPA)	9
1.6	Multiwavelength Fibre Laser	10

1.7	Objective	11
1.8	Thesis Outline	13
	Reference	15
2.	THEORY OF FOUR-WAVE MIXING IN HNLF AND SOA	
2.1	Introduction	21
2.2	Highly Nonlinear Fibres (HNLF)	22
2.2.1	Design of the HNLF	22
2.2.2	Origin of Nonlinear effects	27
2.2.3	Different types of nonlinear effects	31
2.2.4	FWM effect	33
2.3	Semiconductor Optical Amplifier (SOA)	40
2.3.1	Optical gain in semiconductors.	42
2.3.2	Gain saturation and nonlinearities	48
2.3.3	FWM effect	53
2.4	Summary	60
	Reference	61
3.	CHARACTERISATION OF HNLFs AND SOAs USING FOUR WAVE MIXING TECHNIQUES	
3.1	Introduction	66
3.2	Highly Nonlinear Fibre (HNLF)	68
3.2.1	Experimental setup for characterizing the HNLF	69
3.2.2	Determination of the ZDW	70
3.2.3	Determination of chromatic dispersion	83
3.2.4	Determination of nonlinear coefficient	85
3.3	Semiconductor Optical Amplifier (SOA)	88
3.3.1	Gain Performance of SOA	88
3.3.2	FWM effect	95

3.4	Summary	108
	Reference	109
4.	WAVELENGTH CONVERSION USING FWM EFFECT	
4.1	Introduction	114
4.2	Dual-wavelength Fibre laser	115
4.3	FWM effect in HNLF	121
4.3.1	The generation of a wavelength conversion in HNLF by using a dual-wavelength fibre laser.	121
4.3.2	Wideband wavelength conversion in HNLF	131
4.3.3	FWM Effect in ring configuration	140
4.4	FWM effect in SOA	149
4.4.1	Generation of wavelength conversion in SOA by using dual-wavelength fibre laser.	151
4.4.2	Wide-band of wavelength conversion in FWM effect of SOA by using dual-wavelength fibre laser.	155
4.4.3	Pulse Wavelength Conversion in SOA	161
4.4.4	Generation of FWM by using dual-wavelength fibre laser from O band to C band	170
4.5	Summary	184
	Reference	185
5.	FWM APPLICATION IN FIBRE OPTICAL PARAMETRIC AMPLIFIER (FOPA) AND MULTIWAVELENGTH FIBRE LASER	
5.1	Introduction	193
5.2	FOPA	193
5.2.1	Principle of FOPA	195
5.2.2	Basic Equations of FOPA	197

5.2.3	Demonstration of single pump FOPA in a HNLF	200
5.3	Multiwavelength fibre laser	204
5.4	Summary	213
	Reference	214
6.	CONCLUSION AND FUTURE WORKS	
6.1	Conclusion	217
6.1.1	Nonlinear characterization	217
6.1.2	Wavelength conversion based on FWM	219
6.1.3	Development of FOPA and multiwavelength fibre laser	220
6.2	Future Work	221
	APPENDIX	
A	Selected Papers Related to this Work	
B	Selected Paper Based on the Study of Nonlinear Parameter from this Thesis	

LIST OF FIGURES

1 INTRODUCTION

- 1.1 Schematic of the nonlinear effects in fibre optics. 5

2 THEORY OF FOUR WAVE MIXING IN HNLF AND SOA

- 2.1 The index of refractive profile of common graded-index fibre. 23
- 2.2 Fibre losses as a function of Δn . 25
- 2.3 HNLF design. The materials and the concentration of the dopants used for the core and cladding are shown in the figure. 25
- 2.4 Spectrum of FWM terms generated in a three wavelength system with input fields at ω_1 , ω_2 and ω_3 . The number “ ijk ” means the frequency of that term is at $\omega_4 = \omega_1 + \omega_2 - \omega_3$. 34
- 2.5 Wavelength arrangements satisfying the phase matching condition in the zero-dispersion wavelength region. (a) Completely nondegenerate case (b) Partially degenerate case. 38

2.6	Illustration of physical processes involved in dynamic carrier heating and spectral hole burning.	52
2.7	Schematic of a FWM processes in SOA. A_i , $i = 1, 2, 3, 4$ are the pump, signal, conjugate, cs and conjugate, cs', respectively.	54

3 CHARACTERISATION OF HNLFs AND SOAs USING FOUR WAVE MIXING TECHNIQUE

3.1	Schematic diagram for generating FWM effect in the HNLF.	69
3.2	Wavelength arrangements satisfying the phase-matching condition in the ZDW region (a) non-degenerate case, (b) partially degenerate case [22].	72
3.3	The FWM efficiency, η as a function of relative pump wavelength $\lambda_p - \lambda_0$ in partially degenerate FWM.	73
3.4	(a) The FWM spectrum by varying the pump and signal wavelength (b) the spectrum of FWM power against converted wavelength.	75
3.5	(a) The FWM spectrum by varying the pump and fix the signal wavelength (b) the FWM efficiency against pump wavelengths.	77
3.6	Spectrum of FWM	79
3.7	The FWM power of tuning signal wavelength for different pump wavelength.	80
3.8	The FWM efficiency as a function of signal wavelength of HNLF.	81

3.9	Optical power of FWM as a function of signal wavelength.	83
3.10	The chromatic dispersion coefficient of HNLF with our proposed technique.	85
3.11	Experimental setup for ASE measurement of SOA	89
3.12	Spontaneous emission spectrum of the SOA for different total current.	90
3.13	(a) Gain and (b) noise figure as a function of input power at a fixed signal wavelength of 1500 nm, 1550 nm and 1580 nm.	92
3.14	Gain (dB) and Noise Figure (dB) of SOA against different test signal wavelengths at -30 dBm and 0 dBm.	94
3.15	Experiment setup for measure FWM in the SOA.	96
3.16	Optical spectrum of FWM after the SOA. The wavelength separation between the pump and the probe is 0.5 nm. The input power of the pump and probe beams is 12 dBm and 8 dBm, respectively. The wavelength of the FWM is about $2\lambda_{PUMP}-\lambda_{PROBE}$.	98
3.17	Picture of the FWM generation	98
3.18	Measured FWM power (circled) as a function of the wavelength separation between the pump and the probe beams. The pump wavelength, input pump power and signal pump power of 1543 nm, 12 dBm and 10 dBm, respectively. The solid line is the calculated result using typical parameter values.	100
3.19	Measured FWM signal as a function of the total current of the SOA. Wavelength separation between the pump and signal wavelength is 0.5 nm, input pump power of 12 dBm and input signal power of 10 dBm.	101

4 WAVELENGTH CONVERSION USING FWM EFFECT

4.1	The experimental setup for tunable dual-wavelength fibre laser.	117
4.2	Characterization of AWG by using white light source, with outputs at a particular channel.	118
4.3	The dual-wavelength with channels spacing.	119
4.4	SMSR and peak power with different wavelength channels (dual-wavelength output are taken as 9 and 24, 10 and 23, 11 and 22 and soon).	120
4.5	Schematic diagram for generating FWM in a HNLF using a dual-wavelength fibre laser incorporating AWG as the tuning element.	123
4.6	Spectra of the FWM at different pump wavelengths for different AWG channels.	124
4.7	FWM conversion efficiency versus wavelength detuning in HNLF.	126
4.8	Measurement of conversion efficiency in the OSA.	126
4.9	The ASE spectrum of the 11m metrogain EDF.	127
4.10	FWM output power versus wavelength detuning between pump and signal.	128
4.11	FWM output power versus input pump power.	129
4.12	Optical signal to noise ratio versus wavelength detuning.	130
4.13	Schematic diagram for generating FWM effect in a highly nonlinear fibre using dual-wavelengths fibre laser incorporating AWG as a tuning element.	134

4.14	The value of FWM conversion efficiency for different AWG's channels.	134
4.15	The typical output spectra at pump 1, signal and pump 2, as well as their converted signals (sideband fields) C2 and S2 when wavelength of pump 1, signal and pump 2 are 1538.3 nm, 1541.5 nm and 1530 nm.	136
4.16	The output spectra of S2, Pump 2 and C2 when the wavelength of Pump 1 and signal are 1538.3 nm and 1541.5 nm; (a) Pump 2 is 1460 nm and their input power is 3.86 dBm; (b) Pump 2 is 1530.2 nm and their input power is 3.00 dBm; (c) Pump 2 is 1640 nm and their input power is 3.36 dBm.	138
4.17	The conversion efficiency and the optical signal to noise ratio against the converted.	140
4.18	Schematic diagram for generating FWM effect in a ring configuration	142
4.19	Power spectra at the output of the fibre.	144
4.20	FWM conversion efficiency versus the signal wavelength, P_S , with HNLF fitting pump wavelength, P_P , at 1590 nm.	145
4.21	FWM conversion efficiency versus the signal wavelength, P_S , with HNLF fitting pump wavelength, P_P , at 1590 nm by using ring and linear cavity.	146
4.22	FWM conversion efficiency versus 1490 nm LD pump power.	147
4.23	SNR against signal wavelength, P_S , keeping pump wavelength, P_P , fixed at 1590 nm in HNLF.	148
4.24	SNR against signal wavelength, P_S , keeping pump wavelength, P_P , fixed at 1590 nm in HNLF by using ring and linear cavity.	148

4.25	The experimental setup for FWM effect in SOA by using dual-wavelength fibre laser.	152
4.26	The FWM spectrum from OSA.	153
4.27	The conversion efficiency and SNR versus wavelength channels.	154
4.28	Setup on wavelength conversion using assisted pump.	156
4.29	The full, S-band, C-band and L-band spectrum of wavelength conversion.	158
4.30	Effect of the assisted pump on the conversion efficiency versus the wavelength conversion.	160
4.31	Plot of the output SNR against the wavelength conversion.	161
4.32	Setup on wavelength conversion using orthogonal polarized pump four-wave mixing in SOA.	163
4.33	Output spectra without inserted modulated input signal (a) dual-wavelength output of Bi-EDF ring cavity showing the oscillating at λ_{P1} of 1540.0 nm and λ_{P2} of 1541.5 nm (b) an insertion of SOA, four wave mixing is generated whereby λ_{C4} of 1538.4 nm and λ_{C5} of 1543.2 nm are due to four wave mixing.	164
4.34	The spectra signal of orthogonal polarized pump scheme before connected with optical bandpass filter (a) $\lambda_{P1} \geq \lambda_{P2}$ (b) $\lambda_{P1} \leq \lambda_{P2}$.	166
4.35	The output signal after the optical bandpass filters (a) λ_{C1} (b) λ_{C2} .	167
4.36	The converted signal at wavelength 1532.8 nm and 1534.5 from input signal at wavelength 1547.0 nm after passing through the SOA.	169
4.37	Experimental setup.	173

4.38	Output spectrum of channels 23 and 24 of the AWG after the ASE output from the 1310 nm SOA.	174
4.39	The spectrum of dual-wavelength fibre laser with two dual-wavelength side bands together with the 1550 nm signal.	175
4.40	Spectrum from O-band to C-band (a) before the 1310nm SOA (b) after the 1310nm SOA.	177
4.41	The O-band spectrum; (a) before SOA (b) after SOA.	179
4.42	The C-band spectrum; (a) before SOA (b) after SOA	181
4.43	Graphical illustration of wavelength conversion.	183

5 FWM APPLICATION IN FIBRE OPTICAL PARAMETRIC AMPLIFIER (FOPA) AND MULTIWAVELENGTH FIBRE LASER

5.1	Configuration of a single pump FOPA.	195
5.2	Configuration of a two-pump FOPA.	196
5.3	Gain shape versus pump wavelength location.	199
5.4	Gain spectrums for a single pump FOPA.	200
5.5	Schematic diagrams for generating FWM effect in a ring configuration.	201
5.6	Power spectra at the output of the fibre.	202
5.7	Gain versus signal wavelength, $P_{in} = -34$ dBm	204

5.8	Experimental Setup of HLNLF based Multi-Wavelength Fibre Laser in a Ring Cavity Configuration.	207
5.9	Free-Running Spectrum of the FWM (without pump and signal wavelengths).	208
5.10	Power spectra at the output of the fibre.	210
5.11	Number of generated wavelengths (lines) based on FWM in HNLN with different EDFA pump powers against the signal wavelength, λ_s .	211
5.12	Output Power Stability of the Generated Wavelengths based on FWM. Points in the Graph Indicate the Output Power of the Various Generated Wavelengths such as E ₁ , D ₁ , C ₁ , C ₂ , D ₂ and E ₂ of Figure 4	212

LIST OF TABLES

3 CHARACTERISATION OF HNLFs AND SOAs USING FOUR WAVE MIXING TECHNIQUE

3.1 Parameters of HNLF. 87

6 CONCLUSION AND FUTURE WORKS

6.1 Comparison of two different pump sources for wavelength conversion configuration. 219

ACRONYMS

ATT	Attenuator
AWG	Arrayed Waveguide Grating
ASE	Amplified Spontaneous Emission
Bi-EDF	Bismuth Erbium Doped Fibre
CD	Chromatic Dispersion
CH	Carrier Heating
CW	Continuous Wave
DFB	Distributed Feedback
EDFA	Erbium Doped Fibre Amplifier
EDF	Erbium Doped Fibre
FOPA	Fibre Optic Parametric Amplifier
FWM	Four Wave Mixing
HNLF	Highly Nonlinear Fibre
LiNbO ₃	Lithium niobate
MCVD	Modified Chemical Vapour Deposition
MZM	Mach Zehnder Modulator
NPR	Nonlinear Polarization Rotation
OCS	Optical Channel Selector
OFS	Optical Fibre Solutions
OSK	Oscilloscope
OSA	Optical Spectrum Analyzer
PBC	Polarization Beam Combiner
PC	Polarization Controller
PD	Photodetector
SBS	Stimulated Brillouin Scattering
SFG	Sum Frequency Generation
SHB	Spectra Hole Burning

SHG	Second Harmonic Generation
SLM	Sagnac Loop Mirror
SMF	Single Mode Fibre
SMSR	Sidemode Suppression Ratio
SNR	Signal to Noise Ratio
SOA	Semiconductor Optical Amplifier
SPM	Self Phase Modulation
SRS	Stimulated Raman Scattering
TBF	Tunable Bandpass Filter
TLS	Tunable Laser Source
VAD	Vapour Axial Deposition
WDM	Wavelength Division Multiplexing
WXC	Wavelength Cross Connect
XPM	Cross Phase Modulation
ZDW	Zero Dispersion Wavelength

NOMENCLATURE

ν_P ,	Frequency of the pump
ν_A	Frequency of the acoustic phonon
ν_S	Frequencies of the stokes
ν_{AS}	Frequencies of anti-stokes
ν_B	Brillouin shift
V_A	Acoustic velocity
N	Refractive index
λ_P	Pump wavelength
Δn	Variation of refractive index
n_2	Nonlinear coefficient
I	Optical intensity
V	Normalized frequency
A_{eff}	Effective fibre core area
r	Core radius
ϵ_0	Vacuum permittivity
χ	Electric susceptibility
E	Electric field
P	Polarization
α	Absorption coefficient
P_{NL}	Nonlinear polarization
ω	Frequency
η	FWM efficiency
n_{nl}	Nonlinear refractive index
n_l	Linear refractive index
n_{eff}	Effective refractive index
$\Delta\beta$	Phase mismatching

β	Propagation constant
β_2	The group velocity dispersion parameter
θ_+	Relative phase
D	Degeneracy factor
L_{eff}	Effective length
L	Length
γ	Nonlinear coefficient
Dc	Fibre chromatic dispersion
$dD/d\lambda$	Dispersion slope
$u_{cvk}(r)$	Periodicity of the crystalline lattice
$m_{c,v}^*$	Effective mass of the carrier
$H(x)$	Heaviside function
\hbar	Planck's constant
$E_{nc,v}$	Energy level resulting from carrier confinement
$E_{c,v}$	Carrier energy
$E_{fc,v}$	Quasi-fermi level of the conduction and valence band
c	Speed of light
k_B	Boltzman's constant
T	Lattice temperature
μ	Momentum matrix element
T_2	Dephasing time
$\rho_j(\omega_0)$	Joint density of states
N	Carrier density
q	Electron charge
τ_s	Spontaneous carrier lifetime
$G(N)$	Gain constant per unit length
P_s	Saturation power
Ω	Channel spacing
a	Gain factor

α	Linewidth enhancement factor
G_0	Normalization gain
$h_{ch}(t)$	The gain to a change in the carrier temperature
ϵ_{ch}	Strength of the carrier process
ϵ_{sh}	The strength of the spectral hole burning
Γ	Overlap integral
A	Cross-sectional area
$h\nu$	Photon energy
τ_c	Cavity lifetime.

CHAPTER 1

INTRODUCTION

1.1 Fibre Optical Communication System

Communication systems can be broadly defined as systems which enable the transfer of information from one point to another over a distance. These kinds of systems are frequently achieved by superimposing or modulating the information to be transferred onto an electromagnetic wave which acts as a carrier for the information signal. Optical carrier waves or light for communication has been used for many years. As early as 1880 Alexander Graham Bell reported the transmission of speech using a beam of light.

In the intervening years, new technologies slowly took root that would ultimately solve the problem of optical transmission, although it took a considerable amount of time before it was adapted for communication. These technologies generally depended on the phenomenon of total internal reflection, which is the ability to confine light in a material surrounded by other materials with lower refractive indices such as glass in air. In 1854, John Tyndall demonstrated light guiding by guiding light in a jet of water flowing from a tank. By the turn of the century, inventors realized that bent quartz rods could carry light. Proposals for optical communication via dielectric waveguided and optical fibres fabricated from glass were made almost

simultaneously in the mid 1960s when the loss in glass was still in the order of 1000 dB/km, which is much larger than the 5 – 10 dB/km in the then widely used coaxial cable. In January 1966, Charles K. Kao and his colleague, George Hockman, demonstrated that the inherent loss in glass could potentially be removed. They concluded that the fundamental limitation for light attenuation in glass is less than 20 dB/km [1], which is a key threshold value for the feasibility of optical communications. This important prediction started a revolution in fibre optic communication technologies and eventually led to Charles K. Kao receiving the 2009 Nobel Prize in physics for his “groundbreaking achievement concerning the transmission of light in fibres for optical communication” [1]. By 1979, further progress in fabrication technology resulted in a loss of only 0.2 dB/km in the 1500 nm region [2], which is the minimum loss level allowed by the fundamental process of Rayleigh scattering [3].

Even though fibre optic technology is only roughly 25 years old, it has progressed quite rapidly. For instance, the development of optical amplifiers is considered as a key contributor, especially the Erbium Doped Fibre Amplifiers (EDFA) because of its wide gain bandwidth. The wavelength-division multiplexing (WDM) channels, in an EDFA can be amplified simultaneously and transmitted over long distance. However, the implementation of optical amplifiers magnifies the effects of optical nonlinearities in the transmission fibres. These nonlinearities will limit the information capacity of lightwave communications. This type of limitation can be overcome by various compensation techniques such as fibre lasers, amplifiers, switches, multiplexer, demultiplexer, generation of short pulses and wavelength conversion.

1.2 History of Nonlinear Optics

The first functioning laser by T. H. Maiman [4] in 1960 at Hughes Research Laboratories was generated by using the solid state flashlamp-pumped synthetic ruby crystal and produced a red laser light. The advent of this laser gave birth to a new field of optics called nonlinear optics which was due to the response of atoms to intense electromagnetic fields and can no longer be taken to be linear in the electric field. The observation of second harmonic generation [5] in 1961 was soon followed with the discovery of a large number of nonlinear processes such as stimulated Raman scattering (SRS) [6], stimulated Brillouin scattering (SBS) [7] and four wave mixing (FWM) [8].

The nonlinearity cannot be observed inside the silica fibres that were available during the 1960s due to very high losses. This situation was changed when scientists working at Corning [9] were able to reduce losses in silica fibres dramatically in 1970s. Soon after that, Stolen's group at Bell Laboratories used silica fibres to demonstrate a variety of nonlinear effects, including, SBS, SRS, self-phase modulation (SPM) and FWM. These silica fibres are capable of carrying large amounts of information over long repeater-less spans, making optical communications the backbone of today's telecommunication networks. The emergence of multimedia services and the internet has resulted in an explosion in both traffic and bandwidth demand. As a result of this, the development of an all-optical signal processing devices and technologies has become essential to tackle the performance limitation that otherwise result from the unavoidable conversion between the optical and electrical domains. Typical all-optical signal processing devices are based on the nonlinear properties of optical fibres or semiconductor optical amplifiers (SOA), and excellent results have been achieved by both devices based on SOAs and optical fibres. However, devices based on optical fibres would normally be made by very long

optical fibres (typically in km range) to achieve the required nonlinear effects. The use of such a long fibres makes it impractical for uses outside of the laboratory, apart from the added complication of the difficulty in maintaining the polarization of the light when the fibre is in operation. This is because optical fibres, normally made of silica have low values of effective nonlinearity. One way of producing fibres with a high value of effective nonlinearity is to use glass with a higher nonlinear refractive index value n_2 such as chalcogenide [10] or lead silicate [11]. Although high values of effective nonlinearity can be achieved, integration with that transmission fibre (silica) could be a problem. Therefore, there is a need to produce silica optical fibres with a high value of effective nonlinearity to achieve low loss in the transmission wavelength band. One technique to increase the nonlinearity inside the silica fibre is to control the core size and the refractive index different by using the vapour axial deposition (VAD) process. In this process, the nonlinear fibre is achieved by stretching and overloading the fibre performs several times before drawing the fibre performs into fibre. Dopants such as GeO_2 and P_2O_5 are used to increase the refractive index of pure silica and are suitable for the core, while materials such as boron and fluorine are used for the cladding because they decrease the refractive index of silica. The high nonlinearity in the fibre is achieved when the core size is decreased with high effective refractive index.

1.3 Fibre Nonlinearities Effect

The response of optical fibre to light waves becomes nonlinear when the intensity of the light wave is high enough. This caused by the anharmonic motion of bound electrons under the influence of the applied field. Nonlinear effects in fibre optics typically consist of the refractive index effect and stimulated scattering effects. These effects are categorized as shown in Figure 1.1. Stimulated scattering is manifested as an intensity dependent gain or loss, while the nonlinear index gives rise to an intensity dependent phase of optical field [12]. These nonlinearities become a problem in WDM systems. However, this nonlinearity can be used as optical switches or amplifier or wavelength converter or multiwavelength to overcome the problem make by these effects in the WDM system.

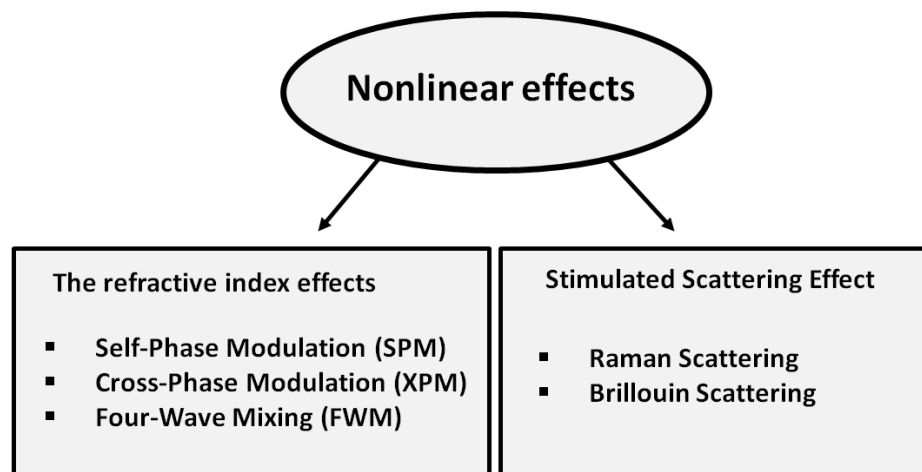


Figure 1.1 Schematic of the nonlinear effects in fibre optics.

In the next subsections, the nonlinear effects in optical fibres that are relevant to the study in this thesis namely SRS, SBS, SPM, cross-phase modulation (XPM) and FWM will be described briefly.

1.3.1 Stimulated Raman Scattering (SRS)

The Raman effect was first discovered in 1928 by C. V. Raman [13]. In general, spontaneous Raman scattering happens when a beam of light illuminates a transparent material (which can be solid, liquid or gas). A fraction of the incident light will be scattered to new frequencies. The light that is scattered to a lower frequency is called the frequency stokes and the light that is scattered to a higher frequency is called the frequency anti-stokes. The scattering occurs as a result of the interaction between the light and molecular vibrations of the medium and hence the extent of the frequency shift depends on the frequency of the molecular vibrations of the medium.

1.3.2 Stimulated Brillouin Scattering (SBS)

The Brillouin effect was first discovered in 1922 by Leon Brillouin [14]. Brillouin scattering, like Raman scattering, involves an interaction between an incident wave, a scattered wave and a phonon. However, unlike Raman scattering, ‘acoustic’ rather than ‘optical’ phonons are involved. The fact that acoustic phonons have much lower energies makes the frequency shift in Brillouin scattering very small (roughly 11 GHz or 0.08 nm at 1550 nm). In this process phonons

may either be created or absorbed, resulting in Stokes or anti-Stokes scattered waves. Following conservation of energy

$$\nu_P = \nu_S + \nu_A \quad 1.1$$

$$\nu_P + \nu_A = \nu_{AS}$$

where ν_P , ν_A , ν_S and ν_{AS} are the frequencies of the pump, acoustic phonon, stokes wave and anti-stokes wave, respectively. Therefore, the magnitude of the Brillouin shift is found to be

$$\nu_B = \frac{2V_A n}{\lambda_P} \quad 1.2$$

where V_A is the acoustic velocity in the fibre, n is the refractive index of the fibre and λ_P is the pump wavelength.

1.3.3 Self-Phase Modulation (SPM)

SPM is the change of phase in the optical pulse due to the change in refractive index caused by the intensity of the pulse. The varying refractive index of the medium is due to the optical Kerr effect [15]. The phase shift in the pulse produced by varying the refractive index leads to a change of the pulse's frequency spectrum. This variation of refractive index can be described by

$$\Delta n = n_2 I \quad 1.3$$

where n_2 is the nonlinear coefficient and I stands for optical intensity. The temporal dependence of the phase shift is considered in SPM.

1.3.4 Cross Phase Modulation (XPM)

XPM is the phenomenon where the intensity of one beam influences the phase change of another beam. In essence, it is the change of the optical phase of one light beam caused by the interaction with another beam in a nonlinear medium, specifically a Kerr medium [15]. This can be described by a refractive index change of

$$\Delta n(\lambda_2) = 2n_2 I(\lambda_1). \quad 1.4$$

XPM leads to an interaction of laser pulses and channel crosstalk in a medium.

1.3.5 Four Wave Mixing (FWM)

FWM occurs when two or more frequencies (or wavelengths) of light are transmitted together through a fibre. Provided that phase matching conditions are satisfied, a new frequency of light is generated using the power from the original frequencies [16], which will be discussed in detail in the next chapter 2. FWM is a nonlinear process that contributes to the generation of a new frequency and has applications in the development of tunable lasers, wavelength conversion fibre optic parametric amplifier (FOPA) and multiwavelength fibre laser.

1.4 Wavelength Conversion

A wavelength converter is a device that takes data from an input channel at a particular wavelength and sends this data out on a different wavelength channel. In large networks (as opposed to point-to-point links) the number of different wavelength channels may not be large enough to support the large number of wavelength cross connect (WXC) nodes needed in the network. When two data streams at the same wavelength are to be routed at the same output, one of the channels will be blocked since there is competition between the two different data-streams for the same wavelength. Wavelength conversion is one solution for reducing the blocking probability by converting the wavelength to another wavelength [17]. In addition, wavelength converters increase the flexibility and capacity of the network for a fixed set of wavelength [18] [19]. Wavelength conversion can be performed by ultrafast wave mixing techniques based either on FWM in an SOA or nonlinear fibre. It is also the only method that allows simultaneous conversion of one set of multiple input wavelengths to another set of multiple output wavelengths. The wave mixing wavelength conversion can potentially operate with signals modulated at over 100 Gb/s bit-rates [20].

1.5 Fibre Optic Parametric Amplifier (FOPA)

Parametric amplification is a well-known phenomenon in materials which has the second order electric susceptibility, χ^2 [21]. However, it can also be obtained in optical fibre by utilizing the χ^3 nonlinear behaviour. With the development of new high-power light sources and fibres with a nonlinear parameter which is 5 – 10 times higher than conventional fibres [22] [23], as well as the need of amplification outside the conventional erbium band, there has been an increased

interest in methods such as FOPA. A FOPA based on highly efficient FWM, have been experimentally investigated since the late 1980s [24]. It offers a wide gain bandwidth, similar to a Raman amplifier, as well as having noise penalties lower than the 3 dB quantum limit [25]. Additional advantages include transparent wavelength conversion [26] and the phase conjugation of the signals [27]. If the pump is intensity modulated, it also can be used for a return-to-zero (RZ) pulse generation, as well as optical sampling or demultiplexing.

1.6 Multiwavelength Fibre Laser

Over the past decades, multiwavelength fibre lasers have aroused considerable interest due to their comprehensive application in the fields of the dense wavelength division multiplexing systems, fibre optic sensing and microwave photonics. The requirements for multiwavelength sources include a large number of channels over a broad bandwidth, precise and stable spacing, narrow linewidth and small power fluctuation. This can be achieved by using the FWM effect in nonlinear fibre. This fibre laser has a more stabilized output as a result of the balance between FWM and the mode competition in the EDF, which is useful for applications in wavelength converters, for the determination of nonlinear parameters as well as for multiwavelength laser source for the WDM system [28] – [30].

1.7 Objective

This thesis is intended

- a) To provide a comprehensive study of the FWM effect in highly nonlinear media and their possible applications in telecommunications.

The nonlinear behaviours of interest in this work are in the HNLF and SOA media, both of which are chosen to demonstrate the different principles of nonlinear behaviour. The nonlinear parameters in HNLF and SOA such as the zero-dispersion wavelength (ZDW), chromatic dispersion (CD), nonlinear coefficient, FWM power and FWM efficiency are discussed in depth in this thesis. The determination of fibre nonlinear parameters conventionally employ the interferometric technique since this experimental technique is relatively accurate compared to other methods. However, this technique is quite difficult and inconvenient for nonlinear measurement. Therefore, non-interferometric techniques such as self-phase modulation (SPM), cross phase modulation (XPM) and FWM are preferable due to their simplicity. In general, self phase modulation (SPM) [31] or cross phase modulation (XPM) [32] techniques require short pulses and small chromatic dispersion and they only give access to the nonlinear coefficient value. More recently, partially degenerated FWM which is described in detail in chapter 2 was shown to be a viable method to simultaneously measure the nonlinear parameters. There are several reports that this scanning FWM experiments can be used to measure ZDW, CD, and the non-linear refractive index both individually [33], [34], [35] and simultaneously [36], [37]. Therefore, several FWM methods are studied in order to establish the best method which agrees with both theoretical calculation and experimental data. From our results, the relevant region for wavelength

conversion by using the FWM technique is identified. This is presented in detail in chapter 3.

- b) To concern with wavelength conversion via the FWM technique in HNLF and SOA.

The basic principle of wavelength conversion is the interaction of two wavelength laser sources, commonly referred to as a dual-wavelength laser source, and they are conventionally injected externally into a nonlinear medium, which then converts the so-called pump sources into a different wavelength [38] [39] [40] [41]. However, in this study, the proposed configuration of a wideband tunable wavelength conversion in HNLF and SOA employed a self-constructed tunable dual-wavelength fibre laser by utilizing the 24 Channel Arrayed Waveguide Gratings (AWG) as a wavelength selector for the laser source. The proposed wavelength conversion will be characterized by the FWM conversion efficiency and conversion power as well as the signal to noise ratio (SNR). The results from this study are important as tool in future WDM-based high speed optical networks because it provides simultaneous conversion of a single data channel into different channels without requiring multiple optical–electronic–optical transponders. The results obtained are discussed in Chapter 4.

- c) To develop the FOPA and multiwavelength fibre laser system with the capability to act as an amplifier as well as multi wavelength sources.

Previous studies of FOPAs employed high power pump and have reported of round 29 dB [42], 70 dB [43] and 49 dB [44]. However, in this thesis, a new configuration of FOPA with a relatively low pump power is demonstrated. The proposed FOPA system can be used in a

wide range application especially in telecommunication where they can replace the existing FOPA systems used as pulse sources, demultiplexer, preamplifier and wavelength converter. This is in contrast to a multiwavelength fibre laser which is generated by the HNLF and can be used as a source for the WDM system. In an earlier work [45] the generation of 5 stable multi-wavelengths has been demonstrated based on the FWM effect in this type of fibre with a SNR of 20 dB. However, it required a very long length of optical fibre (in km) as well as a very high gain amplifier to produce the multi-wavelength fibre laser giving a saturated output power of around 30 dBm [46]. Therefore, in this thesis, a new simple configuration of stable multiwavelength fibre laser employed the FWM effect is designed and discussed. The output power, on/off gain as well as number of lines generated and stability of laser of proposed FOPA and multiwavelength fibre laser are measured in order to obtain the efficiency.

1.8 Thesis Outline

This thesis is divided into six chapters. Chapter 2 provided an overview background on the fundamentals of the nonlinear effect in HNLF and SOA based on the FWM effect. In the HNLF, the design of the fibre and principle of FWM is described in this chapter. The other explanation is about the optical gain, gain saturation and principle FWM in the SOA.

Chapter 3 describes numerically and experimentally nonlinear characterisation of both HNLF and SOA using the FWM technique. Based on this technique, the ZDW, CD, dispersion slope and nonlinear coefficient could be determined in the HNLF. In the SOA medium, the gain performance is investigated to obtain the gain saturation and nonlinearity of the SOA. By using

the FWM technique, the FWM efficiency of SOA and HNLF is obtained approximately similar between numerical and experimental.

Chapter 4 demonstrates various new architectures for the construction of new and novel wavelength converters using either HNLF or SOA as the gain medium to increase the efficiency of FWM. In the first part of this chapter, the generation of dual-wavelength fibre laser is explained. A self-constructed dual-wavelength fibre laser is produced as it is more cost effective compared to the tunable laser source (TLS). Then, the generation of FWM wavelength converter in the SOA and HNLF is investigated. This will be discussed in detail for both FWM degenerates and FWM non-degenerate case. Based on this technique, the wideband wavelength converter is obtained. Following this, the generation of a wavelength converter in a ring configuration by using two independence TLS where it uses a lower pump power is discussed.

In addition to the application of wavelength converters in HNLF and SOA, others applications such as parametric amplifiers and multiwavelength fibre lasers in HNLF are also discussed in Chapter 5. In this chapter, the FOPA system is a design to obtain the highest and flattest gain by using lower pump powers. A compact ring configuration multiwavelength fibre laser utilizing the FWM effect is discussed. Based on the design, the highest SNR, many lines of signal and stable spectrum is obtained.

The works presented in this thesis are summarized and concluded in Chapter 6. A recommendation for further research is also presented in this chapter.

Reference

- [1] K. O. Kao and G. A. Hockam, "Dielectric-fibre surface waveguides for optical frequencies," IEE Proceeding J., vol. 133, pp. 1151-1158, 1996.
- [2] T. Miya, Y. Terunuma, T. Hosaka and T. Miyashita, "Ultimate low-loss single mode fibre at 1550 nm," Electron. Lett., vol. 15, pp. 106-108, 1979.
- [3] G. E. Keiser, "Optical fibre communication, 3rd Ed." McGraw Hill, pp. 106-108 (1979).
- [4] T. H. Maiman, "Stimulated optical radiation in ruby," Nature, vol. 187, pp. 493-494, 1960.
- [5] P. A. Franken, A. E. Hill, C. W. Peters, and G. Weinreich, "Generation of optical harmonics," Phys. Rev. Lett., vol. 7, pp. 118-119, 1961.
- [6] E. J. Woodbury and W. K. Ng, "Ruby laser operation in the near IR," Proc. IRE, vol. 50, pp. 2367, 1962.
- [7] R. Y. Chiao, C. H. Townes, and B. P. Stoicheff, "Stimulated Brillouin scattering and coherent generation of intense hypersonic waves," Phys. Rev. Lett., vol. 12, pp. 592-595, 1964.
- [8] R. L. Carman, R. Y. Chiao, and P. L. Kelly, "Observation of degenerate stimulated four-photon interaction and four-wave parametric amplification," Phys. Rev. Lett., vol. 17, pp. 1281-1283, 1966.
- [9] F. P. Kapron, D. B. Keck, and R. D. Maurer, "Radiation losses in glass optical waveguides," Appl. Phys. Lett., vol. 17, pp. 423-425, 1970.
- [10] T. Kanamori, Y. Terunuma, S. Takahashi and T. Miyashita, "Chalcogenide glass fibres for mid-infrared transmission," Journal of Lightwave Techno., vol 2, pp. 607-613, 1984.

- [11] M. A. Newhouse, D. L. Weidman and D. W. Hall, "Enhanced nonlinearity single mode lead silicate optical fibre," *Optics Letters*, vol. 15, pp. 1185-1187, 1990.
- [12] I. P. Kaminow and T. L. Koch, "Optical fibre telecommunication IIIA," Academic Press, 1997.
- [13] C. V. Raman and K. S. Krishnan, "A new type of secondary radiation," *Nature*, vol. 11, pp. 1503-1509, 2003.
- [14] L. Brillouin, "Diffusion de la lumiere et des rayons X par un corps transparent homogene: influence de l'agitation thermique," *Opt. Exp.*, vol.17, pp. 88-122, 1922.
- [15] G. P. Agarwal, "Fibre optic communication systems," John Wiley & Sons, 2002.
- [16] R. Billington, "A report of four-wave mixing in optical fibre and its metrological application," NPL report COEM, pp. 24, 1999.
- [17] C. A. Brackett, A. S. Acompora, J. Sweitzer, G. Tangonan, M. T. Smith, W. Lennon, K. C. Wang and R. H. Hobbs, "A scalable multiwavelength multihop optical network: A proposal for research on all-optical network," *J. Lightwave Technol.*, vol, 11, pp. 736-753 1993.
- [18] M. J. O'Mohony, "The potential of multiwavelength transmission," *Proc ECOC'94*, vol. 2, pp. 589-892, 1994.
- [19] N. Wauters, P. Demester, "Wavelength requirement and survivability in WDM cross-connected network," *Proc ECOC'94*, vol. 2, pp. 589-592, 1994.
- [20] S. J. B. Yoo, "Wavelength conversion technologies for WDM network applications," *J. Lightwave Technol.*, vol. 14, pp. 955-966, 1996.

- [21] S. K. Choi, R. D. Li, C. Kim and P. Kumar, "Travelling-wave optical parametric amplifier: Investigation of its phase sensitive and phase insensitive gain response," J. Opt. Soc, Amer. B, vol. 14, pp. 1564-1575, 1997.
- [22] M. Onishi, T. Okuno, T. Kashiwida, S. Ishikawa, N. Akasaka and M. Nishimura, "Highly nonlinear dispersion shifted fibre and their application to broadband wavelength converter," Opt. Fibre Technol., vol. 4, pp. 204-214, 1998.
- [23] D. L. Philen, D. W. Peckham and I. Brener, " Measurement of the nonlinear index of refraction, n_2 for various fibre types," Proc. Optical Fibre Communication Conf. Vol. 4, Baltimore, MD, pp. 184-186, Paper ThL5, 2000.
- [24] J. A. Levenson, I. Abram, T. Rivera and P. Grangier, "Reduction of quantum noise in optical parametric amplification," J. Opt., Soc., Amer. B, vol. 10, pp. 2233-2238, 1993.
- [25] W. Imajuku, A. Takada and Y. Yamabayashi, "Inline coherent optical amplifier with noise figure lower than 3 dB quantum limit," Electron. Lett., vol. 36, pp. 63-64, 2000.
- [26] M. Westlund, J. Hansryd, P. A. Andrekson and S. N. Knudsen, "Transparent wavelength conversion in fibre with 24 nm pump tuning range," Electron Lett., vol. 38, pp. 85-86, 2002.
- [27] C. J. McKinstrie, S. Radic, C. Xie, "Phase conjugation driven by orthogonal pump waves in birefringent fibres," J. Opt., Soc. Am. B, vol. 20, pp. 1437, 2003.
- [28] X. Liu, "Self-stabilizing effect of four-wave mixing and its applications on multi-wavelength erbium-doped fibre lasers," Photonics Techno. Lett. IEEE, vol. 17, pp. 2541-2543, 2005.

- [29] S. W. Harun, S. Shahi, H. Ahmad, "Bismuth erbium-doped fibre based multi-wavelength laser assisted by four-wave mixing process," *IEICE Electronics Expr.*, vol. 6, pp. 40-43, 2009.
- [30] Shtainhart, R. Segal, A. Tsherniak, "Wavelength division multiplexing," *Networks, Radar Communication*, 1999.
- [31] R. H. Stolen and C. Lin, "Self-phase modulation in silica optical fibres," *Physical Review A*, vol. 17, pp. 1448-1453, 1978.
- [32] T. Kato, Y. Suetsugu, M. Takagi, E. Sasaoka, and M. Nishimura, "Measurement of the nonlinear refractive index in optical fibre by the cross-phase-modulation method with depolarized pump light," *Opt. Lett.*, vol. 20, 988-990, 1995.
- [33] S. E. Mechels, J. B. Schlager and D. L. Franzen, "Accurate measurements of the zero-dispersion wavelength in optical fibres," *J. Res. Natl. Inst. Stand. Technol.*, vol. 102, pp. 333-347, 1997.
- [34] D. H. Kim, S. H. Kim, J. C. Jo, S. K. Kim and S. S. Choi, "Novel measurement of linear dispersion slope near the zero dispersion wavelength for four wave mixing," in *Proceedings of Nonlinear Optics'98*, 168, 1998.
- [35] L. Prigent and J. P. Hamaide, "Measurement of fibre nonlinear Kerr coefficient by four wave mixing," *IEEE Photon. Technol. Lett.*, vol. 5, 1092-1096, 1993.
- [36] P. S. Andre A. L. J. Teixeira, M. Lima, J. F. da Rocha and J. L. Pinto, "Nonlinear refractive index and chromatic dispersion simultaneous measurement in non zero dispersion shift optical fibres," *ICTON*, pp. 111-114, 2002.

- [37] H. Chen, "Simultaneous measurement of non linear coefficient, zero-dispersion wavelength and chromatic dispersion in dispersion-shifted fibres by four-wave mixing," *Opt. Commun.*, vol. 220, 331-335, 2003.
- [38] I. Zacharopoulos, I. Tomkos, D. Syvridis, F. Girardin, L. Occhi, and G. Guekos, "Influence of phase mismatch on a spectral inverter based on four wave mixing in dispersion shifted fibre at 10Gb/s," *IEEE Photon. Technol. Lett.*, vol. 11, pp. 430-432 1999.
- [39] S. Watanabe and T. Chikama, "Highly efficient conversion and parametric gain of nondegenerate forward four-wave mixing in a single mode fibre," *Electron. Lett.*, vol. 30, pp. 163-164, 1994.
- [40] D. M. Patrick and R. J. Manning, "20 Gbit/s wavelength conversion using semiconductor nonlinearity," *Electron Lett.*, vol. 30, pp. 252–254, 1994.
- [41] N. C. Kothari and D. J. Blumenthal, "Influence of gain saturation, gain asymmetry, and pump/probe depletion on wavelength conversion efficiency of FWM in semiconductor optical amplifiers," *IEEE J. Quantum Electron.*, vol. 32 pp. 1810–1816, 1996.
- [42] T. Yamamoto and M. Nakazawam, "Active optical pulse compression with a gain of 29 dB by using four wave mixing in an optical fibre," *IEEE Photon. Technol. Lett.*, vol. 9, pp. 1595-1597, 1997.
- [43] T. Torounidis, P. A. Andrekson and B. Olsson, "Fibre optical parametric amplifier with 70 dB gain," *IEEE Photon. Technol. Lett.*, vol. 18, pp. 1194-1196, 2006.
- [44] J. Hansryd and P. A. Andrekson, "Broadband continuous wave pumped fibre optical parametric amplifier with 49 dB gain and wavelength conversion efficiency," *IEEE Photon. Technol. Lett.*, vol. 13, pp. 194-196, 2001.

- [45] Y. G. Han, T.V. A. Tran and S. B. Lee, "Wavelength spacing tunable multiwavelength erbium doped fibre laser based on four wave mixing of dispersion shifted fibre," Opt. Lett., vol. 31, pp. 697-699, 2006.
- [46] D. S. Moon, U. C. Paek, Y. Chung, "Multiwavelength lasing oscillations in an erbium doped fibre laser using a few mode fibre Bragg grating," Opt. Express, vol. 12, pp. 6147-6152, 2004.

CHAPTER 2

THEORY OF FOUR-WAVE MIXING IN HNLF AND SOA

2.1 Introduction

Throughout this research, HNLFs and SOAs will be used as the primary nonlinear gain media in generating the FWM effect and designing the wavelength converter, FOPA and multiwavelength fibre laser. Therefore, it is critical that the nonlinear characteristics of these gain media be properly understood before any further work can be carried out.

This chapter is divided into two main sections. The first section will examine the HNLF, looking initially on the design and structure of the fibre, and subsequently focusing on the FWM effect in the HNLF. The second part of this chapter will focus on the SOA, examining its gain saturation and the principles of nonlinearity involved, with a particular focus on the FWM effect.

2.2 Highly Non-Linear Fibres (HNLF)

This section will focus on the design and structure of the HNLF, as well as examining its nonlinear characteristics.

2.2.1 Design of the HNLF

The design of the HNLF does not deviate significantly from that of conventional optical fibres. As such, HNLFs can be manufactured using the same process as conventional silica based Single-Mode Fibres (SMF-28s). Figure 2.1 shows the refractive index n profile of a graded-index fibre. The graded-index profile is easier to manufacture than a step-index because of the nature of the manufacturing process. Normally the core is doped with dopants like GeO_2 or P_2O_5 to raise the value of the refractive index (n) of the core. Possible dopants for the cladding include boron or fluorine to decrease n in the cladding, but a cladding is not normally doped due to cost considerations. If doping is used in the cladding, it can decrease n in the cladding and help to match the softness of the cladding to that of the core, so the fabric preform will not crack during the handling or cooling process after glass forming. In the case of where GeO_2 is used as the core dopant and fluorine cladding dopant, which has been found a ratio of $\Delta^+ : \Delta^- \approx 3:1$ is optimal. In Figure 2.1, the dashed line shows different level of n of pure SiO_2 , Δ^+ shows the increase of n in the core because of the core dopants, and Δ^- shows the decrease of n in the cladding because of the cladding dopants. Conventionally, Δ^+ and Δ^- are represented as a percentage of n of SiO_2 .

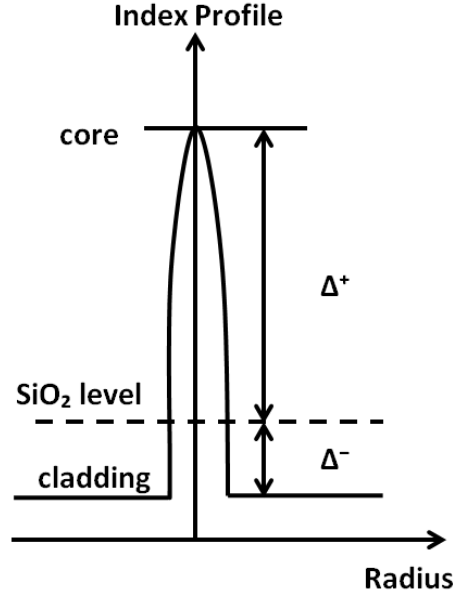


Figure 2.1 The index of refractive profile of common graded-index fibre.

Although other glass materials containing TeO_2 or B_2O_3 have much higher nonlinearity than silica fibre [1], silica glass is still a better choice for making nonlinear fibre due to its low loss in the transmission wavelength band. The low nonlinearity can be compensated by a long effective length. Other advantages of using SiO_2 -based fibre include ZDW controllability and the ease of connection to a transmission fibre. The ZDW controllability is important in FMW and FOPA applications as the ZDW has to be located near the pump wavelength in order to achieve optimum phase matching. SiO_2 -based fibre structure is easier to control in the manufacturing process. The ZDW of a fibre can be managed by changing the core size. Today most transmission fibres are SiO_2 -based, therefore SiO_2 -based HLNFs will be the easiest material to interface with transmission fibres. The splicing process is more reliable and the splice loss can be reduced to less than 1 dB even if there is a large mode-field diameter (MFD) size mismatch.

A simple design to achieve high nonlinearity is to decrease the core size. However, this means that Δ^+ has to be increased simultaneously because the normalized frequency V of the fibre has to be smaller than a critical value (for example, $V \leq 2.405$ for step-index fibre) to maintain single-mode operation of the fibre. V is proportional to $r\sqrt{\Delta^+}$ [2], where r is the core radius, so the decrease in the cores size r has to be accompanied by an increase in Δ^+ to maintain single-mode operation. Higher Δ^+ also increases the confinement of the optical field modes and hence a reducing effective fibre core area, A_{eff} . The increase in Δ^+ can be achieved by a higher percentage of GeO_2 doping in the fibre core. Furthermore, as GeO_2 has larger n_2 than SiO_2 , a higher doping level of GeO_2 will further increases the nonlinearity of the fibre [3]. The highest doping level in the core is limited not only by the manufacturing process but also by the doping level achieve in the cladding, because the core and cladding softness need to match, as mentioned earlier. The highest Δ^- possible to maintain reasonable loss in the case of fluorine doping is 0.45 % (Figure 2.2). For the particular HNLF presented in this work, the Δ^- is $\sim 0.45\%$ and the Δ^+ is carefully adjusted to 2.8%. The profile as a function of radius of the HNLF is shown Figure 2.3.

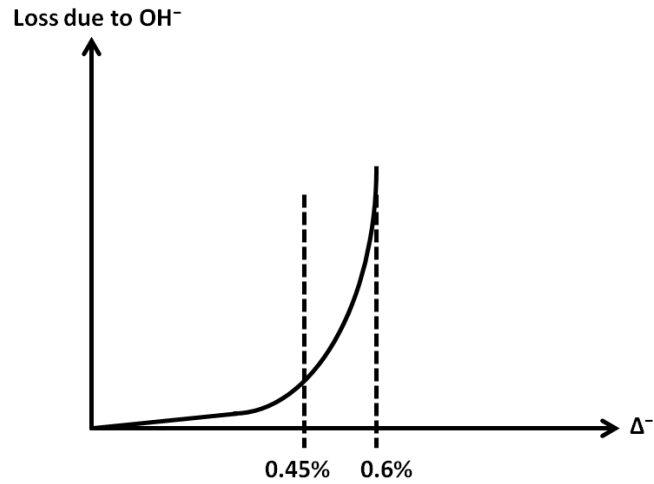


Figure 2.2 Fibre losses as a function of Δ^-

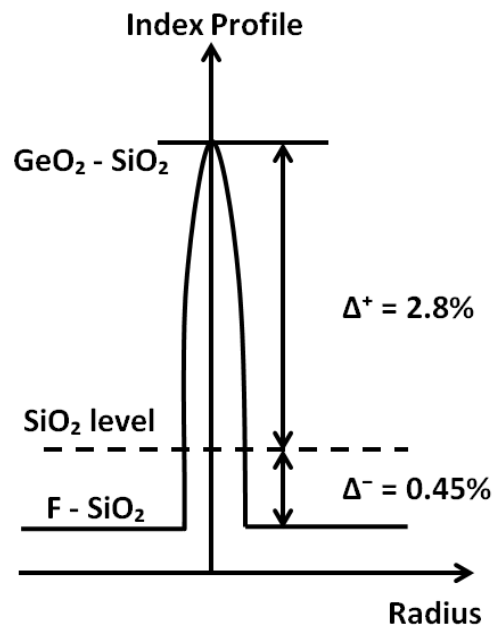


Figure 2.3 HNLF design. The materials and the concentration of the dopants used for the core and cladding are shown in the figure.

Some of the design choices made to enhance the fibre nonlinearity result in an increase in fibre loss [3]. This loss can be acquired by utilizing a deeply depressed ring and a very high core index. By carefully tuning the widths of the core and depressed ring, the dispersion slope can be controlled. The standard HNLF has a core with a high and almost flat refractive index. This fibre allows close control of the fibre dispersion as well as the fibre effective area, which is the main contributor to the fibre non-linearity. The vapour axial deposition (VAD) process also supports HNLF [4] by stretching and overloading the fibre preforms several times before drawing the fibre perform into fibre. The core index profiles usually obtained with the VAD process is graded. The smaller the core, the more time this stretching and overloading operation has to be repeated and therefore the larger the variation in the core size, which then increases the longitudinal ZDW. This problem, however, can be solved by controlling the fabrication process more carefully.

The relationship between effective area and MFD has been evaluated using a far field scanner, and is given by

$$A_{eff} = 0.957 * \frac{\pi}{4} MFD^2. \quad 2.1$$

This gives a HNLF effective area median value of $12.0 \mu\text{m}^2$, whereas for the median value of the Kerr coefficient (n_2) of a standard HNLF is approximately $3.1 \times 10^{-20} \text{ m}^2/\text{W}$ giving a median value for the nonlinear coefficient of approximately $10.8 \text{ W}^{-1} \text{ km}^{-1}$ at 1550 nm.

2.2.2 Origin of Nonlinear effects

When light propagates in a medium, it induced a polarization, P . This polarization is induced by the anharmonic motion of the bound charges in the medium to the applied electric field, E described as

$$P = \epsilon_0 \chi E, \quad 2.2$$

where ϵ_0 is the vacuum permittivity and χ is the electric susceptibility of the medium. An intense light beam propagating through an optical fibre will further induce nonlinear polarization in the fibre giving rise which gives rise to nonlinear effect. The relationship between the P and the applied field is given by [5]

$$P = \epsilon_0 (\chi^1 \cdot E + \chi^2 : EE + \chi^3 : EEE + \dots), \quad 2.3$$

where ϵ_0 is the vacuum permittivity and $\chi^{(j)}$ ($j=1, 2, 3, \dots$) is j^{th} order susceptibility. The linear susceptibility, χ^1 is the dominant contribution to P and its effects are included through the refractive index, n , and the absorption coefficient, α . The second order susceptibility, χ^2 is responsible for nonlinear process such as second harmonic generation (SHG) and sum frequency generation (SFG). However, it is nonzero only for media that lack inversion symmetry at the molecular level [6]. As silica glass is an amorphous with a macroscopic inversion symmetry that forbids second order nonlinear processes. Therefore, the third order susceptibility, χ^3 is responsible for lowest order nonlinear effects in fibres [6].

P and E in 2.3 can be expanded in a Taylor series and evaluated at $E = 0$ yielding [5]

$$P = a_1 E + \frac{1}{2} a_2 E^2 + \frac{1}{6} a_3 E^3 + \dots, \quad 2.4$$

where a_1 , a_2 and a_3 are the first, second and third derivatives of P with respect to E . These coefficients are the characteristic constants of the medium. Clearly, $a_1 = \varepsilon_0 \chi^1$, $a_2 = \varepsilon_0 \chi^2$ and $a_3 = 24 \chi^3$, where χ is the linear susceptibility, related to the dielectric constant and the refractive index of the material by $n^2 = \varepsilon/\varepsilon_0 = 1 + \chi$. The first term denotes the linear response of the fibre polarization to an electric field, whereas the second and third order nonlinear polarization behaviour, respectively. It is customary to write 2.3 in the form

$$P = \varepsilon_0 \chi^1 E + \frac{1}{2} \varepsilon_0 \chi^2 E^2 + 4 \chi^3 E^3 + \dots. \quad 2.5$$

It is convenient to write the polarization density in 2.5 as a sum of linear ($\varepsilon_0 \chi^1 E$) and nonlinear (P_{NL}) parts [6]

$$P = \varepsilon_0 \chi^1 E + P_{NL}, \quad 2.6a$$

$$P_{NL} = \frac{1}{2} \varepsilon_0 \chi^2 E^2 + 4 \chi^3 E^3. \quad 2.6b$$

In the nonlinear (P_{NL}) parts, the first term is vanished for optical fibre, therefore 2.6b become

$$P_{NL} = 4\chi^3 E^3. \quad 2.7$$

Therefore, the lowest order term nonlinear effects in optical fibres originated from the third order susceptibility, χ^3 , which is responsible for phenomena such as the Kerr effects and FWM. The Kerr effect is also referred to nonlinear refraction which is defined as the dependence of the refractive index of the fibre core on the intensity of a propagating electric field. For an electric field,

$$E = E_0 \cos(\omega t - kz). \quad 2.8$$

And by employing trigonometric relations, the polarization P_{NL} in 2.7 can be expressed as follows

$$P_{NL}(\omega) = \frac{3}{4}(4)\chi^3 E_0^2 E_0 \cos(\omega t - kz),$$

$$P_{NL}(\omega) = 3\chi^3 E_0^2 E_0 \cos(\omega t - kz). \quad 2.9$$

The polarization component at a frequency ω in 2.9 corresponds to an incremental change of the susceptibility, χ_{eff} at that particular frequency and is

$$\varepsilon_0 \Delta\chi = \frac{P_{NL}(\omega)}{E} = 3\chi^3 E_0^2 = 6\chi^3 \eta I, \quad 2.10$$

where $I = E_0^2/2\eta$ is the optical intensity of the initial wave. Since $n_l^2 = 1 + \chi$, it have $2n_l \Delta n = \Delta\chi$, so this is equivalent to an incremental refractive index $\Delta n = \Delta\chi/2n_l$

$$\Delta n = \frac{3\eta}{\varepsilon_0 n_l} \chi^3 I \equiv n_{nl} I, \quad 2.11$$

where the nonlinear refractive index (optical Kerr coefficient), n_{nl}

$$n_{nl} = \frac{3\eta_0}{n_l^2 \varepsilon_0} \chi^3. \quad 2.12$$

Thus, the change in the refractive index is proportional to the optical intensity. The effective refractive index is therefore a linear function of the optical intensity, I ,

$$n_{eff} = n_l + n_{nl} I. \quad 2.13$$

In 2.13, the first term is the linear refractive index while the second term represents the nonlinear refractive index. Higher order terms are negligible and hence neglected.

For fused silica fibres, $n_l \approx 1.46$ and $n_{nl} \approx 3.2 \times 10^{-20} \text{ m}^2/\text{W}$ [7]. For the propagation of a mode carrying 100 mW of power in a single mode fibre with an effective mode area $\approx 50 \text{ } \mu\text{m}^2$, the resultant intensity is $2 \times 10^9 \text{ W/m}^2$ and the change in refractive index due to nonlinear effect is,

$$\Delta n = n_{nl}I \approx 6.4 \times 10^{-11}. \quad 2.14$$

2.2.3 Different types of nonlinear effects

Nonlinear effects are divided into two classes or categories, namely, elastic and inelastic nonlinear effect. For the inelastic case, energy is exchanged between the electromagnetic field passing through the fibre and the fibre itself. Behaviours which fall under this category include stimulated Raman scattering (SRS) and stimulated Brillouin scattering (SBS), both of which relate to the vibrational excitation modes of the glass material used for the fabrication of the fibre. The fundamental difference between SBS and SRS results from the participation of optical phonons in the case of SRS and acoustic phonons in SBS. In particular, acoustic phonons correspond to sound waves propagating within the medium and, due to their acoustic nature; they have much lower energies than optical phonons.

For the second category, the elastic case, there is no energy exchange between the propagating electric field and the dielectric medium due to change in the refractive index of the medium with optical intensity. The power dependence of the refractive index is responsible for the Kerr effect. Depending upon the type of input signal, this Kerr nonlinearity manifests itself in three different effects such as self phase modulation (SPM), cross phase modulation (XPM) and FWM. In this

class, the third-order polarization played the main role in the nonlinear behavior where P_{NL} can be expressed as [7]

$$P_{NL} = \varepsilon_0 \chi^3 : EEE,$$

$$P_{NL} = \hat{x} \frac{1}{2} \sum_{j=1}^4 P_j \exp[i(k_j z - \omega_j t)] + c.c.. \quad 2.15$$

For each P_j , $j=1-4$, there are many terms of products of the three electric fields. If take P_4 as an example, it can be expressed as

$$P_4 = \frac{3\varepsilon_0}{4} \chi_{xxxx}^3 \{ [|E_4|^2 + 2(|E_1|^2 + |E_2|^2 + |E_3|^2)] E_4 + 2E_1 E_2 E_3 \exp(i\theta_+) + 2E_1 E_2 E_3^* \exp(i\theta) + \dots \},$$

Where

$$\theta_+ = (\beta_1 + \beta_2 + \beta_3 - \beta_4)z - (\omega_1 + \omega_2 + \omega_3 - \omega_4)t,$$

$$\theta_- = (\beta_1 + \beta_2 - \beta_3 - \beta_4)z - (\omega_1 + \omega_2 - \omega_3 - \omega_4)t. \quad 2.16$$

The term in 2.16 that is proportional to $|E_4|^2 E_4$ is responsible for SPM, which is the influence of a field (E_4 in this case) on its own phase because the only term involved is the field itself. The terms proportional to $|E_j|^2 E_4$, $j=1, 2, 3$ are responsible for XPM. XPM is the phase change due

to the fields other than the target field. The remaining terms in 2.16 are responsible for FWM. The efficiency of FWM is high when the relative phase (θ_+ and θ_- in this example) of P_4 and the mixing term nearly vanishes. This requires matching of the frequencies as well as of the propagation constants. The term associated with θ_+ in 2.16 is responsible for the frequency conversion $\omega_4 = \omega_1 + \omega_2 + \omega_3$. The phase matching of this process also requires

$$\beta_1 + \beta_2 + \beta_3 - \beta_4 = 0. \quad 2.17$$

The term associated with θ_- is responsible for the frequency conversion is $\omega_4 + \omega_3 = \omega_1 + \omega_2$. The phase matching condition of this process requires

$$\beta_1 + \beta_2 - \beta_3 - \beta_4 = 0. \quad 2.18$$

The frequency conversion process $\omega_4 = \omega_1 + \omega_2 + \omega_3$ is not of high interest in optical fibres because the phase-matching condition is difficult to satisfy.

2.2.4 FWM effect

Parametric processes are light processes that arise from light induced modulation on various media parameters such as the refractive index. Parametric processes include the FWM effect, harmonic generation and FWM parametric amplification [6]. In FWM, there are two methods to generate new frequency components; by using two strong pumps ($\omega_1 \neq \omega_2$) or one strong pump ($\omega_1 = \omega_2$). The one pump case is also termed the degenerate case, whereas the two pump case is called the non-degenerate case. Following convention, the pumps are labelled as 1 and 2, the

signal is 3 and the idler is 4. For example, ω_1 and ω_2 are the pump frequencies, ω_3 is the signal frequency and ω_4 is the idler frequency.

In the non-degenerate case, three wave of frequencies ω_1 , ω_2 and ω_3 generate the frequency $\omega_4 = \omega_1 + \omega_2 - \omega_3$ through the FWM process. For a three wavelength system, nine FWM terms exist as illustrated in Figure 2.4. In general, in N-wavelength system, the number of FWM terms is [6]

$$N_{FWM} = \frac{1}{2}(N^3 - N^2). \quad 2.19$$

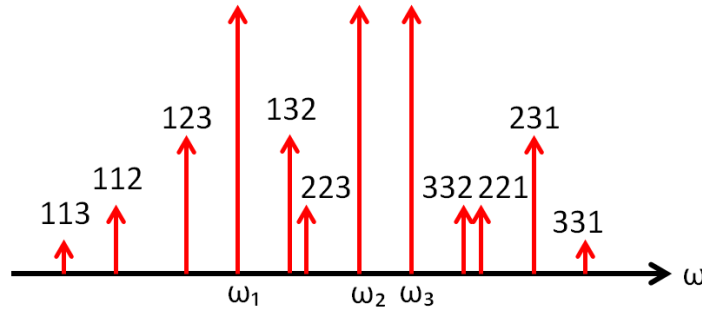


Figure 2.4 Spectrum of FWM terms generated in a three wavelength system with input fields at ω_1 , ω_2 and ω_3 . The number “ ijk ” means the frequency of that term is at

$$\omega_4 = \omega_1 + \omega_2 - \omega_3.$$

The time-averaged optical power $P_4(L, \Delta\beta)$ generated through the FWM process for the frequency component ω_4 is written as [8]

$$P_4(L) = \frac{\eta}{9} D^2 \gamma^2 P_1 P_2 P_3 e^{-\alpha L} L_{eff}^2, \quad 2.20$$

where P_i , $i = 1, 2, 3$ are the input power ($L = 0$) at the respective frequencies ω_i . The parameter D is the degeneracy factor, and $D = 6$ for three tone products ($f_1 \neq f_2 \neq f_3 \neq f_4$).

The effective fibre length, L_{eff} is defined as

$$L_{eff} \equiv \int_0^L \exp(-\alpha z) dz = \frac{1 - \exp(-\alpha L)}{\alpha}, \quad 2.21$$

where α is the absorption coefficient and the nonlinear coefficient, γ is given by [6]

$$\gamma = \frac{n_2 \omega}{c A_{eff}}, \quad 2.22$$

where A_{eff} is the effective fibre core area, n_2 is defined in 2.14 and is related to the third order susceptibility χ^3 [5] by

$$n_2 = \frac{3}{4\epsilon_0 c n_0^2} \text{Re}(\chi^3), \quad 2.23$$

where ω is the angular frequency, c is the speed of light, and A_{eff} again is the effective core area. Clearly the coefficient γ is frequency dependent because of the ω factor. However, if the frequency spread between ω_1 to ω_4 is small, γ can be assumed to be approximately constant for simplicity.

Finally, η in 2.20 represents the dependence of FWM efficiency on the phase mismatching $\Delta\beta$. it can be written as [9]

$$\eta = \frac{\alpha^2}{\alpha^2 + \Delta\beta^2} \left[1 + \frac{4e^{-\alpha L} \sin^2\left(\frac{\Delta\beta L}{2}\right)}{(1 - e^{-\alpha L})^2} \right], \quad 2.24$$

with a propagation constant of

$$\Delta\beta \equiv \beta_1 + \beta_2 - \beta_3 - \beta_4.$$

The maximum value of η is 1, which occurs when the phase matching condition is satisfied, i.e., $\Delta\beta = 0$. Expanding the propagation constant in a Taylor series about $\omega_0 = 2\pi c/\lambda_0$ and retaining terms up to third order in $\omega - \omega_0$, we obtain [10],

$$\beta(\omega) = \beta(\omega_0) + (\omega - \omega_0) \frac{d\beta}{d\omega}(\omega_0) + \frac{1}{2}(\omega - \omega_0)^2 \frac{d^2\beta}{d\omega^2}(\omega_0) + \frac{1}{6}(\omega - \omega_0)^3 \frac{d^3\beta}{d\omega^3}(\omega_0)$$

$$\begin{aligned} \beta(\omega) = & \beta(\omega_0) + (\omega - \omega_0) \frac{d\beta}{d\omega}(\omega_0) - (\omega - \omega_0)^2 \frac{\pi\lambda^2}{c} D_c(\omega_0) \\ & + (\omega - \omega_0)^3 \frac{\pi\lambda^4}{3c^2} \left\{ \frac{2}{\lambda} D_c(\omega_0) + \frac{dD_c}{d\lambda} \right\} \end{aligned}$$

$$\beta(\omega) = \beta(\omega_0) + (\omega - \omega_0) \frac{d\beta}{d\omega}(\omega_0) + (\omega - \omega_0)^3 \frac{\pi\lambda^4}{3c^2} \frac{dD_c}{d\lambda}, \quad 2.25$$

where λ is wavelength, c is light velocity, D_c is the fibre chromatic dispersion (CD) and ω_0 is the zero-dispersion frequency. Generally, D_c dominates, and the contribution of $dD_c/d\lambda$ can be neglected at the wavelength far from ZDWs around 1300 nm and 1550 nm. At the zero CD wavelength, $D_c = 0$ and the dispersion slope $dD_c/d\lambda$ must be included. Using 2.25, 2.24 is rewritten as [10]

$$\Delta\beta = -\frac{\lambda^4\pi}{c^2} \frac{dD_c}{d\lambda} \{(\omega_4 - \omega_0)^3 + (\omega_3 - \omega_0)^3 - (\omega_1 - \omega_0)^3 - (\omega_2 - \omega_0)^3\}$$

$$\begin{aligned} \Delta\beta = & -\frac{\lambda^4\pi}{c^2} \frac{dD_c}{d\lambda} \{(\omega_1 - \omega_0) + (\omega_2 - \omega_0)\} \cdot \{(\omega_1 - \omega_0) - (\omega_3 - \omega_0)\} \\ & \cdot \{(\omega_2 - \omega_0) - (\omega_3 - \omega_0)\} \end{aligned}$$

$$\Delta\beta = -\frac{\lambda^4\pi}{c^2} \frac{dD_c}{d\lambda} \{(\omega_1 - \omega_0) + (\omega_2 - \omega_0)\} \cdot (\omega_1 - \omega_3)(\omega_2 - \omega_3) \quad 2.26$$

where the relation of $\omega_4 = \omega_1 + \omega_2 - \omega_3$ is used. 2.26 describe the phase mismatching in the ZDW region. It is noted that the phase-matching condition is always satisfied when the ZDW is positioned at the middle between two light of ω_1 and ω_2 frequencies, i.e., $\omega_1 - \omega_0 = -(\omega_2 - \omega_0)$. In this condition, since $\omega_4 = \omega_1 + \omega_2 - \omega_3 = 2\omega_0 - \omega_3$, then, $\omega_3 - \omega_0 = -(\omega_3 - \omega_0)$. Thus, FWM light is generated at the side opposite the ω_3 frequency light wavelength with the zero-dispersion wavelength as the centre point. The wavelength arrangement for this phase-matched condition is illustrated in Figure 2.5 (a).

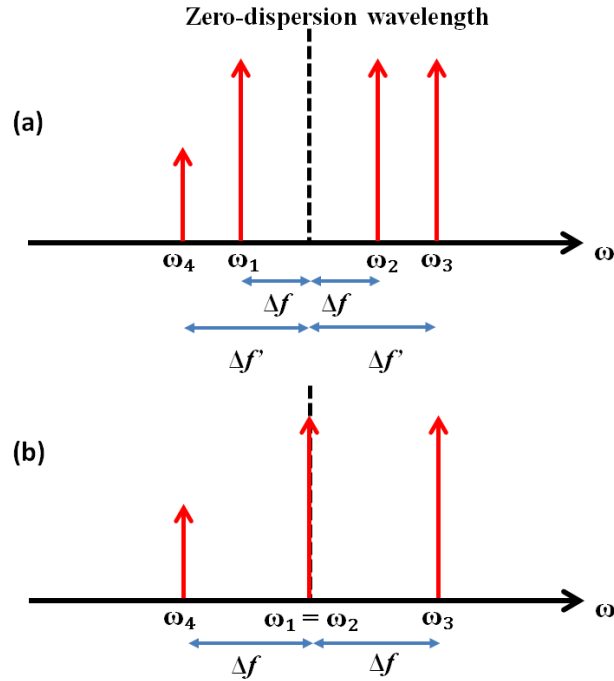


Figure 2.5 Wavelength arrangements satisfying the phase matching condition in the ZDW region (a) completely nondegenerate case (b) partially degenerate case.

In the degenerate case in which only one pump exist, i.e., $\omega_1 = \omega_2$, where it consider only three term in 2.27, and the frequency relationship between ω_1 , ω_3 and ω_4 becomes

$$\omega_4 = 2\omega_1 - \omega_3. \quad 2.27$$

In this case ($\omega_1 = \omega_2$), the phase mismatching from 2.26 is rewritten as

$$\Delta\beta = -\frac{\lambda^4\pi}{c^2} \frac{dD_c}{d\lambda} 2(\omega_1 - \omega_3)^2(\omega_1 - \omega_0). \quad 2.28$$

It is noted in 2.28 that the phase matching condition is always satisfied when ω_1 coincides with the ZDW, i.e., $\omega_1 = \omega_0$. The wavelength arrangement for this phase matched condition is illustrated in Figure 2.2 (b). The generated wave efficiency, η with respect to phase mismatch $\Delta\beta L$ can be expressed as

$$\eta = \frac{P_4(L, \Delta\beta)}{P_4(L, \Delta\beta = 0)} = \frac{\alpha^2}{\alpha^2 + \Delta\beta^2} \left[1 + \frac{4e^{-\alpha L} \sin^2\left(\frac{\Delta\beta L}{2}\right)}{(1 - e^{-\alpha L})^2} \right], \quad 2.29$$

where the total incident power in this case is $P_0 = P_1$ which can be expressed as

$$P_4(L) = \frac{\eta}{9} D^2 \gamma^2 P_1^2 P_3 e^{-\alpha L} L_{eff}^2. \quad 2.30$$

where the parameter D is 3 for two-tone products ($f_1 = f_2 \neq f_3$).

2.3 Semiconductor Optical Amplifier (SOA)

The semiconductor material systems for laser fabrication are generally of two main types, the GaAs/GaAlAs system and InP/InGaAsP system. GaAs/GaAlAs devices typically have lasing wavelengths in the range between 700 nm and 900 nm while InP/InGaAsP devices generally lase at longer wavelengths within the 1100 nm to 1600 nm range. The longer wavelength lasers are important for long-haul optical communication because at these wavelengths silica fibres have extremely low attenuation (as low as 0.2 dB/km at 1550 nm).

Laser operation of a semiconductor p-n junction device was first demonstrated by four independent research groups within six weeks of one another in 1962 [11] – [14]. Initially, due to the severe heating problems caused by the high lasing threshold current, lasing action could only be generated continuously at low temperatures or in pulse form at room temperature, and device lifetimes were also short. Since then, semiconductor lasers have developed at a remarkable pace [15] – [18]. Fabrication technology and device design have progressed to the point where highly reliable lasers with extrapolated room temperature lifetimes of a century are routinely produced.

Because of their low cost, reliability, low power consumption and capability for high-speed modulation, semiconductor lasers are technologically attractive sources of coherent optical radiation for a variety of applications. Most notably, semiconductor lasers are playing an integral part in the ever-expanding lightwave communications industry. One of the most important characteristics for semiconductor lasers used in lightwave communication systems is the direct modulation bandwidth; ultrafast intraband dynamics and inter quantum well carrier transport.

When the cleaved facets of a semiconductor laser are anti-reflection coated, the device is referred to as a semiconductor optical amplifier (SOA). Two types of SOA's can be distinguished, Fabry-

Perot amplifier and travelling wave amplifier. The former is essentially a laser biased above transparency but below lasing threshold. The result is an amplifier having a series of narrow bandpasses with resonant-enhanced gain as the envelope. With the latter, on the other hand, great care is exerted to make the reflectivity of both facets as low as possible, typically as low as 10^{-4} to 10^{-5} . The device will amplify the incident signal in a single pass through the active region, thus with little cavity-resonance effects in the gain spectrum.

Research on SOA's dates back to the 1960's, soon after the invention of semiconductor lasers [19], [20]. However, it was only during the 1980's that they were developed for practical applications, largely motivated by potential applications in lightwave communication systems [21] – [25]. Early studies were conducted on Fabry-Perot amplifiers [19] – [21], but more recent research has concentrated on travelling-wave amplifiers [26] – [28]. Several ways of suppressing the end reflectivity have been demonstrated to obtain traveling-wave operation. These include multi-layer anti-reflection coating [26], angled facet [27] and window facet structures [28].

SOA's have been used as pre-amplifiers [29] and in-line amplifiers [30] in a number of lightwave transmission system experiments. They have also been employed to overcome distribution losses in local area networks [31]. However, SOA's initially developed for optical amplification; have in recent years largely given up the role in the 1500 nm communication window to Erbium-doped fibre amplifiers which are far superior as optical amplifiers [32]. SOA's have nevertheless found other “unconventional” applications to which a large body of research has been devoted in recent years [33] – [36]. These efforts include using SOA nonlinearities to achieve important functionalities for lightwave communication systems such as broadband wavelength conversion [33], [34] all optical clock recovery [35] and ultrafast optical

signal processing [36]. In addition, SOA's are important components in photonic integrated circuits [37].

In this section, optical gain in semiconductors is discussed theoretically. Gain nonlinearities, which are responsible for nonlinear applications of SOA's, and the physical processes associated with these nonlinearities, i.e., dynamic carrier heating and spectral hole burning are also investigated.

2.3.1 Optical gain in semiconductors.

The wave function of an electron in a given band (conduction or valence) in semiconductor can be written as

$$\psi_{c,v}(r) = u_{c,vk}(r)e^{ik \cdot r}, \quad 2.31$$

where the subscripts c and v denote for conduction and valence bands, respectively, and $u_{cvk}(r)$ is the periodicity of the crystalline lattice. The “propagation” constant k is quantized and its components are given by

$$k_j = \frac{2\pi m}{L_j}, \quad 2.32$$

where $j = x, y, z$, m is an integer and L_j is the length of the crystal in the j direction. The k space volume for each electronic state is thus $8\pi^3/V$ where V is the crystal's physical volume. The number of electronic states per band for a value of k between k and $k + dk$ is given by

$$\rho(k)dk = \frac{k^2 V}{n^2} dk, \quad 2.33$$

where a factor of two has been added to account for the two spin states of electrons for each k eigenvalue.

Using the parabolic band approximation

$$E(k) = \frac{\hbar^2 k^2}{2m_{c,v}^*}, \quad 2.34$$

where $m_{c,v}^*$ is the effective mass of the carrier in the respective band and the energy E is measured from the band edge extremum, the density of states per unit energy interval can be readily expressed as

$$\rho_{c,v}(E) = \sum_{n=1}^{\infty} \frac{m_{c,v}^*}{\pi \hbar^2} H(E - E_{nc,v}), \quad 2.35$$

where $H(x)$ is the Heaviside function is equal to unity when $x > 0$ and is zero when $x < 0$, \hbar is Planck's constant and $E_{nc,v}$ is the n^{th} discrete allowable energy level resulting from carrier

confinement in the quantum well. The above expression gives the density in a quantum well SOA where the electron and holes are confined to planes of motion.

These available states are partially filled by carriers. Under electrical pumping, the probability function describing the filling of the states reaches a quasi-equilibrium described by the Fermi-Dirac law

$$f_{c,v}(E_{c,v}) = \frac{1}{1 + e^{(E_{c,v} - E_{fc,v})/k_B T}}, \quad 2.36$$

where $E_{c,v}$ and $E_{fc,v}$ are the carrier energy and the quasi-fermi level of the conduction and valence band, k_B is Boltzman's constant and T is the lattice temperature of the SOA. In thermal equilibrium, a single Fermi energy applies to both conduction and valence bands, respectively. Under the conditions in which the thermal equilibrium is disturbed, such as via electrical pumping, two separate Fermi level E_{fc} and E_{fv} , called quasi Fermi levels, are used for each of the bands. In this case the electron density N and hole density P can be written as

$$N = \int_0^\infty f_c(E) \rho_c(E) dE,$$

$$P = \int_0^\infty f_v(E) \rho_v(E) dE. \quad 2.37$$

To calculate the optical gain for a semiconductor system, we begin from a two level discrete atomic or electronic medium. We assume that the population densities of lower and upper levels N_1 and N_2 , respectively and the energy difference between the two levels is $\hbar\omega_0$. The complex susceptibility, χ , of such a system can be found using the density matrix formalism and it is given by [28]

$$\chi(\omega) = -\frac{\mu^2 T_2 (N_2 - N_1) [(\omega_0 - \omega) T_2 - i]}{\epsilon_0 [1 + (\omega - \omega_0)^2 T_2^2]}, \quad 2.38$$

where μ is the momentum matrix element and T_2 is a dephasing time introduced phenomenologically.

In a direct gap semiconductor, the minimum in the conduction band and the maximum in the valence band occur at the same value of the wave vector k . Since the momentum of the photon carriers is negligible compared to the carrier momentum $\hbar k$, radiative transitions occur between electrons and holes of essentially same wave vectors. In the case of such a semiconductor system, modification to the density inversion $N_2 - N_1$ can be achieved by first considering the contribution from electrons with a value of the wave vector between k and $k + dK$. Their contribution to the density inversion is found to be

$$d(N_2 - N_1) = \frac{1}{V} \rho(k) dk \{f_c(E_a)[1 - f_v(E_b)] - f_v(E_b)[1 - f_c(E_a)]\},$$

$$d(N_2 - N_1) = \frac{1}{V} \rho(k) dk [f_c(E_a) - f_v(E_b)], \quad 2.39$$

where $E_a = \hbar^2 k^2 / 2m_c^*$ and $E_b = \hbar^2 k^2 / 2m_v^*$ are the energy levels corresponding to the wave vector value k in the conduction and valence bands, respectively. Substituting 2.39 for $(N_2 - N_1)$ in 2.38 gives the total complex susceptibility in a semiconductor

$$\chi(\omega) = -\frac{\mu^2 T_2 (N_2 - N_1) [(\omega_0 - \omega) T_2 - i]}{\epsilon_0 [1 + (\omega - \omega_0)^2 T_2^2]} [f_c(E_a) - f_v(E_b)] \rho(k) dk. \quad 2.40$$

Note that there exists the following relation;

$$\hbar\omega_0 = (E_c - E_a) - (E_v - E_b) = E_g + \hbar^2 k^2 / 2m_r^*, \quad 2.41$$

where E_c, E_v are energy levels of the conduction band minimum and the valence band maximum, respectively; $E_g = E_c - E_v$ is the band gap, and m_r^* is the reduced mass given by the relation $m_r^{*-1} = m_c^{*-1} + m_v^{*-1}$. Employing equation 2.33 and 2.41, we can redefine the independent variable in 2.40 into ω_0 and obtain the following expression for the complex susceptibility

$$\chi(\omega) = -\frac{1}{\epsilon_0 \hbar} \int_{E_g/\hbar}^{\infty} \mu^2(\omega_0) T_2 \rho_j(\omega_0) \frac{(\omega_0 - \omega) T_2 - i}{1 + (\omega_0 - \omega)^2 T_2^2} [f_c(\omega_0) - f_v(\omega_0)] d\omega_0, \quad 2.42$$

where $\rho_j(\omega_0)$ is the joint density of states, given by

$$\rho_j(\omega_0) = \frac{1}{2\pi^2} \left(\frac{2m_r^*}{\hbar} \right)^{3/2} (\omega_0 - E_g/\hbar)^{1/2} \quad 2.43$$

In addition, as the explicit expressions for the Fermi functions appearing in 2.42 are given by

$$f_c(\omega_0) = \frac{1}{1 + \exp \left[\frac{m_r^*}{m_c^*} (\hbar\omega_0 - E_g) + E_c - E_{fc} \right] / k_B T}$$

$$f_v(\omega_0) = \frac{1}{1 + \exp \left[-\frac{m_r^*}{m_c^*} (\hbar\omega_0 - E_g) + E_v - E_{fc} \right] / k_B T} \quad 2.44$$

It follows that the gain constant can then be expressed as

$$G(\omega) = \frac{k}{n^2} \text{Im}[\chi(\omega)]$$

$$G(\omega) = \frac{k}{n^2 \epsilon_0 \hbar} \int_{E_g/\hbar}^{\infty} \mu^2(\omega_0) \rho_j(\omega_0) [f_c(\omega_0) - f_v(\omega_0)] \frac{T_2 d\omega_0}{1 + (\omega - \omega_0)^2 T_2^2} \quad 2.45$$

where n is refractive index of the semiconductor material and $k = \omega n/c$ is the wave number of the incident optical field at an optical frequency of $\omega/2\pi$. Since ω and E_g/\hbar are in the order of

10^{15} s^{-1} and T_2^{-1} is typically in the order of 10^{13} s^{-1} , $\frac{T_2}{1+(\omega-\omega_0)^2 T_2^2}$ can be approximated as $\pi\delta(\omega - \omega_0)$ when the integral in 2.45 is evaluated. This leads to

$$G(\omega) = \frac{\mu^2}{\lambda\epsilon_0 n\hbar} \left(\frac{2m_r^*}{\hbar}\right)^{3/2} (\omega - E_g/\hbar)^{1/2} [f_c(\omega) - f_v(\omega)]. \quad 2.46$$

The gain profile also depends sensitively on the carrier temperature, which affects the Fermi distribution functions, as expressed in 2.45. In the next part, saturation of semiconductor optical gain due to carrier temperature increase will be discussed.

2.3.2 Gain saturation and nonlinearities.

Gain saturation, an important property of semiconductor lasers and amplifiers, can be understood by an analysis of the rate equation. The carrier density, N at an injected current, I in the presence of the optical power, P can be obtained by solving the rate equation

$$\frac{dN}{dt} = \frac{1}{qV} - \frac{N}{\tau_s} - \frac{G(N)}{A\hbar\omega} P + D\nabla^2 N, \quad 2.47$$

where q is the electron charge, V is the active layer volume, τ_s is the spontaneous carrier lifetime, $G(N)$ is the gain constant per unit length as given by 2.46, A is the cross section area of the optical guided mode and D is the carrier diffusion coefficient. This rate equation can be derived from the density matrix formalism combined with the rate equation approximation and can also be understood intuitively from the viewpoint of carrier number bookkeeping.

In the case of semiconductor optical amplifiers, the carrier density N is also a function of longitudinal location z . The solution of the above equation is complicated because of the presence of the diffusion term. The main effect of the carrier diffusion is to wash out the carrier gradient in the longitudinal direction. To a good degree of approximation, this term can be ignored in the case of travelling wave amplifiers. The carrier density N thus satisfied the simpler rate equation

$$\frac{dN}{dt} = \frac{1}{qV} - \frac{N}{\tau_s} - \frac{G(N)}{A\hbar\omega}P. \quad 2.48$$

To simplify 2.48, the optical gain is assumed to vary linearly with the carrier density N , i. e.,

$$G(N) = a(N - N_0), \quad 2.49$$

where a is the differential gain and N_0 is the carrier density at which the active region become transparent. Under a condition of steady operation, i.e., injection current I and optical power P are constant, the carrier density is found to be

$$N = \frac{I\tau_s/qV + N_0P/P_s}{1 + P/P_s}, \quad 2.50$$

where P_s is the saturation power given by

$$P_s = \frac{A\hbar\omega}{a\tau_s}. \quad 2.51$$

A gain saturation behaviour can thus be expressed as

$$G(N) = a(N - N_0) = \frac{a(I\tau_s/qV - N_0)}{1 + P/P_s} = G_0 S, \quad 2.52$$

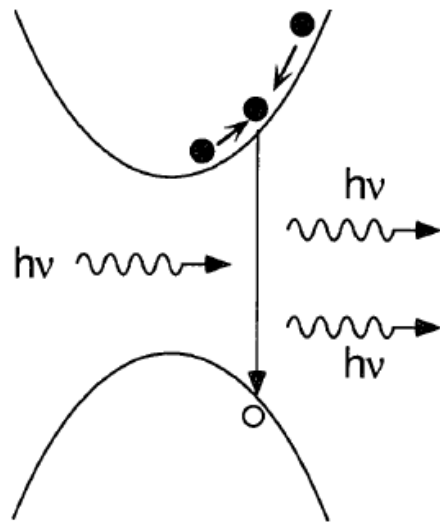
where $G_0 = a(I\tau_s/qV - N_0)$ is the unsaturated optical gain in absence of input optical field, and where we introduced a saturation factor S , which is a function of z and is given by

$$S(z) = \frac{1}{1 + P(z)/P_s}. \quad 2.53$$

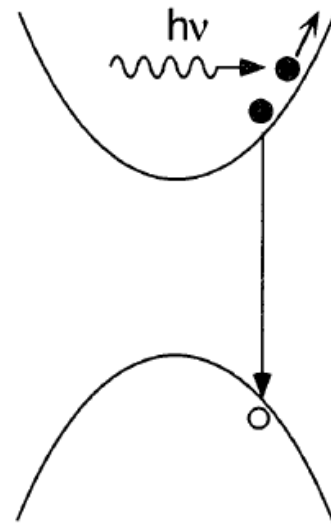
Physically, the gain saturation is caused by stimulated emission through which carrier density is reduced by the input optical field. This saturation phenomenon is usually referred to as the interband gain saturation. There exists yet another type of gain saturation, resulting from various intraband processes. In this case, the occupation probability of the carriers in each energy band, rather than the actual carrier population, is altered by the input optical field. This leads to intraband gain saturation, also known as the nonlinear gain effect which is often phenomenologically represented by a nonlinear gain coefficient, ϵP , as defined in the relation $G(N, P) = G(N, 0)/1 + \epsilon_P P$.

Intraband processes that cause gain nonlinearity typically include dynamic carrier heating and spectral hole burning. Carrier heating produces a similar distribution, either by stimulated emission removing carrier that are cooler than the intraband average or by free carrier absorption exciting carriers to a higher energy level. Carrier-phonon scattering, with a characteristic time constant of 500 – 1000 fs, allows carriers to relax to the lattice temperature. This results in a Fermi-Dirac distribution of the carriers that is at the temperature of the lattice, but that is characterized by a different quasi-Fermi, as shown in Figure 2.6.

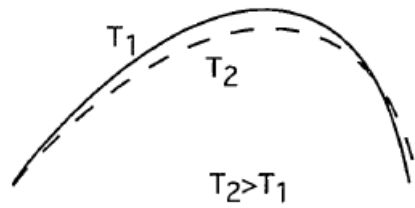
Spectral hole burning, on the other hand, refers to a spectrally local gain reduction due to the input optical field which is shown in Figure 2.6. Stimulated emission removes carriers at states in the band corresponding to the photon energy. It has burned a hole in the quasi-equilibrium carrier intraband distribution. Carrier-carrier scattering, with a characteristic time constant of 50 – 200 fs, will cause carriers to fill the hole and reach a thermal distribution.



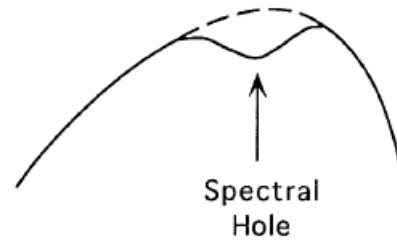
(a) Stimulated Emission



(b) Free Carrier Absorption



(c) Carrier Heating Effect



(d) Spectral Hole Burning

Figure 2.6 Illustration of physical processes involved in dynamic carrier heating and spectral hole burning.

2.3.3 FWM effect

Physical mechanisms responsible for FWM are interband gain saturation; arising from stimulated emission, and intraband gain nonlinearities; resulting from intraband dynamics. In the former, carrier density is modulated by the optical beating of pump and probe, while in the latter, the carrier density remains unchanged but intraband occupancy probability is modulated. Both mechanisms can create dynamic gain and index gratings along the amplifier length. The subsequent scattering of pump and probe fields from these gratings results in the generation of two new side bands. This is the basic process of FWM in SOA's.

The principle of FWM as shown in Figure 2.7 requires a strong pump and probe to be injected in the SOA with frequencies ω_p and ω_s respectively, with the condition that the channel spacing ($\Omega = \omega_p - \omega_s$) is of the same state of polarization. Through the mechanisms of carrier density modulation, carrier heating and spectral hole burning, dynamic gratings are formed in the SOA carrier density and distribution. The input waves then scatter off of the resulting dynamic gain and index gratings. The pump scattering also generates two waves, one at the probe frequency and one at $\omega_{cs} = 2\omega_p - \omega_s$. The probe scattering also generates two waves, one at the pump frequency and one at $\omega_{cs'} = 2\omega_s - \omega_p$. The most interesting of the scattered waves is the converted signal at ω_{cs} . As will be shown, it is more efficiently generated than the other converted wave and additionally it is proportional to the phase conjugate of the input signal.

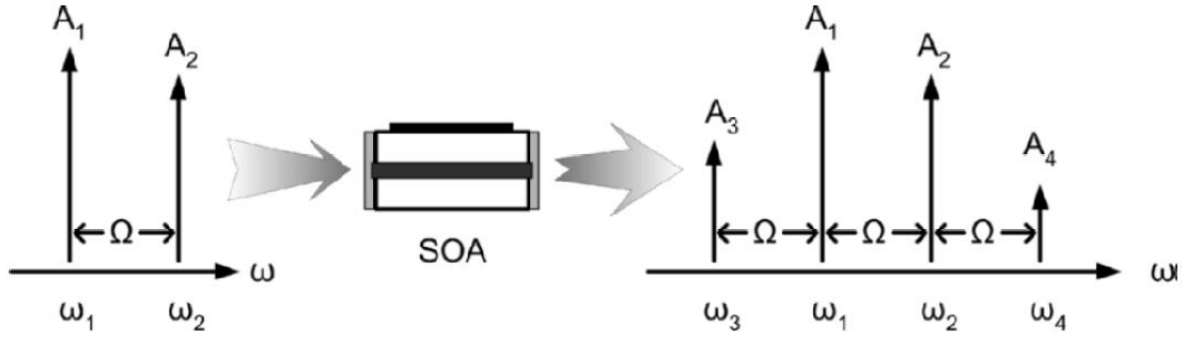


Figure 2.7 Schematic of a FWM processes in SOA. A_i , $i = 1, 2, 3, 4$ are the pump, signal, conjugate, cs and conjugate, cs', respectively.

FWM in a semiconductor medium generated by intraband occupancy modulation was first analyzed by Agrawal [38]. His theory, based on density-matrix equations, included contributions from interband carrier density modulation and spectral hole burning. Modelling the nonlinearities involved in FWM, it is possible to predict the converted signal generation efficiency.

Beginning with the wave equation for an electromagnetic field [38]

$$\nabla^2 E - \frac{n^2}{c^2} \frac{d^2 E}{dt^2} = \frac{1}{\epsilon_0 c^2} \frac{d^2 P}{dt^2}, \quad 2.54$$

and assuming $P = \epsilon_0 \chi(N)E$ for the electric polarization, 2.54 becomes

$$\nabla^2 E - \left[\frac{n^2}{c^2} + \frac{\chi(N)}{c^2} \right] \frac{d^2 E}{dt^2} = 0. \quad 2.55$$

Assuming a solution of the form $E(z, t) = E_0(z)e^{i(kz - \omega t)}$, with k_0 defined as the solution for k when $P = 0$, the solution then becomes

$$E(z, t) = E_0(z) \exp i \left(\left[k_0 + k_{nl} - i \frac{G}{2} \right] z - \omega t \right), \quad 2.56$$

with

$$k_{nl} = \frac{k_0}{2n^2} \text{Re}[\chi(N)].$$

Assuming all three waves in the SOA, the pump, the probe and the converted signal are polarized along the TE mode, the total electric field can be written as

$$E(z, t) = E_{\text{pump}} + E_{\text{probe}} + E_{\text{converted signal}},$$

$$E(z, t) = E_p(z)e^{i(k_p z - \omega_p t)} + E_s(z)e^{i(k_s z - (\omega_p - \Omega)t)} + E_{cs}(z)e^{i(k_{cs} z - (\omega_p - \Omega)t)}, \quad 2.57$$

where k_i and ω_i are the propagation constant and frequency of the i^{th} wave, respectively. The nonlinear contribution to the wavenumber is assumed to be

$$k_{nl} = \frac{1}{2} \left[\alpha a(N - N_0) - \epsilon_{ch} \beta \int_0^\infty dt' h_{ch}(t') |E(t - t')|^2 \right], \quad 2.58$$

where a is the gain factor, α is the linewidth enhancement factor, G_0 is the normalization gain, β is the linewidth enhancement factor temperature, $h_{ch}(t)$ is the response functions of the gain to a change in the carrier temperature, and ϵ_{ch} is the strength of the carrier process, respectively. Equation 2.58 can be written in the same form with $h_{ch}(t)$ and ϵ_{ch} being replaced by $h_{sh}(t)$, the response functions in the intraband population distribution, and ϵ_{sh} , the strength of the spectral hole burning nonlinear process, respectively. The contributions of carrier heating and spectral hole burning are introduced phenomenologically. The functional dependence follows that measured in [39]; with the spectral hole burning response function being linear with respect to carrier density below transparency and zero at transparency, and with the carrier heating response function non-zero at transparency. There is a small carrier density dependency to carrier heating, however this is neglected.

The carrier density in the SOA is determined by the equation

$$\frac{dN}{dt} = \frac{I}{qV} - \frac{N}{\tau_s} - g|E(z, t)|^2, \quad 2.59$$

where I is the injection current, q is the charge of an electron, V is the volume of the SOA's active region, and τ_s is the spontaneous lifetime. The carriers will respond to the beating of the pump and the probe, producing a modulation on N at the beat frequency. Assuming a form for N of

$$N = \bar{N} + \Delta N e^{-i\Omega t} + \Delta N^* e^{i\Omega t}, \quad 2.60$$

and using this and Equation 2.57 in equation 2.59, ignoring terms proportional to ϵ_{ch} and ϵ_{sh} , it is possible to solve for the time-independent terms. One result gives

$$a(\bar{N} - n_0) = \frac{\bar{g}}{1 + \frac{P_t(z)}{P_s}} = S(z)\bar{g}, \quad 2.61$$

where $\bar{g} = \frac{aI\tau_s}{qV} - an_0$ is the small signal gain $P_t(z) = |E_p(z)|^2 + |E_q(z)|^2 + |E_{cs}(z)|^2$ is the total power, $S(z) = \frac{1}{1 + \frac{P_t(z)}{P_s}}$ is a saturation parameter whose functional form is determined by the initial gain function assumed is the saturation power.

Using these results in the wave equation, under the slowly varying approximation, it is possible to derive approximate travelling wave equations. Under the assumption of $\Omega\tau_s \gg 1$, which is true for the region of detuning which we are interested in a wavelength converter, 2.57 can be simplified as [39]

$$\frac{dE_p}{dz} = \frac{1}{2}[-\gamma_{sc} + C_1S(z)]E_p$$

$$\frac{dE_s}{dz} = \frac{1}{2}[-\gamma_{sc} + C_1S(z) - F_1(\Omega)S(z)]E_s$$

$$\frac{dE_{cs}}{dz} = \frac{1}{2}[-\gamma_{sc} + C_1S(z) - F_1(\Omega)S(z)]E_{cs} - \frac{|E_p|^2 E_s^*}{P_s} [F_2(\Omega) + F_3(\Omega)S(z)] \quad 2.62$$

where

$$C_1 = (1 - i\alpha G)$$

$$F_1(\Omega) = i\Omega\tau_s C_1 \frac{|E_p|^2}{P_s}$$

$$F_2(\Omega) = \frac{G}{2} \frac{(1 - i\beta)\epsilon_{ch}P_s}{(1 - i\Omega\tau_1)(1 - i\Omega\tau_2)}$$

$$F_2(\Omega) = \frac{G}{2} \frac{(1 - i\alpha)}{\left(1 + \frac{P_t(z)}{P_s} + i\Omega\tau_s\right)} + \frac{G}{2} \frac{\epsilon_{sh}P_s}{(1 - i\Omega\tau_s)}$$

and where τ_1 and τ_2 are the time constants associated with carrier heating and spectral hole burning respectively, and γ_{sc} has been introduced phenomenologically to account for waveguide propagation losses. Equation 2.62 shows that the converted signal generated is proportional to the phase conjugate of the input signal, demonstrating the converter's potential as a phase conjugate and also revealing the fundamental modulation format insensitivity of a FWM converter. Additionally, it should be noted that a similar set of equations could be developed for the FWM converted signal at $\omega_{cs'}$. These equations reveal a reduced conversion efficiency since this converted signal generated is proportional to $|E_s|^2 E_p^*$.

It is possible to obtain a closed form solution from these travelling wave equations, without the simplification of assuming $\Omega\tau_s \gg 1$. Solving for the conversion efficiency,

$$\eta = \frac{|E_{cs}(z)|^2}{|E_s(0)|^2}$$

$$\eta = \left| \frac{A_{cd}e^{i\phi_{cd}}}{1 - i\Omega\tau_s} + \frac{A_{ch}e^{i\phi_{ch}}}{(1 - i\omega\tau_1)(1 - i\omega\tau_2)} + \frac{A_{sh}e^{i\phi_{sh}}}{1 - i\Omega\tau_2} \right|^2 \quad 2.63$$

where the magnitudes and phases of the contributing mechanism, A_i and ϕ_i for I carrier density modulation (cd), carrier heating (ch) and spectral hole burning (sh), are given by [38]

$$A_{cd}e^{i\phi_{cd}} = \left[\frac{P_t(z)}{P_t(0)} \right]^{\frac{1}{2}} \frac{|E_p(0)|^2 \ln \left[\frac{g_0}{g} \right]}{2P_t(0)} (1 - i\alpha)$$

$$A_{ch}e^{i\phi_{ch}} = \left[\frac{P_t(z)}{P_t(0)} \right]^{\frac{1}{2}} \frac{|E_p(0)|^2 \ln \left[\frac{g_0}{g} \right]}{2P_t(0)} \frac{G_0}{G} \left[1 + \frac{(g + 1) \ln \frac{g_0}{g}}{2(g - 1)} \right] (1 - i\beta)$$

$$A_{sh}e^{i\phi_{sh}} = \left[\frac{P_t(z)}{P_t(0)} \right]^{\frac{1}{2}} \frac{|E_p(0)|^2 \ln \left[\frac{g_0}{g} \right]}{2P_t(0)} \epsilon_{sh} P_s \quad 2.64$$

where g and g_0 are the facet-to-facet gain and small signal gain, respectively. From this, the functional dependence of the conversion efficiency on the detuning frequency is described. Each

of the three mechanisms has a contributing magnitude and phase, with the magnitude attenuated for increasing detuning by $\frac{1}{1-i\Omega\tau_i}$ as the nonlinearity becomes less able to respond to the higher frequencies. Carrier heating is attenuated by two time constant; τ_1 which corresponds to the carrier phonon scattering time governing the relaxation of hot carrier, and τ_2 which corresponds to the delay in the turning on of carrier heating.

Note: The equations written are taken from the references quoted earlier.

2.4 Summary

Based on the literature, nonlinear fibres can be divided into four categories, namely, narrow core fibres with silica cladding, microstructure fibres, non silica fibres such as chalcogenide, bismuth oxide and tellurite oxide and tapered fibres with air cladding. Silica glass (HNLF) is still a better choice for making nonlinear fibre because of its low loss in the transmission wavelength band compared to glass with higher nonlinearity. In the HNLF design which used the MCVD process; we require a deeply depressed ring and a very high core index for increasing the fibre loss. This is to control the fibre dispersion inside the fibre. In this fibre, the nonlinear effect can be divided into two classes which are inelastic (SRS and SBS) and elastic (SPM, XPM and FWM) effects. However, in this thesis, FWM is of interest as it is more suitable for application as a wavelength converter, FOPA and multiwavelength fibre laser. Most explanation is based on the non-degenerate and degenerate FWM case for HNLF and SOA. A semiconductor laser with a cleaved facet and with anti-reflection coating is called a SOA. They can be classified as either the Fabry-Perot or the travelling wave amplifier. SOA's can be used as an amplifier or as a nonlinear medium. In the latter case, gain nonlinearities, which are responsible for nonlinear applications

of SOA's, and the physical processes associated with these nonlinearities, i.e., dynamic carrier heating and spectral hole burning were discussed in detail in this chapter. This will be applied in explaining the experimental results which will be discussed in the next chapter.

Reference

- [1] E. M. Vogel, M. J. Weber and D. M. Krol, "Nonlinear optical phenomena in glass" Physics and Chemistry of Glasses, vol 32, pp. 231-254, 1991.
- [2] L. Kazovsky, S. Benedetto and A. Willner, "Optical fibre communication systems," Artech House, Boston, 1996.
- [3] M. J. Holmes, D. L. Williams and R. J. Manning, "Highly nonlinear optical fibre for all optical processing applications," IEEE Photon. Technol. Lett., vol 7, pp. 1045-1047, 1995.
- [4] J. Hiroishi, N. Kumano, K. Mukasa, R. Sugizaki, R. Miyabe, S. Matsushita, H. Tobioka, S. Namiki and T. Yagi, "Dispersion slope controlled HNL-DSF with high γ of $25 \text{ W}^{-1} \text{ km}^{-1}$ and band conversion experiment using this fibre," Proc ECOC 02, paper PD1.5, 2002.
- [5] Y.R. Shen, "Principles of Nonlinear Optics," Wiley, New York, 1984.
- [6] G. P. Agrawal, 3rd Edition of Nonlinear Fibre optics, Academic Press, San Diego, 2001.
- [7] S. P. Singh and N. Singh, "Nonlinear effects in optical fibres; origin, management and applications," Progress in Electromagnetic Research, PIER, 73, pp. 249-275, 2007.
- [8] K. O. Hill, D. C. Johnson, B. S. Kawasaki, and R. I. MacDonald, "CW three-wave mixing in single mode optical fibres," J. Appl. Phys., vol 49, pp. 5098-5106, 1978.

- [9] N. Shibata, R. P. Braun and R. G. Waarts, "Phase-mismatch dependence of efficiency of wave generation through four wave mixing in a single mode optical fibre," IEEE J. Quantun Electron., vol QE_23, pp. 1205-1210, 1987.
- [10] K. Inoue, "Four-wave mixing in the zero-dispersion wavelength regions," J. Lightwave Technol., vol. 10, pp. 1553-1561, 1992.
- [11] R. N. Hall, G. E. Fenner, J. D. Kingley, T. J. Soltys and R. O. Carlson, "Coherent light emission from GaAs junctions," Phys. Rev. Lett., vol. 9, pp. 366-368, 1962.
- [12] M. I. Nathan, W. P. Dumke, G. Burns, F. H. Dill, and G. Lasher, "Stimulated emission of radiation from GaAs p-n junctions," Appl. Phys. Lett., vol. 1, pp. 62-64, 1962.
- [13] N. Holonyak, Jr., and S. F. Bevacqua, "Coherent (visible) light emission from Ga ($_{As1-x}P_x$) junctions," Appl. Phys. Lett., vol. 1, pp. 82-83, 1962.
- [14] T. M. Quist, R. H. Rediker, R. J. Keyes, W. E. Krag, B. Lax, A. L. McWhorter and H. J. Zieger, "Semiconductor maser of GaAs," Appl. Phys. Lett., vol. 1, pp. 91-92, 1962.
- [15] H. Kressel and J. K. Butler, "Semiconductor lasers and Heterojunction LED's", Academic Press, 1978.
- [16] H. C. Casey, Jr. and M. B. Panish, "Heterostuctures Lasers: Part A," Academic Press, 1978.
- [17] G. P. Agrawal and N. K. Dutta, "Long-wavelength semiconductor laser," Van Nostrand Reinhold, 1986.
- [18] P. S. Zory, Jr., Ed. "Quantum well lasers," Academic Press, 1993.
- [19] J. W. Crowe and R. M. Craig, Jr., "Small signal amplification in GaAs lasers," Appl. Phys. Lett., vol. 4, pp. 57, 1964.

- [20] W. F. Kosonocky and R. H. Cornley, "GaAs laser amplifiers," IEEE J. Quantum Electron., vol. 4, pp. 125, 1968.
- [21] Y. Yamamoto, "Characteristics of AlGaAs Fabry-Perot cavity type laser amplifiers," IEEE J. Quantum Electron., vol. 16, pp. 1047-1052, 1980.
- [22] J. C. Simon, "Semiconductor laser amplifiers for single mode fibre communications," J. Optical Commun., vol. 4, pp. 51-62, 1983.
- [23] J. C. Simon, "GaInAsP semiconductor laser amplifiers for single mode fibre communications," IEEE J. Lightwave Technol., vol. 5, pp. 1286-1295, 1987.
- [24] M. J. O'Mahony, "Semiconductor laser optical amplifiers for use in future fibre system," IEEE J. Lightwave Technol., vol. 6, pp. 531, 1988.
- [25] N. A. Olsson, "Lightwave systems with optical amplifiers," IEEE J. Lightwave Technol., vol. 7, pp. 1071-1082, 1989.
- [26] T. Saitoh, T. Mukai and O. Mikami, "Theoretical analysis and fabrication of antireflection coatings on laser diode facets," IEEE J. Lightwave Technol., vol. 3, pp. 288-293, 1985.
- [27] C. E. Zah, J. S. Osinski, C. Caneau, S. G. Menocal, L. A. Reith, J. Salzman, F. K. Shokoohi and T. P. Lee, "Fabrication and performance of 1.5 μm GaInAsP travelling wave laser amplifiers with angled facets," Electron. Lett., vol. 23, pp. 990-992, 1987.
- [28] N. A. Olsson, R. F. Kazarinow, W. A. Nordland, C. H. Henry, M. G. Oberg, H. G. White, P. A. Garbinski and A. Savage, "Polarization independence optical amplifier with buried facets," Electron. Lett., vol. 25, pp 1048- 1049, 1989.
- [29] N. A. Olsson, and P. A. Garbinski, "High sensitivity direct detection receiver with a 1.5 μm optical preamplifier," Electron. Lett., vol. 22, pp 1114- 1116, 1986.

- [30] M. G. Oberg, N. A. Ollson, L. A. Koszi and G. J. Przybylek, "313 km transmission experiment at 1 Gbit/s using optical amplifiers and a low chirp laser," *Electron. Lett.*, vol. 24, pp 38-39, 1988.
- [31] W. I. Way, C. E. Zah and T. P. Lee, "Applications of travelling wave laser amplifiers in subcarrier multiplexer lightwave systems," *IEEE Trans. Microwave Theory Tech.*, vol. 38, pp. 534-545, 1990.
- [32] T. Li, "The impact of optical amplifiers on long distance lightwave telecommunication," *Proc. IEEE*, vol. 81, pp. 1633-1646, 1993.
- [33] M. C. Tatham, G. Sherlock and L. D. Westbrook, "20 nm wavelength conversion using nondegenerate four wave mixing," *IEEE Photon. Tech. Lett.*, vol. 5, pp. 1303-1306, 1993.
- [34] J. Zhou, N. Park, K. J. Vahala, M. A. Newkirk and B. I. Miller, "Four wave mixing wavelength conversion efficiency in semiconductor travelling wave amplifiers measured to 65 nm of wavelength shift," *IEEE Photon. Technol. Lett.*, vol. 6, pp. 984-987, 1994.
- [35] L. E. Adams, E. S. Kintzer and J. G. Fujimoto, "All-optical clock recovery using a mode locked figure eight laser with a semiconductor nonlinearity," *Electron. Lett.*, vol. 30, pp. 1696-1697, 1994.
- [36] S. Shimada, K. Nakagawa, M. Saruwatari and T. Matsumoto, "Very high speed optical signal processing," *Proc. IEEE*, vol. 81, pp. 1633-1646, 1993.
- [37] T. L. Koch and U. Koren, "Semiconductor photonic integrated circuits," *IEEE J. Quantum Electron.*, vol. 27, pp. 641-653, 1991.
- [38] G. P. Agrawal, "Populations pulsations and nondegenerate four wave mixing in semiconductor lasers and amplifiers," *J. Opt. Soc. Am. B*, vol. 5, pp. 147-158, 1988.

- [39] K. L. Hall, G. Lenz, E. P. Ippen, U. Koren and G. Raybon, "Carrier heating and spectral hole burning in strained layer quantum well laser amplifiers at 1.5 μm ," Appl. Phys. Lett., vol. 61, pp. 2512-2514, 1992.

CHAPTER 3

CHARACTERISATION OF HNLFs AND SOAs USING FOUR WAVE MIXING TECHNIQUE

3.1 Introduction

Nonlinear processes which involve the modulation of the refractive index of glass are commonly referred to as parametric process and can be divided into two categories, namely, FWM and harmonic generation. Both processes operate on a somewhat similar principle; whereby the magnitude of the polarization terms in each process are governed by the nonlinear susceptibility, thus serving as a source to excite other electromagnetic waves with different frequencies and wave vectors [1], [2]. As discussed in Chapter 2, these process have both second and third order nonlinear susceptibility, whereby a second order non-linear effects cover the parametric effects of second-harmonic generation [3] and sum-frequency generation [4]; while third order nonlinear effects encompass the FWM and parametric amplification, respectively. Second order effects will vanish in silica fibres as explained previously [1], [2], [5], thereby allowing third order effects to become the dominant factor of the nonlinear behaviour in optical fibres. Amongst the various third order effects, the FWM effect is one of the prevalent effect in optical fibres and whose nature involves the interaction of two optical waves propagating in a fibre to generate new

waves [2], [3]. This effect is both a disadvantage as well as an advantage, as it can cause severe system degradation in multichannel transmissions, but can also be utilized for unique applications such as wavelength generation.

FWM efficiency in optical fibres depends strongly on phase matching and the ZDW, which in turn is determined by the chromatic dispersion. The key parameters in enabling a broad and highly efficient FWM process are a high effective nonlinearity per unit length, a low chromatic dispersion with a low dispersion slope and short fibre length [6], [7]. The most critical of these factors is a high effective nonlinearity per unit length, which provides the means for a highly efficient FWM process and allows for enhanced wavelength conversion efficiency. By operating close to the ZDW of a fibre with a low dispersion slope, the linear phase mismatch between the interacting waves is decreased, thereby allowing operation over a broad wavelength region.

The FWM process occurs when photons from one or more waves are annihilated and new photons are created at different frequencies, such that the net energy and momentum are conserved during the parametric interaction. In order to generate the FWM effect (and also parametric effects), a specific set of frequencies and specific nonlinear refractive index is necessary [2]. In this regard, it is obvious that the generation of the FWM effect in an optical fibre is very much different from that of other optical gain media, such as the SOA, whereby in the optical fibre the FWM process depended strongly on phase mismatching inside the fibre, whereas in the SOA the FWM process is dependent on the intraband and interband interactions. Interband FWM generation requires carrier density modulation involving electron-hole recombination at relatively low wavelengths and is typically limited by the carrier lifetime and a wavelength shift of <0.1 nm [8], [9]. In contrast, interband FWM involves the modulation of the occupational probability within an energy band to

respond on a time scale of <1 ps and provide wavelength shifts larger than 10 nm [10]-[12]. For this reason, intraband FWM has become common for practical implementation of wavelength converters, even though the required pump power can exceed 10 mW and the conversion efficiency is typically $<10\%$ [11]-[13].

In this chapter, the optical characterization of the HNLF and the SOA is discussed. In the first part of this chapter, the nonlinear parameters of the HNLF such as ZDW, FWM conversion efficiency, CD and nonlinear coefficient will be examined, while in the second part of the chapter the linear and nonlinear parameters of the SOA such as the gain, noise figure and FWM conversion efficiency will be discussed.

3.2 Highly Nonlinear Fibre (HNLF)

In this research, the HNLF used is manufactured by Optical Fibre Solutions (OFS, a Furukawa company). It combines a high non-linear coefficient with numerically small group velocity dispersion and includes a high delta core, surrounded by a deeply depressed ring and doped with Fluorine. The parameters obtained from the characterization of the HNLF are compared to the specifications from OFS to ensure the accuracy of the characterization procedure. The detailed design and parameters of the HNLF have been given in Chapter 2.

Several methods have been proposed for characterizing the nonlinear behaviour of fibres, most of which are based on the detection of the phase shift caused by self phase modulation (SPM) or on cross phase modulation (XPM). However, these techniques generally need short pulses and a small chromatic dispersion, and only give the Kerr coefficient value. A

more viable approach would be the use of partially degenerated FWM to simultaneously measure the Kerr and dispersion coefficient as described in detail in Chapter 2. As the FWM efficiency curve of an optical fibre as a function of wavelength depends significantly on the CD, the ZDW and the nonlinear coefficient of an optical fibre, the FWM technique has become popular as a tool for measuring these parameters in an optical fibre [14]-[21]. There are several reports on scanning FWM experiments can be used to measure ZDW, CD, and the nonlinear refractive index both individually [17], [19], [20] and simultaneously [15], [21].

3.2.1 Experimental setup for characterizing the HNLF

The experimental setup for the simultaneous measurement of nonlinear coefficient, ZDW and CD in the HNLF via partially degenerated FWM with two pump lasers is shown in Figure 3.1

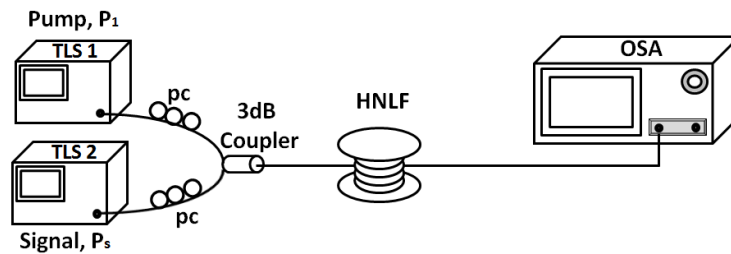


Figure 3.1 Schematic diagram for generating FWM effect in the HNLF.

In the setup, two Yokogawa (AQ2200) Tunable Laser Sources (designated TLS1 and TLS2); with tuning ranges from 1450 nm to 1620 nm and linewidths of 0.015 nm are used as signal, P_s and pump, P_p sources. Both P_p and P_s are combined using a 3 dB coupler and a Polarization Controller (PC) to adjust the polarization of the input signals in order to obtain the maximum FWM efficiency. The HNLF used in this experiment is from OFS with specifications of the nominal ZDW, loss coefficient, dispersion slope and nonlinear parameter of 1531 nm, 0.73 dB/km, 0.007 ps/nm².km and 10.8 (W.km)⁻¹, respectively. A Yokogawa Optical Spectrum Analyzer (OSA) with 0.02 nm resolution bandwidth is used to measure the generated FWM spectrum.

3.2.2 Determination of the ZDW

The development of systems operating within the ZDW region has become important to avoid degradation due to the CD in the high speed transmissions. It is therefore important to study the FWM effect in this wavelength region for high-speed multichannel transmission in order to understand and determine any possible degradation.

The theoretical treatment of fibre FWM in the ZDW region is dependent on the FWM power, FWM efficiency and phase mismatch. The output power from the FWM process can be written as [21, 22]

$$P_F(L, \Delta\beta) = \eta(\Delta\beta) \gamma^2 L_{eff}^2 P_s P_p^2 e^{-\alpha L}, \quad 3.1$$

where P_s and P_p are the two input powers at λ_s and λ_p wavelength, respectively, L is the length of the optical fibre and α is the absorption coefficient. The effective fibre length L_{eff} is defined as

$$L_{eff} \equiv \int_0^L \exp(-\alpha z) dz = \frac{1 - \exp(-\alpha L)}{\alpha}, \quad 3.2$$

and the nonlinear coefficient, γ

$$\gamma = \frac{2\pi n_2}{\lambda A_{eff}}, \quad 3.3$$

where n_2 is the nonlinear index coefficient, A_{eff} is the effective mode area. FWM efficiency, $\eta(\Delta\beta)$ is a coefficient determining the FWM efficiency on phase matching term $\Delta\beta$ and is defined as

$$\eta(\Delta\beta) \equiv \frac{P_F(L, \Delta\beta)}{P_F(L, \Delta\beta = 0)}. \quad 3.4$$

The phase-mismatching term $\Delta\beta$ is defined as the difference between propagation constants of the four waves: $\Delta\beta \equiv \beta_F + \beta_s - 2\beta_p$ where β is the propagation constant. The FWM efficiency and the phase mismatching terms are given as [22], [24]

$$\eta = \frac{\alpha^2}{\alpha^2 + \Delta\beta^2} \left[1 + \frac{2e^{-\alpha L}(1 - \cos(\Delta\beta L))}{(1 - e^{-\alpha L})^2} \right]. \quad 3.5$$

The efficiency, η takes a maximum value of 1 for $\Delta\beta = 0$ which is the value whereby the phase matching condition is satisfied. The phase mismatch at a partially degenerate case is given by

$$\Delta\beta = -\frac{2\pi c\lambda_0^3}{\lambda_p^3\lambda_s^2} \frac{dD_c}{d\lambda} (\lambda_p - \lambda_0)(\lambda_p - \lambda_s)^2. \quad 3.6$$

It is noted in a phase mismatch equation that the phase matching condition is always satisfied when λ_p coincides with the ZDW, λ_0 , i.e., $\lambda_p = \lambda_0$. The wavelength arrangement for this phase-matched condition is illustrated in Figure 3.2.

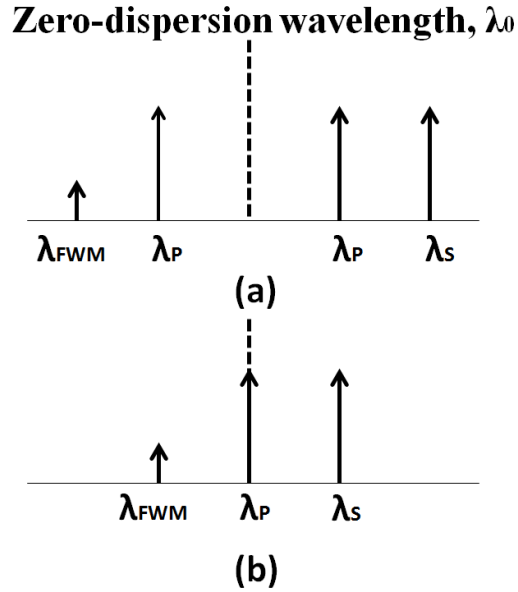


Figure 3.2 Wavelength arrangements satisfying the phase-matching condition in the ZDW region (a) non-degenerate case, (b) partially degenerate case [22].

The dependence of the FWM efficiency, η on the phase mismatching around the ZDW is calculated in the partially degenerate case using 3.5. The results are shown in Figure 3.3, where the FWM efficiency as a function of wavelength difference of $\lambda_p - \lambda_0$ is plotted with an input light wavelength, λ_s set far from λ_p and λ_0 . In the Figure 3.3, the solid and broken lines denote FWM efficiency when the wavelength differences between the pump and probe lights are 14 nm and 5 nm, respectively.

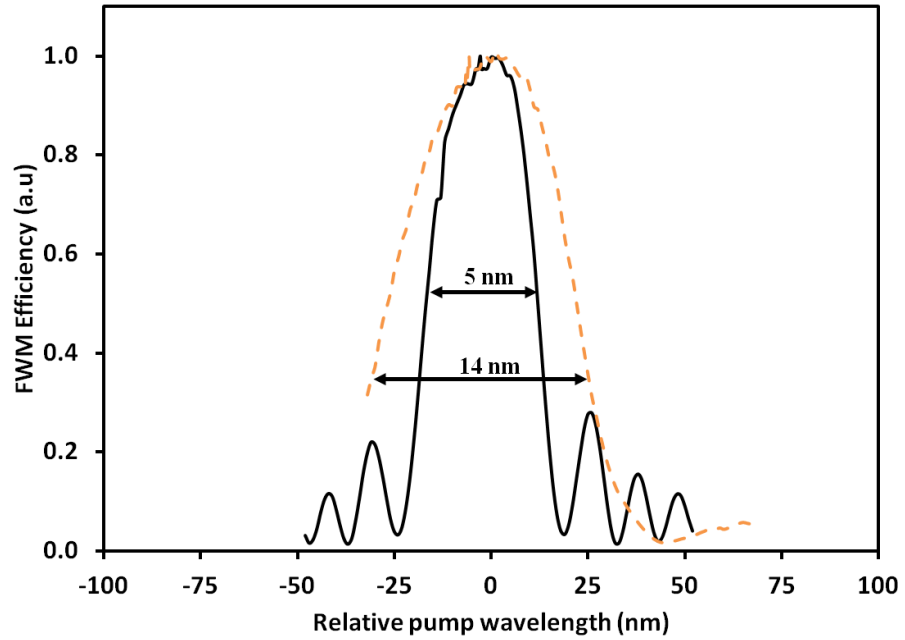
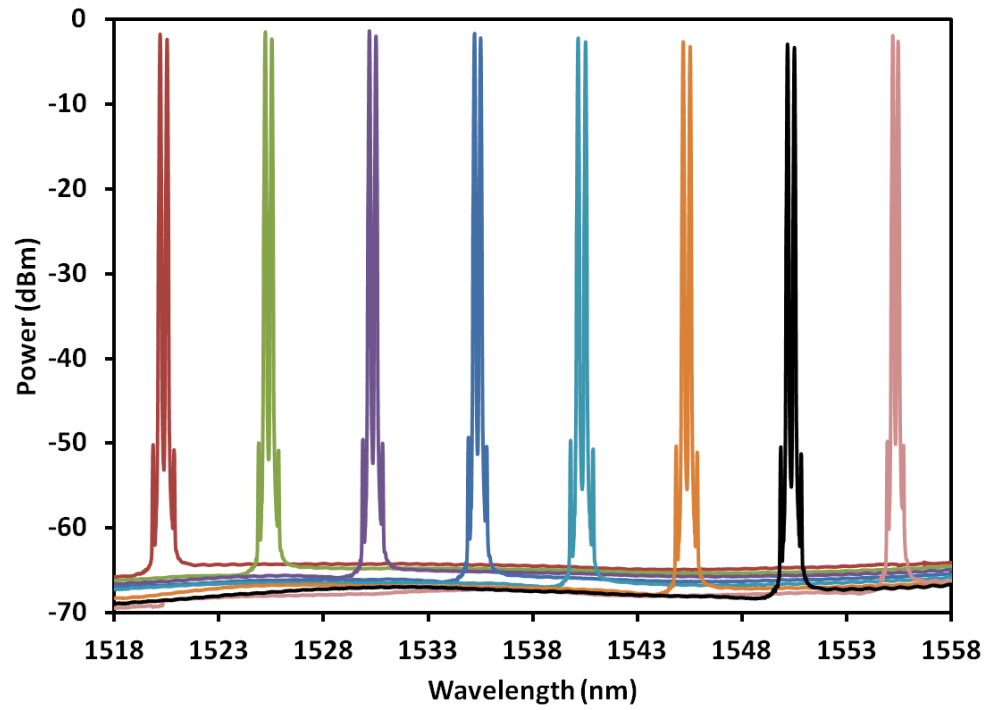


Figure 3.3 The FWM efficiency, η as a function of relative pump wavelength $\lambda_p - \lambda_0$ in partially degenerate FWM.

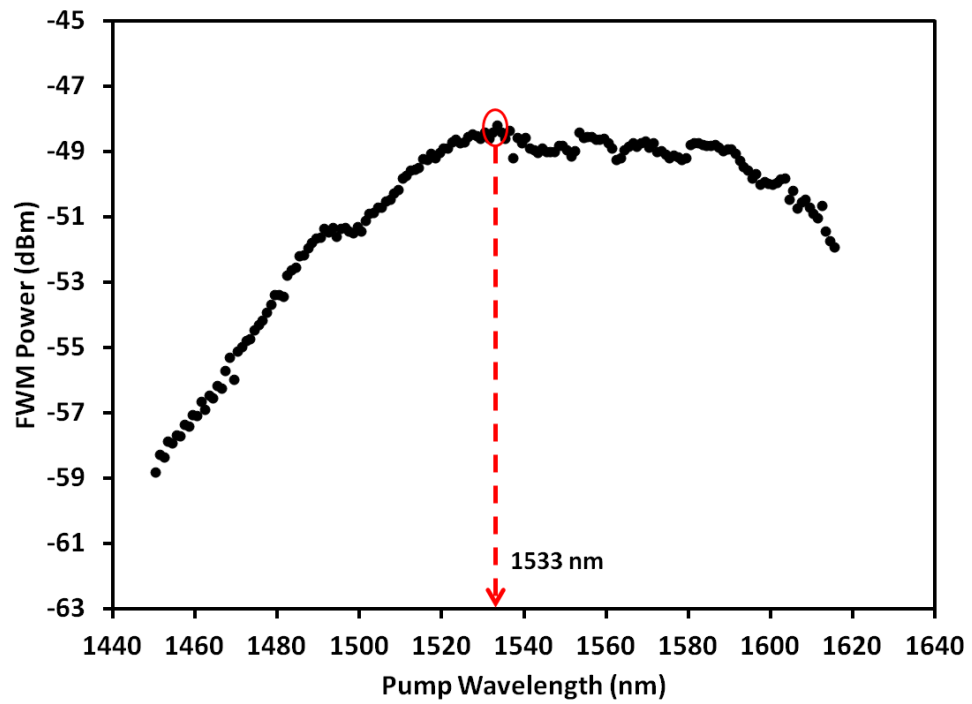
The results show that FWM efficiency is at the maximum when the pump wavelength is at the ZDW region and then rapidly decreases as the pump wavelength is detuned far from the ZDW. The frequency bandwidth within which the FWM light is efficiently generated is

dependent on a wavelength difference between pump and probe light. The phase matched wavelength bandwidth is narrower for the larger wavelength difference [22].

In order to measure the ZDW, λ_o , several techniques which utilises the FWM effect are used. The first techniques accomplishes by varying the pump and signal wavelengths based on setup from Figure 3.1, with a wavelength detuning of 0.4 nm in order to obtain the highest values of FWM power in the range 1450 nm to 1620 nm, shown in Figure 3.4 (a). In order to determine the ZDW, a TLS with broad tuning range is needed in this experiment. The scanning pump laser wavelength must pass over the ZDW of the HNLF in order to obtain a phase matched FWM efficiency curve for a HNLF. Figure 3.4 (a) shows that the generation of this idler depends on the power of the pump and signal wavelengths, when a strong pump transfers its power to create the converted signal. To achieve higher converted signal output power, the pump power should be greater than the signal power and this also can be achieved by using the polarization controller. Hence, the highest converted signal output power of -48.17 dBm is obtained when the pump and signal powers are set to 12.9 dBm and 12 dBm respectively. Figure 3.4 (b) shows that the value of FWM power starts to increase from 1450 nm to 1520 nm, after which it becomes flat with a 0.5 dB power fluctuations in the region of 1526 nm to 1539 nm at FWM power of -48.17 dBm. After this region, the power decreases rapidly as the signal wavelength increases into L-band region. It is shown that high power is needed to exceed the FWM threshold power and subsequently generate the new wavelength (sideband) based on the FWM effect. By employing this technique, we found that the ZDW located in the region between 1526 nm to 1539 which difficult to determine the exact value of λ_o . In this wavelength range, higher power value of FWM converter is obtained at 1533 nm. Therefore, this technique is not suitable in determining an exact value of λ_o .



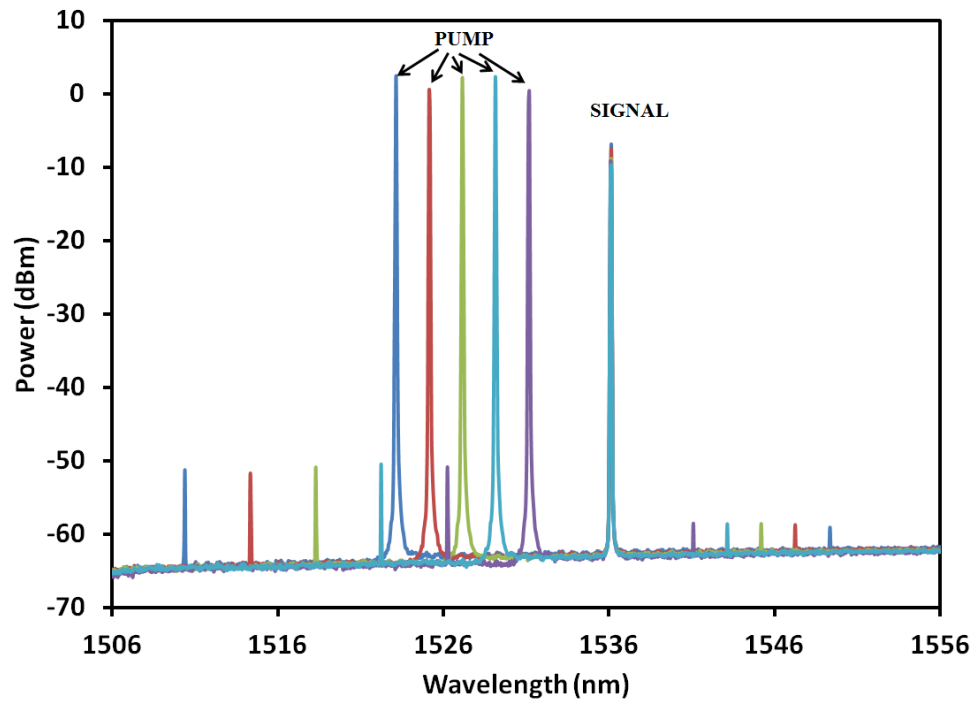
(a)



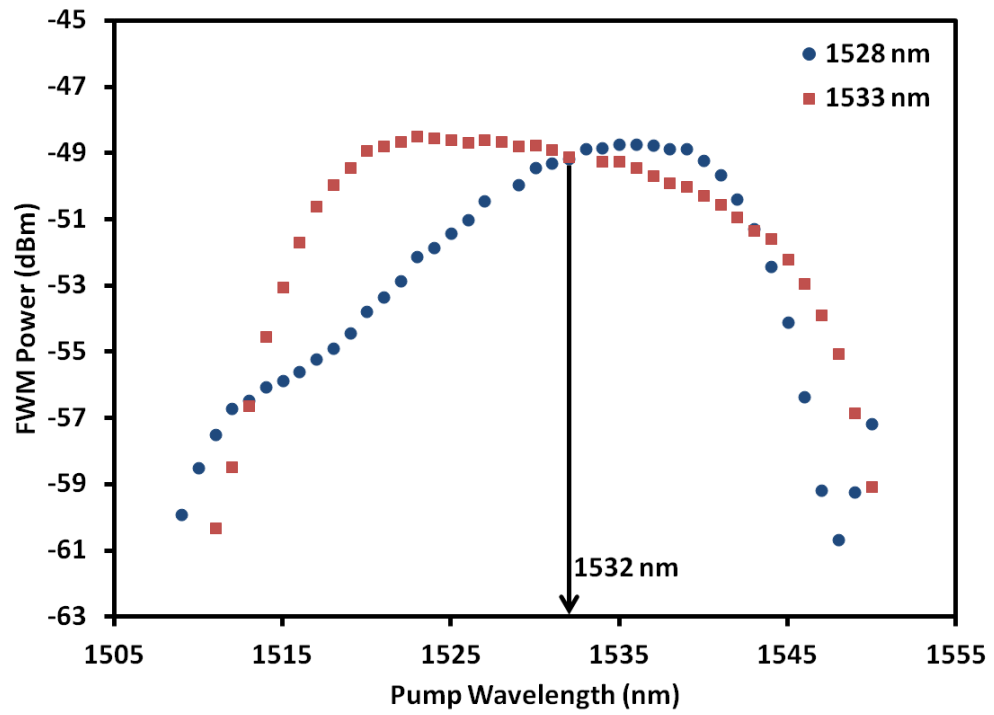
(b)

Figure 3.4 (a) The FWM spectrum by varying the pump and signal wavelength (b) the spectrum of FWM power against converted wavelength.

In the second technique, the pump wavelength is tuned to roughly the value of λ_o , while the probe light wavelength is fixed. Most research teams, such as those led by D. H. Kim [19], L. Prigent [20], K. Inoue [22] [25] and J. X. Feng [23] use this technique to map λ_o . This technique however assumes λ_o is completely uniform, i.e. with no fluctuations within tenth of nanometre along the entire length of the fibre. In long fibres (km), however, this is impossible due to perturbations in the line created during the fabrication process, and therefore λ_o must necessarily fluctuate along the fibre length. The HNLF used in this setup has a length of 100 m, and in this case λ_o can be considered to be uniform. In this experiment, the pump wavelength is varied from 1510 nm to 1550 nm at two different signal wavelengths of 1528 nm and 1533 nm. The value of a signal wavelength is chosen due to the maximum FWM power when the pump wavelength is around λ_o . Figure 3.5 (a) show the FWM spectrum when the signal wavelength is fixed at the power of -2 dBm and the pump wavelength is varied at the power of 12 dBm. From this spectrum, the FWM power is measured and the resulting spectrum is shown in Figure 3.5 (b). A 3 dB bandwidth of these spectra are 19 nm and 28 nm for the 1528 nm and 1533 nm, respectively. Thus, the frequency bandwidth within which the FWM light is efficiently generated is wide when the signal wavelength is position at maximal FWM wavelength. Figure 3.5 (b) shows the same FWM power at pump wavelength of 1532 nm and it also illustrates the clash point FWM power between both signal wavelengths. This is because the phase-matching condition is completely satisfied at that point where it can be assumed as a ZDW, λ_o . Therefore, the ZDW obtained from this technique is 1532 nm, which is approximately the ZDW value as provided by the manufacturer.



(a)



(b)

Figure 3.5 (a) The FWM spectrum by varying the pump and fix the signal wavelength (b) the FWM efficiency against pump wavelengths.

In the final technique, the same setup as employed in the second technique was used, but with the pump wavelength being fixed and the signal wavelength being varied from the S-band to L-band. The ZDW is also assumed to be uniform due to the shorter HNLF length (100 m). In this experiment, the intensity of the FWM converter is measured for every tuned signal wavelength over its entire wavelength range from 1500 nm to 1600 nm with a wavelength detuning range of 125 GHz of between the signal and pump which is shown in Figure 3.6. The pump and signal powers are set at 5.5 mW and 4.25 mW to measure the highest FWM conversion efficiency. Figure 3.7 shows the variation of the pump wavelength from 1516 nm, 1518 nm, 1526 nm, 1528 nm, 1533 nm, 1535 nm, 1544 nm and 1545 nm against a varying signal wavelength from 1500 nm to 1600 nm for every pump wavelength. Based on this figure, it can be seen that a full width at half maximum for the FWM generated signals are larger for a smaller wavelength difference between the pump and signal lights due to the phase matched wavelength bandwidth. The phase matched bandwidth within which the FWM light is efficiently generated depends on the wavelength difference between the pump and signal wavelength, and is satisfied at a wavelength spacing region of 1 nm until 15 nm. Above a spacing of 15 nm, the FWM power decreases as illustrated when using the pump wavelength below the ZDW ($\lambda_P < \lambda_0$). However, when the pump wavelength is above the ZDW ($\lambda_P > \lambda_0$) (until 19 nm at the pump wavelength of 1550 nm), an increase in the FWM power can be observed. In this case, a maximum FWM efficiency at 1550 nm can be achieved. However, a narrow phase matching is illustrated when using the pump wavelength of 1550 nm. Consequently, it is difficult to apply this method in other applications such as wavelength converters where it needs a broader phase matched bandwidth. For that reason, the pump wavelength should use at the wavelength nearest to the ZDW. To determine the ZDW, the wavelength spacing is tuned from 10 nm

to 15 nm where the clash of spectrum FWM power can be observed as the ZDW of HNLF. Based on this technique, a ZDW of 1531 nm is successfully obtained where it is similar to the manufacturer's specifications.

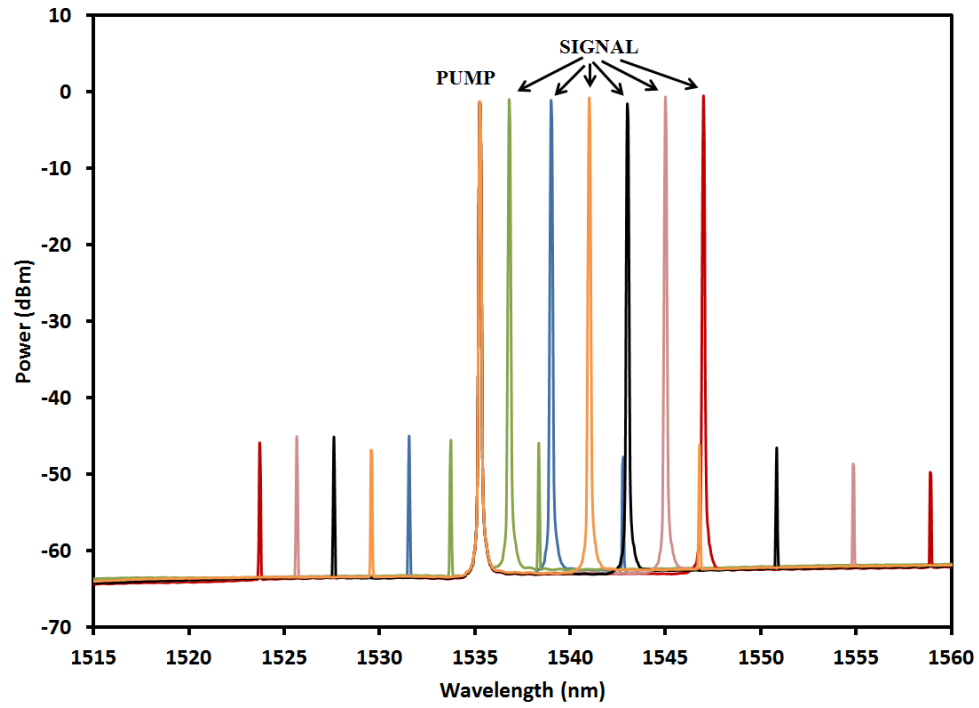


Figure 3.6 Spectrum of FWM

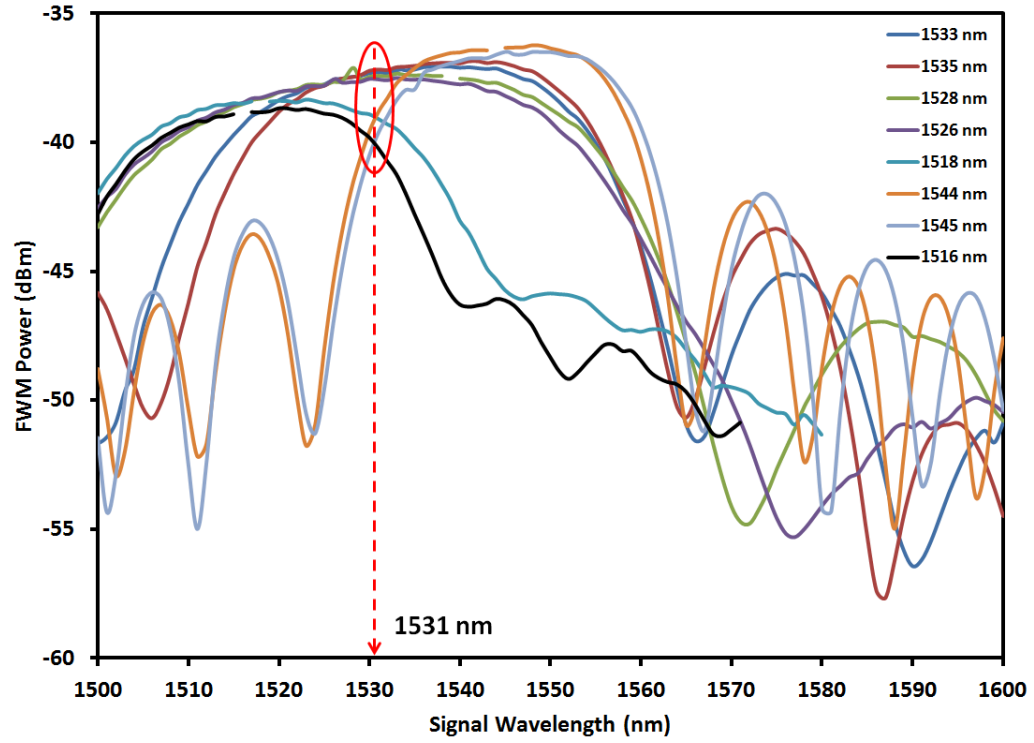


Figure 3.7 The FWM power of tuning signal wavelength for different pump wavelength.

In order to verify ZDW, we compared the measured value with our calculated result obtained from equation 3.1 and 3.5, which requires the FWM power and FWM efficiency. These values can be obtained by first setting the pump wavelength to a value which is less than the ZDW value ($\lambda_p < \lambda_0$) stated by the manufacturer. Equation 3.5 requires the HNLF fibre length, L , absorption coefficient, α , as well as the dispersion slope at 1550 nm, $dD_c/d\lambda$, which we obtained from the manufacturer's data sheet with values of $L = 100$ m, $\alpha = 0.000168 \text{ m}^{-1}$, $dD_c/d\lambda = 0.007 \text{ ps}/(\text{nm}^2 \cdot \text{km})$, respectively. Before discussing the experimental results, it is worth noting that due to the limitations of the OSA, the measured FWM efficiency and power, η and P , respectively, will never be able to reach the minimum value, i.e. $\eta = 0$ and $P = -75$. In fact, the low sensitivity of the OSA means that we can only measure noise at low values of η and P . From Figure 3.8, it is clear that the theoretical and

experimental values of the FWM efficiency are similar and follow a similar trend when we used the experimental value of the ZDW at 1531 nm obtained via the third technique. However, there is a slight discrepancy when we used the first and second techniques to calculate the FWM efficiency, which implies that the third technique is the most suitable one to employ for FWM efficiency calculations. This technique is much superior to other techniques such as frequency-domain phase shift [26], modulation instability amplification [27] and the differential phase shift [26] in determining the ZDW due to the accuracy of the technique as well as simplicity of the setup.

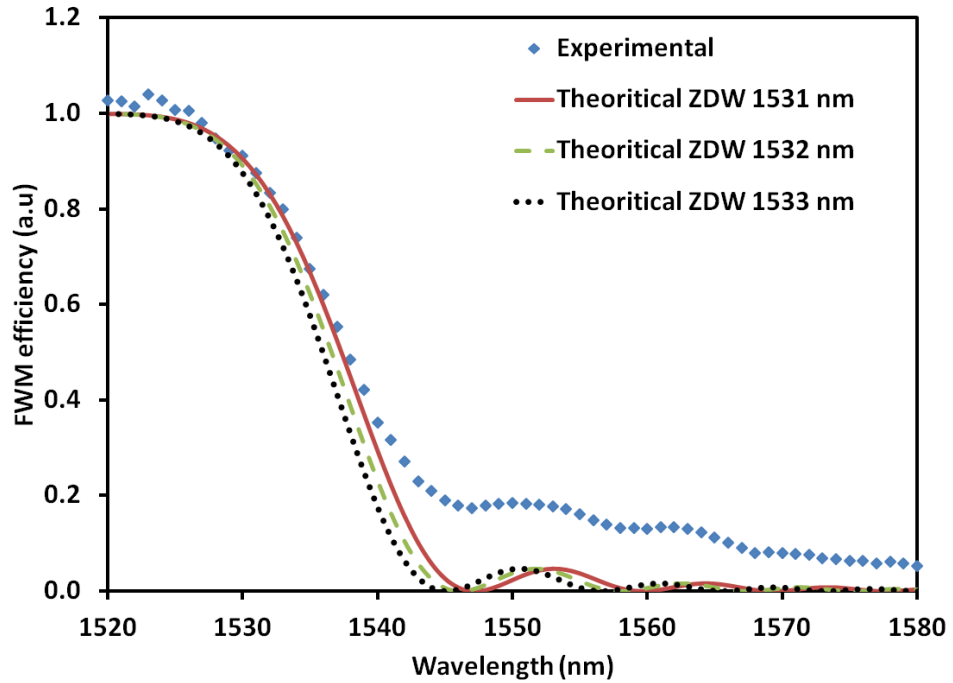


Figure 3.8 The FWM efficiency as a function of signal wavelength of HNLf.

The FWM efficiency is essentially based on the FWM power that is obtained from the experimental value shown in Figure 3.9. In this figure, the highest FWM power of -38.5 dBm at 1520 nm is found and observed to be almost constant from 1520 nm to 1532 nm with 1 dB fluctuation power. It then decreases from -39.2 dBm to -46.1 dBm between 1532 nm to 1547 nm, respectively before increasing again to round 0.2 dB at 1552 nm. This spectrum is observed to behave almost like a cosine spectrum due to the changes in dispersion along the whole length at the HNLF. In addition to the experimental results, Figure 3.9 also shows the numerical spectrum of FWM power based on the ZDW at 1531 nm, 1532 nm and 1533 nm, respectively. This spectrum can be obtained by inserting the FWM efficiency value from Figure 3.8 into equation 3.1. Therefore, the numerical spectrum of 1531 nm illustrates the same pattern as that of the experimental spectrum due to the fact that the nonlinear parameters in the equation 3.1 are constant for both cases. For this reason, the other ZDW measurements (at 1532 nm and 1533 nm) gave the different values in the FWM power. These differences can cause the value of CD and the nonlinear coefficient to change, which will be explained in the next section of this thesis.

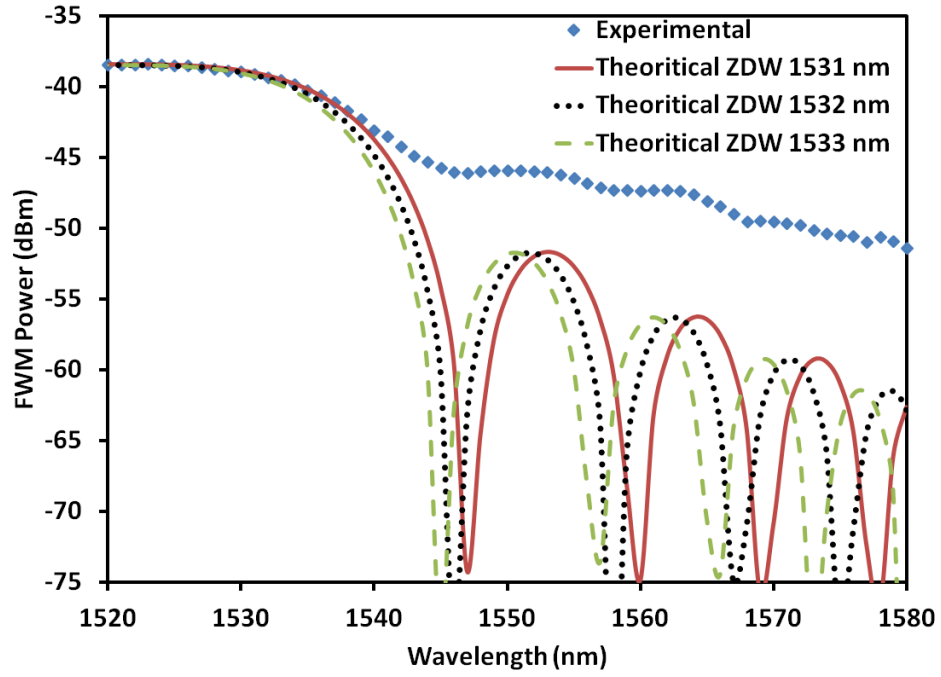


Figure 3.9 Optical power of FWM as a function of signal wavelength.

3.2.3 Determination of chromatic dispersion

In addition to the determination of the ZDW in the HNLF, this technique can also be used in the measurement of the CD in HNLF. In this case, it is referred to as the normalized FWM efficiency, η , as stated in Equation 3.5. To determine the CD, the following equation is employed,

$$\Delta\beta = \frac{2\pi\lambda^2}{c} D \cdot \Delta f^2, \quad 3.7$$

with the dispersion parameter, $D = \frac{-2\pi c}{\lambda^2} \beta_2$, and β_2 is the group velocity dispersion parameter. From equation 3.7, it is assumed that the minima of P_{FWM} occurs when

$\Delta\beta.L/2 = k.\pi$, where k is integer. This is due to the phase mismatch between the signals that propagating inside the fibre. For fixed channel spacing, the P_{FWM} minima can be observed. From equation 3.7, P_{FWM} appear after every $2\pi/\Delta\beta$ meter. Similarly, the minima for P_{FWM} for a fibre with a fixed length of L are located at a channel spacing of,

$$\Delta f_k = \sqrt{\frac{k.c}{\lambda^2.D.L}}, \quad 3.8$$

where k is the integer.

As the nonlinear behaviour is only able to shift certain characteristics of the FWM up or down, an analysis of the FWM signal power minima can be used to measure the dispersion of the optical fibre. The total fibre will also allow us to estimate the nonlinearity of the fibre. The setup for this measurement requires only two laser diodes with a tuning range of less than 1 nm and a proper length of the fibre. To calculate the fibre dispersion it is necessary to find the channel spacing for which P_{FWM} reaches its first minimum and the calculated CD coefficient $D(\lambda)$ as

$$D = \frac{c}{\lambda^2 \Delta f^2 L}. \quad 3.9$$

The channel spacing for P_{FWM} reaches its first minimum can be obtained from the FWM power of tuning signal wavelength for different pump wavelength which is shown in Figure 3.7. Figure 3.10 shows the CD coefficient $D(\lambda)$ of a HNLF is obtained from the proposed method. From this figure, the second order dispersion coefficient $dD(\lambda)/d\lambda$ which is related

to the dispersion slope of the HNLF is also obtained. The red empty dots show the measurement result by using the third technique for a 100 m length of HNLF where it is in good agreement with those of the manufacturer's datasheet. However, from this figure, the experimental result was obtained only from 1525 nm to 1545 nm due to the limitation of ZDW bandwidth in the FWM technique. This limitation is a drawback of this technique.

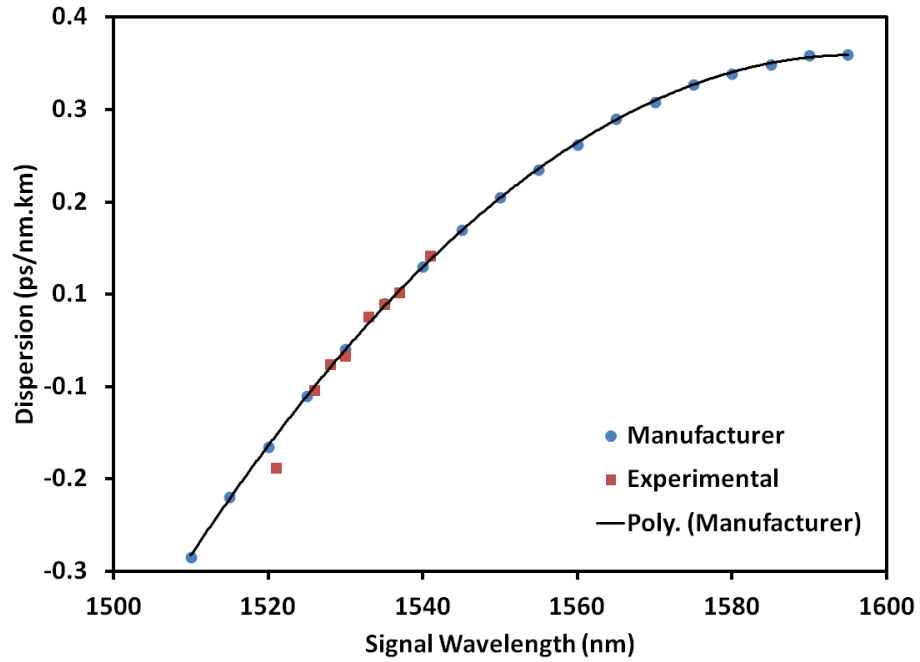


Figure 3.10 The chromatic dispersion coefficient of HNLF with our proposed technique.

3.2.4 Determination of nonlinear coefficient

The measurement of nonlinear coefficients of the HNLF is based on the measurement of the FWM effect on a dual wavelength laser, with optical beat signals propagating through the fibre. The measured FWM signal intensity versus wavelength is analysed to extract the fibre nonlinear coefficient, dispersion and slope dispersion by tuning the signal laser wavelength while the pump laser wavelength is fixed which is shown in Figure 3.11. The

maximum power of the converted wavelength is obtained by adjusting the two PCs as shown in Figure 3.1 for each measurement. The maximum FWM signal power can be used to determine the nonlinear coefficient by carefully measuring input pump powers, fibre length and fibre loss.

To analyze the nonlinearity in the HNLF, the nonlinear coefficient, γ , is estimate using equation 3.10

$$\gamma = \sqrt{\frac{P_{FWM}}{\eta P_s P_p^2 e^{-\alpha L} L_{eff}^2}}, \quad 3.10$$

where P_{FWM} is the FWM power, P_p is the input pump power, P_s is the input signal power, L is the fibre length and α is the fibre attenuation coefficient. The effective length of the fibre L_{eff} takes into account the decrease in power due to attenuation and is defined as:

$$L_{eff} = \frac{1 - e^{-\alpha L}}{\alpha}. \quad 3.11$$

By adjusting the signal power, pump power, converted power and the normalized FWM efficiency, the nonlinear coefficient for the HNLF is estimated by using equation 3.10. Therefore, the value of the nonlinear coefficient by all the FWM techniques are obtained as $10.7 \text{ W}^{-1}\text{km}^{-1}$, $10.9 \text{ W}^{-1}\text{km}^{-1}$ and $11.0 \text{ W}^{-1}\text{km}^{-1}$ at 1531 nm, 1532 nm and 1533 nm respectively.

Table 3.1 shows all parameters that are measured by all techniques compared to the manufacturer datasheet. In this table, the nonlinear coefficient of HNLF that obtained from

manufacturer is estimated from the effective area. Nevertheless, by using the proposed technique which is used FWM effect, the nonlinear coefficient of the HNLF is similar to the manufacturer datasheet with an error of about 0.93%. However, using the first technique, a dispersion slope @ 1550 nm, ZDW and nonlinear coefficient of $0.0065 \text{ ps.nm}^{-2}\text{km}^{-1}$, 1533 nm and $11.0 \text{ W}^{-1}\text{km}^{-1}$ is obtained with an error of about 2%. In the second technique with a 1% error is observed the dispersion slope @ 1550 nm of $0.006 \text{ ps.nm}^{-2}\text{km}^{-1}$, ZDW of 1532 nm and nonlinear coefficient of $10.9 \text{ W}^{-1}\text{km}^{-1}$.

Table 3.1 Parameters of HNLF

Parameter	unit	Manufacturer	Experimental		
			1	2	3
Length	m	100	100	100	100
Dispersion Slope @ 1550 nm	$\text{ps}/(\text{nm}^2.\text{km})$	0.007	0.0065	0.0060	0.0070
ZDW	nm	1531	1533	1532	1531
Nonlinear coefficient	$\text{W}^{-1}\text{km}^{-1}$	10.8	11	10.9	10.7
Fibre attenuation	dB/km	0.73	0.73	0.73	0.73

3.3 Semiconductor Optical Amplifier (SOA)

Optical amplifiers, as the name implies, are devices that amplify an input optical signal. There are two main types of optical amplifiers: the semiconductor optical amplifier (SOA) and the fibre amplifier. In an SOA, light is amplified when it propagates through a semiconductor medium fabricated in the form of a waveguide, while in a fibre amplifier, light is amplified when it travels through a fibre doped with rare earth ions (such as Er^{3+}). SOAs require external current to produce gain, as compared to fibre amplifiers which use pump lasers for the same purpose. The SOA is a device which is similar to a semiconductor laser; hence its operating principle, fabrication and design are also similar when the current is injected into an SOA but below the lasing threshold, the device acts as an optical amplifier for incident light waves, but more interestingly is that above this threshold it acts as a nonlinear medium. In general these nonlinearities can cause problems such as frequency chirping and generation of second or third order inter-modulation products in transmissions, but can also be turned into an advantage for the development of functional devices such as wavelength converters.

3.3.1 Gain Performance of SOA

In order to analyse the gain performance of an ultra-wide band SOA, the Amplified Spontaneous Emission (ASE) spectrum is analyzed. Therefore, a simple experiment was done as shown in Figure 3.11. The setup for the SOA is comprised of a single device with an output port connected to the OSA and without any connection at the input port.

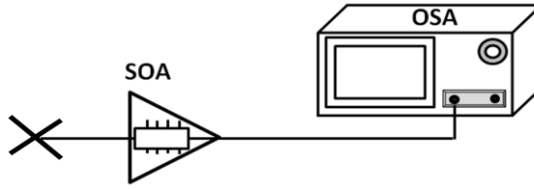


Figure 3.11 Experimental setup for ASE measurement of SOA

Figure 3.12 shows the Amplified Spontaneous Emission (ASE) spectrum of the ultra-wide band SOA at different injection currents. When the total currents of the SOA increases from 70 mA to 390 mA, the total spontaneous emission power increases, along with a gain peak shift from 1530.76 nm to 1487.44 nm, since the gain profile is generally similar to the spontaneous emission profile. It can be seen that the ASE output power generated by the SOA shifts towards the shorter wavelength region as the injection current is increased. This is attributed to the energy absorbed by the excited electrons from the lower energy level state to the higher energy level state, which is then de-excites, emitting a photon with the same energy as the excited electron. The increase in the energy of the photon therefore results in shorter wavelengths. Some ripples are also observed in the spontaneous emission spectrum which is attributed to the residual reflectivity on the facets of the SOA.

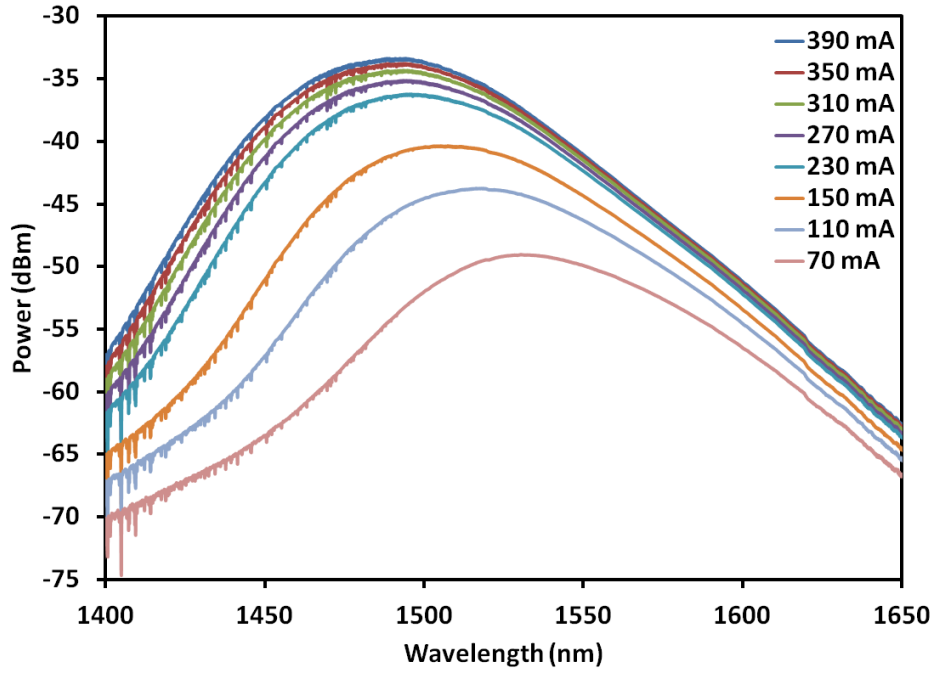


Figure 3.12 Spontaneous emission spectrum of the SOA for different total current.

Figure 3.13 (a) show the dependence of the measured gain on output power at three different signal wavelengths of 1500 nm, 1550 nm and 1580 nm. This dependence could be described as [28], [29]

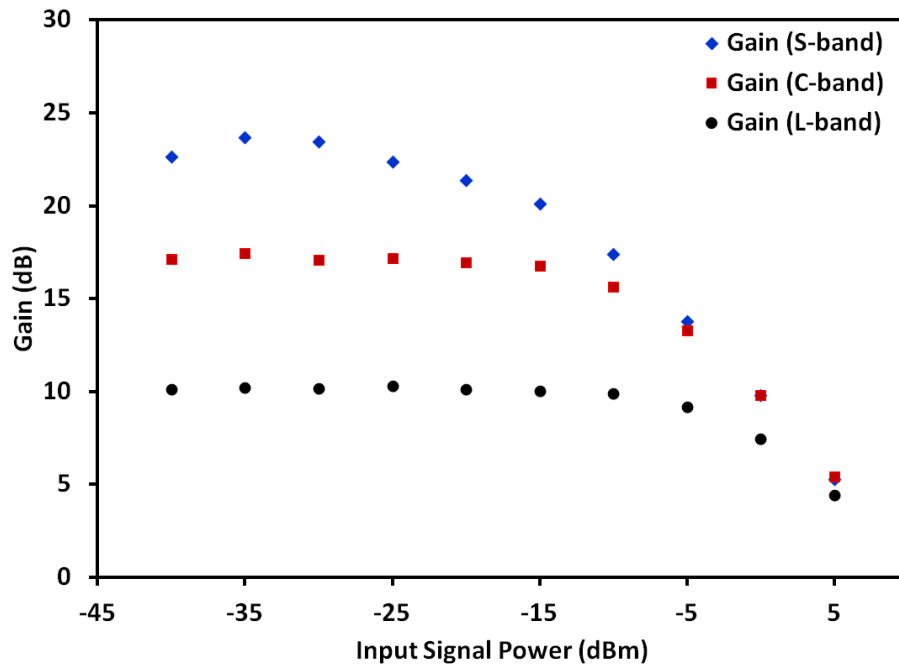
$$g = \frac{g_0}{1 + P/P_s}, \quad 3.12$$

where g_0 is the small signal gain and P_s is the saturation power where it is defined as

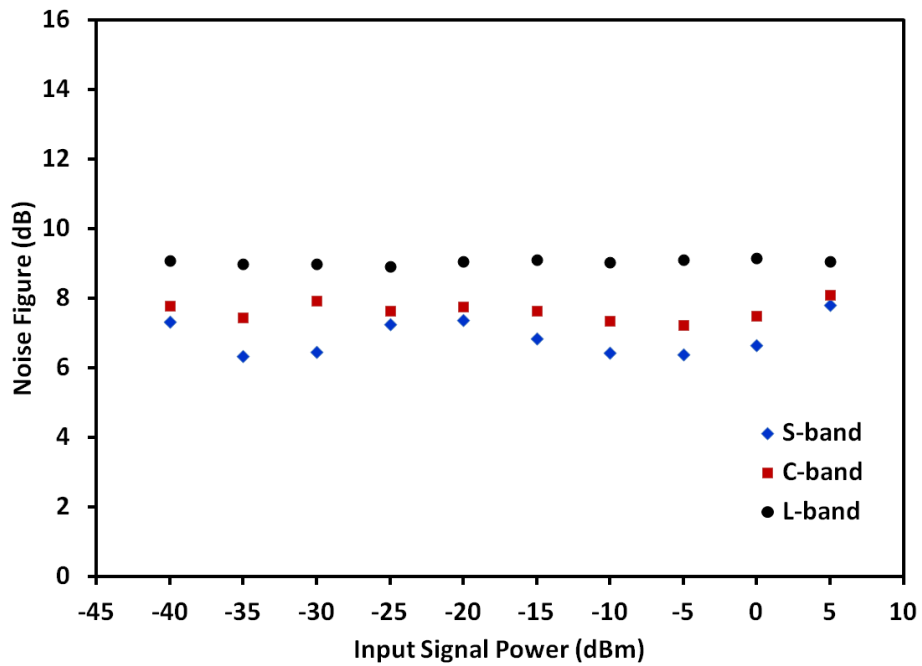
$$P_s = \frac{Ahv}{\Gamma a \tau_c}, \quad 3.13$$

where A is the cross-sectional area of the waveguide mode, $h\nu$ is the photon energy of the signal, Γ is the overlap integral, α is the absorption coefficient and τ_c is the cavity lifetime. The gain decreases with increasing input power, and this phenomenon is called gain saturation. In the experiment, the pump power is fixed at 160 mW. From Figure 3.13 (a), the gain is decreased from the maximum value of 23.7 dB (at -35 dBm) to the minimum value of 5.41 dB (at 5 dBm) with input signal wavelength of 1500 nm. The saturation output power is obtained at an input signal of -10 dBm. On the other hand, for a signal wavelength of 1550 nm the gain drops from its maximum value of 17.4 dB to the minimum value of 4.42 dB. The saturation power is estimated to be about -5 dBm at the C-band input signal power. In the L-band region, the gain decreases from its maximum value of 10.2 dB at the input signal power of -35 dBm to the minimum value of 5.41 dB at an input signal power of 5 dBm. From the figure, and using the output power at which the gain is 3 dB below its unsaturated value, the saturation gain for this region is determined to be at 0 dBm. The gain at 1500 nm is higher than that at 1550 nm and 1580 nm by approximately 6.3 dB and 17.5 dB for all input signal powers tested as shown in Figure 3.10. This is attributed to the fact that the rate of energy transfer from L-band and C-band to S-band is higher at 1500 nm rather than at 1550 nm and 1580 nm.

The characteristics of the SOA noise figure against input signal powers is also shown in Figure 3.13 (b) for three signal wavelengths of 1500 nm, 1550 nm and 1580 nm. As shown in the figure, the noise figures obtained are approximately at approximately 9.1 dB, 7.2 and 6.4 dB at the saturated gain region for input signal wavelengths of 1500 nm, 1550 nm and 1580 nm, respectively. This figure shows the value of noise figure is inverted to the gain where the S-band region encounters higher gain but a lower noise figure as compared to the L-band gain and noise figure.



(a)



(b)

Figure 3.13 (a) Gain and (b) noise figure as a function of input power at a fixed signal wavelength of 1500 nm, 1550 nm and 1580 nm.

The gain and noise figure spectra of the SOA is shown in Figure 3.14 for input signal powers of -30 dBm and 0 dBm using the same pump power of 150 mW. At input signal power of -30 dBm, the gain spectrum increased from 17.17 dB to 21.72 dB within a wavelength region from 1460 nm to 1475 nm. The stable region of gain for the low signal is observed at the 1475 nm to 1520 nm region, where the gain fluctuates by approximately 2 dB, while in the other areas the gain fluctuation is 5 dB or more. Above 1544 nm, the gain decreases as the wavelength increases from above 20 dB to less than 5 dB at 1610 nm. For this low power, the gain follows the spectrum of the ASE as the ASE power is dependent on the wavelength in the SOA. This figure that the NF is relatively stable in the region of 1460 nm to 1595 nm for the low signal values with a fluctuation of roughly 3 dB. However, above 1595 nm, the NF increases slightly to the saturation power of SOA. Unlike the case of the input signal at -30 dBm, the gain and noise figure of the SOA for the high signal is flat and stable as seen in Figure 3.14. The average gain at all wavelengths is approximately 9 dB, while the noise figure is approximately 7 dB. Both the gain and noise figure show a stable and flat spectrum, with fluctuations of 3 dB observed in the noise figure above a wavelength region of 1595 nm whereby the noise figure fluctuates by approximately 6 dB. This is due to the SOA being saturated by the high input signal, resulting in the clamping of the gain [30].

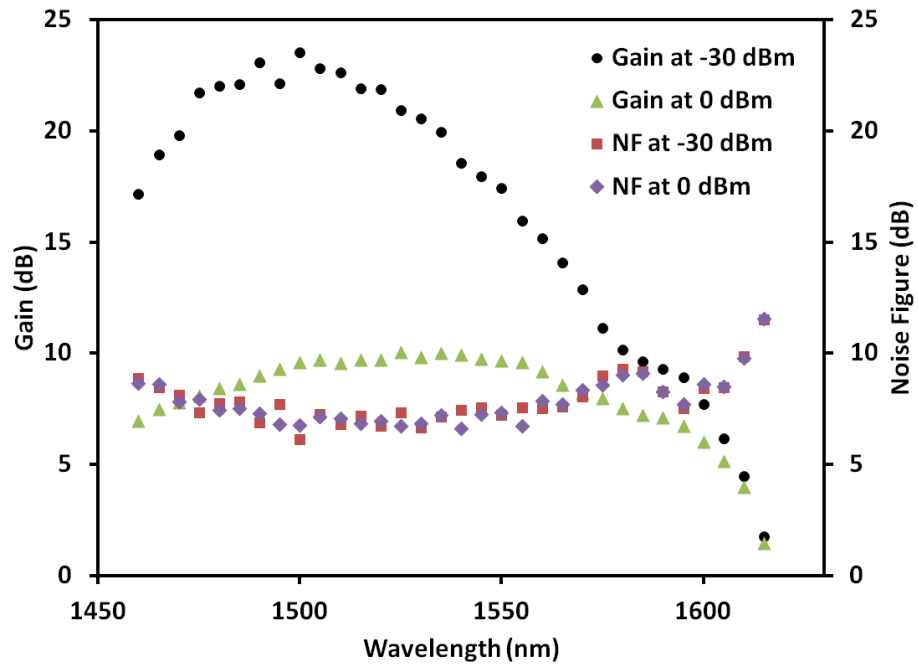


Figure 3.14 Gain (dB) and Noise Figure (dB) of SOA against different test signal wavelengths at -30 dBm and 0 dBm.

Although some experiments have demonstrated the potential application of SOA in optical communication, the SOA still need to overcome several drawbacks before their use becomes practical. The first drawback is their large coupling loss. Even though the SOA can have a gain as high as 24 dB, the usable gain is reduced by 2 to 20 dB because of the large loss occurring at the input and output ends. The second drawback is that the lifetime of the upper state in SOA is 1 ns, so the typical modulation bandwidth of the SOA is limited to only several GHz, which limits the application of SOA in high speed communications. The third drawback is the strong nonlinear effects in SOA, such as gain saturation SPM, XGM and FWM, which introduce a large amount of multichannel crosstalk in WDM (Wavelength Division Multiplexing) communication systems. Additionally, gain ripples due to residual facet reflectivity and polarization sensitivity can

also limit the deployment and efficiency of SOAs. As a result of the above factors, fibre amplifiers have dominated in the modern optical communication systems, while SOAs only have found some applications where they can be monolithically integrated, such as within the transmitter or receiver. Since late 1980s however, nonlinear effects in SOA have attracted increasing interest and have found some more potential applications utilizing the nonlinear effect in SOA. In the next part, the FWM effect is studied in two sections SOA and as well as its applications in optical communication.

3.3.2 FWM effect

FWM in an SOA is a third-order nonlinear effect and has attracted much interest since a late 1980s [8], [31], [32]. Because of its ultra high speed of response (up to THz) [33] and large operating wavelength range [11], [34], FWM in an SOA has been proposed as a technique for wavelength conversion, optical demultiplexing and also for clock recovery.

Figure 3.15 shows the experimental setup where two light beams, called the pump (with frequency ω_0) and probe (with frequency ω_1) respectively, are coupled into the SOA, which is then further coupled into the output spectrum of the SOA. This setup is similar to the setup in Figure 3.1 but in different nonlinear medium and it also used the third technique method measurement (with the pump wavelength being fixed and the signal wavelength being varied). It is due to has proved that the third technique is the best method to measure the nonlinear parameters for each fibre and waveguide. From the figure, two additional sidebands are observed to be generated at frequencies $2\omega_0 - \omega_1$ and $2\omega_1 - \omega_0$, respectively. As the pump and probe beams correspond to the clock and incoming data signals respectively in the transmission system, the input power of the pump beam is generally is

much higher than that of the probe beam. Therefore, the power of the sideband wavelength closer to the pump wavelength is much higher than that of the other sideband wavelength. In this work, the FWM or the FWM signal refers to the signal with the frequency $2\omega_0 - \omega_1$. In the measurement, the pump and probe beams emitting at frequency ω_0 and ω_1 are obtained from two single wavelength Distributed Feedback (DFB) lasers. Since the gain is polarization dependent in the case of the SOA and there is a birefringence effect in a bulk SOAs, two polarization controllers (PC) are used as shown in Figure 3.14 to adjust the polarization states of the input beams until the FWM signal reaches the maximum. The FWM signal intensity at the frequency of $2\omega_0 - \omega_1$ is measured by an OSA. Since the wavelength separation between the pump and the probe is generally quite small (less than 30 nm), the wavelength of the FWM beam is about $2\lambda_0 - \lambda_1$.

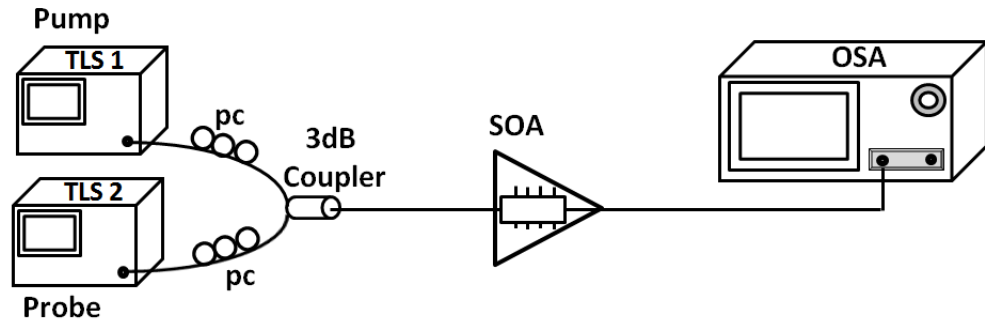


Figure 3.15 Experiment setup for measure FWM in the SOA.

A representation of the energy bands in the SOA is shown in Figure 3.16 and can help in the understanding of the generation of the FWM in a SOA. A beating signal with a frequency $\omega_0 - \omega_1$ is produced in the SOA due to the interaction between the pump and the

probe beam. This beating signal causes the oscillation of the carrier in the energy bands through interband process or intraband process and heats the carrier (oscillation of the carrier through interband process is called carrier density modulation, while through intraband process, is called the nonlinear gain effect [35]). In the intraband process, the wavelength separation is generally small; as such the quantum of the oscillation with energy $\hbar(\omega_0 - \omega_1)$ could be absorbed by an electron at the pump energy level shown in Figure 3.17, which will then jump to a higher energy level. When this electron makes a transition to the valence band, a FWM photon with energy $\hbar(2\omega_0 - \omega_1)$ is given out. This is a typical two-photon process. When the wavelength separation is large, the interband transition cannot respond to the beating signal, and in this case the two photon process used to generate the FWM signal will take place only within the conduction band, since intraband process can respond much faster to signals.

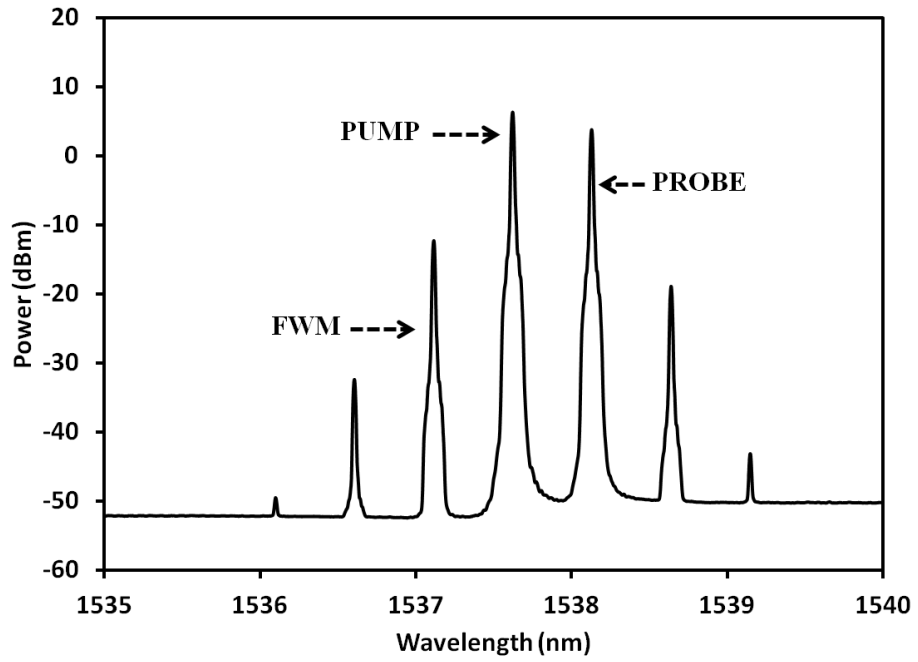


Figure 3.16 Optical spectrum of FWM after the SOA. The wavelength separation between the pump and the probe is 0.5 nm. The input power of the pump and probe beams is 12 dBm and 8 dBm, respectively. The wavelength of the FWM is about $2\lambda_{PUMP} - \lambda_{PROBE}$.

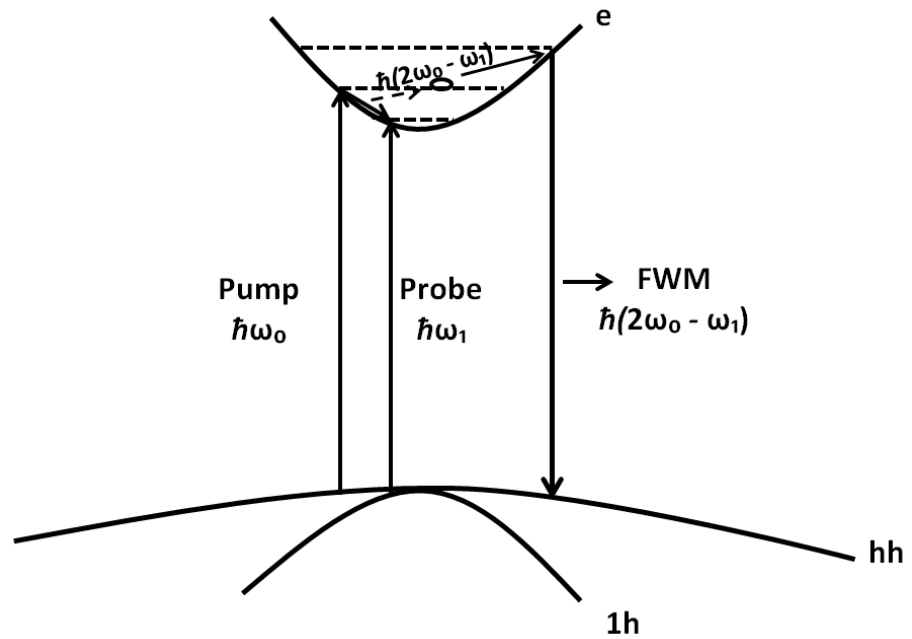


Figure 3.17: Picture of the FWM generation.

Figure 3.18 shows the FWM efficiency for different wavelength separation. The FWM efficiency, η is calculated from the measured value of I_{FWM} and I_I from setup in Figure 3.15 is given by:

$$\eta = I_{FWM}/I_I, \quad 3.14$$

where I_{FWM} and I_I are the FWM and the probe intensities respectively. The FWM signal power at a frequency of $2\omega_0 - \omega_1$ is approximately proportional to $(I_0)^2 I_1$ where I_0 and I_1 are the pump and probe intensities, respectively. The measured FWM efficiency (circle points) as a function of this wavelength separation is shown in Figure 3.17 when the pump wavelength is fixed. Based on the experimental result, the highest FWM efficiency of -7.2 dB is obtained at a wavelength separation of 0.7 nm. Also, the solid line shown is the numerical value calculated using typical parameter values. Both the experimental and calculated results show that the FWM efficiency is higher if the wavelength separation is smaller, and is asymmetric with respect to $\lambda_d = \lambda_1 - \lambda_0$.

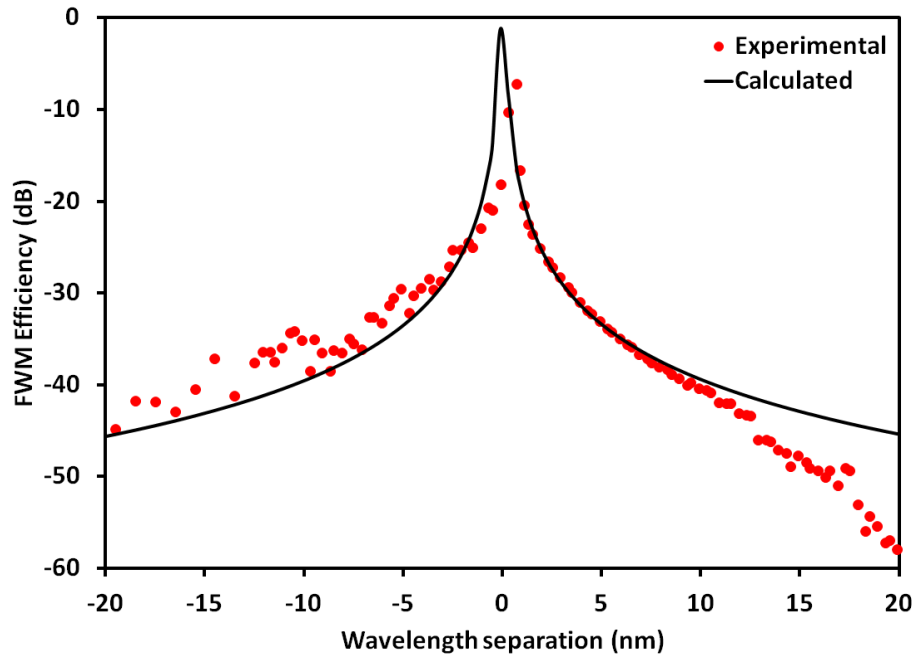


Figure 3.18 Measured FWM power (circled) as a function of the wavelength separation between the pump and the probe beams. The pump wavelength, input pump power and signal pump power of 1543 nm, 12 dBm and 10 dBm, respectively. The solid line is the calculated result using typical parameter values.

The FWM efficiency also depends on the gain of SOA as shown in Figure 3.14. With an increase in the current the gain in the SOA increases, thereby increasing the FWM efficiency. Figure 3.19 shows the highest FWM efficiency of -7.7 dB is achieved at an SOA current of 390 mA when using a wavelength separation between the pump and signal wavelengths of 0.7 nm with input pump power of 12 dBm and input signal power of 10 dBm. Furthermore, it also shows the SNR (signal to noise ratio) against the SOA current reaches 38.3 dB for an SOA current of 390 mA.

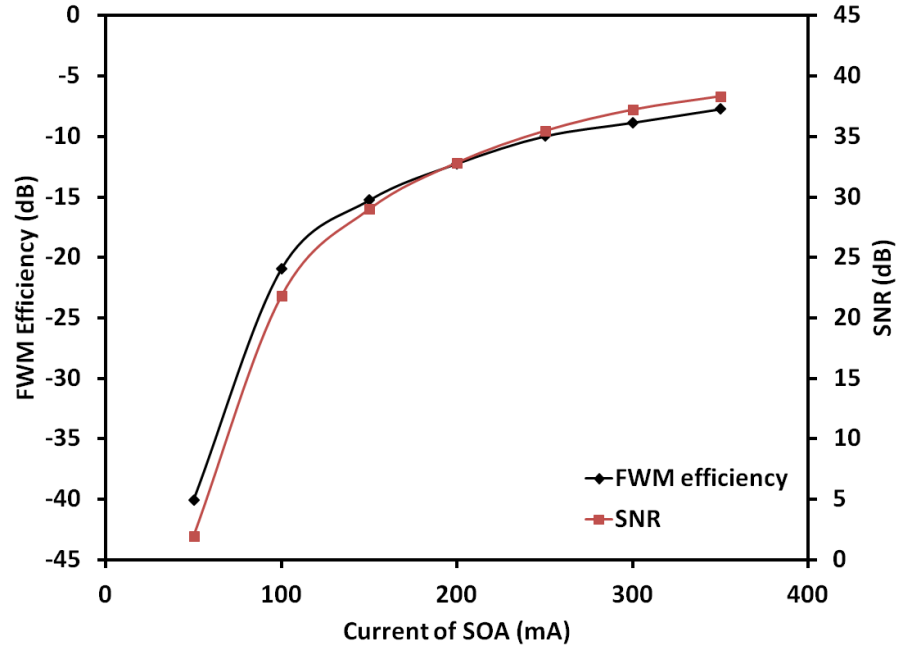


Figure 3.19 Measured FWM signal as a function of the total current of the SOA.

Wavelength separation between the pump and signal wavelength is 0.5 nm, input pump power of 12 dBm and input signal power of 10 dBm.

As discussed above, the mechanisms responsible for the generation of FWM in a SOA are carrier density modulation and nonlinear gain effects [35] [36]. The carrier density modulation has a time constant in the range of 0.1 to 0.5 ns. It also has been proposed that there are two kinds of nonlinear gain effects: dynamic carrier heating and spectral hole burning. The former has a time constant 0.6 ps, and the latter can occur on a faster time scale of less than 0.1 ps [32]. Due to the huge difference between the times constant, carrier density modulation only dominates the generation of FWM when the wavelength separation between the pump and the probe is less than 0.5 nm, while the nonlinear gain effect dominates when the wavelength separation is larger than 1.0 nm.

In this section, the FWM effect within the SOA is analysed in detail. The susceptibility χ is a tensor, which depends on the optical field intensity in the case of high input power. This could be described by expanding the susceptibility as a power series in the optical field E

$$\chi = \chi + \chi^2 E + \chi^3 EE + \dots, \quad 3.15$$

where χ is the small signal gain or linear susceptibility and χ^2 and χ^3 are the higher order nonlinear susceptibilities. The third order susceptibility χ^3 gives rise to all the significant nonlinear effects in a SOA such as FWM and SPM. The induced nonlinear polarization due to χ^3 could be expressed as

$$P = \varepsilon_0 \chi^3 EE \cdot E, \quad 3.16$$

For the FWM case, the third order susceptibility can be considered to come from the carrier density modulation due to the beating between the pump and the probe, so the equation can be written as

$$P = \varepsilon_0 \frac{\partial \chi(N)}{\partial N} n_1 \cdot E, \quad 3.17$$

where n_1 is the modulated carrier density and $N \gg n_1$. It has also been deduced that the susceptibility $\chi(N)$ is related to the carrier density N by [37]

$$\chi(N) = -\frac{nc}{\omega_0} (\alpha + i) g(N), \quad 3.18$$

where $g(N)$ is the gain defined as

$$g(N) = \frac{g_0}{1 + P/P_S},$$

where g_0 is small signal gain and P_S is saturation power. The quantity α is the linewidth enhancement factor, which is defined as

$$\alpha = \frac{\delta n_R}{\delta n_I}, \quad 3.19$$

where n_R and n_I are the real and the imaginary parts of the refraction index.

In FWM, the pump and probe beating frequency

$$\omega_d = \omega_0 - \omega_1, \quad 3.20$$

is relatively small. The pump beam is generally much more intense than the probe beam, i.e., $E_1 \ll E_0$ (E_0 , E_1 correspond to the electrical field of the pump and probe). The carrier density N is described by the following rate equation in the SOA when a current I is applied,

$$\frac{dN}{dt} = \frac{I}{eV} - \frac{N}{\tau_c} - \frac{g(N)}{H\omega_0} |E|^2, \quad 3.21$$

where τ_c is the carrier lifetime. Since the length of the SOA is typically less than 1 mm, phase matching conditions can be considered satisfied for the pump and probe power, thus The optical field can be described as follows

$$E = E_0 \exp(-i\omega_0) + E_1 \exp(-i\omega_1 t). \quad 3.22$$

Therefore,

$$|E|^2 = |E_0|^2 + |E_1|^2 + 2\{E_0^* E_1 \exp[-i(\omega_0 - \omega_1)t]\}. \quad 3.23$$

It is expected that the carrier density will also be modulated by the beating frequency ω_d , such that:

$$N(t) = \bar{N} + n_1 \exp(-i\omega_d t). \quad 3.24$$

Since $E_1 \ll E_0$, it have $\bar{N} \gg n_1$, substituting 3.23 and 3.24 into 3.21 will give

$$\bar{N} = \frac{\frac{I}{eV} \tau_c + \frac{|E_0|^2}{P_S} N_t}{1 + \frac{|E_0|^2}{P_S}}$$

and,

$$n_1 = \frac{-(\bar{N} - N_t) \frac{E_0^* E_1}{P_S}}{1 + \frac{|E_0|^2}{P_S} - i\omega_d \tau_c}. \quad 3.25$$

By substituting equation 3.18 and 3.25 into the equation 3.17, the induced nonlinear polarization due to the beating signal between the pump and the probe in the SOA can be obtained.

The optical fields in the SOA satisfy the Maxwell's equation,

$$\nabla^2 E - \frac{n^2}{c^2} \frac{\partial^2 E}{\partial t^2} = \frac{1}{\epsilon_0 c^2} \frac{\partial^2 P}{\partial t^2}. \quad 3.26$$

In the FWM process, generally $I_{FWM} \ll I_1 \ll I_0$ where I_{FWM} , I_0 , I_1 are the FWM, the pump and the probe power, respectively. Substituting equation 3.17 into 3.26 gives us the coupled equations for the electric fields of the pump, the probe and the FWM beam [37],

$$\frac{dE_0}{dZ} = \frac{1}{2} g(1 - i\alpha) E_0,$$

$$\frac{dE_1}{dZ} = \frac{1}{2} g(1 - i\alpha) E_1,$$

$$\frac{dE_{FWM}}{dZ} = \frac{1}{2} g(1 - i\alpha) E_{FWM} - \frac{1}{2} g \sigma E_1^* E_0^2,$$

and,

$$\sigma = \frac{1 - i\alpha}{1 + \frac{|E_0|^2}{P_s} - i\omega_d \tau_c} \cdot \frac{1}{P_s} + \frac{1 - i\beta}{1 - i\omega_d \tau_n} \cdot \frac{1}{P_n}, \quad 3.27$$

where P_n , τ_c and τ_n are the relaxation time constant corresponding to carrier density modulation and nonlinear gain effects, respectively, and the other terms have been defined earlier. B is the ratio of the real and imaginary parts of the refractive index change induced

by gain nonlinearity. The gain g is defined by equation 3.18 if we are considering the gain saturation.

If $I_0(0) < I_S$, it neglects the $|E_0|^2/I_S$ term in the denominator of σ . Also, for $g \equiv g_0$, the equations for E_0 and E_1 are easily solved and substituting the solutions into the equation for E_{FWM} , as follows:

$$\frac{dE_{FWM}}{dZ} = AE_{FWM} - Be^{CZ}, \quad 3.28$$

where

$$A = \frac{1}{2}g(1 - i\alpha),$$

$$B = \frac{1}{2}g \left[\frac{1 - i\alpha}{1 - i\omega_d\tau_c} \cdot \frac{1}{P_S} + \frac{1 - i\beta}{1 - i\omega_d\tau_n} \cdot \frac{1}{P_n} \right] \cdot I_0(0) \cdot E_1(0), \text{ and}$$

$$C = \frac{1}{2}g(3 - i\alpha). \quad 3.29$$

$I_0(0)$ and $E_1(0)$ are the pump intensity and the field of the probe at $Z=0$, respectively. Using the boundary condition, $E_{FWM}(Z=0) = 0$, the solution of the above is

$$E_{FWM}(Z) = \frac{B}{A - C}(e^{CZ} - e^{AZ}). \quad 3.30$$

Thus the FWM power at $Z=L$ is

$$I_{FWM} = E_{FWM}(L) \cdot E_{FWM}^*(L). \quad 3.31$$

Therefore, the expression of the CW FWM power is:

$$I_{FWM} = \frac{1}{4} \left| \frac{1 - i\alpha}{1 - i\omega_d \tau_c} \cdot \frac{1}{P_s} + \frac{1 - i\beta}{1 - i\omega_d \tau_n} \cdot \frac{1}{P_n} \right|^2 I_0^2(0) I_1(0) f(G), \quad 3.32$$

where $G = e^{gL}$ is the total gain of SOA

$$f(G) = G^3 - G. \quad 3.33$$

In the above calculation, the absorption loss as well as the reflection loss on the interfaces between the insertion and active areas has been neglected. Although many simplifying assumptions have made, the above equation is still a good approximation if for reasonable values of the total gain of the SOA. The calculated I_{FWM} (solid curve) used the typical parameter values such as $\tau_c = 352$ ps, $\tau_n = 0.48$ ps, $P_s = 10$ mW, $I_0(0) = 12$ dBm, $I_1(0) = 10$ dBm and $G = 13$ dB in equation 3.32. Figure 3.14 shows the calculated values of FWM efficiency obtain when used the FWM power by using equation 3.32. Based on equation 3.32, the FWM power will increase if the pump power increase. The FWM power is also proportional to the $f(G)$, thus the CW power is higher in SOA with high gain, which is consistent with the result shown in Figure 3.15.

It can also be seen in Figure 3.14 that, the calculated results shows that the FWM power on the up conversion side ($\lambda_d > 0$) is higher than that of the down conversion side ($\lambda_d < 0$) for the same absolute value of λ_d . This because for $\lambda_d > 0$, the effect of carrier density modulation and nonlinear gain in the generation of the FWM add constructively [35], while for $\lambda_d < 0$, the two mechanism counteract each other, which results in minimum FWM efficiency, especially when λ_d is about -0.1 nm. It also shows that for $\lambda_d > 1.0$ nm, the mechanism of carrier density modulation could be neglected and the nonlinear gain effects dominate in the generation of the FWM signal.

3.4 Summary

In this chapter, the nonlinear parameters of HNLF and SOA are discussed. In the case of the HNLF, three techniques to generate and modify the FWM effect such as varying the pump and signal wavelength, varying the pump and fixing the signal wavelength and fixing the pump and varying the wavelength is used to determine the best way to characterize the nonlinear parameters such as ZDW, CD and nonlinear coefficient. This was followed by a description of the gain performance of ultra wide band SOA using the ASE of SOA for different currents, gains and noise figures. By using these parameters, the gain saturation of this SOA is obtained to determine the nonlinear characterise such as nonlinear coefficient and FWM power of SOA. In the next chapter, applications of nonlinear media are investigated using two different gain media of HNLF and SOA. Various configurations of FWM effects will be proposed and demonstrated for wavelength converters, amplifiers and multiwavelength applications.

Reference

- [1] J. A. Armstrong, N. Bloembergen, J. Ducuing, and P. S. Pershan, "Lightwave interact", Phys. Rev., vol. 127, pp. 1918-1939, 1962.
- [2] G. P. Agrawal, 3rd Edition of Nonlinear fibre optics, Academic Press, San Diego, 2001.
- [3] Y. Yamamoto, K. Iga, K. Yamamoto and K. Morito, Handbook of integrated optics, Tayloc and Francis, 2006.
- [4] Ivan Avrutsky and Richard Soref, "Phase-matched sum frequency generation in strained silicon waveguides using their second-order nonlinear optical susceptibility," Opt. Express, vol. 19, pp. 21707-21716, 2011.
- [5] R. W. Boyd, Nonlinear optics, Academic Press, San Diego, CA, 1992.
- [6] J. Hansryd, P. A. Andrekson, M. Westlund, J. Li and P. Hedekvist, "Fiber based optical parametric amplifiers and their applications," IEEE J. Sel. Tp. Quantum Electronics, vol. 8, pp. 506-519, 2002.
- [7] O. Aso, S. Arai, T. Yagi, M. Tadakuma, Y. Suzuki and S. Namiki, "Broadband four wave mixing generation in short optical fibers," Electron. Lett., vol. 36, pp. 709-711, 2000.
- [8] G. P. Agrawal, "Population pulsation and nondegenerate four wave mixing in semiconductor lasers and amplifiers," J. Opt. Soc. Amer. B, vol. 5, pp. 147-159, 1988.
- [9] M. P. Dlubek, S. N. Kaunga-Nyirenda, A. J. Phillips, S. Sujecki, I. Harrison and E. C. Larkins, "Experimental verification of the existence of optically induced carrier pulsations in SOAs," Opt. Commun., vol 283, pp. 1481-1484, 2010.

- [10] G. P. Agrawal, "Highly nondegenerate four wave mixing in semiconductor lasers due to spectral hole-burning," *Appl. Phys. Lett.*, vol. 51, pp. 302-304, 1987.
- [11] J. Zhou, N. Park, K. J. Vahala, M. A. Newkirk and B. I. Miller, "Four wave mixing wavelength conversion efficiency in semiconductor travelling-wave amplifier measured to 65 nm of wavelength shift," *IEEE Photon Technol. Lett.*, vol. 6, pp. 984-987, 1994.
- [12] A. Mecozzi, S. Scotti, A. Dottavi, E. Iannone and P. Spano, "Four wave mixing in travelling wave semiconductor amplifier," *IEEE J. Quantum Electron.*, vol. 31, pp. 689-699, 1995.
- [13] A. Dottavi, E. Iannone, A. Mecazzi, S. Scotti, P. Spano, R. Dall'Ara, J. Eckner and G. Guekos, "Efficiency and noise performance of wavelength converters based on FWM in semiconductor optical amplifier," *IEEE Photon. Technol. Lett.*, vol. 7, pp. 357-359, 1995.
- [14] C. Vinegoni, H. Chen, M. Leblac, G. W. Schinn, M. Wegmuller and N. Gisin, "Distributed measurement of chromatic dispersion and nonlinear coefficient in low-PMD dispersion-shifted fibers," *IEEE Photon. Technol. Lett.*, vol. 15, pp. 739-741, 2003.
- [15] P. S. Andre A. L. J. Teixeira, M. Lima, J. F. da Rocha and J. L. Pinto, "Nonlinear refractive index and chromatic dispersion simultaneous measurement in non zero dispersion shift optical fibers," *ICTON*, pp. 111-114, 2002.
- [16] D. Marcuse, A. R. Chraply and R. W. Tkach, "Effect of fiber nonlinearity on long-distance transmission," *J. Lightwave Technol.*, vol. 9, pp. 121-128, 1991.

- [17] S. E. Mechels, J. B. Schlager and D. L. Franzen, "Accurate measurements of the zero-dispersion wavelength in optical fibers," J. Res. Natl. Inst. Stand. Technol. 102, pp. 333-347, 1997.
- [18] C. Mazzali, D. F. Grosz and H. L. Frahnito, "Simple method for measuring dispersion and nonlinear coefficient near the zero dispersion wavelength of optical fibers," IEEE Photon. Technol. Lett., vol. 11, pp. 252-253, 1999.
- [19] D. H. Kim, S. H. Kim, J. C. Jo, S. K. Kim and S. S. Choi, "Novel measurement of linear dispersion slope near the zero dispersion wavelength for four wave mixing," Proceedings of Nonlinear Optics'98, pp. 168, 1998.
- [20] L. Prigent and J. P. Hamaide, "Measurement of fiber nonlinear kerr coefficient by four wave mixing," IEEE Photon. Technol. Lett., vol. 5, pp. 1092-1096, 1993.
- [21] H. Chen, "Simultaneous measurement of non linear coefficient, zero-dispersion wavelength and chromatic dispersion in dispersion-shifted fibers by four-wave mixing," Opt. Commun., vol. 220, pp. 331-335, 2003.
- [22] K. Inoue, "Four-wave mixing in the zero-dispersion wavelength regions," J. Lightwave Technol., vol. 10, pp. 1553-1561, 1992.
- [23] J. X. Feng and Z. X. Min, "Determination of zero-dispersion wavelength by four-wave mixing," J. Chin. Phys. Lett., vol. 23, pp. 1507-1510, 2006.
- [24] N. Shibata, R. P Braun and R. G. Warrts, "Phase-mismatch dependence of efficiency of wave generation through four-wave mixing in a single mode fiber," IEEE J. Quantum Electron., QE-23, pp. 1205-1211, 1987.
- [25] K. Inoue, "Experimental study on channel crosstalk due to fiber four-wave mixing around the zero-dispersion wavelength", J. Lightwave Technol., vol. 12, pp. 1023-1028, 1994.

- [26] S. E. Mechels, J. B. Schlager and D. L. Franzen, "Accurate measurement of the zero-dispersion wavelength in optical fibers," J. Res. Natl. Inst. of Stand. Techno., vol. 102, pp. 333-347, 1997
- [27] C. Mazzali, D. F. Grosz, and H. L. Fragnito, "Simple method for measuring dispersion and nonlinear coefficient near the zero-dispersion wavelength of optical fibers," IEEE Photonics Technology Letters, vol. 11, pp. 251-253, 1999.
- [28] T. Saitoh, T. Mukai, "Gain saturation characteristics of travelling-wave semiconductor laser amplifiers in short optical pulse amplification," IEEE J. Quantum Electron, vol. 26, pp. 2086-2094, 1990.
- [29] S. Ruiz-Moreno, J. Guitart, "Behavior of a travelling wave semiconductor optical amplifier," IEEE Proceedings-J, vol. 140, pp. 39-43, 1993.
- [30] M. J. Connelly, Semiconductor optical amplifiers, Kulwer Academic Publishers, Dordrecht, 2004.
- [31] G. P. Agrawal, "Four-wave mixing and phase conjugation in semiconductor laser media," Optics Lett., vol. 12, pp. 260-262, 1987.
- [32] F. Favre and D. L. Guen, "Four wave mixing in traveling wave semiconductor laser amplifier," IEEE J. Quantum Electron., vol. 26, pp. 858-864, 1990.
- [33] J. Zhou, N. Park, J. W. Dawson and K. J. Vahala, "Terahertz four-wave mixing spectroscopy for study of ultrafast dynamics in a semiconductor optical amplifier," Appl. Phys. Lett., vol. 63, pp. 1179-1181, 1993.
- [34] A. D'ottavi, P. Spano, G. Hunziker, R. Paiella, R. Dall'Ara, G. Guekos and K. J. Vahala, "Wavelength conversion at 10 Gb/s by four wave mixing over a 30 nm interval," IEEE Photonics Technol. Lett., vol. 10, pp. 952-954, 1998.

- [35] L. F. Tiemeijer, "Effect of nonlinear gain on four wave mixing and asymmetric gain saturation in a semiconductor laser amplifier," *Appl. Phys. Lett.*, vol. 59, pp. 499-501, 1991.
- [36] K. Kikuchi, M. Kakui, C. E. Zah and T. P. Lee, "Observation of highly non-degenerate four wave mixing in 1.5 μm travelling-wave semiconductor optical amplifiers and estimation of nonlinear gain coefficient," *IEEE J. Quantum Electron.*, vol. 28, pp. 151-156, 1993.
- [37] G. P. Agrawal, N. K. Dutta, 2nd edition *Semiconductor laser*, Van Nostrand Reinhold, NY, 1993.

CHAPTER 4

WAVELENGTH CONVERSION USING FWM EFFECT

4.1 Introduction

The use of FWM for wavelength conversion attracted considerable attention during the 1990s because of its potential application in WDM lightwave systems [1] – [5]. Wavelength conversion is a key requirement in realizing an all-optical system. It also ensures future seamless network evolution that can provide the switching of wavelengths from long haul system to access network without the need to convert from optical signal to an electrical one. The function of a wavelength converter is to convert one or more of wavelengths from a WDM network into a desired wavelength or group of wavelengths without significant distortion in the output signals. There are many optical wavelength conversion techniques that have been reported such as the use of the nonlinear behaviour in the HNLF and also the use of SOA as a nonlinear medium, to name a few. The common approach in achieving wavelength conversion is through XPM [6] [7], XGM [8] [9] and through FWM [10] – [13]. Among these methods, FWM provides advantages approach due to its simplicity and unique characteristics of providing the preservation of amplitude and phase, data format and bit rate transparencies.

A large number of the FWM effect in this chapter is generated by using a dual-wavelength fibre laser for wavelength conversion. The dual-wavelength fibre laser used in this thesis is

more cost effective and inexpensive as compared to the TLS. It allows for a smooth wavelength tuning over a wide range and has high performance stability. In the first part of this chapter, the discussion will focus on the generation of a dual-wavelength fibre laser and subsequently will move on to wavelength conversion via FWM in HNLF and SOA.

4.2 Dual-wavelength fibre laser

The generations of dual-wavelength fibre lasers have attracted considerable interests especially for possible application as alternative laser sources for wavelength division multiplexing (network) and wavelength conversion. Generally, these lasers operate with an erbium doped fibre (EDF) as the active gain medium. Interest in the erbium doped fibre is primarily due to its compact size and simplicity. There is an issue in generating multiwavelength outputs from EDF which is largely due to the homogeneous broadening exhibited by this material. This inhibits operation of more than one wavelength due to the gain competition. To overcome this, many methods have been used such as cooling the EDF in liquid nitrogen [14] [15], using hybrid gain medium and sagnac loop mirror [16] – [20], elliptical EDF [21] [22], cavity loss controlled [23] [24] and self injected laser diode, [25] [26] among others [27] – [29]. In this section, the generation of a stable dual-wavelength fibre laser using an arrayed waveguide grating (AWG) in a ring cavity is demonstrated. This dual-wavelength fibre laser can be tuned from 18.1 nm to 0.8 nm with the output power of -3 dBm. To obtain the stable dual-wavelength fibre laser, the cavity loss control method is used for this research.

The configuration of the proposed setup of the tunable dual-wavelength fibre laser with a ring configuration is shown in Figure 4.1 [30]. The dual-wavelength fibre laser uses a 5 m metrogain EDF with absorption coefficients of 11.9 dB m^{-1} at 979 nm and 16.4 dB m^{-1} at 1531 nm as a gain medium. A 980 nm laser diode with a pump power of 110 mW is connected to the EDF via a 1550/980 nm wavelength division multiplexer (WDM) coupler. The propagation of the 980 nm pump light through the WDM coupler to the EDF creates an Amplified Spontaneous Emission (ASE) which then circulates inside the cavity in a clockwise direction. This ASE is then filtered as it enters an Arrayed Waveguide Grating (AWG) which works as a multiplexer that slices the ASE source into 16 different channels in the C-band region. The AWG has been optimized for use in the C-band region with a 100 GHz narrow band transmission which is equivalent to a 0.8 nm of interval spacing (from two adjacent channels). There are 16 lasing wavelengths from channels 1 (1536.7 nm) to 16 (1548.6 nm). The output of the dual-wavelength fibre laser is then connected to the variable coupler which acts as a cavity controller. One leg of the variable coupler is connected to an OSA and the other leg provides feedback for the laser by connecting it to the 1550 nm input port of the WDM coupler. An isolator is inserted to ensure a unidirectional propagation of the laser inside the cavity and also to enhance the Side Mode Suppression Ratio (SMSR) by compressing the backward ASE for full optimization of the master laser output power.

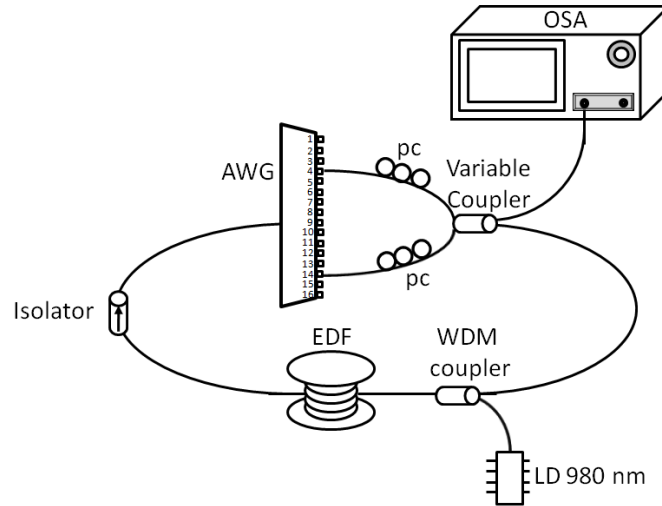


Figure 4.1 The experimental setup for tunable dual-wavelength fibre laser [30].

Figure 4.2 shows the characterization of one of the 24 channels of the AWG with the input beam having a broad spectrum spanning from 1250 nm to 1600 nm (from a white light source). From the figure, multiple wavelengths output were observed at different channels tested. These include of output wavelengths at 1271.35 nm, 1309.15 nm, 1349.75 nm, 1392.8 nm, 1438.3 nm, 1487.3 nm, 1539.45 nm and 1595.8 nm with an average peak power of -72 dBm. Different channels will have a similar behaviour of producing three peaks at different wavelengths.

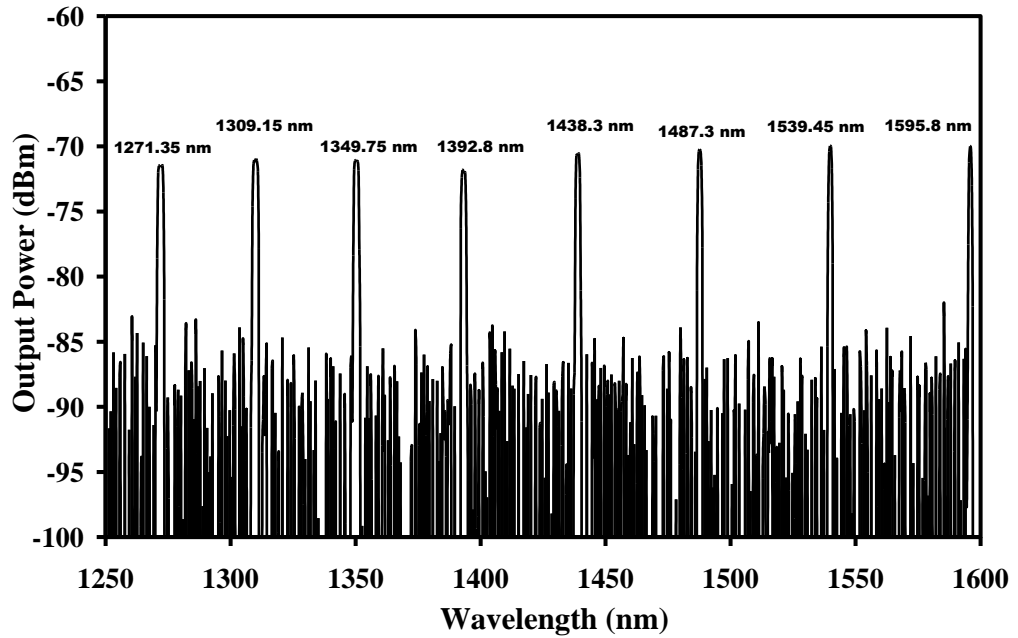


Figure 4.2 Characterization of AWG by using white light source, with outputs at a particular channel [30].

Figure 4.3 shows the different channel combinations such as 9 and 24, 10 and 23 until towards channel 16 and 17. It gave the narrowest tunable spacing of about 0.8 nm (channels 16 and 17) to the widest spacing of 12.4 nm (channels 9 and 24). Since this design is specifically for C-band region, lasing was observed from channels 9 to 24 at wavelengths 1536.7 nm to 1548.6 nm. Employing a longer gain medium and a higher pump power, a wider tuning range can be achieved.

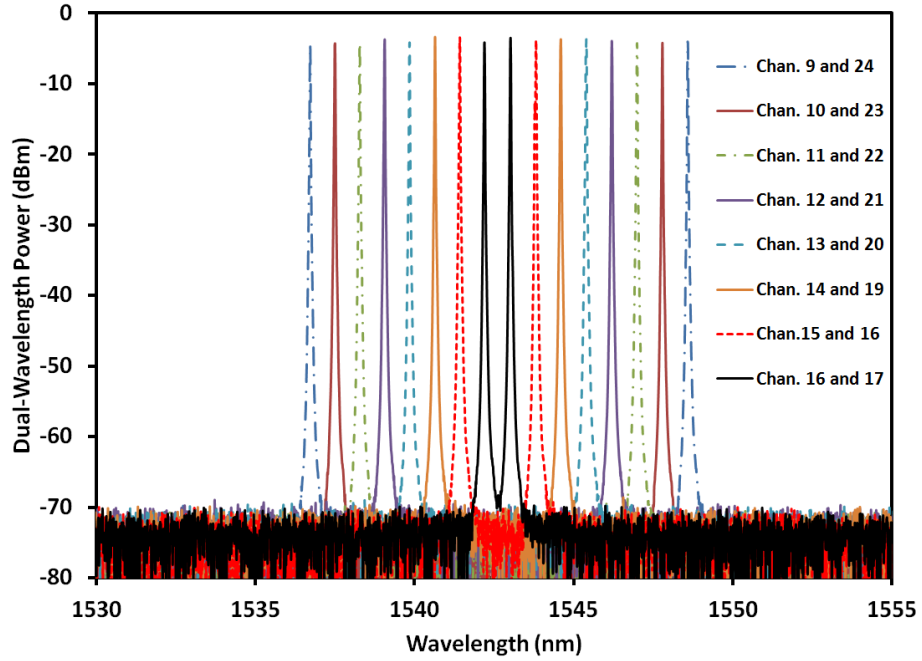


Figure 4.3 The dual-wavelength with channels spacing [30].

The output power of the dual-wavelength fibre lasers and its SMSR is shown in Figure 4.4. They are taken in pairs, such as channels 9 and 24, channels 10 and 23, channels 11 and 22 and subsequently channels 16 and 17. The average output power is about -3.74 dBm and has a power variation among the channels of less than 2 dB. This can be further improved by fine tuning the variable attenuator, and nearly equal amplitude of the dual-wavelengths peaks can be achieved. On the other hand, the average value of the SMSR is about 66.8 dB giving an indication that the signals are of good optical quality with a SMSR variation among the channels of less than 2 dB.

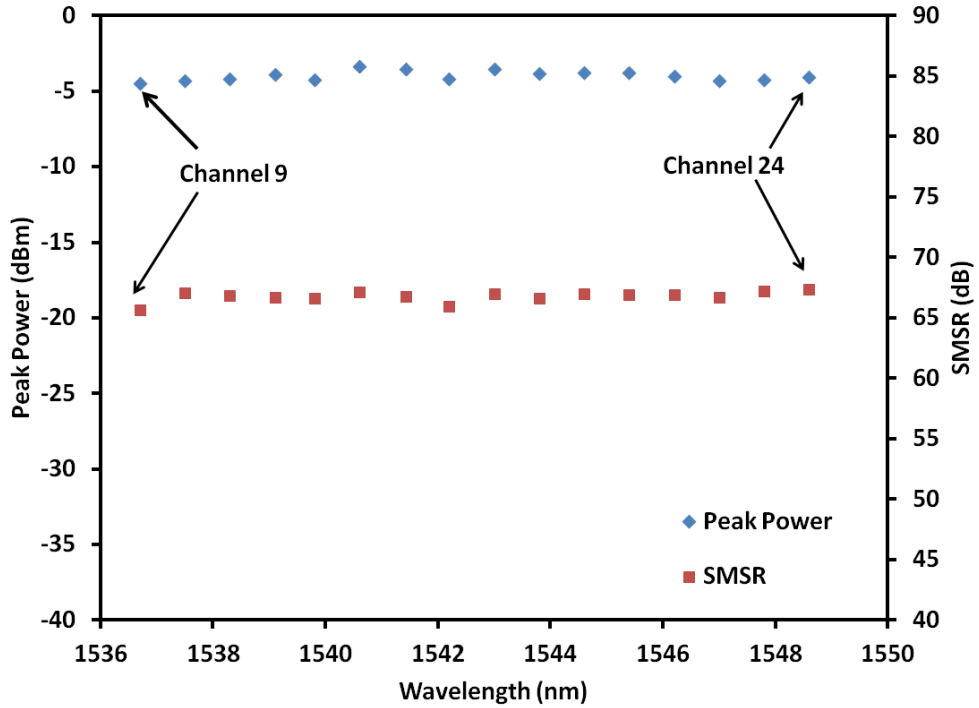


Figure 4.4 SMSR and peak power with different wavelength channels (dual-wavelength output are taken as 9 and 24, 10 and 23, 11 and 22 and soon) [30].

In this section, a dual-wavelength fibre laser using an EDF as a linear gain medium in combination with an AWG in to provide the necessary channel spacing tunability is demonstrated. The output power of the dual-wavelength fibre laser is balanced by controlling the cavity loss in the dual-wavelength fibre laser by using variable coupler. The widest spacing obtained from the dual-wavelength fibre laser is 11.9 nm from channel 9 at 1536.7 nm to channel 24 at 1548.6 nm while the narrowest spacing was obtained at approximately 0.8 nm from channel 16 at 1542.2 nm to channel 17 at 1542.0 nm. The SMSR of the dual-wavelength fibre laser is approximately 66.8 dB with fluctuations of less than 2 dB, indicating good stability for numerous applications. The advantage of this

system is its ability to generate an equal powered and stable dual-wavelength output from a homogenously broadened gain medium by carefully controlling the cavity losses in the setup. The next stage of this research is to elaborate on the role of the dual-wavelength fibre laser used in HNLF and SOA for wavelength conversion application.

4.3 FWM effect in HNLF

Following the discussion on the production of a dual-wavelength fibre laser, wavelength conversion can now be investigated. The specification of the nonlinear fibre that has been used in the thesis is discussed in detail in chapter 3. In this section, the discussion is divided into two subsections, namely, the generation of wavelength conversion by using a dual-wavelength fibre laser and the best configuration of wavelength conversion generation when used two tunable lasers source.

4.3.1 The generation of a wavelength conversion in HNLF by using a dual-wavelength fibre laser.

In this part, the generation of a wavelength conversion in HNLF by using a dual-wavelength fibre laser is described [31]. Figure 4.5 shows the proposed ring cavity experimental setup which uses an 11 m of Metrogain erbium doped fibre from Fibercore as an ASE source as well as the gain medium. The EDF has an Erbium ion concentration of 900 ppm and absorption coefficients of 18.06 dB m^{-1} and 11.3 dB m^{-1} at 1530 nm and 980 nm, respectively. In this experimental setup, a high-power EDFA pumped with a 980 nm

wavelength light from two semiconductor laser diodes is demonstrated. The outputs from the two 980 nm pump LD modules are 215 mW each. They are combined using a polarization beam combiner (PBC). The output is then connected to the ring cavity via a 980/1550 nm WDM coupler and directed into the ring cavity. The combined pump power that travels in a clockwise direction is then absorbed by the EDF. The emission of the C-band ASE output from the EDF will travel through a 1x24 AWG and is sliced into 24 individual output wavelengths from each channel output. The 1x24 channels output will cover the wavelength range from 1530.473 nm to 1548.613 nm with an interchannel spacing of 100 GHz. Two selected channels from the AWG outputs are connected to the polarization controllers for output optimization before being connected to a 2x1 variable optical coupler. The variable optical coupler is connected to an optical isolator to complete the ring cavity which allows the light to propagate in single direction only. In the AWG channels, the signal wavelength is fixed at 1548.6 nm (channel 24) and the pump wavelength is varied from 1530.5 nm (channel 1) to 1545.4 nm (channel 23). The chosen channels are then connected to the variable optical coupler via a PC as illustrated in Figure 4.5. The PC is used to maximize the matching of the polarization state of a pump and signal power. The dual-wavelength fibre laser is generated at the output port of the variable optical coupler and travels in a clockwise direction and will be amplified again by the gain medium. The high output power from the dual-wavelength fibre laser will travel through the 100 m HNLF which acts as the nonlinear medium to generate the FWM output wavelength. Finally, the output end of the HNLF is connected to a 90/10 coupler with the 10% port connected to an optical spectrum analyzer (Yokogawa AQ6370B) and the 90% port completes the loop by connecting to the AWG.

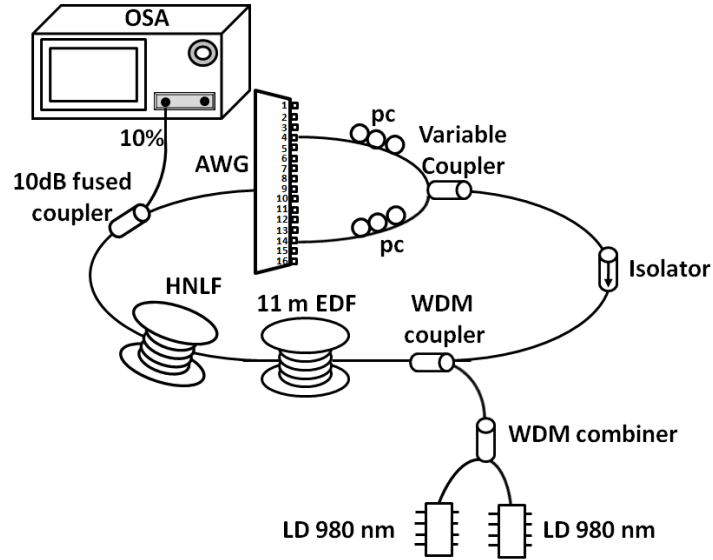


Figure 4.5 Schematic diagram for generating FWM in a HNLf using a dual-wavelength fibre laser incorporating AWG as the tuning element [31].

The dual-wavelength fibre laser provides the required source for generating the converted signal based on FWM in the highly nonlinear optical fibre in the ring cavity as shown in Figure 4.6. The generation of this converted signal depends on the power of the pump and signal wavelengths where a strong pump transfers its energy to create this converted signal as shown in Figure 4.6. To achieve the highest converted signal output power, the pump power should be higher than the signal power and this can be done by controlling the cavity loss using a variable optical coupler. Hence, the highest output power of the converted signal of -16.8 dBm is obtained when the pump and signal powers are set at +13.3 dBm and +5 dBm respectively. From Figure 4.6, it can be inferred that the converted signal power increases when the pump power approaches the signal power. In addition, an additional idler wavelength is generated when the pump power is almost the same as the signal power.

This is due to the fact that the power of the first idler which is enough to generate the additional idler wavelength.

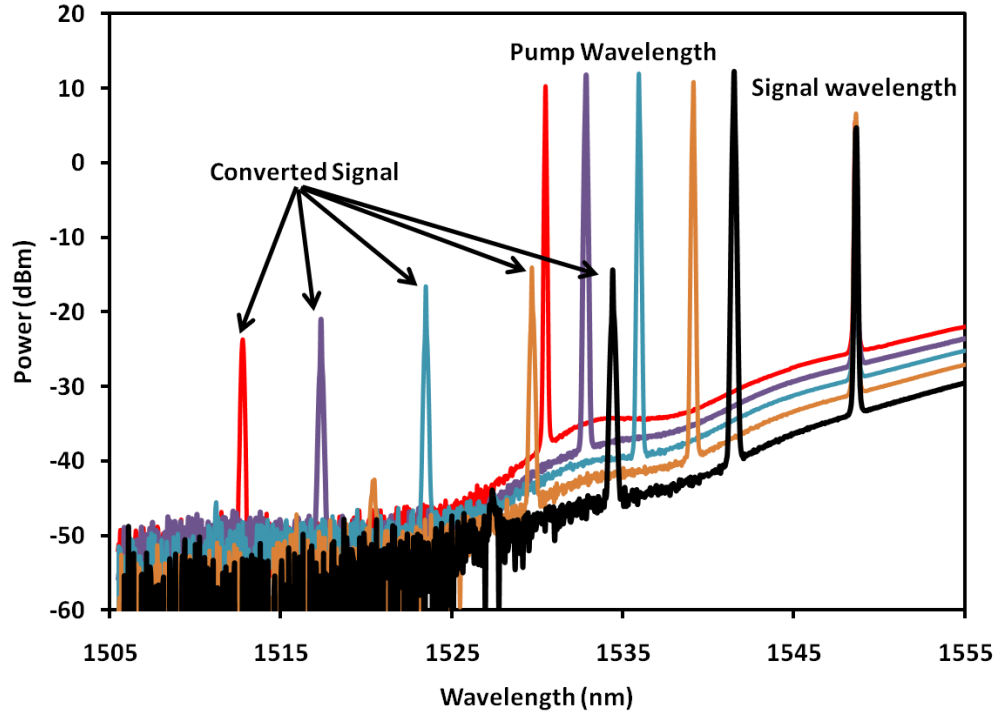


Figure 4.6 Spectra of the FWM at different pump wavelengths for different AWG channels [31].

In Figure 4.7, the FWM conversion efficiency of the dual-wavelength fibre laser as a function of wavelength detuning is plotted based on theoretical and experimental values. The squares represent the experimental data while the curve is a trend line fitted to the data. The maximum FWM conversion efficiency has been fitted to the experimental data. As shown in Figure 4.7, a FWM conversion efficiency of roughly -12 dB is obtained. Measurements of the FWM conversion efficiency from the spectrum was obtained by using OSA and is shown in Figure 4.8, where the FWM conversion efficiency is given as

$\eta(\text{dB}) = P_{\text{signal}}(\text{dBm}) - P_{\text{FWM}}(\text{dBm})$. The calculation of the FWM conversion efficiency depends on the phase mismatch around the ZDW. However, the FWM conversion efficiency obtained experimentally rapidly decreases when the wavelength detuning exceeds 12 nm which is 3 nm shorter than the calculated value of 15 nm. A possible reason for this discrepancy is the larger phase mismatch experienced at larger wavelength separation [32]. Theoretically, the FWM conversion efficiency is higher when the pump wavelength is at the ZDW. Conversely, from the experiments which were carried out, the FWM conversion efficiency at the ZDW at the same wavelength detuning is lower compared to the one in the 1560 nm region due to the higher ASE level in this region as shown in Figure 4.9. This is due to the fact that the emission from the 11 m EDF is being shifted to a longer wavelength. In short, the use of the longer EDF contributes to a higher output power which will enhance the FWM effect. However, the maximum FWM conversion efficiency has shifted to a longer wavelength, specifically to the 1560 nm region. In this experiment, the work to measure the FWM conversion efficiency curve in the 1560 nm region is limited by the operating wavelength of AWG which covers the wavelength range from 1530.5 nm to 1548.6 nm.

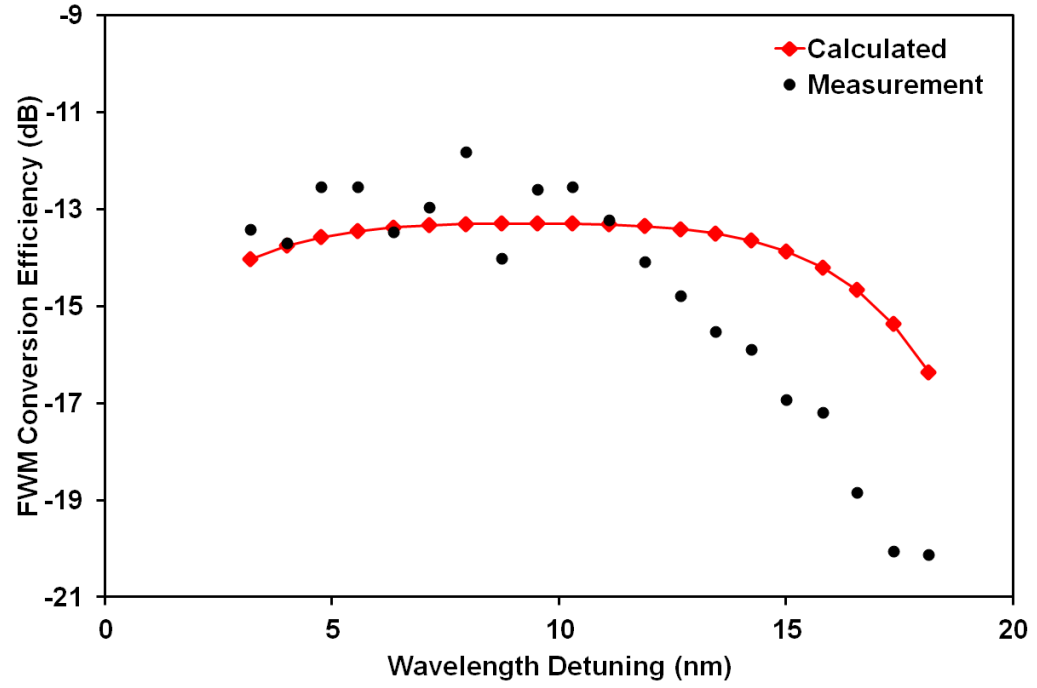


Figure 4.7 FWM conversion efficiency versus wavelength detuning in HNLF [31].

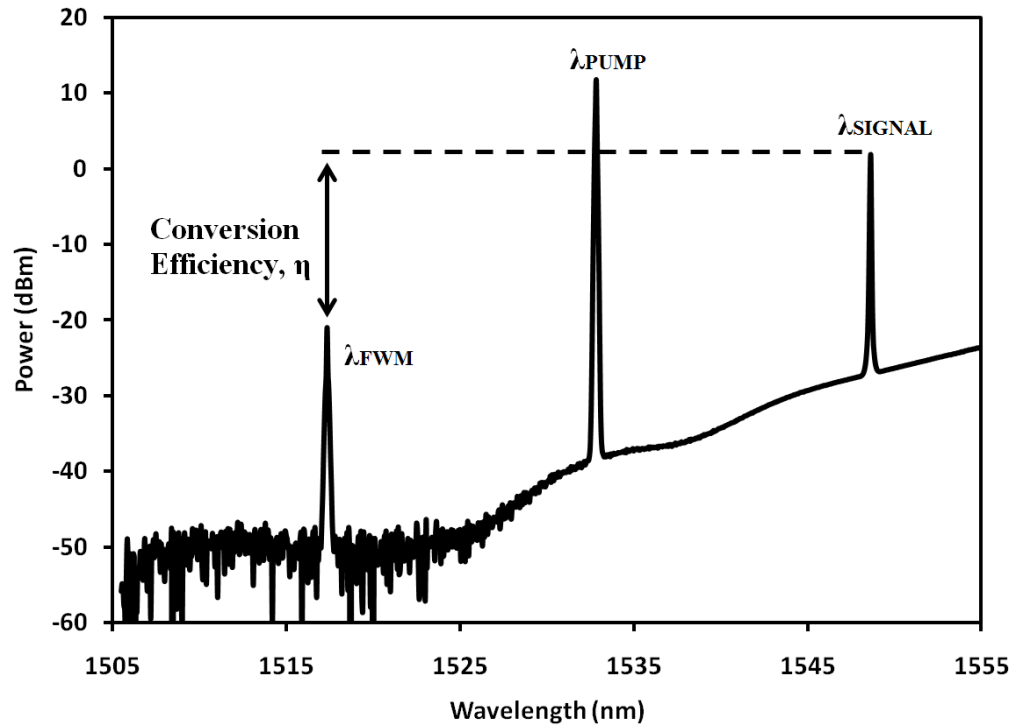


Figure 4.8 Measurement of conversion efficiency in the OSA [31].

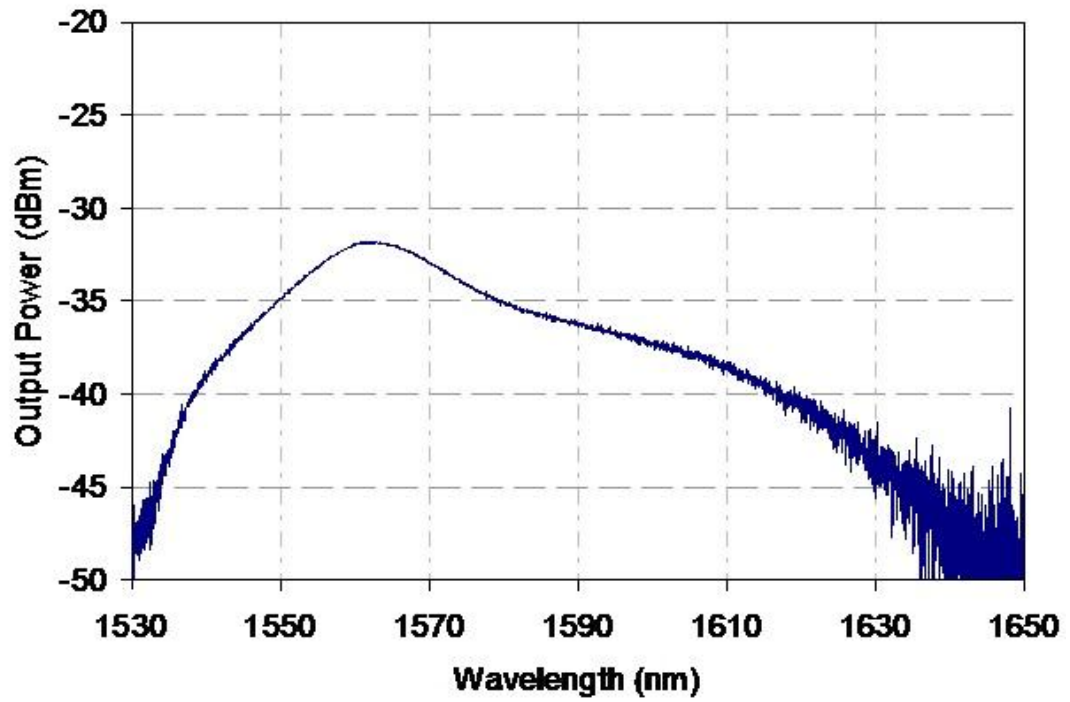


Figure 4.9 The ASE spectrum of the 11m metrogain EDF [31].

The FWM output power obtained from both calculations and experimental data is presented in Figure 4.10. It shows that the FWM output power is around -22 dBm when the wavelength is varied from 5 nm to 15 nm, with the input pump and signal powers set at +13.3 dBm and +5 dBm, respectively. However, the FWM output power obtained from measurements varies from -16 dBm to -20 dBm with a wavelength detuning from 3 nm to 18 nm, respectively. The output power slowly decreases when the wavelength detuning is increased and this can be expected from our calculation.

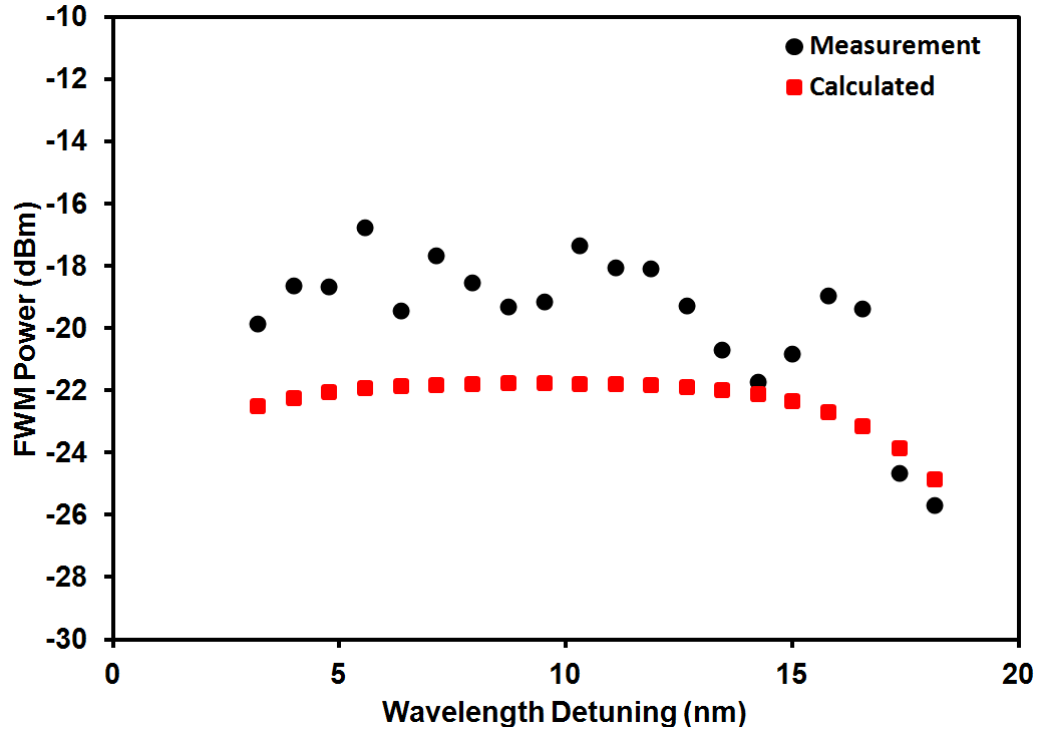


Figure 4.10 FWM output power versus wavelength detuning between pump and signal [31].

Figure 4.11 shows the variation of conversion efficiency of FWM with pump power for a wavelength detuning of 8 nm in a HNLF with a length of 100 m. The conversion efficiency of FWM is proportional to the pump and signal power as shown in Figure 4.11. Since the fibre laser power plays an important role in the generation of FWM, it is important to have a high pump power to obtain the high conversion efficiency of FWM. A power of 21.4 mW (+13.3 dBm), for example, is required to obtain a conversion efficiency of -11 dB. However, if the pump power is less than 1 mW, the conversion efficiency drops by about 19 dB compared to the maximum value.

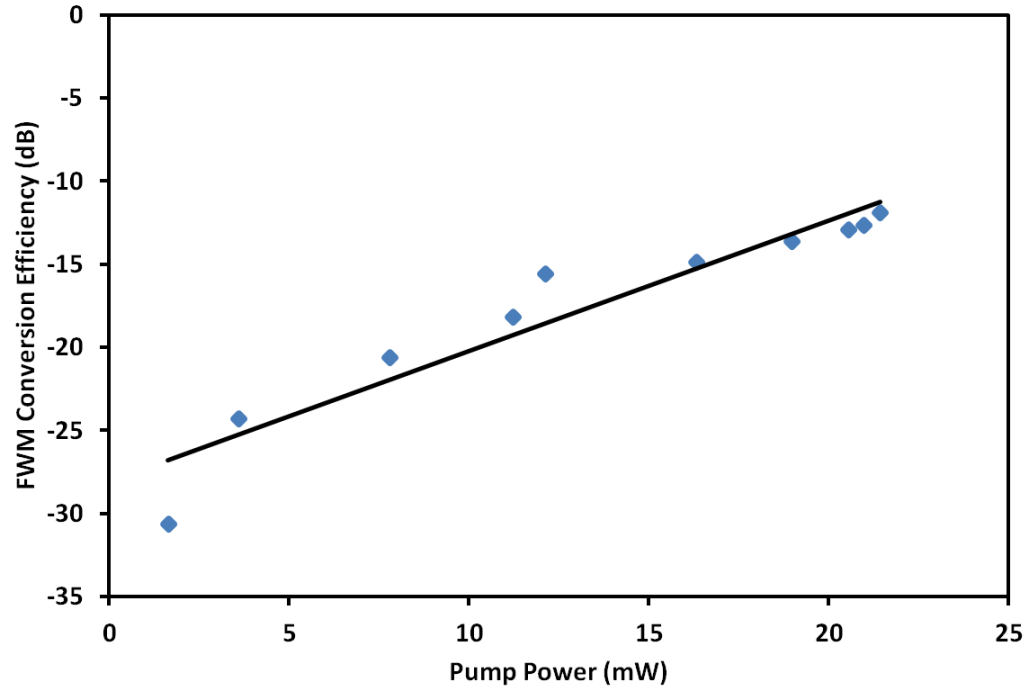


Figure 4.11 FWM output power versus input pump power [31].

Figure 4.12 shows the SNR of the converted signal against the wavelength detuning. Our results show that the SNR varies between 30 dB and 40 dB with a wavelength detuning of up to 15 nm. Figure 4.12 also shows that closer wavelength detuning results in lower SNR because the peak of the FWM product power overlaps with the ASE generated by the EDF. The characteristics of the FWM in dual-wavelength fibre laser of the HNLF are important for wavelength conversion to avoid distortion of the output signal.

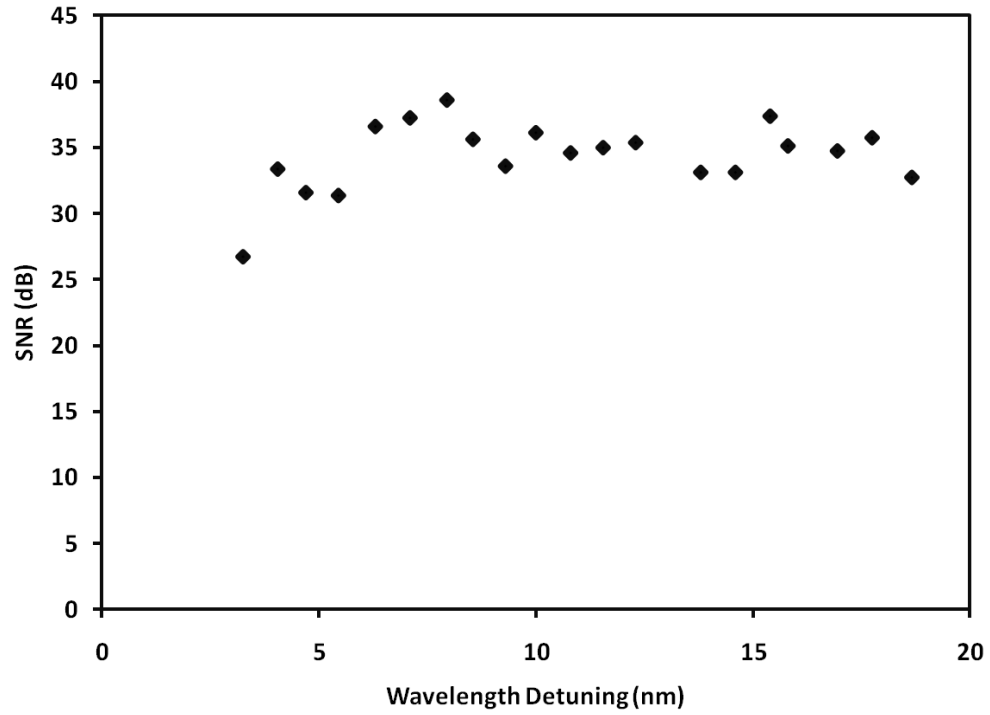


Figure 4.12 Optical signal to noise ratio versus wavelength detuning [31].

The proposed experiment obtained an higher conversion efficiency, at -11 dB, as compared to others researchers whose using two independent tunable laser sources (TLS) in generating four wave mixing effect in nonlinear fiber, having the conversion efficiency of -20 dB [33] and -13 dB [34], taken at the same nonlinear coefficient. This indicates that the dual-wavelength fibre laser can be employed as a device to generate FWM in the HNLF for wavelength conversion applications.

4.3.2 Wideband wavelength conversion in HNLF

In this part, a novel S+C+L tunable wavelength conversion via a dual-wavelength fibre laser in a HNLF is demonstrated. The widely tunable wavelength conversion operates with only one external pump laser. Generally, in FWM light of three different wavelengths are launched into a fiber, giving rise to a new wavelength (known as an idler). The wavelength of the idler does not coincide with the other input signals. Usually, most researchers such as Z.G. Lu [35] and Y. P. Yatsenko [36] used tunable laser source as their pump and signal source for obtain the new wavelength by using FWM effect in the highly nonlinear fiber. Z.G. Lu demonstrated the 380 nm ultra broadband wavelength converter based on co-polarized dual pumping FWM technique in a photonic crystal fiber. However, the TLS is not cost effective due to the availability of fiber laser. Recent work [37], [38] uses similar configuration from a single ring to a double ring, and having Semiconductor Optical Amplifiers (SOAs) as the non-linear gain medium for the observation of the FWM effect. Their range is limited to 40 nm only. As well as SOAs, a 100 m length of dispersion shifted fiber is also used as the non-linear medium with a dual-wavelength fiber laser as the pump and signal source [39]. Their wavelength conversion range however is only limited to the C-band region.

In this paper, we demonstrate a novel wideband wavelength conversion using a dual-wavelength fiber laser in a highly non-linear fiber (HNLF) with a high non-linear coefficient combined with a numerically small group dispersion velocity. The fluorine-doped fiber has a high delta core and is surrounded by a deeply depressed ring and thus is not based on the photonic crystal structures. This is an extension of our earlier work [31], which gives an interesting experimental result of a wide-band, tunable wavelength

conversion range from 1460 nm to 1640 nm as it is to the author's knowledge the longest wavelength conversion and hopping range to date, based on simple HLNFs, although there are wider ranges that have been obtained using HNL-PCFs. Additionally, the proposed setup employs the use of an AWG that allows for efficient channel selection and therefore the highest wavelength conversion efficiency.

Figure 4.13 shows the same proposed of ring configuration as with the earlier experimental setup which uses 11 m of Metrogain erbium doped fibre (DL1500L, Fibercore Ltd.) as the medium for amplified spontaneous emission (ASE) as well as the gain medium. The light outputs from the two 980 nm pump LD modules are 215 mW each where they are combined using a polarization beam combiner (PBC). The output is then connected to the ring cavity via a 980 /1550 nm WDM coupler and directed into the ring cavity. The combined pump power that travels in a clockwise direction is then absorbed by the EDF. The erbium ions will be excited and will then reemit an optical output at 1550 nm in the form of the ASE. From the measurement, the average ASE output power is 20.2 dBm with an output emission in the C-band. The emission of C-band ASE output from the EDF will then travel through a 1x24 AWG which will be sliced into 24 individual output wavelengths coming from 24 channels. The channels are then connected to a variable optical coupler via a PC as illustrated in Figure 4.13, where it is used to optimize the matching of the polarization state of pump and signal powers. The dual-wavelengths fibre laser is generated at the output port of the 2x1 variable optical coupler and travels in the clockwise direction. The dual-wavelength that has been created is then combined with a TLS by using another 50/50 fused coupler. In this experiment, the most suitable dual-wavelength fibre laser is chosen by oscillating the dual-wavelength fibre laser without

injecting the signal from the TLS. In this situation, the dual-wavelengths which are combined by a 2x1 variable optical coupler will be amplified by an EDFA and further generate a FWM effect in the HNLF, simultaneously. The highest value of the FWM conversion efficiency is selected by tuning the AWG's channel. This is one of the novelties of this configuration in which the dual-wavelength fibre laser can give the highest FWM conversion efficiency in the nonlinear fibre can be selected independently as provided by the AWG channels. Through this selection, channels 11 and 15 gave the highest value of FWM conversion efficiency when compared to other channels as shown in Figure 4.14. Therefore, channels 11 and 15 which are at 1541.54 nm and 1538.3 nm are selected as pump and signal wavelengths. The TLS, whose polarization can be adjusted with the incorporation of PC's, is subsequently launched into the cavity. This TLS is denoted as a pump wavelength with an average output power of 10.8 dBm and it can be tuned from 1400nm to 1680nm with a linewidth of 0.015 nm. The combination of the dual-wavelength and the TLS created three wavelengths inside the ring cavity which is then amplified by the EDFA to produce the triple wavelengths output power necessary in generating the FWM effect. At this point, the triple wavelength acts as a signal and pump to produce multiple wavelengths output as the light propagates in the 100 m highly nonlinear fibre by virtue of the FWM effect. The output of the HNLF is tapped out from the 90/10 coupler where a larger portion of light is allowed to oscillate in the ring cavity. The output spectrum is measured using an OSA (Yokogawa AQ6370B) with a resolution 0.002nm.

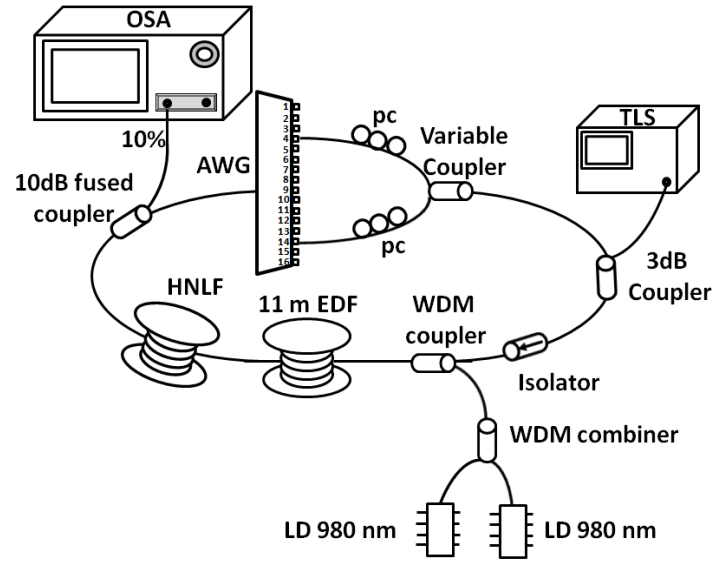


Figure 4.13 Schematic diagram for generating FWM effect in a HNLF using dual-wavelengths fibre laser incorporating AWG as a tuning element.

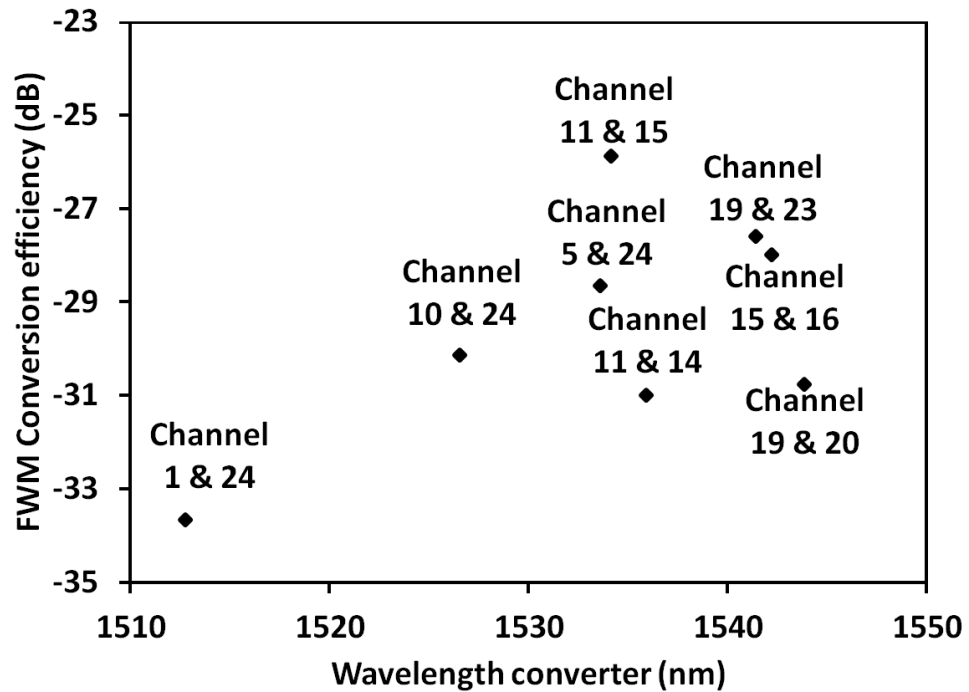


Figure 4.14 The value of FWM conversion efficiency for different AWG's channels.

In this experiment, the generated triple wavelength is a combination of the dual-wavelength fibre laser and TLS and is shown in Figure 4.15 where it is marked as pump 1, signal and pump 2, respectively. Due to the beating of pump 1, signal and pump 2, they experience an index-modulated grating within the HNLF. This process generates two sidebands C2 (a conjugate of signal) and S2 (a replica of signal) around pump 2, divided by a spacing of Δf and having the states of polarization of pump 2. In this experiment, the intensities of C2 and S2 are measured for every different wavelength of pump 2 over the entire wavelength range of between 1460 nm to 1640 nm with 100 GHz of detuning depending on the spacing of the signal and pump 1. The intensities of two sidebands C2 and S2 also depend on the dual-wavelength operation where channel 11 (1538.3 nm) and channel 15 (1541.5 nm) are selected as pump 1 and signal, respectively. Figure 4.15 shows the typical output spectrum of pump 1, pump 2 and signal that creates FWM after passing through the HNLF. The pump 1, signal and pump 2 wavelengths of 1538.3 nm, 1541.5 nm and 1530 nm with injected powers of 10.3 dBm, 5 dBm and 3.86 dBm, respectively are used.

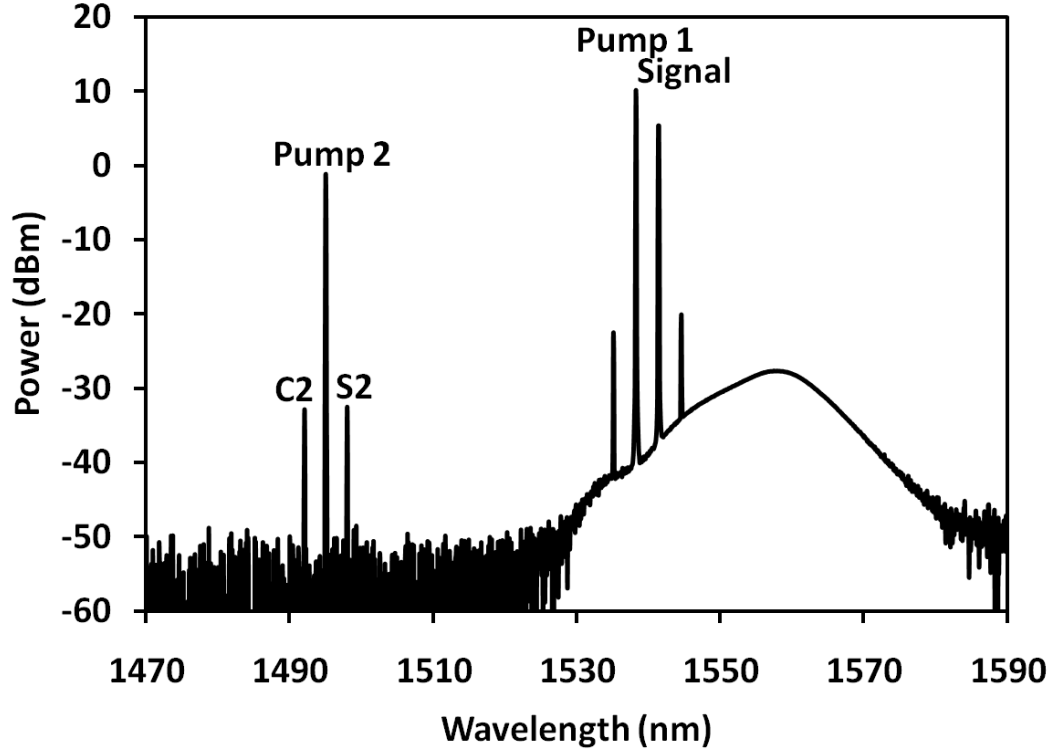
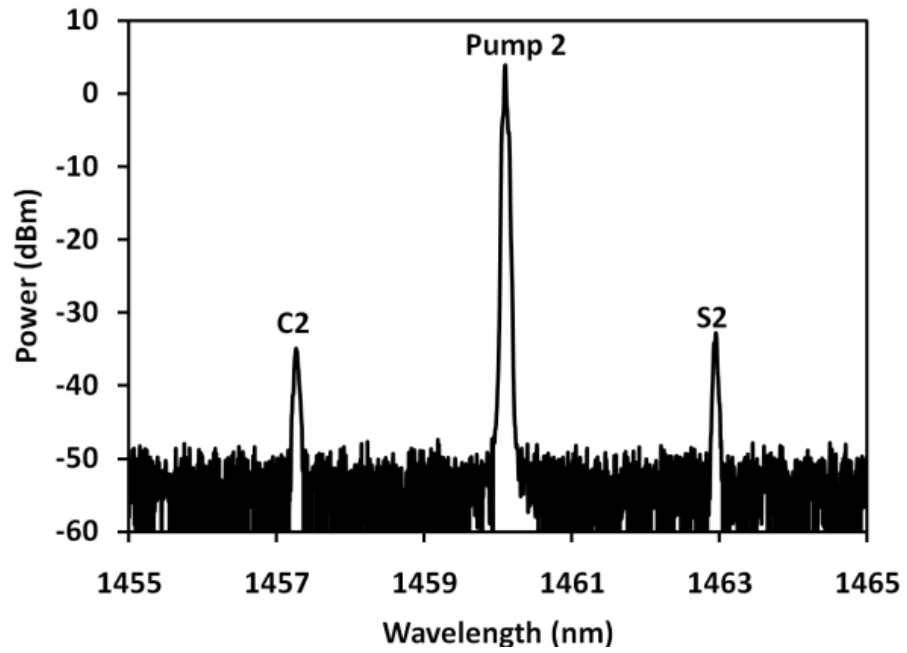
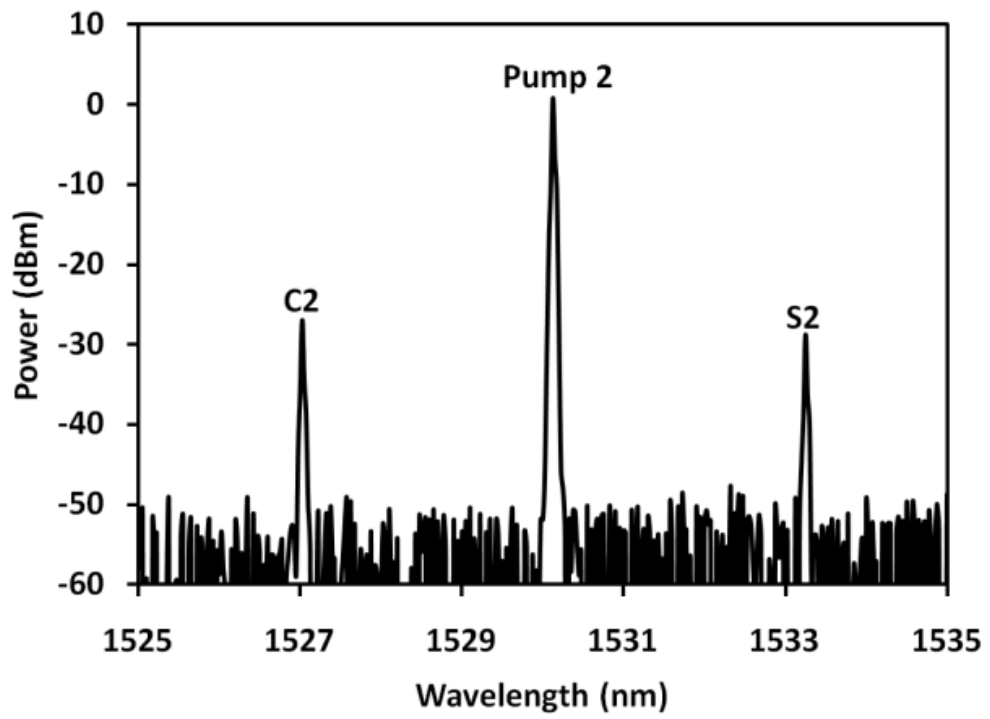


Figure 4.15 The typical output spectra at pump 1, signal and pump 2, as well as their converted signals (sideband fields) C2 and S2 when wavelength of pump 1, signal and pump 2 are 1538.3 nm, 1541.5 nm and 1530 nm.

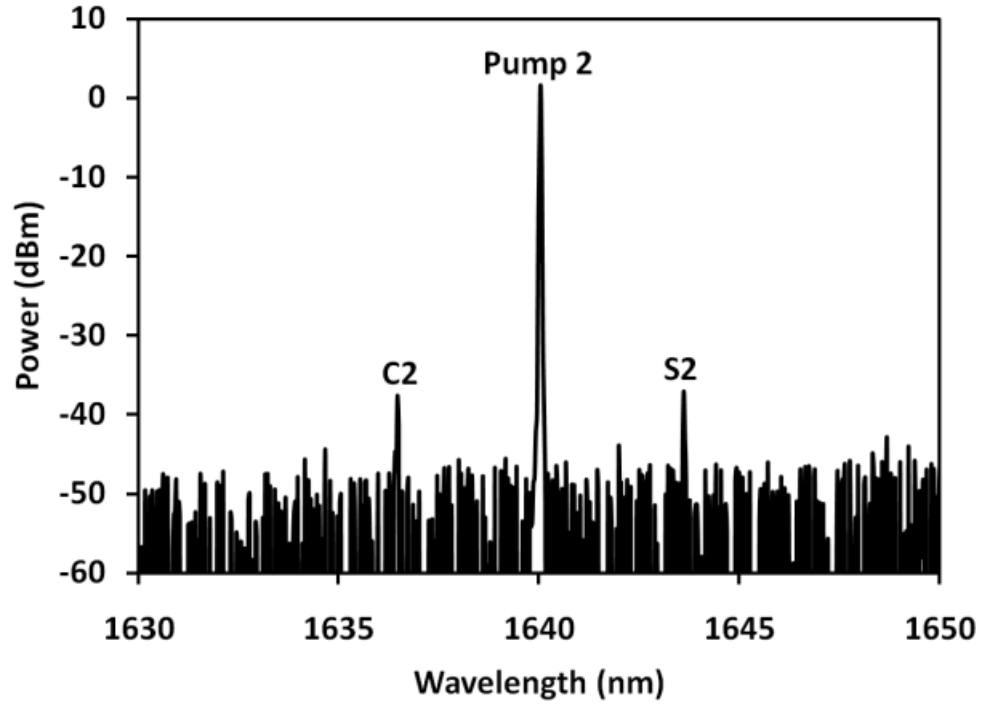
To investigate the tunability of the proposed wavelength conversion technique, the input powers of pump 1 and signal are fixed at 10.3 dBm and 5 dBm, at wavelengths of 1538.3 nm and 1541.5 nm, respectively. The wavelength of pump 2 is then changed from 1460 nm to 1640 nm by using the TLS. The converted signals C2 and S2 are observed through the whole tuning range (1460 nm to 1640 nm). Figure 4.16 (a), (b) and (c) show the output spectra of S2, pump 2 and C2 at different wavelength values. Our results presented below clearly show that by using the proposed the ultra-broadband tunable wavelength conversion configuration with a tunable range of over 180 nm can be achieved.



(a)



(b)



(c)

Figure 4.16 The output spectra of S2, Pump 2 and C2 when the wavelength of Pump 1 and signal are 1538.3 nm and 1541.5 nm; (a) Pump 2 is 1460 nm and their input power is 3.86 dBm; (b) Pump 2 is 1530.2 nm and their input power is 3.00 dBm; (c) Pump 2 is 1640 nm and their input power is 3.36 dBm.

The efficiency of the proposed configuration, certain characterization of FWM such as the conversion efficiency and the SNR are measured from results shown in Figure 4.17. The conversion efficiency is obtained by changing the wavelength of pump 2 while keeping pumps 1 (1538.3 nm) and signal (1541.5 nm) at a constant 10.3 dBm and 5 dBm, respectively. During the measurement, the input pump power of pump 2 is about 3 dBm and its wavelength changes from 1460 nm to 1640 nm. The maximum power of the converted wavelength is obtained by adjusting the three PCs as shown in Figure 4.13 for

each measurement. The conversion efficiency is calculated as a ratio of the power of the converted signal C2 to the input signal. Results indicate that the FWM conversion efficiency is approximately -20 dB within the 70 nm tuning range with a 3 dB fluctuation. However, as the converted wavelength is tuned over the 70 nm tuning range, the conversion efficiency drops rapidly due to the effect of chromatic dispersion in the fibre as stated by K. Inoue [40]. The figure also shows the optical signal to noise ratio (SNR) versus wavelength that shows the SNR being maintained above 30 dB at around the 70 nm tuning range. The SNR is stable between the wavelengths of 1470 nm to 1550 nm, and drops rapidly at longer wavelengths. This indicates that the data signal within this region can be converted efficiently. However, conversion can still be realized at longer wavelengths with a higher degree of degradation. This can be improved by using higher pump and signal powers which cannot be realized at this moment due to the limitations of the high power laser.

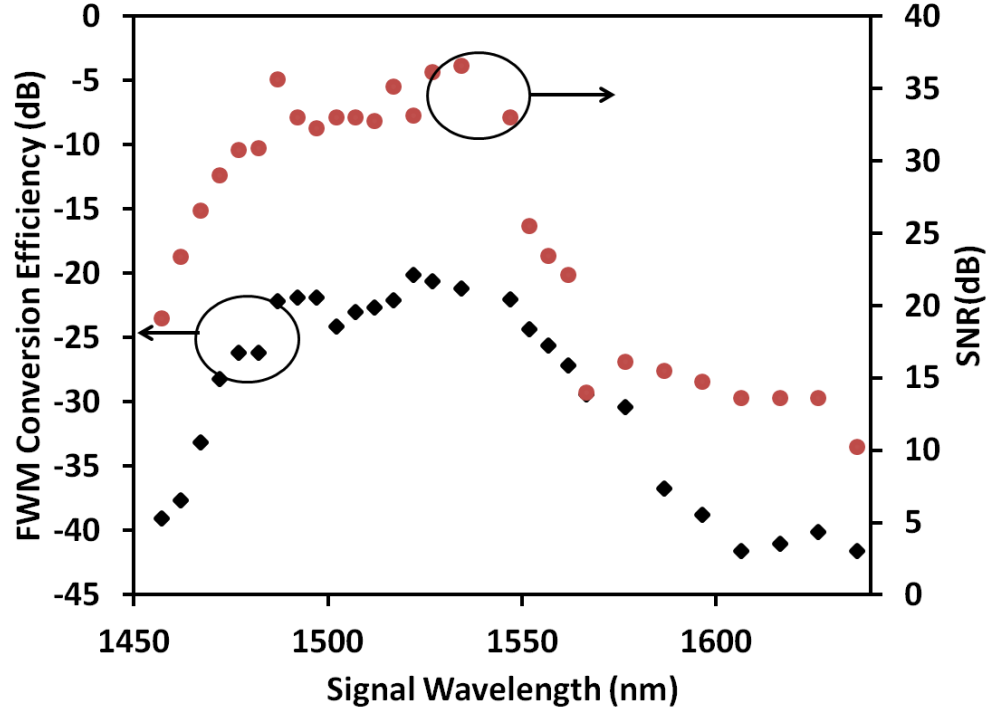


Figure 4.17 The conversion efficiency and the optical signal to noise ratio against the converted.

4.3.3 FWM Effect in ring configuration

The final discussion section of HNLFs is the generation of wavelength conversion in the ring configuration by using 2 TLSs with a lower pump power than the previous configuration [41]. One of the key issues in FWM is the conversion efficiency, whereby a recent work by Petit et. al. [42] uses a high power laser operating at 28 dBm to generate the FWM effect in a HNLF. The conversion efficiency achieved is only -5 dB in a 120 m length of HNLF with the nonlinear coefficient of $\gamma = 12 \text{ W}^{-1}\text{km}^{-1}$. Similarly, works by Dahan et. al. [43] also obtained a conversion efficiency of -5 dB while using a high pump power and a signal laser operating at 22 dBm in a 1000 m HNLF (nonlinear coefficient

$\gamma = 10.5 \text{ W}^{-1}\text{km}^{-1}$). The pump power of this proposed setup is lower, at 12.8 dBm, as compared to similar system using HNLF, having an average output power of 28 dBm [42] and 21.3 dBm [43], taken at the same conversion efficiency. Therefore, this system is simple and not cost effectively for the communication system.

As discussed above these methods require high power lasers with a long length of HNLF. In this part, an effective method is proposed whereby a lower pump power and signal are used in 100 m HNLF giving higher conversion efficiency of -4 dB and also a better SNR ratio of 43 dB. An additional interesting result of this work is that the FWM conversion efficiency is as broad as 20 nm of the 3 dB bandwidth.

Figure 4.18 shows a schematic structure of the FWM embedded within a HNLF in a ring configuration. The main components are an erbium-doped fibre which acts as an optical amplifier, a 100 m long HNLF, an optical circulator and an output coupler. The EDFA consists of the 11m Metrogain erbium doped fibre (DF1500L, Fibercore Ltd.) where it is pumped by a laser diode with pump power of 90 mW at 1490 nm. The other components are an isolator 2 which forces the oscillation in a counter-clockwise direction, an optical circulator that provides a means of injecting the dual-wavelength input into the ring cavity and a 90/10 coupler to extract the signal into the OSA.

The input signal for the FWM in the HNLF configuration is taken from two TLSs with a pump wavelength, P_P , at 1590 nm and output power of 12.8 dBm is used. The other signal, which is referred to as the input signal, P_S , is from another TLS with an output power of 10.8 dBm and the input signal wavelength tuned from 1570 nm to 1600 nm. An output linewidth of these TLSs are roughly 0.015 nm. Both of these signals are made to pass through a polarization state to synchronize the two signals to satisfy phase matching

condition in the HNLF. These two signals then combine with a 3dB coupler where the output port is connected to port 1 of the optical circulator via the isolator 1. This combination signal of dual-wavelength (P_P and P_S) is then emitted into port 3 of the circulator in the ring cavity. This setup takes advantage of the low isolation loss of the circulator from port 1 to port 3. The circulator principal should ideally give the highest isolation lost from port 1 to port 3. However, in reality, the isolation is just about 45 dB which lead to the signal leakage from port 1 to port 3. The combined signal will travel to the EDFA to be amplified and then travels to the HNLF to generate the required FWM. Careful adjustments of the PCs are required so as to provide the right conditions necessary for phase matching, which will then generate a new wavelength from the FWM process. The output signal is detected using an OSA which is connected to the 10% port of the 90/10 coupler.

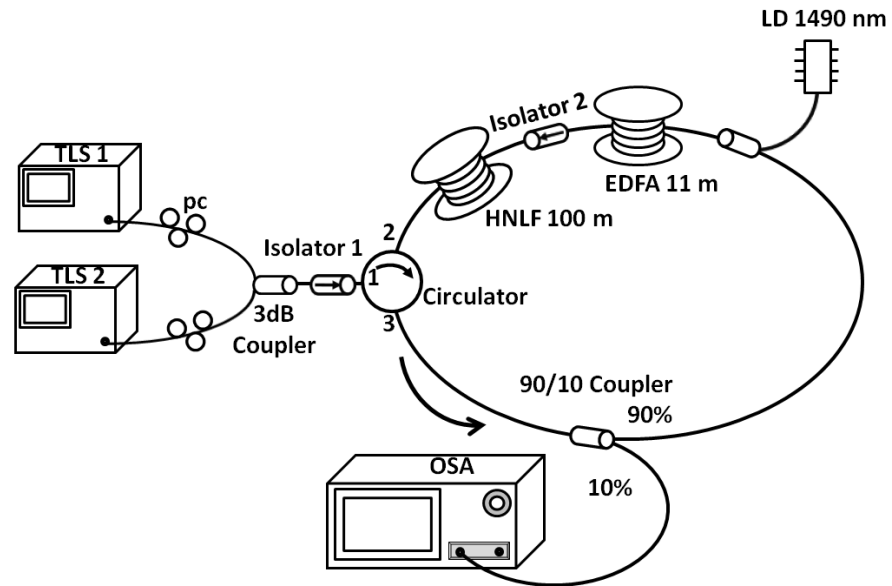


Figure 4.18 Schematic diagram for generating FWM effect in a ring configuration [41].

The dual-wavelength input into the ring cavity are set at 1590 nm and 1591 nm for the P_P , and P_S , respectively, which is launched into the ring cavity via the optical circulator and moves in a counter-clockwise direction. This dual-wavelength signal will experience amplification in the EDF gain medium and then travels toward the HNLF. In this nonlinear medium, FWM takes place and generates the multiple outputs as shown in Figure 4.19 when the necessary phase matching condition is satisfied. From the figure, we can conclude that the input signals P_P and P_S generate C_1 and C_2 due to FWM. As the intensity of conversion wavelengths C_1 and P_P are very high, the interaction between them can also generate the new wavelengths D_1 and P_S , which in this case will enhance P_S . Subsequently, C_2 and P_S will generate new wavelengths at D_2 and P_P . Similarly, signals at C_1 and D_1 will generate E_1 and also signals at C_2 and D_2 will generate E_2 . This process will be repeated and is dependent upon the signal power levels of the interacting waves. The interest in conversion signals will depend largely on the power levels of the ‘free-running’ spectrum. At this power level, the FWM power increases when the pump wavelength is located near its peak. Therefore, by using the ring cavity, it gave the highest peak of conversion wavelength when compared to the linear cavity in the same HNLF and pump power level which is shown in Figure 4.19.

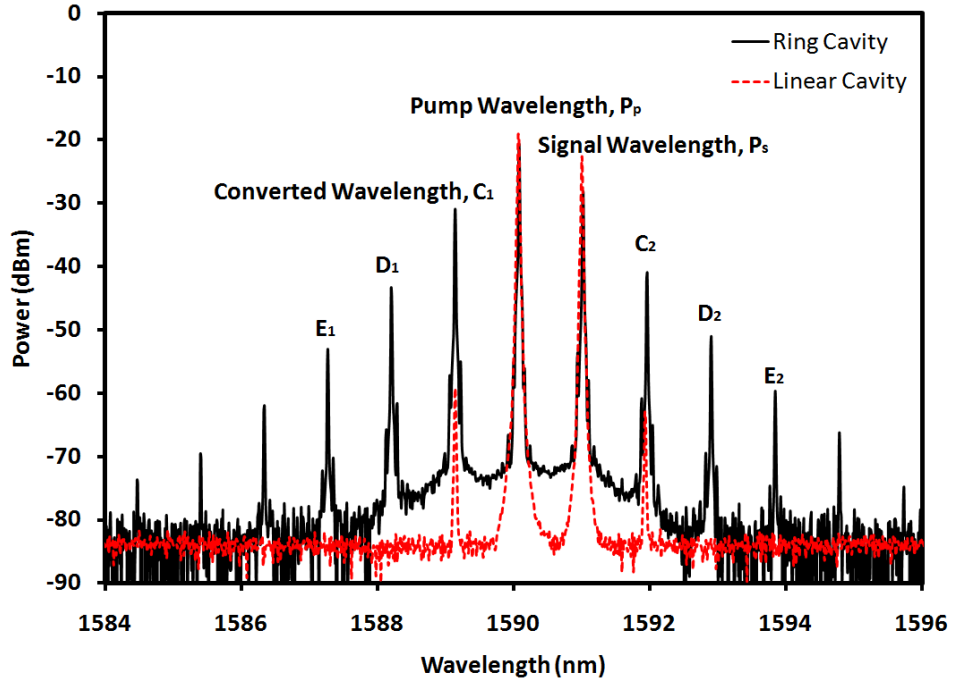


Figure 4.19 Power spectra at the output of the fibre [41].

An important parameter for FWM is a conversion efficiency shown in Figure 4.20 whereby the signal wavelength is varied from 1573 nm to 1600 nm while keeping the pumping wavelength fixed at 1590 nm for the case of the first converted signal, C_1 . Measurement of the conversion efficiency from the spectrum obtained using the OSA, where the FWM conversion efficiency, η (dB) is defines as $P_S(\text{dBm}) - P_{C1}(\text{dBm})$. As the detuning of P_S from 1573 nm to 1580 nm, the conversion efficiency increases from -13.42 dB to -5.69 dB. The conversion efficiency plateaus off at 1580 nm until 1600 nm with a value of -4 dB. The fluctuation is only about 2 dB within a region of 20 nm as shown in Figure 4.20. This measurement can be extended into the C-band region if a shorter length of EDF is used.

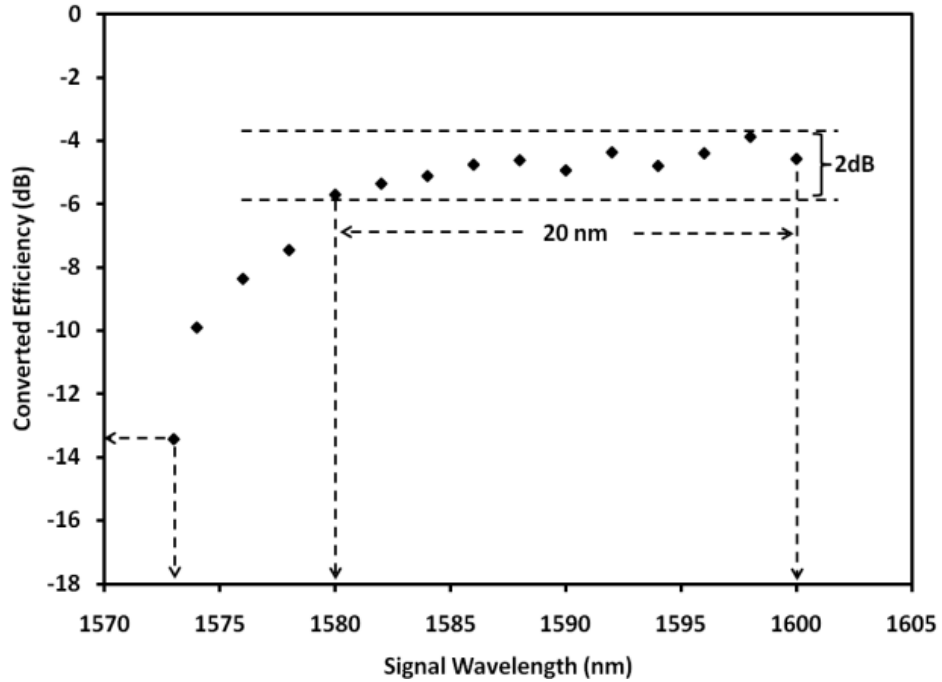


Figure 4.20 FWM conversion efficiency versus the signal wavelength, P_S , with HNLf fitting pump wavelength, P_P , at 1590 nm [41].

Figure 4.21 show the FWM conversion efficiency against the signal wavelength in the ring and linear cavity. By using the same pump power, we observed a higher rate of FWM conversion efficiency in the ring cavity when compared to a linear cavity within the 30 dB bandwidth. The FWM conversion efficiency for a ring cavity is -4 dB while for a linear cavity it was maintained at -38 dB. In essence, the high conversion efficiency for FWM generally requires a high pump power laser (high cost and complicated system), but this restriction can be removed by employing a ring cavity, with certain conditions.

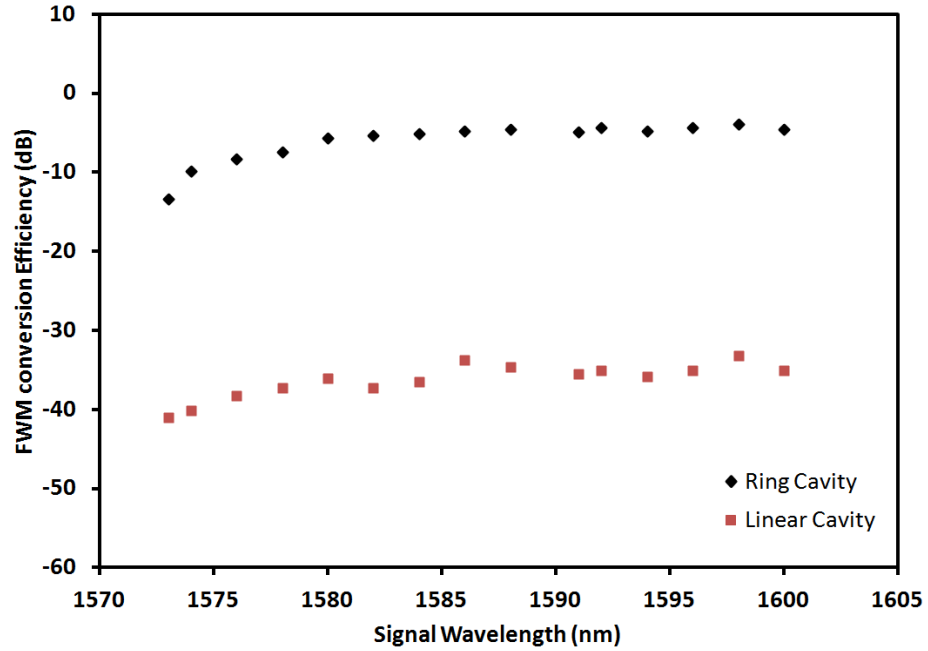


Figure 4.21 FWM conversion efficiency versus the signal wavelength, P_S , with HNLF fitting pump wavelength, P_P , at 1590 nm by using ring and linear cavity [41].

In Figure 4.22, the conversion efficiency against the laser diode pump wavelength is shown. It can be seen that the conversion starts at roughly 27 mW and increases as the pump power is increased. The novelty of this experiment is that higher conversion efficiency can be achieved at a lower laser pump power as compared to a linear cavity by using the same HNLF and laser pump power. The proposed design leads to a higher amplification by the EDF caused by the circulation inside the ring cavity. The other important parameter in the FWM experiment is the SNR ratio which is shown in Figure 4.23 and 4.24. The definition of the SNR [dB] is the measure of the ratio of signal power to noise power in an optical channel. Measurements are taken by after the signal wavelength, P_S , is varied while keeping the pump wavelength, P_P , constant at 1590 nm, as in the case in Figure 4.23. As the signal increases from 1573 nm to 1576 nm, the SNR improves from

30 dB to 43 dB. Further increases of the P_s do not change the SNR very much as it plateaus off after 1576 nm. The peak to peak variation within a region of 24 nm is only about 1 dB. In addition to the conversion efficiency, we also compared the SNR in linear and ring cavity, illustrated in Figure 4.24, whereby the SNR of the ring cavity obtained is higher than the linear cavity in the range of 20 dB.

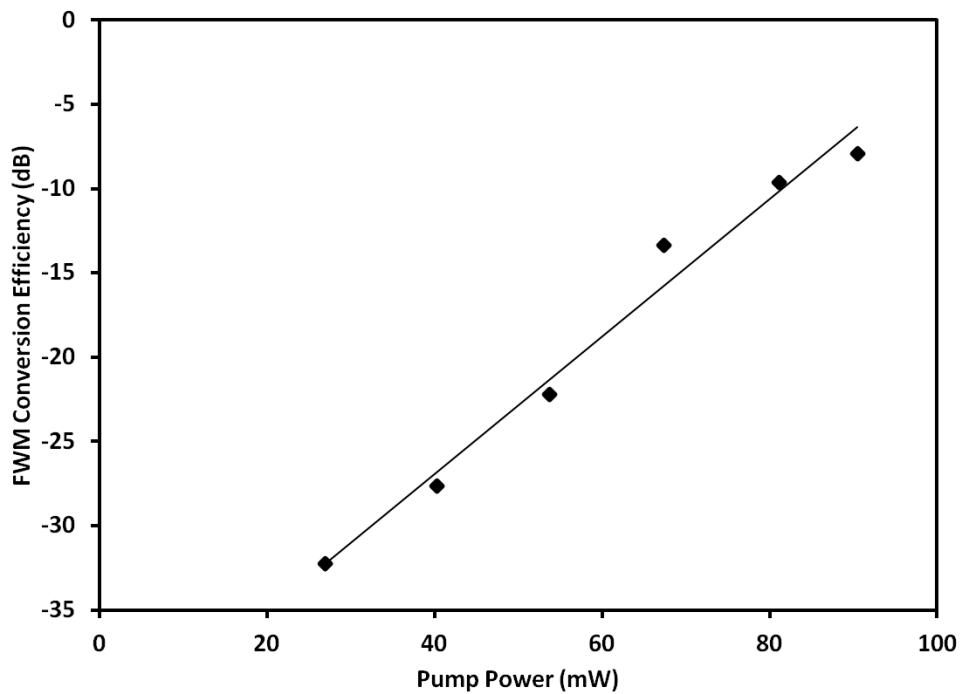


Figure 4.22 FWM conversion efficiency versus 1490 nm LD pump power [41].

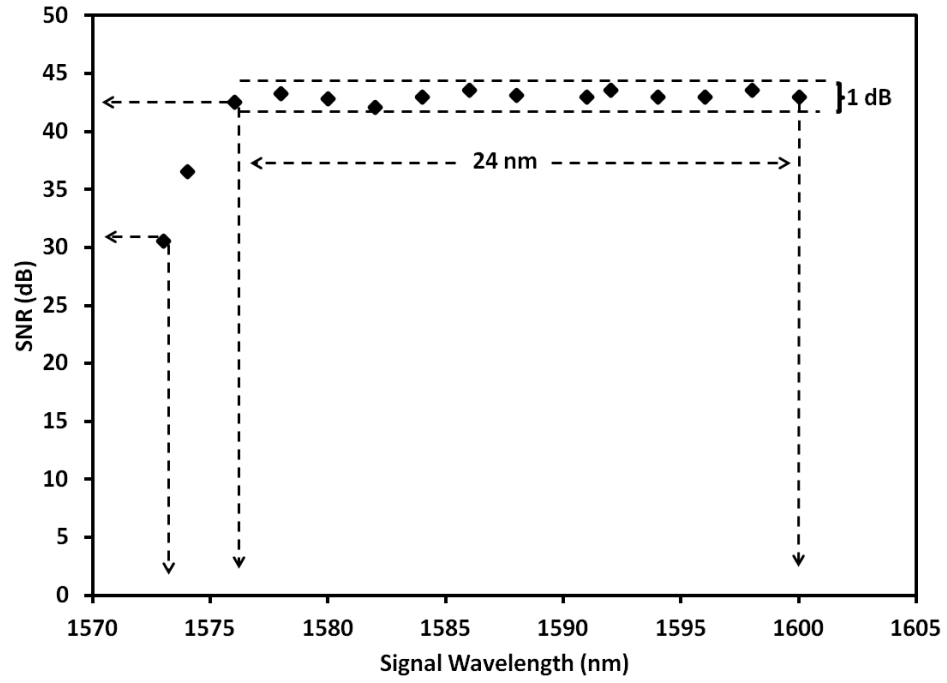


Figure 4.23 SNR against signal wavelength, P_s , keeping pump wavelength, P_p , fixed at 1590 nm in HNLF [41].

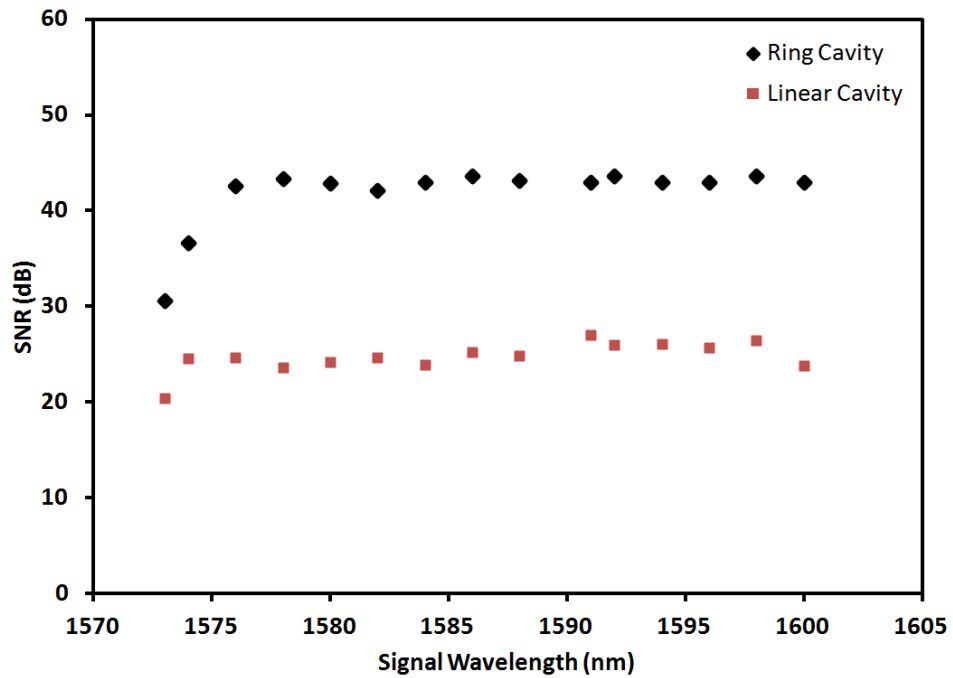


Figure 4.24 SNR against signal wavelength, P_s , keeping pump wavelength, P_p , fixed at 1590 nm in HNLF by using ring and linear cavity [41].

The proposed experiment demonstrates an efficient system for generating FWM in a 100 m HNLF using a ring configuration which, to our knowledge, is the first of its kind to be reported. The measured conversion efficiency is about -4 dB which is the highest conversion efficiency using a 90 mW pump power laser at 1490 nm and SNR of 43 dB for the case of the first converted signal, C_1 . This experimental setup exhibits a flat conversion efficiency as well as SNR over a span of 20 nm. In short, the proposed technique will be of suitable application for wavelength conversion in many practical communication systems.

4.4 FWM effect in SOA

FWM in SOA is a third order nonlinear effect and has attracted much interest since late 1980s. Because of its ultra high speed of response (up to THz) and large operating wavelength range, FWM in a SOA has been proposed as a technique for wavelength conversion [44], optical demultiplexing and clock recovery in high speed optical transmission systems. The generation of the FWM effect is associated with the nonlinearity of the SOA. It is principally caused by carrier density pulsation, carrier heating and spectra hole burning changes induced by the amplifier input signal [44]. The mechanism of generating FWM is based on wavelength detuning whereby in a detuning above a few nm, a mechanism called the carrier density modulation happens [45]. Such a mechanism falls within the category of interband effects that change the carrier density due to the depletion caused by stimulated emission. For wavelength detuning below a few nm, the FWM generated is based on the intraband effect where it is associated with two phenomena; spectra hole burning (SHB) and carrier heating (CH). In the SHB mechanism, an optical input signal create holes and changes the intraband carrier distribution producing

modulation of the occupation probability of carriers within the energy band. The CH phenomena on the other hand are caused by the removal of low energy levels of free carriers via stimulated emission if they are transferred to a higher level due to free carrier absorption [45].

Recently, the FWM effect in SOAs has become a promising technique with regards to wavelength conversions. Wavelength conversions are important tools in future WDM-based high speed optical networks because it provides simultaneous conversion of a single data channel into different channels without the necessity of multiple optical–electronic–optical transponders. Wavelength conversion which utilizes FWM has two basic schemes known as, the co-polarized pump scheme and an orthogonal polarized pump scheme [46]. If a CW pump beam is injected together with a signal pulse train consisting of a pseudorandom sequence of “1” and “0” bits inside a parametric amplifier, the idler wave is generated through FWM only when the pump and signal are present simultaneously. As a result, the idler wave appears in the form of a pulse train consisting of same sequence of “1” and “0” bits as the signal. In effect, FWM transfers the signal data to the idler at a new wavelength with perfect fidelity. It is also able to improve the signal quality by reducing intensity noise [46].

In this part, the degenerate and the non-degenerate case of the FWM effect by using dual-wavelength fibre laser in SOA is discussed. The next part of this section shows the applications of the FWM effect in SOAs in the wavelength conversion. The final part, our discussion of the dual-wavelength fibre laser in SOA will involve the generation of the wavelength conversion in C-band region from the O-band source signal. This description will show the FWM power, conversion efficiency and SNR of FWM in SOA.

4.4.1 Generation of wavelength conversion in SOA by using dual-wavelength fibre laser.

In this part, the dual-wavelength fibre laser is used to generate the FWM effect inside the SOA which acts as the nonlinear medium as well as the amplifier. The fibre laser can independently operate as a dual-wavelength source in a CW mode as well as an efficient wavelength conversion based on the FWM effect owing to the parametric phenomenon due to the nonlinearity of the SOA. However, the new wavelength that generated from the SOA dual-wavelength fibre laser has lower FWM power, FWM conversion efficiency and SNR as compared to the dual-wavelength laser (TLSS). However, this design has the advantages of compatibility, compact size and is simple to implement in current communication system. In this design, the dual-wavelength fibre laser can be tuned around the AWG channels. Therefore, the widest wavelength bandwidth is 18.1 nm (Channel 1 to Channel 24) between the wavelengths of wavelength of 1530.5 nm to 1548.6 nm.

The schematic layout of the dual-wavelength fibre laser is illustrated in Figure 4.25. The experimental setup consists of a 1550 nm SOA, AWG, variable coupler, 2 PC and an isolator. The SOA is responsible for initiating the lasing in the system by generating an ASE, which then passes through the 10 dB fused coupler and sliced by AWG channel. The SOA is biased with a 300 mA current which is equivalent to a 5 dBm output power. A dual-wavelength fibre ring laser was formed by emitting two selected wavelengths simultaneously by using AWG in the laser cavity. The dual-wavelength fibre laser then acts both as pump and probe, each having an individual PC, which is then combined via a variable coupler. Then, this fibre laser is rotated clockwise into the SOA to generate the converted signal by using the FWM effect where the power of the converted signal can be

controlled by using a variable coupler. The use of the variable coupler is important to control the cavity loss inside the cavity. A fibre isolator is used to ensure unidirectional operation of the laser and to reduce instabilities due to the component reflections. The PCs allow the polarization of two input waves to be aligned with each other as well as the proper axis of the SOA. Each PC is composed of a combination of a half-wave plate, a quarter-wave plate and a half-wave plate. The 10% of 10 dB fused coupler is tapped after the SOA for observing the FWM spectrum at OSA.

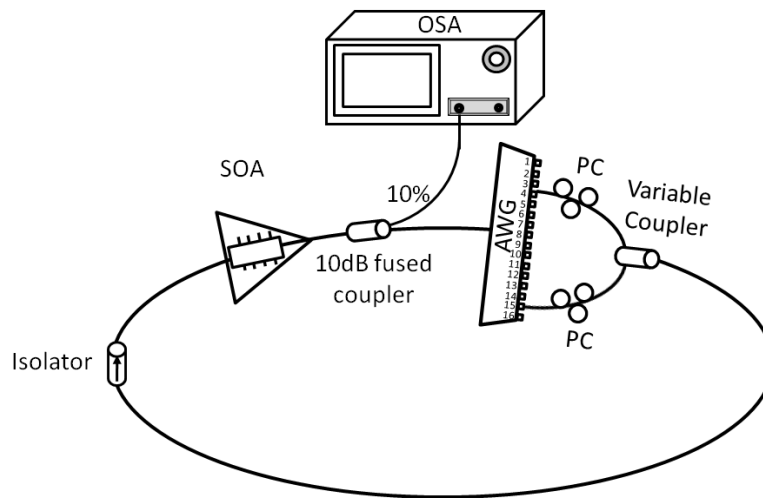


Figure 4.25 The experimental setup for FWM effect in SOA by using dual-wavelength fibre laser.

The output spectrum of the source is shown in Figure 4.26 where the pump is fixed at channel 1 (1530.5 nm) and the probe is tuned from channel 6 to 24. The tuning of the probe is initiated from channel 6 due to the fact that the variable coupler could not control the loss

inside the system. From this figure, it can be seen that the flat nature of the dual-wavelength is not an important factor for the FWM process, as the different pump and probe powers are important in the generation of a high intensity converted signal. In the FWM process, two chosen wavelengths (λ_{pump} and λ_{probe}) will generate a converted signal wavelength ($\lambda_{converted\ signal} = 2\lambda_{pump} - \lambda_{signal}$).

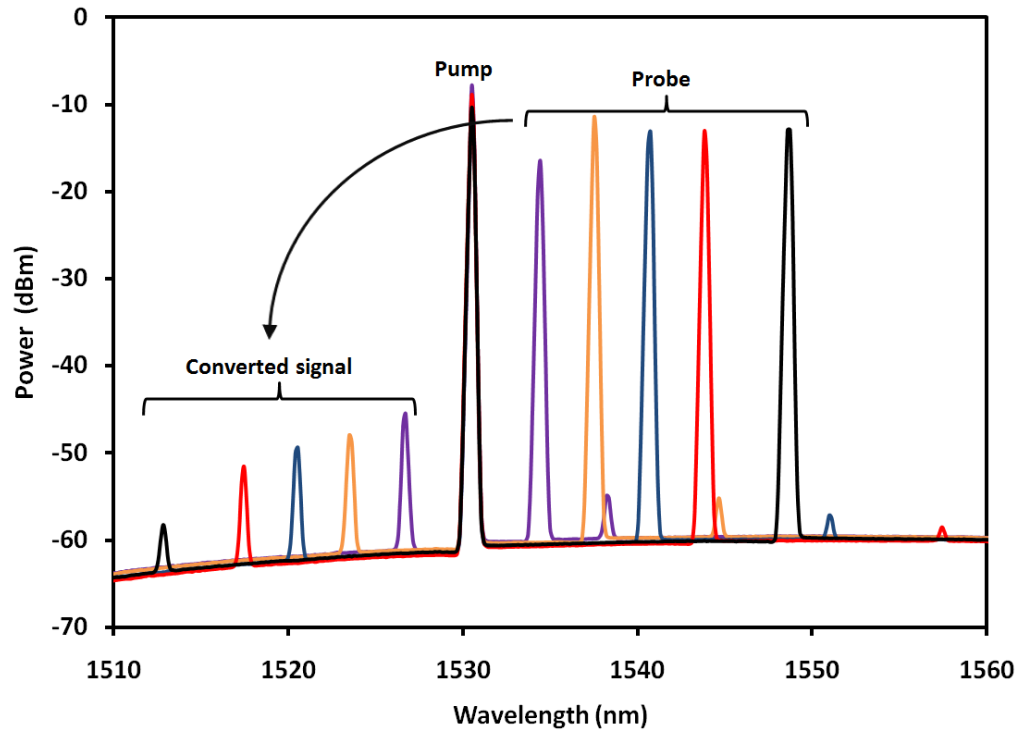


Figure 4.26 The FWM spectrum from OSA.

The FWM conversion efficiency and SNR of the converted signal is measured by changing the probe wavelength, which is also one of the AWG channels. The FWM conversion efficiency in the SOA is defined as the ratio of the converted signal power to the probe

power. The SNR is obtained by dividing the converted signal power with the noise power within 0.1 nm of an optical bandwidth. The FWM conversion efficiency is below -29 dB when the SOA is biased at 390 mA, as shown in Figure 4.27. From this figure, it is evident that the FWM conversion efficiency has the same pattern as the SNR. It also shows the value of the FWM conversion efficiency of channel 1 and 16 highest than channel 1 and 24 due to the increment of the wavelength spacing between the channels. Moreover, the results indicate that at wavelength spacing of 3.9 nm and 18.1 nm, the FWM conversion efficiency reach -29 dB and -45.243 dB and the SNR achieved were 15.6 dB and 5.091 dB, respectively.

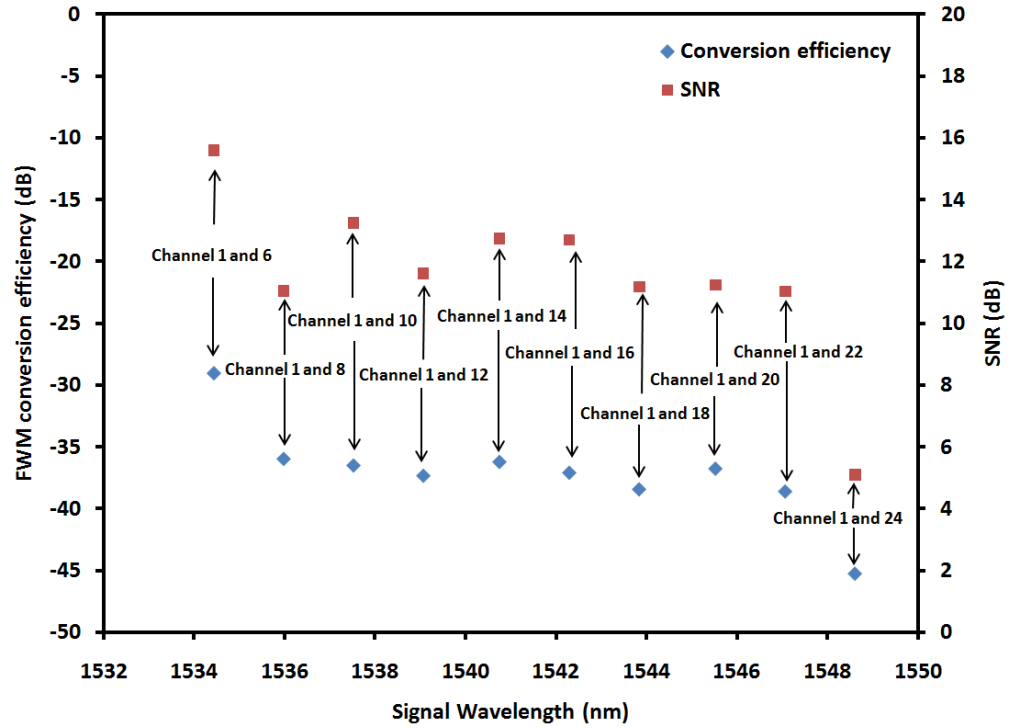


Figure 4.27 The conversion efficiency and SNR versus wavelength channels.

4.4.2 Wide-band of wavelength conversion in FWM effect of SOA by using dual-wavelength fibre laser.

As was discussed previously, wavelength conversion between channels causes a reduction in the intensity of the converted signal and degradation of the SNR. An improved scheme with a wider wavelength tuning range and an increment in the conversion efficiency has been developed using broad assisted pump technique. This work demonstrated that employing an additional so-called ‘assist pump’ in the SOA considerably increased the conversion efficiency and SNR.

As depicted in Figure 4.28, our experiments were performed using a setup similar to that used to generate the wavelength conversion in the SOA with a pump and assisted pump (TLS). A 1550 nm commercial SOA is biased at 300 mA and is placed before the AWG. To ensure the unidirectional operation and to prevent back reflection, an isolator is employed in the setup. The generation of the dual-wavelength fibre laser takes place when the SOA induces ASE which is then circulates inside the cavity in a clockwise direction. The ASE is then sliced by AWG into 24 different channels, with two of the channels, namely channel 1 (pump1, P_1) and channel 24 (probe, P_S) being selected via variable coupler. The variable coupler uses to control the cavity loss in order to balance the power of the two inputs of the dual-wavelength fibre laser (P_1 and P_S). To accomplish this, P_1 and P_S is fixed at 1530.5 nm and 1548.6 nm (channel 1 and 24) and 1539.2 nm and 1540.7 nm (channel 12 and 14) with power of -9.8 dBm and -11.1 dBm (channel 1 and channel 24) and -8.0 dBm and -11.8 dBm (channel 12 and 14), respectively. For the FWM interaction to be efficient, PCs are inserted between the AWG and variable coupler to align the polarization vector of the P_S and P_1 polarization in the SOA. The TLS (pump 2, (P_2)) and

output of variable coupler are then connected to a 3 dB coupler to produce a wider range of wavelengths. The TLS acts as an assisted pump in this system. The P_2 wavelength is varied from 1476 nm to 1600 nm while the power was kept at a constant 10 dBm. P_S , P_1 and P_2 are then combined and injected into an SOA with a small signal gain of 30 dB.

The wavelength detuning ($\Delta\lambda$), defined as the difference between the wavelengths of P_1 and P_S , is set to 1.5 nm (channel 12 and 14) and 18.1 nm (channel 1 and 24) during the experiments. The difference between the wavelengths of the wavelength conversion and P_2 is equals to the detuning $\Delta\lambda$, as indicated in Figure 5.9. Therefore, the wavelength conversion range is $\Delta P + 2 \Delta\lambda$, where ΔP is the pump spacing, which is difference between the wavelengths of P_1 and P_2 . This refers to a down conversion, in which the input probe is converted to a shorter wavelength. For the so-called up-conversion to a longer wavelength, the relative wavelength positions of P_S and P_1 are the same as those for down conversion, but reside at a longer wavelength than P_1 . Accordingly, the wavelength conversion range for the case is $\Delta P - 2 \Delta\lambda$.

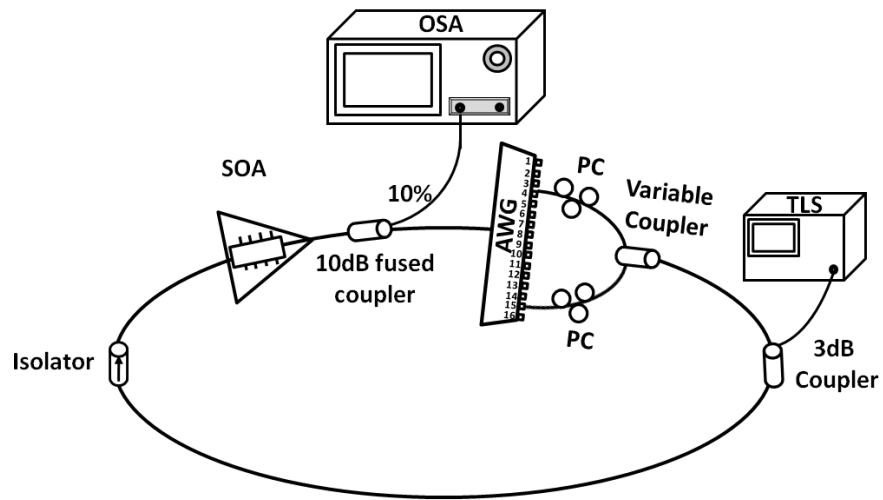


Figure 4.28 Setup on wavelength conversion using assisted pump.

Figure 4.29 show the spectrum of a wide-band wavelength range for two dual-wavelength fibre lasers. Channels 1 and 24 and channels 12 and 14 are illustrated in this part to express the principle of wavelength conversion where the FWM conversion efficiency can be increased by decreasing the wavelength detuning between probe and pump. However, channels 12 and 13 (wavelength spacing of 0.8 nm) is not selected because of the homogeneous effect in the SOA. The combination of the dual-wavelength fibre laser and assisted pump which is shown in full spectrum in this figure generated the triple wavelength (wavelength conversion) in the SOA. The process is due to the beating of P_1 , P_S and P_2 where it experiences an index-modulated grating within the SOA. In this process, it generated two sidebands C_2 (wavelength conversion) and S_2 (a replica of signal) around P_2 , spaced by $\Delta\lambda$ and having the states of polarization of P_2 . In our experiment, the intensities of C_2 and S_2 are measured for every different wavelength of pump 2 over the entire wavelength range of between 1476 nm to 1600 nm with a detuning of 194 GHz and 2291 GHz depending on the spacing of the P_S and P_1 at channels 1 and 24 and channels 12 and 14, respectively. Figure 4.29 show the output spectra of S_2 , P_2 and C_2 at S-band, C-band and L-band spectrum. However, channels 1 and 24 could not generate the wavelength conversion at the C-band region because of the imbalance power of the dual-wavelength fibre laser. This because the TLS is easier to lase compared to dual-wavelength fibre laser, thus, the wavelength conversion unable to generate.

Therefore, the results presented below clearly show that by using the proposed configuration, an ultra-broadband tunable wavelength conversion with a tunable range of over 124 nm can be achieved.

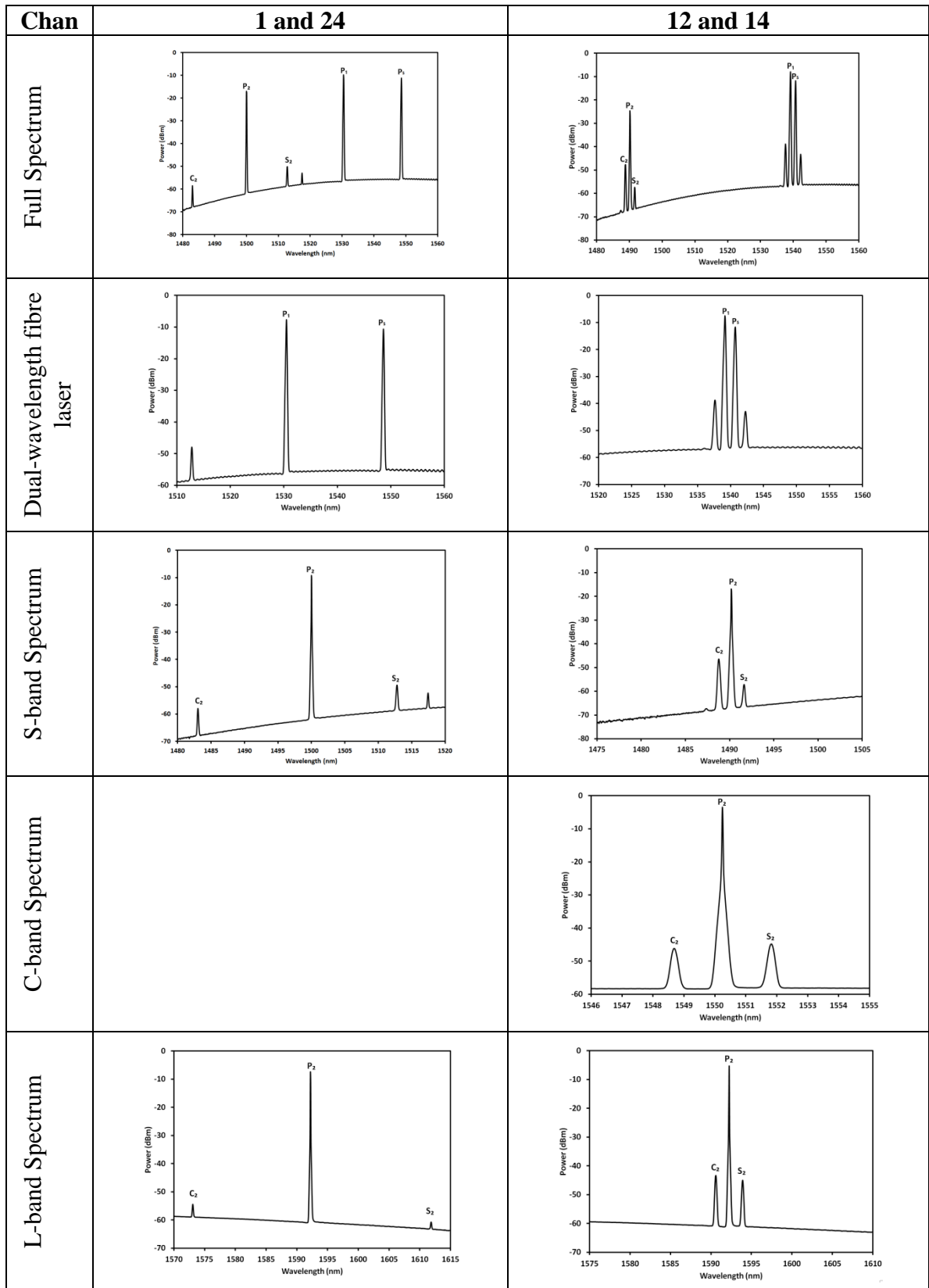


Figure 4.29 The full, S-band, C-band and L-band spectrum of wavelength conversion.

The relationship between the FWM conversion efficiency and wavelength conversion is shown in Figure 4.30. This figure shows a converted wavelength started from 1457.9 nm to 1581.9 nm at channels 1 and 24 while for channels 12 and 14; it began from 1474.5 nm to 1598.5 nm, both of which have a wavelength range of 124 nm. The spectrum of channels 1 and 24 illustrated the increment of the FWM conversion efficiency from -63.7 dB to -29.4 nm at 1457.9 nm and nm 1509.9 nm, respectively. Beyond 1509.9 nm, the FWM conversion efficiency could not be measured as our wavelength conversion simply ceased to work in this particular setup. This occurred as there is an imbalance in the power of the dual-wavelength fibre laser, which is controlled by the TLS. The wavelength conversion then appear to come back online when the wavelengths were at 1551.9 nm and 1581.9 nm with a FWM conversion efficiency of -44.04 dB and -47.62 dB, respectively. The highest FWM conversion efficiency of this channel is around -29.4 dB. The FWM conversion efficiency spectrum of channels 12 and 14 is more stable and is related to the SOA gain spectrum, discussed in chapter 3. The value of the FWM conversion efficiency is 17.4 dB with the conversion bandwidth started from 1474.5 nm until 1598.5 nm. In this region, the FWM conversion efficiency increased from -43.26 dB to -28.74 dB at 1474.5 nm and 1502.5 nm, respectively. This then was maintained at around 1504.5 nm to 1534.5 nm with a 3 dB conversion bandwidth of -28 dB. After that, it dropped until -37.9 dB at 1556.5 nm, before increasing against at 1578.5 nm with FWM conversion efficiency of -29.83 dB. It then went down to -35.17 dB at 1598.5 nm.

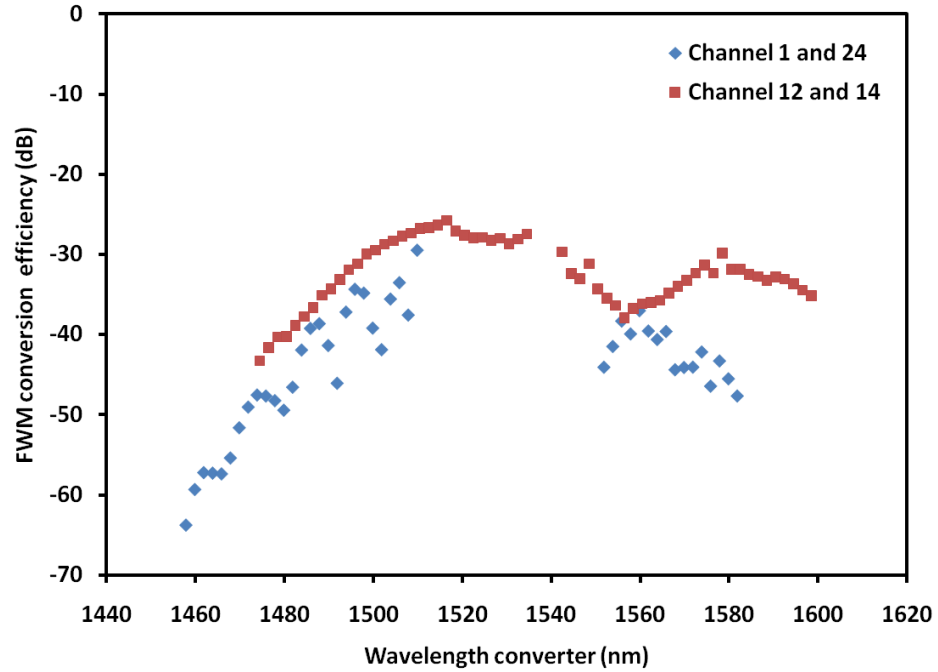


Figure 4.30 Effect of the assisted pump on the conversion efficiency versus the wavelength conversion.

Figure 4.31 plots the output of the SNR against the signal wavelength. The results show that the SNR for channel 1 and 24 increased from 5.0 dB to 20.5 dB in the region of 1457.9 nm to 1495.9 nm before being reduced to 5.5 dB at 1551.9 nm. It then increased again from 5.5 dB to 15.0 dB in the up conversion range in 10 nm and before decreasing to 6.8 dB at a wavelength 1581.9 nm. For channels 12 and 14, SNR was maintained at below 25 dB with a 3 dB FWM conversion efficiency bandwidth of over the 46 nm and then decreased rapidly from 21.4 dB to 9.9 dB in the region of 1520.5 nm to 1556.5 nm. After that, the SNR increased again from 9.9 dB to 18.8 dB at 1556.5 nm to 1580.5 nm.

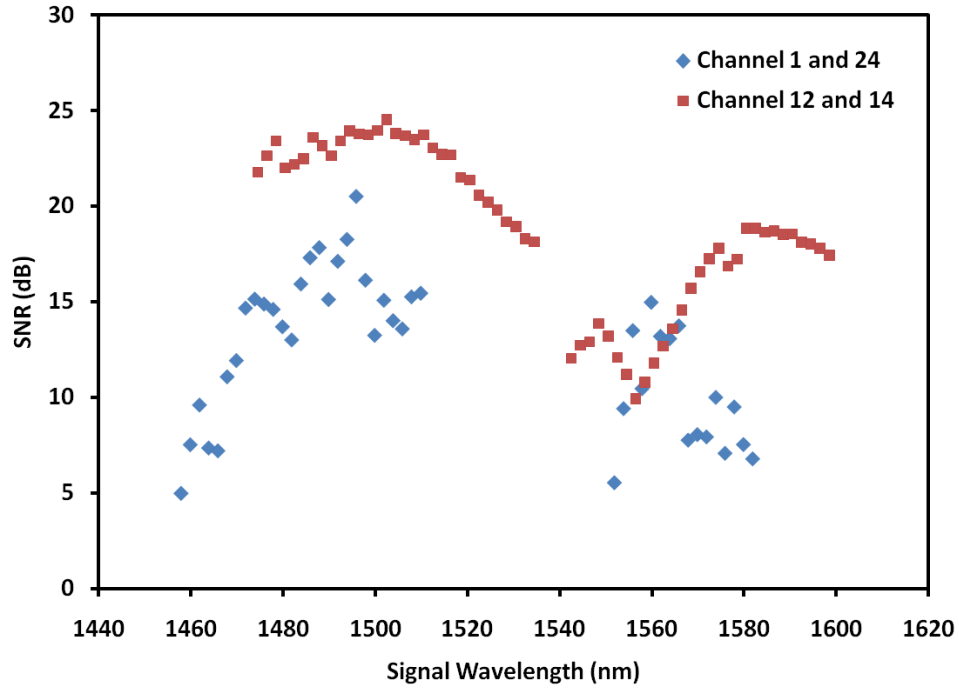


Figure 4.31 Plot of the output SNR against the wavelength conversion.

4.4.3 Pulse Wavelength Conversion in SOA

In this part, we discuss wavelength conversion generated via the FWM effect in SOA when the probe signal is modulated by an internal modulator of TLS [47]. This setup enabled the conversion of data signal from the probe signal with minimal distortion. This therefore proves that the FWM effect is suitable for use in wavelength conversion in the dual-wavelength fibre laser.

The proposed experimental setup is shown in Figure 4.32. This experimental setup consists of ring cavities with gain medium, a 14 meter long EDF, a 48 cm Bismuth-Erbium doped fibre (Bi-EDF) and a 1550nm SOA which contributes to the production of dual-wavelengths and the FWM effect simultaneously. The Bi-EDF is pumped bi-directionally

with two 1480nm laser diodes with a power of 180mW each via a 1480/1550nm WDM with a built-in isolator inside the input WDM. The Bi-EDF plays two important roles here. First, it acts as a gain medium for generating dual-wavelength and second, as a pre amplifier for the FWM effect output enhancement in the SOA. A isolator placed after the Bi-EDF and is used to avoid back scattering inside the cavity, in order to improve the ASE significantly. The 1550nm SOA is used as a nonlinear medium in order to produce the FWM effect. The SOA is biased with a 300mA current which is equivalent to an output power of 5dBm. The 14 meter long EDF has an absorption rate of approximately 4.5 dB/m at 980 nm and is pumped with a 980 nm laser diode at 80mW via a 980/1550 nm WDM. The output end of the EDF is connected to a 90/10 coupler in which the 90% ratio goes to the single input of a 1×24 AWG while the 10% ratio goes to a tunable bandpass filter (TBF) which is further connected to a 50/50 optical coupler. The 50/50 optical coupler splits the optical signal into an OSA and into a photodetector (PD) which is then connected to an oscilloscope (OSK). In this configuration, we selected two channels from the AWG and connected to variable coupler via two PCs. A PC is used to control the polarization state of the two pumps to make it orthogonally polarized. The output of variable coupler is then connected to the 50% leg of a 3dB coupler while the other leg is connected to a TLS. The TLS is modulated by an internal modulator which allows the TLS to act as the input signal for this experiment. The output of the 3dB coupler is connected to the 1480/1550nm WDM which completes the ring cavity configuration.

The generation of the FWM spectra begins with a dual-wavelength fibre laser. First, a balanced dual-wavelength fibre laser has to be produced by controlling both of the cavity losses by using a variable coupler. When the output powers of both wavelengths are almost

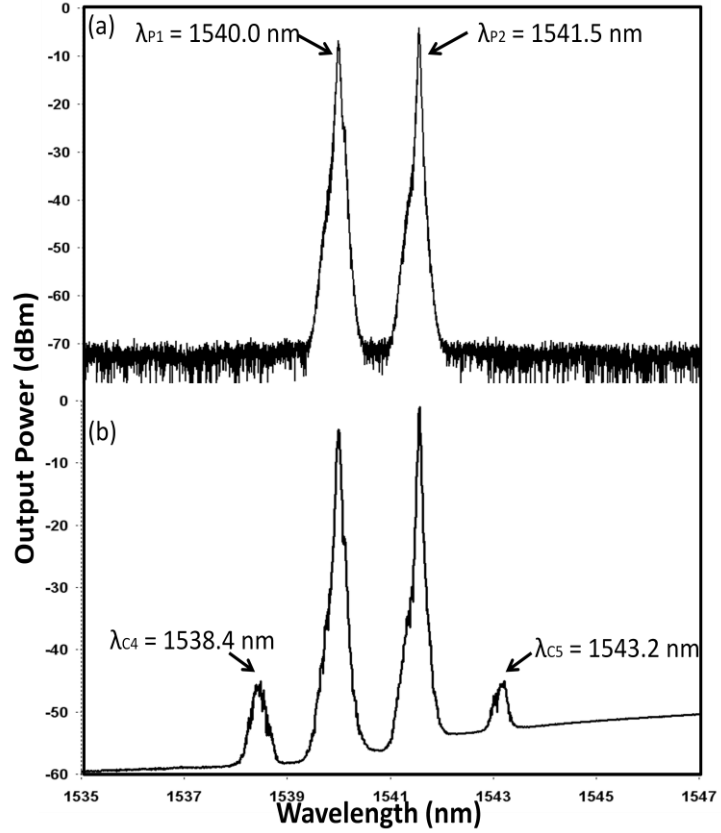


Figure 4.33 Output spectra without inserted modulated input signal (a) dual-wavelength output of Bi-EDF ring cavity showing the oscillating at λ_{P1} of 1540.0 nm and λ_{P2} of 1541.5 nm (b) an insertion of SOA, FWM is generated whereby λ_{C4} of 1538.4 nm and λ_{C5} of 1543.2 nm are due to FWM [47].

Figure 4.34 illustrates the spectra of signals observed when the two polarized pumps (λ_{P1} and λ_{P2}) and the modulated signal (λ_S) are launched into the setup. Due to the interactions between the three input waves, a number of conjugates are generated. They are the two conjugate FWMs (λ_{C4} and λ_{C5}) of λ_{P1} and λ_{P2} , two replicas (λ_{C6} and λ_{C7}) of the signal with wavelength spacing from the signal equal to the spacing of the two pumps and the three

others conjugates which are λ_{C1} , λ_{C2} and λ_{C3} . The components in the spectra have different optical wavelengths that can be expressed as [48] [49]

$$\lambda_{C1} = 2 \times \lambda_{P1} - \lambda_S$$

$$\lambda_{C2} = 2 \times \lambda_{P2} - \lambda_S$$

$$\lambda_{C3} = \lambda_{P1} + \lambda_{P2} - \lambda_S$$

$$\lambda_{C4} = \lambda_{P1} - (\lambda_{P2} - \lambda_{P1})$$

$$\lambda_{C5} = \lambda_{P2} - (\lambda_{P2} - \lambda_{P1})$$

$$\lambda_{C6} = \lambda_S - (\lambda_{P2} - \lambda_{P1})$$

$$\lambda_{C7} = \lambda_S + (\lambda_{P2} - \lambda_{P1}) \quad 4.1$$

The conjugate signals (λ_{C1} and λ_{C2} with 1532.8 nm and 1534.6 nm, respectively) generated by mixing the optical signal of λ_S (1547 nm) with one of the pumps, are called the converted FWMs. Therefore, the novelty of this setup is that, the data from the 1547 nm optical signal can be transferred to the pulse signal at wavelength 1532.8 nm and 1534.6 nm. Figure 4.34 (a) and 4.34 (b) show that the power of the converted signal (λ_{C1}) increases the power of pump 1 (λ_{P1}) is increased, and vice versa. The conjugate signal (λ_{C3}) is generated by mixing the optical signal with both pump signals and is called the non-converted FWM. This can also be called the converted signal when the conjugate signal is λ_{C6} (1545.6 nm). Most references such as [48], [49], [50], [51], used λ_{C6} as their converted

signal, but in this experiment λ_{C1} and λ_{C2} are utilized instead, due to the fact that the power of λ_{C1} is higher than λ_{C6} . Furthermore, λ_{C1} and λ_{C2} also have a wider wavelength detuning of 7 nm, so other components can be filtered out for measuring the converted signal. We must note, however that the conversion efficiency of λ_{C1} and λ_{C2} are -43 dB and -47 dB, respectively, which is quite low for signal conversion. However in this experiment, the signal of λ_{C1} and λ_{C2} still can be converted and detected. The lower conversion efficiency can be attributed to the increment in ASE noise of the amplifier.

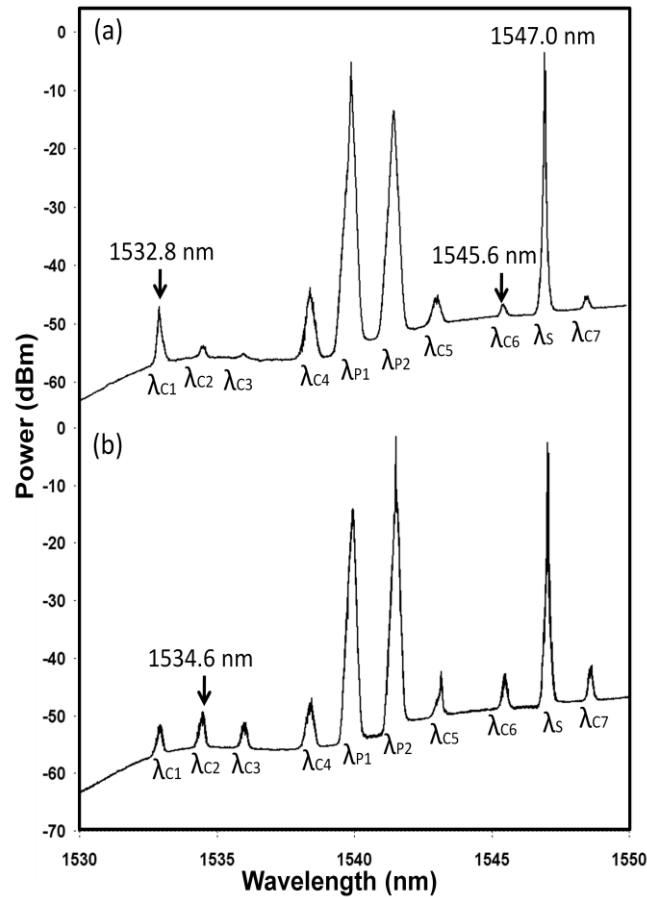


Figure 4.34 The spectra signal of orthogonal polarized pump scheme before connected with optical bandpass filter (a) $\lambda_{P1} \geq \lambda_{P2}$ (b) $\lambda_{P1} \leq \lambda_{P2}$ [47].

The optical bandpass filter is used to selectively pick out λ_{C1} (1532.9 nm) or λ_{C2} (1534.5 nm) by removing the pump signal, the input signal and the other conjugated signals generated by FWM. Figure 4.35 shows the spectra of λ_{C1} and λ_{C2} . The disparity in spectra is due to the difference in polarization of the optical signals, which indicates a special measure for optimization of the system performance against the polarization dependence.

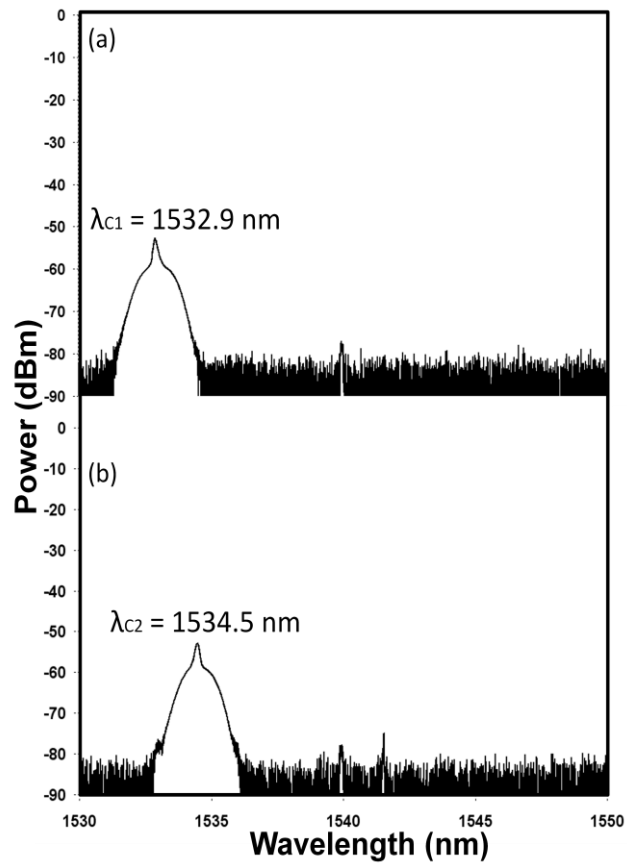


Figure 4.35 The output signal after the optical bandpass filter (a) λ_{C1} (b) λ_{C2} [47].

This spectrum is also observed through an OSK and the non-inverting pulse is obtained as shown in Figure 4.36. Based on the time domain, the input signal, λ_s (1547.0 nm) converts the pulse signal to the converted signal, λ_{C1} (1532.8 nm) or λ_{C2} (1534.5 nm) similar to the frequency modulator. But the converted signal will have a finite rise time and fall time due to the non-zero carrier lifetime. In the case of negligible waveguide losses, the conversion bandwidth is inversely proportional to the spontaneous carrier lifetime but enhanced by the amplifier gain. This bandwidth enhancement is due to propagation effect in the amplifier gain. The slow carrier response at the start of the amplifier leads to a distortion of the optical pulses in the middle of the amplifier. The distorted pulse with strong leading edges then saturates the carrier more rapidly in the last parts of the device leading to an enhanced bandwidth. However, the high data signal could not be tested in this configuration due to the limitation of the equipments in our laboratory.

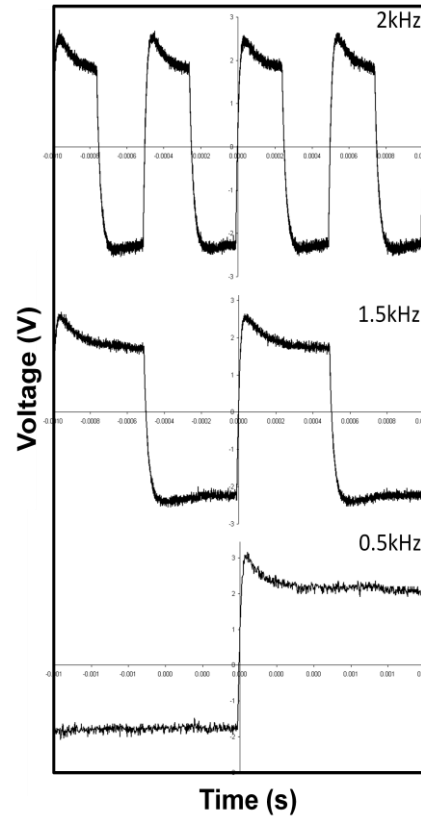


Figure 4.36 The converted signal at wavelength 1532.8 nm and 1534.5 from input signal at wavelength 1547.0 nm after passing through the SOA [47].

4.4.4 Generation of FWM by using dual-wavelength fibre laser from O band to C band

The final stage of our experiments is wavelength conversions which are able to convert wavelengths from the O-band to C-band [52]. This is the most complicated stage as the wavelength conversion takes place at ultra-wideband (O-band to C-band) regions which has considerable attenuation losses. The main reason for the use of this method is the need of telecommunication systems, as it is one of the key components in all-optical communication network using the whole low attenuation bandwidth of the silica fibre [53]. The use of all-optical ultra-wideband wavelength conversions enhances network flexibility, allowing all-optical wavelength converter between different transmission windows, therefore avoiding the bottleneck of optical-electrical-optical conversion. This will be of particular importance at the network interfacing metro-access systems employing the whole low-loss bandwidth of the silica fibre, and the core network traditionally centered in a 1550 nm window. Ultra-wideband wavelength conversions applied in a metro access systems have to deliver high performance while remaining cost-effective. A cost-effective alternative to 1310 to 1550 nm wavelength conversions based on expensive LiNbO_3 waveguides [54], are wavelength conversions employing SOA.

There have been several reports on ultra-wideband wavelength conversion and recently a paper by Lu et. al [55] demonstrated a wideband up-conversion from 1550 nm to 1310 nm based on FWM in a dispersion flattened high nonlinear photonics optical fibre. The experimental setup provides a tunability of over 340 nm. Matsuura et. al [56] provide an approach based on cross gain modulation and cross phase modulation to generate a 300 nm wide ultra-wideband wavelength conversion based on a triple stage SOA. Nonlinear

polarization rotation (NPR) techniques also allowed ultra-wideband wavelength conversion in a single SOA which leads to easier integration in achieving wavelength switching [57]. However, the disadvantages of these techniques are that it has to be properly adjusted and it is difficult to manage.

The primary motivation for this work is to investigate the possibility of using this method for applications in the access network, whereby the signal at 1310 nm can be converted to 1550 nm for effective implementation of an all-optical network. In this thesis, we report a novel method to generate FWM effect from 1310 nm to 1550 nm by using only a single SOA as the nonlinear gain medium for wavelength conversion application. Even though, the NPR technique also uses a single SOA but with the FWM technique, it is much easier to handle. This is the advantage of using the FWM effect and it can potentially be used as a wavelength conversion for optical communication networks.

The proposed experimental setup for generating the FWM effect from 1310 nm (O-band) to 1550 nm (C-band) is shown in Figure 4.37. The setup comprises of two parts labelled A and B. Part A consists of a TLS that can be tuned from 1460 nm to 1580 nm with a linewidth of 0.015 nm. For this experiment the TLS is set at 1542 nm with an output power of 10.0 dBm and is then connected to the Bi-EDF optical amplifier. The Bi-EDF is pumped bi-directionally by two 1480 nm pump lasers operating at an output power of 130 mW. The total pumped power from both ends is therefore 260 mW. The length of the Bi-EDF is 48.2 cm with a dopant concentration of 6300 ppm. The amplified spontaneous emission level of this fibre-based optical amplifier is about -29.49 dBm at 1542 nm. The input signal from the tunable laser is injected into the Bi-EDF through a 1310/1550 nm fused optical coupler. After the optical amplifier, the output signal is measured at 13 dBm by using

optical power meter measurement and is further amplified using a 1550 nm SOA to 16 dBm.

For FWM, at least two wavelengths are required, namely the pump and probe (input signal) which are then coupled into the non linear medium which, in this case, is the 1310 nm SOA. In this experimental setup, three wavelengths are used to generate the FWM as to convert the signal from 1310 nm to 1550 nm, which has a wavelength spacing of about 250 nm in a nonlinear medium.

The three waves are comprised of a 1550 nm pump light for the first part and two 1310 nm lights (pump and probe) of closely spaced wavelengths for the second part (part B) of the experimental setup. The two closely spaced wavelengths at 1310 nm are generated using a 1310 nm SOA as an ASE source as well as the gain medium. The ASE output of the SOA travels to the 1x24 AWG which slices the source signal into multiple individual output wavelengths in the O-band. The sliced wavelengths range from 1301.956 nm to 1316.124 nm with an interchannel spacing of 120 GHz. The measured spacing may not equal the channel spacing of the AWG at 100 GHz. This difference is due to the fact that the AWG used in this experiment is optimized at 1550 nm. At the other end of the AWG, the output of the 24 channels are then connected point to point to the two OCS (1x16) as illustrated in Figure 4.37.

The odd-numbered channels are connected to OCS1 and the even-numbered channels are connected to OCS2. Different sets of two closely spaced wavelengths can be selected from the output of the two OCS which are denoted by λ_1 (channel 23 of OCS1) and λ_2 (channel 24 of OCS2). The output of λ_1 is then connected to an optical attenuator to provide the correct adjustment of the optical power for use in the mixing of this wave in the nonlinear

medium. For wavelength conversion applications, the MZM modulator is connected to one of the legs to provide the data signal. By inserting the MZM modulator, the performance of the output of FWM does not seem to change. This output is then connected to a 1310/1550 nm WDM coupler (C1) at the input end. The other leg is connected to the input signal at 1550 nm from part A. These two wavelengths will then combine at the output end of the coupler which is then connected to one of the input leg of a 3 dB coupler, C2. The other wavelength from the OCS2, λ_2 , is connected to an optical attenuator and then to the other input leg of C2. In the case of C2, a 2x2 coupler is used whereby one of the output legs is connected to an OSA and the other leg to the input of a 1310 nm SOA. This SOA will provide the amplification and also acts as the nonlinear medium for the FWM. The output end of the SOA is then connected to a 90/10 coupler, C3, with the 10% leg connected to another OSA. The 90% leg completes the loop which is connected to AWG.

Figure 4.37 Experimental setup [52].

The results of the above setup are presented in this section. The AWG used in this experiment is an AWG optimized for 1550 nm since the AWG for 1310 nm are not available commercially. The output spectrum of the AWG at different wavelengths other than 1550 nm is investigated and this is done for 1310 nm transmissions. Figure 4.38 shows the output spectrum that has been taken from channels 23 and 24 of the AWG which are from OCS1 and OCS2. The top spectrum is from the output of channel 23 and the bottom is from channel 24. Channel 23 has three peaks at 1278.5 nm, 1316.74 nm and 1357.2 nm respectively. The middle 1316.74 nm peaks has the highest peak power of -20 dBm with the two ‘side lobes’ having peak powers of -55 dBm. Channel 24 also displays the same type of spectrum with a centre peak wavelength of 1317.44 nm and a peak power of -20dBm as well as the two side peaks at 1279.2 nm and 1357.9 nm with peak powers of -55 dBm and -60 dBm respectively.

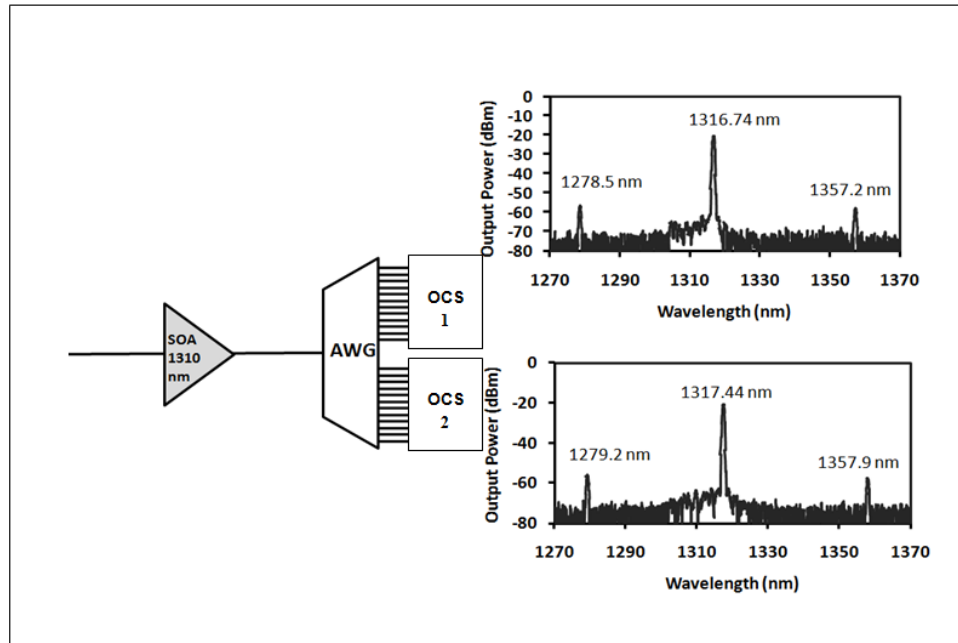


Figure 4.38 Output spectrums of channels 23 and 24 of the AWG after the ASE output from the 1310 nm SOA [52].

From the two spectrums the peak output power of both channels are found to be similar. When these two channels are combined, the spectrum would consist of 6 peaks from both the 1310 nm and the 1550 nm as in Figures 4.39 and 4.40(a), respectively. Figure 4.39 shows the two spectra of channels 23 and 24 with a peak difference of 0.7 nm. The spacing between these peaks is the same as is also observed in other paired channels.

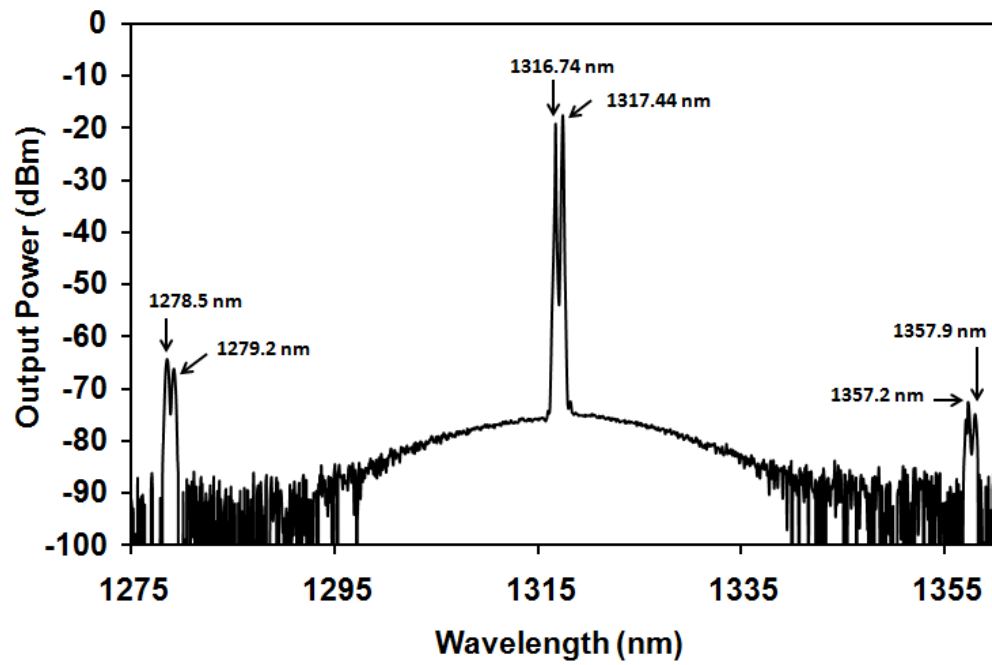
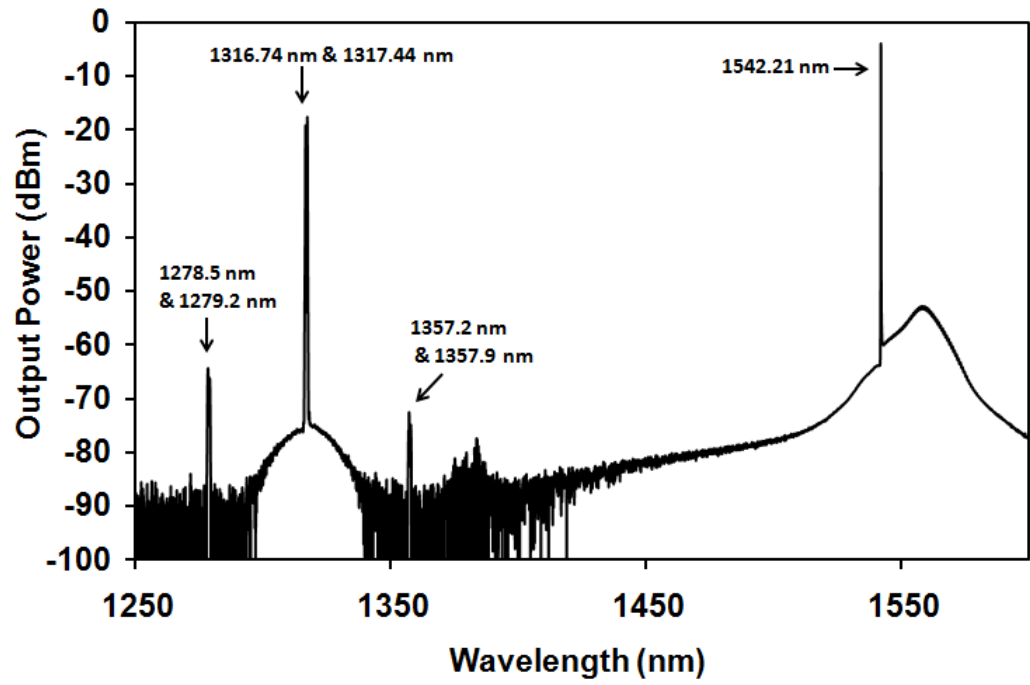
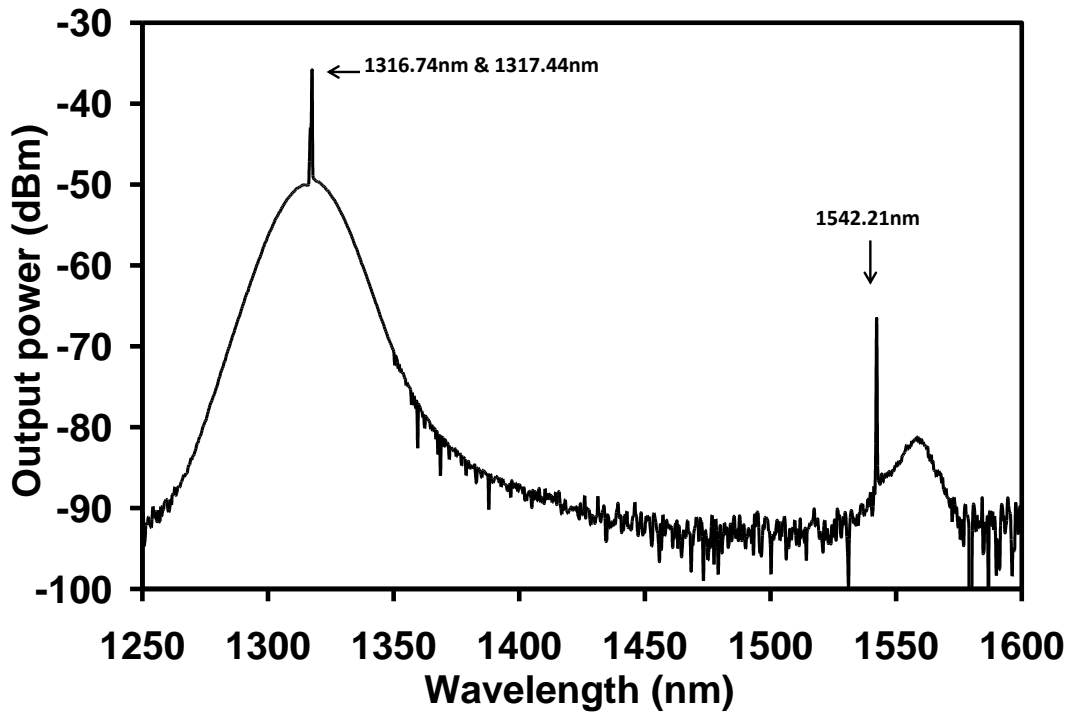


Figure 4.39 The spectrum of dual-wavelength fibre laser with two dual-wavelength side bands together with the 1550 nm signal [52].

Figure 4.40 (a) shows the entire spectrum for the 1310 nm and 1550 nm that is from the O-band to the C-band that is taken from OSA before the 1310 nm SOA. From the spectrum, the 1550 nm output (at 1542.21 nm) is slightly higher by a power difference of 13.627 dB compared to the 1310 nm output (1316.74 and 1317.44 nm). The ‘side-peaks’ have relatively ‘small’ amplitudes, with peak powers of less than -60 dBm as compared to the main peak. These smaller peaks come about from the repetition of outputs at the channels of the AWG as explained earlier. However these peaks are not amplified by the 1310 nm SOA and are eliminated as indicated in Figure 4.40 (b). The use of the 1310 nm SOA as a nonlinear medium has the advantage of allowing signals from 1550nm to pass through with the certain attenuation together with the 1310 nm output. It is worth noting that, if a 1550 nm is used instead of 1310 nm SOA, the signal at 1310 nm will be completely attenuated.



(a)



(b)

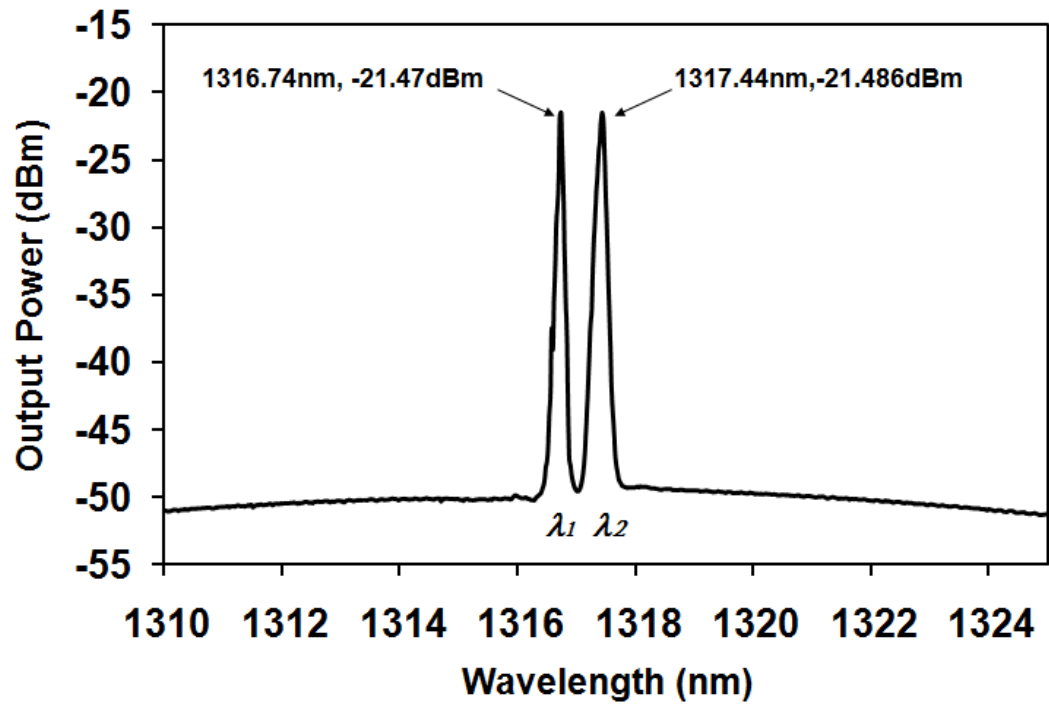
Figure 4.40 Spectrum from O-band to C-band (a) before the 1310nm SOA (b) after the 1310nm SOA [52].

An enlarged trace at 1316.74 nm and 1317.44 nm at peak powers of -21.47 dBm and -21.48 dBm respectively is depicted in Figure 4.41 (a) for the case before a 1310 nm SOA. Figure 5.21(b) shows the trace after travelling through the nonlinear medium at peak powers of -17.57dBm and -16.48 dBm, respectively. In Figure 4.41 (b) the observed two side peaks at 1316.03 nm and 1318.19 nm with peak powers of -72.08 dBm and -72.13 dBm respectively, are due to the four-wave mixing between the interacting waves at 1316.75 nm (λ_1) and 1317.47 nm (λ_2). The generated output due to four-wave mixing can be explained using equation 4.2 [58],

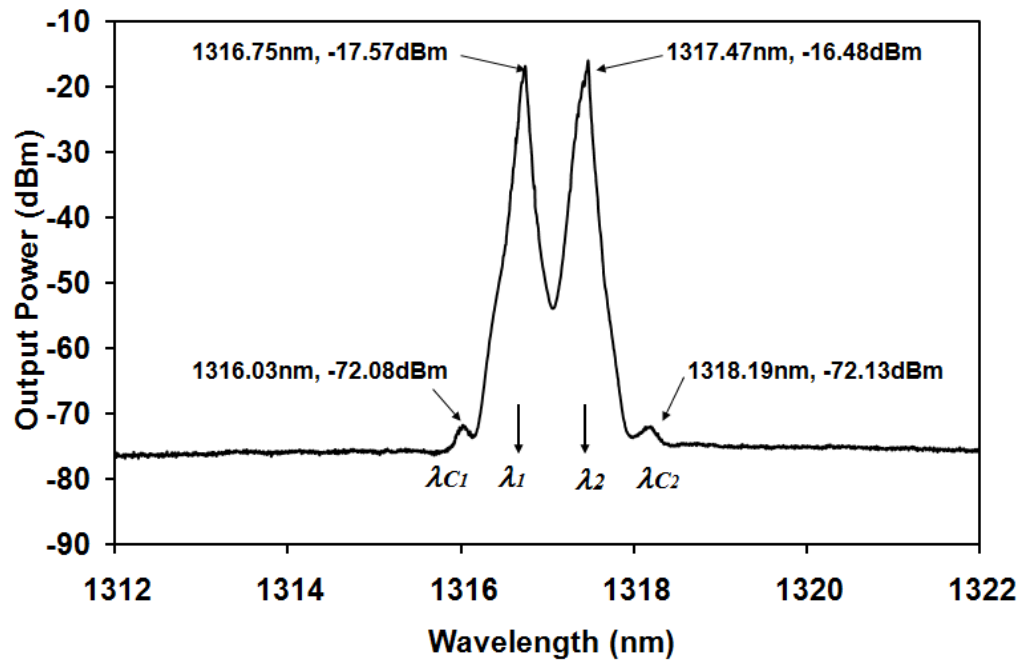
$$\lambda_{c1} = \lambda_1 - (\lambda_2 - \lambda_1)$$

$$\lambda_{c2} = \lambda_2 + (\lambda_2 - \lambda_1) \quad 4.2$$

whereby λ_{c1} =1316.74 nm and λ_{c2} =1317.44 nm. The generation of λ_{c1} and λ_{c2} depends on the wavelength spacing between λ_1 and λ_2 which is 0.72 nm.



(a)



(b)

Figure 4.41 The O-band spectrum; (a) before SOA (b) after SOA [52].

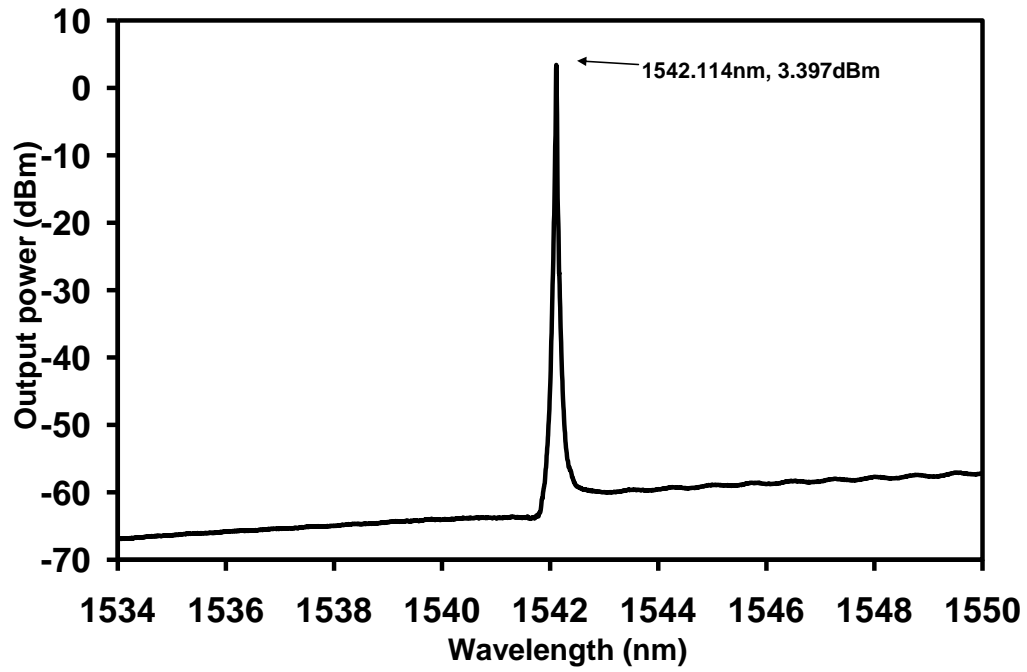
The peaks are denoted by λ_{C1} and λ_{C2} , and the converted wavelengths caused by the two interacting wavelength denoted by λ_1 and λ_2 . This effect is similarly observed at the 1550 nm part of the spectrum as shown in Figure 4.42(a) and 4.42(b). Figure 4.42(a) shows the 1550 nm signal after the 1310 nm SOA with the peak wavelength at 1541.49 nm (λ_{C3}) and 1542.93 nm (λ_{C4}) and peak powers at -80.91 dBm and -80 dBm respectively. This is due to the FWM of the three signals namely λ_1 , λ_2 and λ_{P2} as shown in the above figures. The generated FWM of Figure 4.42(b) can be explained from the equation below based on ref [59]

$$\lambda_{C3} = \lambda_{P2} - (\lambda_2 - \lambda_1) \quad 4.3$$

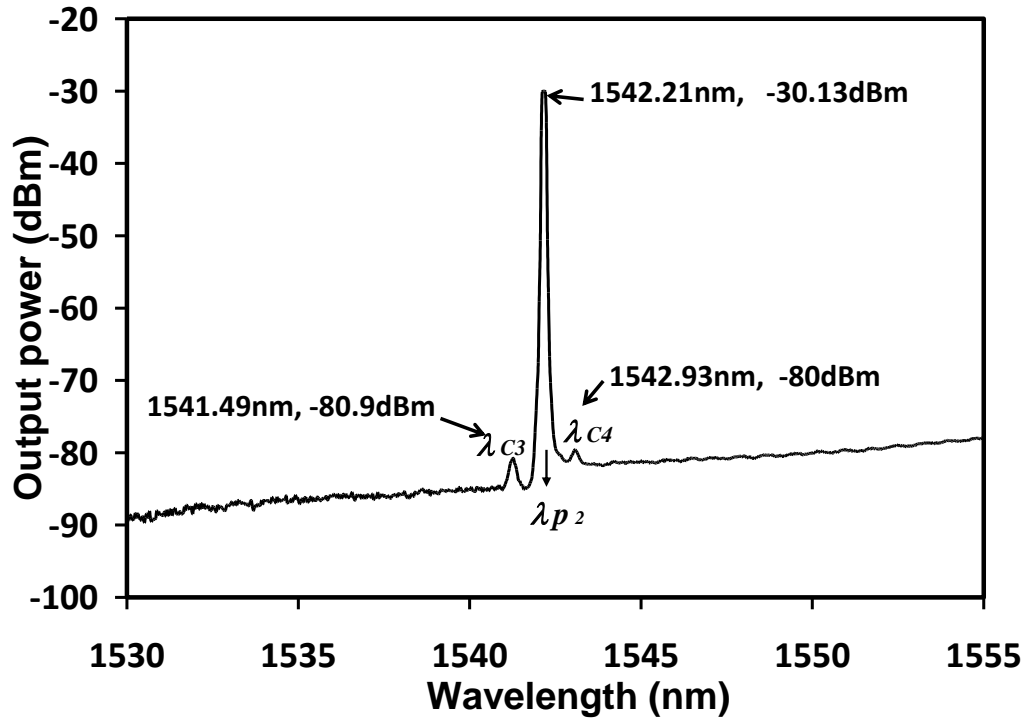
As depicted in Figures 4.42 the values of λ_{P2} , λ_2 and λ_1 are 1542.21 nm, 1317.47 nm and 1316.75 nm, respectively. Inserting these values into equation 4.3 yields $\lambda_{C3} = 1541.49$ nm and this is observed in Figure 4.42 (b). For λ_{C4} , the expression is as given below

$$\lambda_{C4} = \lambda_{P2} + (\lambda_2 - \lambda_1) \quad 4.4$$

Using the same above values would yield $\lambda_{C4} = 1542.93$ nm as observed. The wavelength of the two conjugates namely λ_{C3} and λ_{C4} will depend on the wavelength spacing of 1310 nm dual-wavelength fibre laser.



(a)



(b)

Figure 4.42 The C-band spectrum; (a) before SOA (b) after SOA [52].

The converted signal is determined by the wavelength signal at the 1310 nm region as shown in Figure 4.43. The converted signal in this ultra-wideband regime will depend on the wavelength spacing and the pump spacing. As an example, a signal wavelength of 1316.74 nm will have a wavelength spacing of 0.72 nm and pump spacing of 224.74 nm, and will produce a converted signal at 1542.93 nm. This is verified by the calculation below using equation 4.5

$$\lambda_1 + (\Delta P + 2(\Delta\lambda)) = \lambda_{C4} \quad 4.5$$

Therefore, for a signal wavelength at 1317.47 nm (λ_2), the wavelength conversion will be 1541.49 nm (λ_{C3}) as calculated from the equation below

$$\lambda_2 + (\Delta P + 2(\Delta\lambda)) = \lambda_{C3} \quad 4.6$$

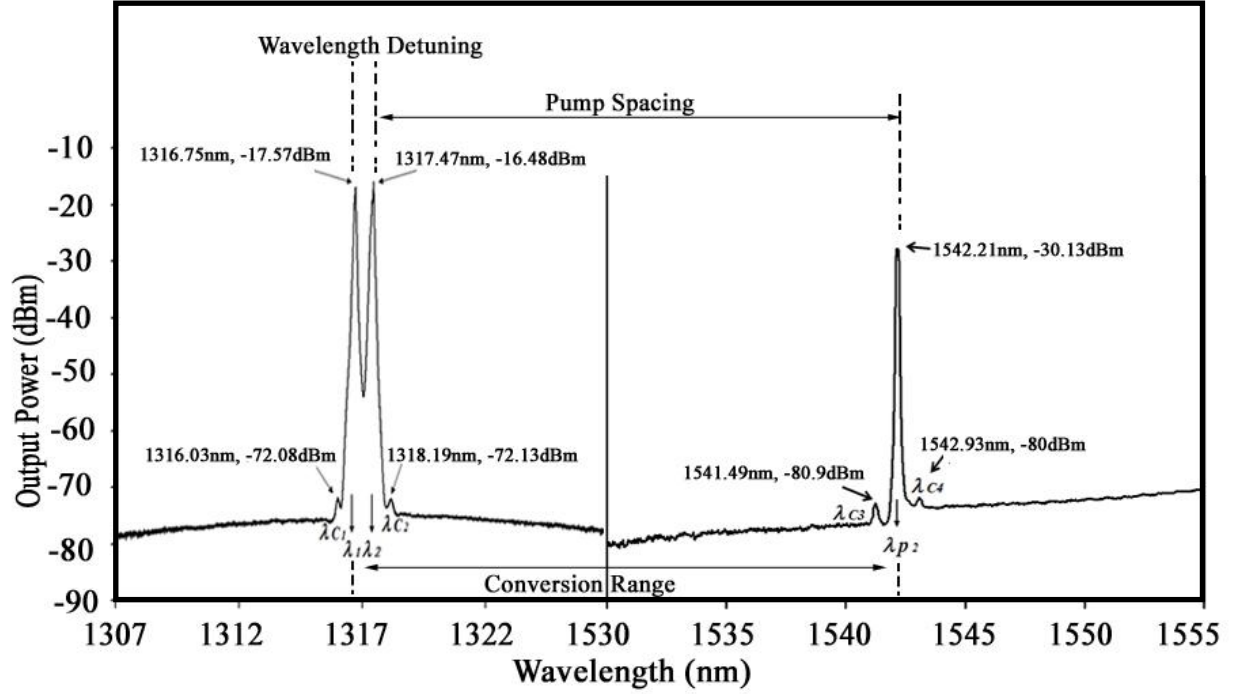


Figure 4.43 Graphical illustration of wavelength conversion [52].

The calculated value corresponds well to the measured value as indicated in Figure 4.44. From these measurements, we have demonstrated a generating wavelength conversion from 1310 nm to 1550 nm with the spacing of 226 nm for wavelength conversion applications. This is the first demonstration of a large spacing down-conversion using an SOA as a nonlinear medium.

There are two other important characteristics of a wavelength conversion namely the conversion efficiency, η , and SNR. The conversion efficiency from the experimental result can be calculated by using equation 4.7

$$\eta = P_{C3} - P_{\lambda 1} \quad 4.7$$

which gives a value of -64.42 dB. This result verifies the theoretical estimation proposed by S. Diez et. al [59], which gives a theoretical conversion efficiency value of -63.3 dB. The SNR that have been obtained is only 3.5 dB. This is due to the fact that the SNRs of the probe lights which are in the C-band region which has higher loss degradation which is largely due to the high absorption loss in 1310 nm SOA.

4.5 Summary

In this chapter, the generation of dual-wavelength fibre laser by using the AWG in a ring cavity has been explained. However, the dual-wavelength fibre laser has a gain competition due to the homogenous broadening exhibited by the EDF material. Therefore, the cavity loss controlled has been used in the generation of dual-wavelength fibre laser.

This followed by a discussion of wavelength conversion by using FWM in the HNLF. In this part, the wavelength conversion in the HNLF by using dual-wavelength fibre laser was investigated in numerically and experimentally. The generation of wideband wavelength conversion is then explained. Both of this configuration, the parameters of FWM conversion efficiency, FWM power and SNR of wavelength conversion have been described. The final part of FWM in HNLF is the generation of wavelength conversion in a ring configuration by using two TLSs which uses a low, rather than the conventional high pump power.

Subsequently, wavelength conversion in the SOA by using a dual-wavelength fibre laser has been investigated. In this section, the generation of pulse wavelength conversion by mixing the optical signals called the non-converted FWM is discussed in detail. Then, the

ultra-wideband wavelength conversion (O-band to C-band) is demonstrated for WDM lightwave application.

The next chapter will describe other applications of FWM effect in HNLF such as FOPA and multiwavelength fibre laser.

Reference

- [1] S. Watanabe and T. Chikama, "Highly efficient conversion and parametric gain of nondegenerate forward four-wave mixing in a single mode fibre," *Electron. Lett.*, vol. 30, pp. 163-164, 1994.
- [2] K. Inoue, "Arrangement of fibre pieces for a wide wavelength conversion range by fiber four wave mixing," *Opt. Lett.*, vol. 19, pp. 1189-1191, 1994.
- [3] X. Zhang and B. F. Jorgensen, "Noise characteristic and optimum length of spectral inversion using four wave mixing in a dispersion shifted fibre," *Opt. Fibre Technol.*, vol. 3, pp. 28-43, 1997.
- [4] I. Zacharopoulos, I. Tomkos, D. Syvridis, F. Girardin, L. Occhi, and G. Guekos, "Influence of phase mismatch on a spectral inverter based on four wave mixing in dispersion shifted fiber at 10Gb/s," *IEEE Photon. Technol. Lett.*, vol. 11, pp. 430-432, 1999.
- [5] E. Ciaramella and S. Trillo, "All optical signal reshaping via four wave mixing in optical fibre," *IEEE Photon. Technol. Lett.*, vol. 12, pp. 849-851, 2000.
- [6] D. M. Patrick and R. J. Manning, "20 Gbit/s wavelength conversion using semiconductor nonlinearity," *Electron Lett.*, vol. 30, pp. 252-254, 1994.

- [7] T. Durhuus, C. Joergensen, B. Mikkelsen, R. J. S. Pedersen, K. E. Stubkjaer, "All optical wavelength conversion by SOA's in a Mach-Zehnder configuration," *IEEE Photonics Tech. Lett.*, vol. 6, pp. 53–55, 1994.
- [8] X. Pan and T. L. Koch, "Intensity noise characteristics of a Mach-Zehnder wavelength converter," *IEEE Photonics Tech. Lett.*, vol. 7, pp. 1276–1278, 1995.
- [9] K. Inoue and K. Oda, "Noise suppression in wavelength conversion using a light injected laser diode," *IEEE Photonic Tech. Lett.*, vol. 7, pp. 500–502, 1995.
- [10] N. Kikuchi and S. Sasaki, "Noise analysis for optical frequency conversion using nearly degenerate four wave mixing in semiconductor optical amplifier," *J. Lightwave Tech.*, vol. 11, pp. 819–828, 1993.
- [11] N. Schunk, G. Grobkopf, R. Ludwig, R. Schnabel and H.G. Weber, "Frequency conversion by nearly-degenerate four wave mixing in travelling-wave semiconductor laser amplifiers," *IEE Proceeding, Part J.*, vol. 137, pp. 209–214, 1990.
- [12] N. C. Kothari and D. J. Blumenthal, "Influence of gain saturation, gain asymmetry, and pump/probe depletion on wavelength conversion efficiency of FWM in semiconductor optical amplifiers," *IEEE J. Quantum Electron.*, vol. 32, pp. 1810–1816, 1996.
- [13] A. D'Ottavi, E. Iannone, A. Mecozzi, S. Scotti, P. Spano, R. Dall'Ara, J. Eckner and G. Guekos, "Efficiency and noise performance of wavelength converters based on FWM in semiconductor optical amplifiers," *IEEE Photonics Tech. Lett.*, vol. 7, pp. 357–359, 1995.
- [14] S. Yamashita and K. Hotate, "Multiwavelength erbium-doped fibre laser using intracavity etalon and cooled by liquid nitrogen," *Electron. Lett.*, vol. 32, pp. 1298–

1299, 1996.

- [15] N. Park and P. F. Wysocki, "24-line multiwavelength operation of erbium-doped fibre-ring laser," *IEEE Photon. Technol. Lett.*, vol. 8, pp. 1459-1461, 1996.
- [16] S. L. Pan, X. F. Zhao, and C. Y. Lou, "Switchable single-longitudinal-mode dual-wavelength erbium-doped fibre ring laser incorporating a semiconductor optical amplifier," *Opt. Lett.*, vol. 33, pp. 764-766, 2008.
- [17] S. Qin, D. Chen, Y. Tang, and S. He, "Stable and uniform multiwavelength fibre laser based on hybrid Raman and erbium doped fibre gain," *Opt. Express*, vol. 14, pp. 10522-10527, 2006.
- [18] H. Ahmad, M. Z. Zulkifli, K. Thambiratnam, S. F. Latif, and S. W. Harun, "High power and compact switchable bismuth based multiwavelength fibre laser," *Laser Phys. Lett.*, vol. 6, pp. 380-383, 2009.
- [19] D. N. Wang, F. W. Tong, Xiaohui Fang, W. Jin, P. K. A. Wai, and J. M. Gong, "Multiwavelength erbium doped fibre ring laser source with a hybrid gain medium," *Opt. Commun.*, vol. 228, pp. 295-301, 2003.
- [20] D. Chen, S. Qin, and S. He, "Channel spacing tunable multiwavelength fibre ring laser with hybrid Raman and erbium doped fibre gains," *Opt. Express*, vol. 15, pp. 930-935, 2007.
- [21] G. Das and J. W. Y. Lit, "L-band multiwavelength fibre laser using an elliptical fibre," *IEEE Photon. Technol. Lett.*, vol. 14, pp. 606-608, 2002.
- [22] G. Sun, Y. Chung, and D. S. Moon, "L-band tunable multiwavelength fibre laser using an unpumped polarization maintaining an erbium-ytterbium double-clad fibre-loop mirror," *Laser Phys.*, vol. 18, pp. 1196-1199, 2008.
- [23] M. Durán-Sánchez, A. Flores-Rosas, R. I. Álvarez-Tamayo, E. A. Kuzin, O. Pottiez,

- M. Bello-Jimenez, and B. Ibarra-Escamilla, "Fine adjustment of cavity loss by Sagnac loop for a dual wavelength generation," *Laser Phys.*, vol. 20, pp. 1270-1273, 2010.
- [24] A. W. Al-Alimi, M. H. Al-Mansoori, A. F. Abas, M. A. Mahdi, and M. Ajiya, "Optimization of tunable dual wavelength erbium-doped fibre laser," *Laser Phys. Lett.*, vol. 6, pp. 727-731, 2009.
- [25] C. H. Yeh, F. Y. Shih, C. H. Wang, Y. F. Wu, and S. Chi, "Cost effective wavelength tunable fibre laser using self seeding Fabry Perot laser diode," *Optics Exp.*, vol. 16, pp. 435-439, 2008.
- [26] P. S. Liang, Z. X. Zhang, Q. Q. Kuang, and M. H. Sang, "All fibre birefringent filter with fine tunability and changeable spacing," *Laser Phys.*, vol. 19, pp. 2124-2128, 2009.
- [27] X. M. Liu, "Broad and tunable multiwavelength fibre laser at the assistance of modulation-instability-assisted four-wave mixing," *Laser Phys.*, vol. 20, pp. 842-846, 2010.
- [28] Z. Y. Liu, Y. G. Liu, J. B. Du, S. Z. Yuan, and X. Y. Dong, "Channel spacing and wavelength switchable multiwavelength erbium doped fibre laser using sampled Hi-Bi fibre grating and photonic crystal fibre loop mirror," *Laser Phys. Lett.*, vol. 5, pp. 122-125, 2008.
- [29] S. W. Harun, M. Z. Zulkifli, and H. Ahmad, "A linear cavity S-band Brillouin/erbium fibre laser," *Laser Phys. Lett.*, vol. 3, pp. 369-371, 2006.
- [30] A. A. Latif, M. Z. Zulkifli, N. A. Awang, S. W. Harun and H. Ahmad, "A simple linear cavity dual-wavelength fibre laser using AWG as wavelength selective mechanism," *Laser Phys.*, vol. 20, pp.2006-2010, 2010.

- [31] N.A. Awang, H. Ahmad, A.A. Latif, M.Z. Zulkifli, Z.A. Ghani, S.W. Harun, "Wavelength conversion based on FWM in a HNLF by using a tunable dual-wavelength erbium doped fibre laser source," *Journal of Modern Optics*, vol. 58, pp. 566-572, 2011.
- [32] L. R. Chen and X. Gu, "Dual-wavelength Yb-doped fibre laser stabilized through four wave mixing," *Optics Exp.*, vol. 15, pp. 5083-5088, 2007.
- [33] P. A. Andersen, T. Tökle, Y. Geng, C. Peucheret, and P. Jeppesen, "Wavelength Conversion of a 40-Gb/s RZ-DPSK Signal Using Four-Wave Mixing in a Dispersion-Flattened Highly Nonlinear Photonic Crystal Fiber" *IEEE Photonics Technology Letters*, vol. 17, pp. 1908-1910, 2005.
- [34] J. Yu and M. F. Huang, "Wavelength conversion for 112Gbit/s PolMux-RZ-QPSK signals based on four-wave mixing in high-nonlinear fiber using digital coherent detection," *Optical Communication*, 2008. ECOC 2008. 34th European Conference, pp.1-2, 21-25 Sept. 2008.
- [35] Z.G. Lu, J.R. Liu, S. Taebi, Y. Song, X.P. Zhang, and T. Hall, "Ultra-broadband wavelength conversion system by using photonic crystal fiber", *Passive Components and Fiber-based Devices IV*, Proc. of SPIE Vol. 6781, 67811L, 2007.
- [36] Y. P. Yatsenko, A.F. Kosolapov, A.E. Levchenko, S.L. Semjonov, and E.M. Dianov, "Broadband wavelength conversion in a germanosilicate-core photonic crystal fiber," *Opt. Lett.* 34, pp. 2581-2583, 2009.
- [37] K. K. Chow, M. W. K. Mak, C. Shu and H. K. Tsang: Widely Tunable All-Optical Wavelength Converter Using a Fiber Ring Cavity Incorporating a Semiconductor Optical Amplifier. *Optics Communications*, vol. 203, pp. 101-106, 2002.

- [38] K. K. Chow, C. Shu, M. W. K. Mak and H. K. Tsang: Widely Tunable Wavelength Converter Using Double Ring Fiber Laser with a Semiconductor Optical Amplifier. *IEEE Photonics Technology Letters*, vol. 14, pp. 1445-1447, 2002.
- [39] J. H. Han, "Four-wave mixing in intra-cavity dual-wavelength fiber ring laser," *Electronics Letters*, vol. 47, pp. 612 -614, 2011.
- [40] K. Inoue, "Four wave mixing in an optical fibre in the zero-dispersion wavelength region," *J. Lightwave Techno.*, vol. 10, pp.1553-1561, 1992.
- [41] H. Ahmad, N. A. Awang, A. A. Latif, M. Z. Zulkifli, Z. A. Ghani, and S. W. Harun, " Wavelength conversion based on four-wave mixing in a highly nonlinear fibre in ring configuration," *Laser Phys. Lett.*, vol. 8, pp. 742–746, 2011.
- [42] S. Petit, T. Kurosu, M. Takahashi, T. Yagi and S. Namiki, "Continuously tunable wavelength converter by four-wave mixing in SBS suppressed highly nonlinear fibre," *Electro. Lett.*, vol. 45, pp. 1084-1085, 2009.
- [43] D. Dahan, E. Shumakher and G. Eisenstein, "A multiwavelength short pulse source based on saturated optical fibre parametric amplification," *IEEE Photonics Techno. Lett.*, vol. 18, pp. 592-594, 2006.
- [44] A. D'Ottavi, Francois Girardin, L. Graziani, F. Martelli, P. Spano, A. Mecozzi, S. Scotti, R. Dall'Ara, J. Eckner, and G. Guekos, "Four-wave mixing in semiconductor optical amplifiers: a practical tool for wavelength conversion" *IEEE J. Selected Topics in Quantum Electron.*, vol. 3, pp. 522-528, 1997.
- [45] H. J. Kim and J. I Song, "An all-optical frequency up-converter utilizing four-wave mixing in a semiconductor optical amplifier for sub-carrier multiplexed radio-overfibre applications," *Optics Exp.*, vol. 15, pp. 3384-3389, 2007.
- [46] M. J. Connelly, *Semiconductor Optical Amplifier*, Kluwer Academic Publishers, 2004.

- [47] N.A. Awang, H. Ahmad, A.A. Latif, M.Z. Zulkifli and S.W. Harun, "Four-wave mixing in dual wavelength fibre laser utilizing SOA for wavelength conversion," *Optik - International Journal for Light and Electron Optics*, vol. 122, pp. 754–757, 2011.
- [48] K. K. Chow, C. Shu, M. W. K. Mak, and H. K. Tsang, "Widely tunable wavelength converter using a double-ring fibre laser with a semiconductor optical amplifier," *IEEE Photonics Techno. Lett.*, vol. 14, pp. 1445-1447, 2002.
- [49] S. Diez, C. Schmidt, R. Ludwig, H. G. Weber, K. Obermann, S. Kindt, I. Koltchanov, and K. Petermann, "Four-wave mixing in semiconductor optical amplifiers for frequency conversion and fast optical switching," *IEEE Journal of Selected Topics in Quantum Electro.*, vol. 3, pp. 1131-1145, 1997.
- [50] C. M. Greco, F. Martelli, A. D'Ottavi, A. Mecozzi, P. Spano, and R. Dall'Ara, "Frequency-conversion efficiency independent of signal-polarization and conversion-interval using four-wave mixing in semiconductor optical amplifiers" *IEEE Photonics Techno. Lett.*, vol. 11, pp. 656-658, 1999.
- [51] Z. J. Lu, L. Dong and J. Yu Chen, " Polarization Insensitive Wavelength Conversion Based On Four-Wave Mixing For Polarization Multiplexing Signal In High-Nonlinear Fibre," *Optics Comm.*, vol. 282, pp. 1274–1280, 2009.
- [52] N. A. Awang, H. Ahmad, A. A. Latif, M. Z. Zulkifli, Z. A. Ghani and S. W. Harun, "O-band to C-band wavelength converter by using four-wave mixing effect in 1310 nm SOA," *J. Modern Opt.*, vol. 57, pp. 2147-2153, 2010.
- [53] J. P. R. Lacey, , G. J. Pendock, and R. S. Tucker, "All-optical 1300 nm to 1550 nm wavelength conversion using cross gain modulation in a SOA," *IEEE Photonic Techno. Lett.*, vol. 8, pp. 885-887, 1996.

- [54] C. Q. Xu, H. Okayama, and M. Kawahara, "Wavelength conversion between two silica loss window at 1.31 and 1.55 μm using different frequency generations," *Elect. Lett.*, vol. 30, pp. 2168-2169, 1994.
- [55] Z. G. Lu, P. J. Bock, J. R. Liu, F. G. Sun, T. J. and Hall, "All-optical 1550 nm to 1310 nm wavelength converter," *Electro. Lett.*, vol. 42, pp. 937-938, 2006.
- [56] M. Matsuura, N. Kishi and T. Miki, "Ultrawideband wavelength conversion using cascaded SOA based wavelength converters," *J. Lightwave Techno.*, vol. 25, pp. 38-45, 2007.
- [57] J. P. Turkiewicz, G. D. Khoe, and H. De Waardt, "All-optical 1310 to 1550 nm wavelength conversion by utilising nonlinear polarization rotation in semiconductor optical amplifier," *Electron. Lett.*, vol. 41, pp. 29-30, 2005.
- [58] D. Nasset, T. Kelly and D. Marcenac, "All-optical wavelength conversion using SOA nonlinearities," *IEEE Communication Magazine*, vol. 36, pp. 56-61, 1998.
- [59] S. Diez, C. Schmidt, R. Ludwig, H. G. Weber, K. Obermann, S. Kindt, I. Koltchanov and K. Petermann, "Four-wave mixing in semiconductor optical amplifiers for frequency conversion and fast optical switching," *IEEE J. Selected Topics in Quantum Electro.*, vol. 3, pp. 1131-1145, 1997.

CHAPTER 5

FWM APPLICATION IN FIBRE OPTICAL PARAMETRIC AMPLIFIER (FOPA) AND MULTIWAVELENGTH FIBRE LASER

5.1 Introduction

In addition to wavelength conversion in HNLF and SOA discussed in the previous chapter, further applications such as FOPA and multiwavelength fibre laser via the FWM effect in the HNLF are discussed in this chapter. FOPAs are used in lightwave systems for several signal-processing applications including optical amplification, phase conjugation and wavelength conversion. While multiwavelength fibre lasers are useful light sources for wavelength division multiplexer, fibre sensor and testing of optical instruments.

5.2 FOPA

FOPA employs the nonlinear phenomenon of FWMs to transfer energy from one or two strong pump fields to weak signal fields. FWM is a parametric process stemming from the third-order nonlinear response of materials [1]. The first experiment that demonstrated FWM in a fibre was done in the year 1974 [1]. FOPA, which is based on FWM inside optical fibres, is attracting considerable attention as they because they can provide

broadband amplification and can thus replace erbium-doped fibre amplified used commonly for signal amplification [2] – [4]. FOPA are multifunctional devices that have been used in a wide range of applications, especially in the telecommunications industry where they have been used as pulse sources, demultiplexers, preamplifiers, wavelength converters and in all-optical sampling [5] – [7]. A feature unique to FOPA is that the idler field is generated during the signal amplification [8]. However, the FOPA is also an ideal candidate for ultrafast, all optical, signal processing because of instantaneous nonlinear electronic response of silica which is responsible for FWM in optical fibres. Moreover, amplification provided by FOPAs has relatively low noise, allowing operation close to the quantum limit [9] – [10].

In this section, the basic principle, system applications and current available technologies of FOPA system are described. Employing a high output power EDFA (several Watts) to amplify the pump signal in the amplifying fibre, researchers such as T. Yamamoto [11], T. Torounidis [12] and J. Hansryd [13] reported FOPA system gains of around 29 dB (1.9 W) [11], 70 dB (1.9 W) [12] and 49 dB (2.0 W) [13]. However, in this experiment, the pump signal which is amplified by a high output power EDFA (0.5 W) is used, although this pump signal has insufficient energy to amplify the signal power directly. Therefore, a ring configuration is used to increase the pump power. This technique could obtain an efficient parametric gain of 28 ± 3 dB within a 30 nm tuning range. This technique also produced an efficient wavelength conversion of -4 ± 1 dB within a 20 nm tuning range. This high gain is achieved using efficient SBS suppression on a pump and amplified signal. A high gain amplifier could be useful as ASE sources, preamplifiers in low bit rate communication systems, or in free space communication system.

5.2.1 Principle of FOPA

FOPA occurs when a strong pump (ω_p) and a weak signal (ω_s) co-propagate in the optical fibre and interact through the Kerr nonlinearity effect after which the two frequencies are beating with each other. This process allows the transfer of energy from the pump to the signal, generating a new wavelength component, thereby acting as a wavelength converter. FOPA can be achieved by either one or two pumps. The configuration of a one pump FOPA is shown in Figure 5.1. It is similar to the other fibre based amplifiers. Due to the presence of the idler, a filter is required after the fibre to filter out a residual pump power, ASE noise and the idler (or the signal if it is intended to be used as wavelength converter). The efficiency of this process is strongly dependant on the pump wavelength. The pump is usually operates near the zero-dispersion wavelength of the fibre for the best phase matching.

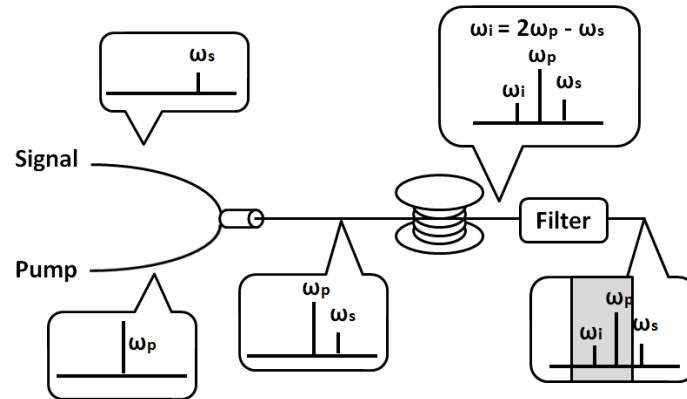


Figure 5.1 Configuration of a single pump FOPA.

Figure 5.2 shows the configuration of a two-pump FOPA system. In this configuration the pumps are placed far from the signal band, which offers several advantages such as a flat gain in wider bandwidth. The wavelength converter is determined by the following relationship

$$\omega_c = \omega_{Pump1} + \omega_{Pump2} + \omega_{signal} \quad 5.1$$

Although the two pump configuration is more complicated, it provides extra degrees of freedom to allow flat gain bandwidth [11] and polarization independent operation [12]. This was not performed in this work due to the limited availability of tunable pump sources with high output power.

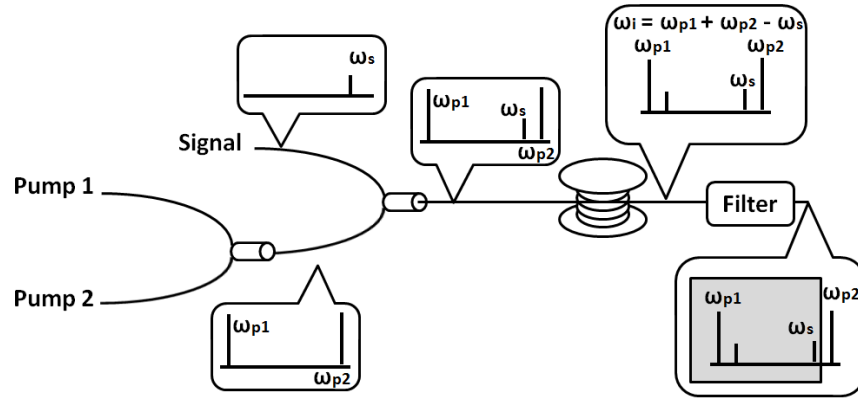


Figure 5.2 Configuration of a two-pump FOPA.

5.2.2 Basic Equations of FOPA

This section explains the gain formula and identifies the important parameters which influence a FOPA. Consider a pump with power P_1 and signal, P_s , with radian frequencies of ω_p and ω_s , respectively, co-propagating in the z direction in a lossless fibre with a nonlinearity coefficient, γ . A parametric gain amplifies the signal as well as an idler arising at $\omega_i = 2\omega_p - \omega_s$.

The signal power gain and idler conversion efficiency are obtained by assuming a single polarization and no pump depletion. Single polarization means that all three waves have the same linear state of polarization. No pump depletion means the pump power is much stronger than the signal power, so that the pump power can be assumed constant throughout the fibre. In the no-depletion approximation the parametric amplification is described by the signal power gain [1];

$$G_s(L) = 1 + \left[\frac{\gamma P_s}{g} \sinh(gL) \right]^2, \quad 5.2$$

where P_s is the signal power in the fibre, γ is the fibre nonlinear coefficient and L is the fibre length. The parametric gain, g is given by [1]

$$g^2 = -\Delta\beta \left(\frac{\Delta\beta}{4} + \gamma P_s \right), \quad 5.3$$

where $\Delta\beta$ is the phase mismatch

$$\Delta\beta = \frac{2\pi\lambda^2}{c} D \cdot \Delta f^2, \quad 5.4$$

with the dispersion parameter, $D = \frac{-2\pi c}{\lambda^2} \beta_2$, β_2 is the group velocity dispersion parameter.

Figure 5.3 shows the spectrum evolution of the gain shape as the pump moves across the ZDW. The thick line in the middle represents a typical plot of fibre dispersion versus wavelength, with a positive dispersion slope. The graph shows that when the pump wavelength satisfies $\lambda_p < \lambda_0$, the gain rapidly falls with distance from the pump. On the other hand, when $\lambda_p > \lambda_0$, the maximum gain is larger and is characterized by a double peak. Figure 5.3 also shows that the gain bandwidth decreased as the pump wavelength is moved away from λ_0 . This is because the phase-mismatch, $\Delta\beta$, grows faster. Therefore, the maximum bandwidth usually occurs when the pump is at a wavelength that is slightly above the ZDW.

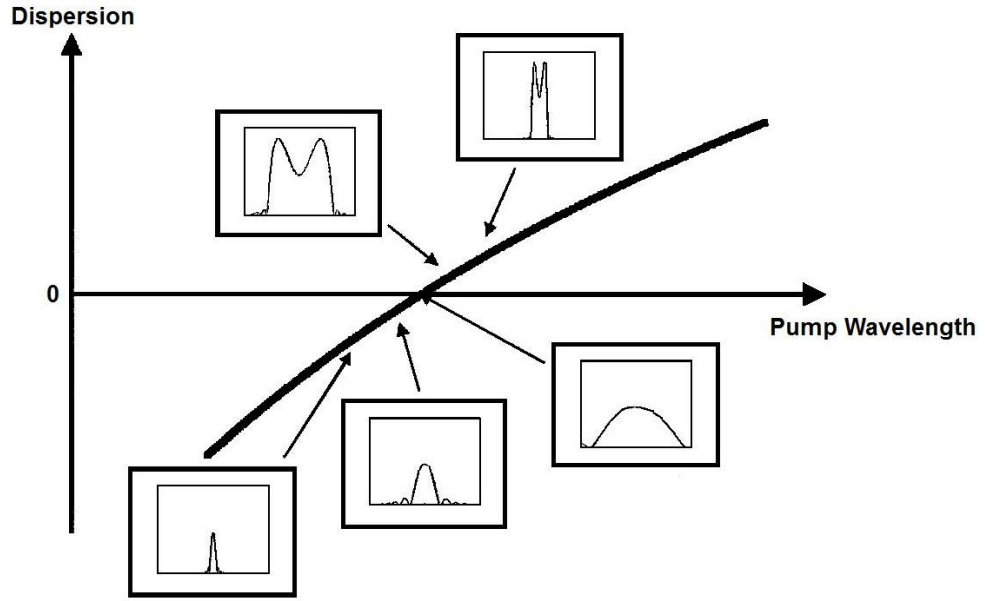


Figure 5.3 Gain shape versus pump wavelength location.

Figure 5.4 shows the theoretical gain spectrum against the signal wavelength for the HNLF. The gain bandwidth of the HNLF, calculated from this figure, is 73 nm. The parameters used in the theoretical gain spectrum are $\lambda_0 = 1531$ nm, $D = 0.007$ ps⁻¹nm⁻¹km⁻¹, $\gamma = 11$ km⁻¹W⁻¹ and $\lambda_p = 1580$ nm. λ_0 is not ideal because it is 49 nm away from the available pump wavelength. However, a significant result can still be obtained despite separation between pump and ZDW.

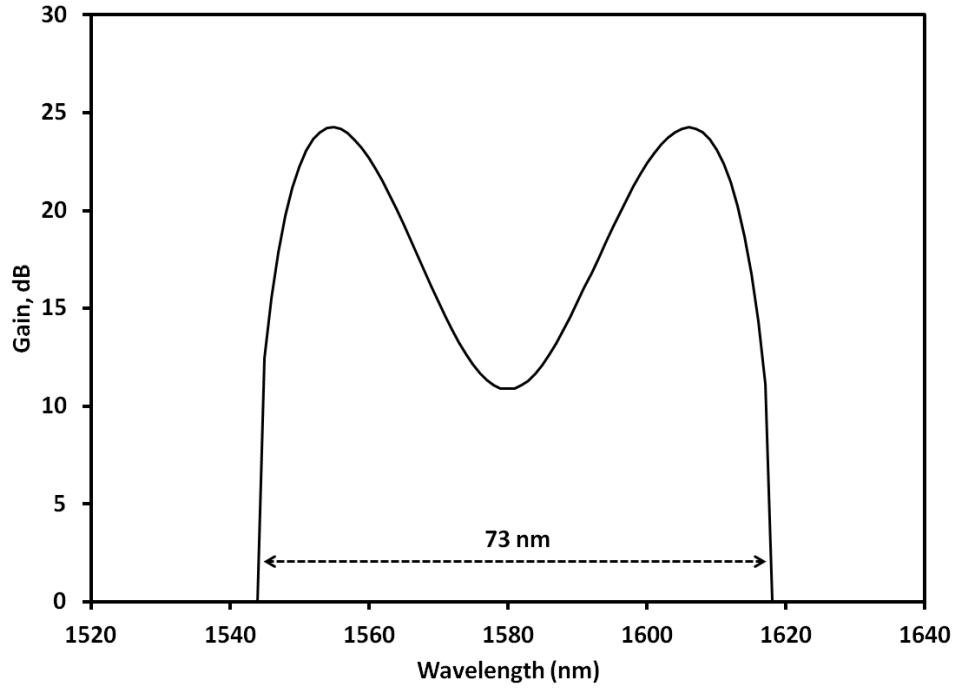


Figure 5.4 Gain spectrums for a single pump FOPA.

5.2.3 Demonstration of single pump FOPA in a HNLF

This section reports the demonstration of a single pump FOPA which utilizes a HNLF as well as a fibre provided by OFS. The experiment setup for the FOPA is shown in Figure 5.5. A TLS1, YOKOGAWA AQ2200 served as the pump signal, P_p . The pump signal is subsequently amplified using an erbium-doped fibre which acts as an optical amplifier via isolator 1. The EDFA consisted of the 11 m Metrogain erbium doped fibre (DF1500L, Fibrecore ltd.) with an Erbium ion concentration of 900 ppm and absorption coefficient of 18.06 dB m^{-1} and 11.3 dB m^{-1} at 1530 nm and 980 nm respectively. The EDF is pumped by a laser diode with pump power of 500 mW at two laser diode pump wavelength 1460 nm and 1490 nm. A PC is used to align the state of polarization of the pump signal. The TLS 2 is used as the signal wavelength, P_s to be amplified by the FOPA system which is

connected to an isolator. The PC at the output of the isolator is employed to align the state of polarization of the signal so as to coincide with the pump's polarization such that the most efficient parametric amplification occurs. The signal and pump are then combined using a 10 dB fused fibre coupler and the output is connected to a 100 m length of HNLF. The HNLF is used as the nonlinear medium to generate FWM when a two closely spaced signal (pump and signal) travel in this fibre. The output signal is detected using an OSA which is connected to the 10% port of the 90/10 coupler. The other coupler port (90% port) is connected to the variable optical coupler which is then used as a pump signal oscillating in a ring configuration to generate the highest output pump power capable to amplify the power signal in the 100 m HNLF.

Figure 5.5 Schematic diagrams for generating FWM effect in a ring configuration [14].

In Figure 5.6 the optical spectra measured by an OSA in Figure 5.5 is shown with the pump turned off and turned on. The wavelength of the signal is at 1585 nm. It can be observed that the signal receives a parametric gain of 28 dB, and a strong idler at 1583 nm is also generated. The input signal power, P_{sin} is -34.8 dBm. The measured optical SNR is 43 dB at the 0.02nm resolution bandwidth, which is limited by the non-ideal suppression of an ASE noise from the 11 m EDFA. The gain (an output power/an input power) is measured by comparing the signal power, P_{sin} , in Figure 5.6 with the signal and idler power, P_{sout} and P_{iout} , respectively.

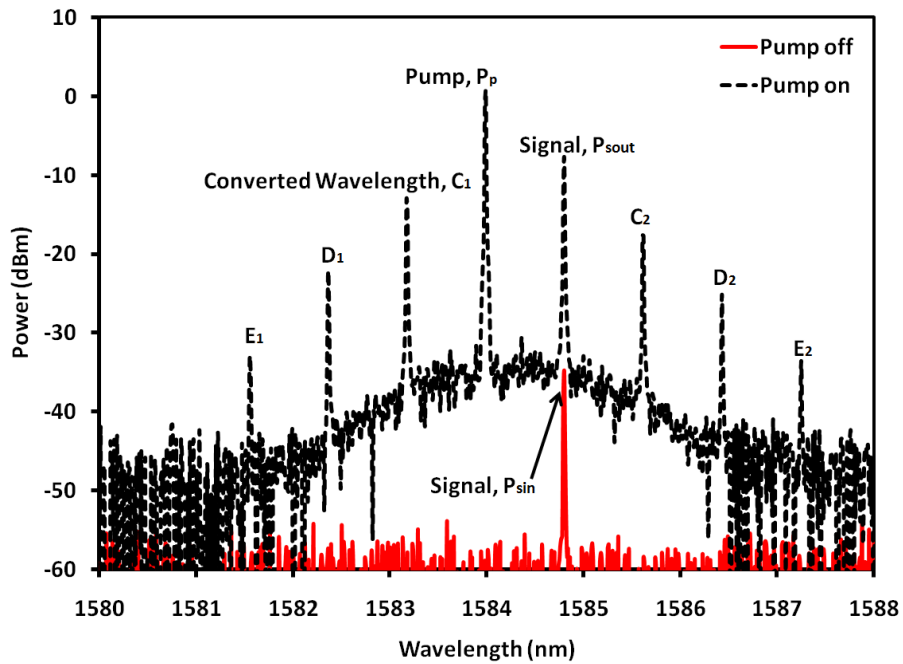


Figure 5.6 Power spectra at the output of the fibre [14].

Figure 5.7 shows the obtained on-off gain versus signal wavelength into the HNLF. An on-off gain of 28 dB is obtained, but it does not account for the losses in the fibre, e.g. splice losses and 90/10 coupler losses. The gain can be more appropriately measured by taking the on-off gain and reducing the loss between the input and output power. The highest black box gain measured is 18.2 dB for a signal wavelength at 1575 nm, which corresponds to a 18.2 dB gain ($28 - 9.8 = 18.2$ dB) gain [14], whereby the insertion loss for the 90/10 coupler is 9.8 dB. These measurements are taken by varying the signal wavelength, P_s , and the pump wavelength, P_p is fixed at 1585 nm, as in the case shown in Figure 5.6. As the signal is increased from 1564 nm to 1570 nm, the on/off gain is improved from 11.62 dB to 27.35 dB. Further increases of P_s do not change the on/off gain much as it plateaus between 1570 nm to 1594 nm. The peak to peak variation within a region of 22 nm is only about 3 dB. Hansryd et. al [13] reported that the generation of FOPA system needs a maximum output power of 2.0 W to obtain 49 dB of on/off gain and Torounidis, et. al [12] reported the FOPA can be achieved at 70 dB on/off gain with 2.8 W of output power with -48 dBm of input power. However, in this study, an output power of only 400 mW [14] is used to oscillate the laser with the large portion of 90/10 coupler used to increase the output pump power so that it capable to transfer the energy into signal power. The output power was limited by both a saturation effects from the ASE and the SBS on the amplified signal.

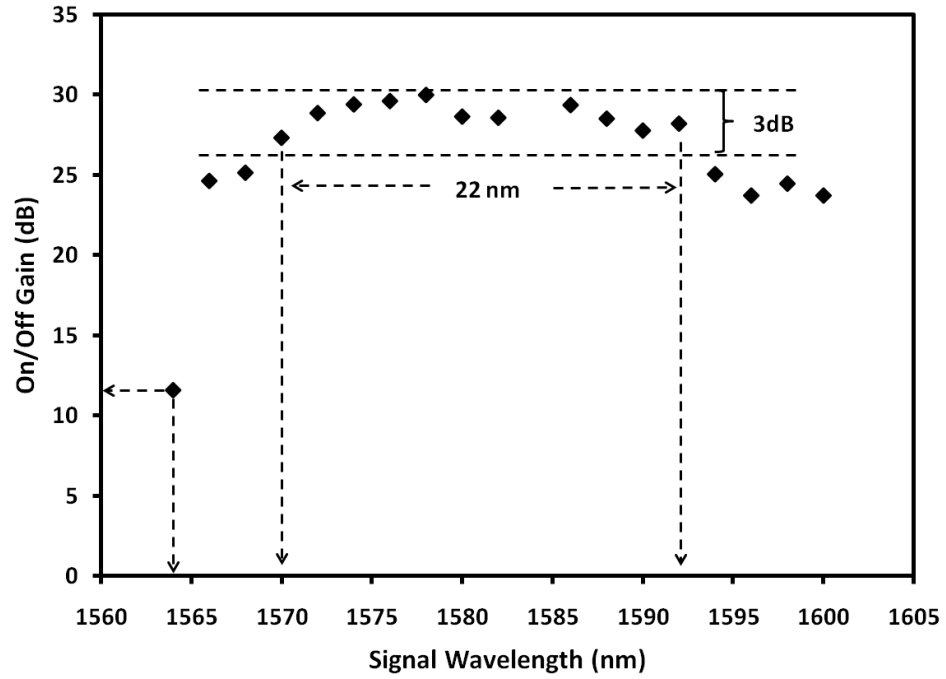


Figure 5.7 Gain versus signal wavelength, $P_{in} = -34$ dBm [14].

5.3 Multiwavelength fibre laser

Multi-wavelength fibre lasers are of great interest for many applications in optical communications such as wavelength division multiplexing, fibre optic sensor and wavelength conversion [15] – [17]. This has been reported and investigated using various gain media such as EDFs [15] [17] and also in SOAs [19]. EDF based multi-wavelengths sources are of special interest due to their advantages such as low cost, low threshold power, high power conversion efficiencies and its compatibility with existing optical communications infrastructure [16]. However, there are many difficulties in the realization of multi-wavelength fibre sources due to issues of strong mode competition in EDFAs and also significant fluctuations in the output power stability, making them unsuitable for practical applications. Among these issues, mode competition is the most difficult to

overcome as it arises from the homogeneous line broadening in the EDF. The FWM effect can be employed to generate a stable multiwavelength output in the HNLF, and is investigated here.

In this section, a compact ring configuration multiwavelength fibre laser utilizing the FWM effect in a short length HNLF is demonstrated. In an earlier work [17] the generation of five stable multi-wavelengths has been demonstrated based on the FWM effect on this type of fibre with a SNR of 20 dB. Generally, the generation of the multi-wavelength output based on the FWM effect in the HNLF uses a very long fibre and a very high gain amplifier with a saturated output power of around 30 dBm [18]. Most of the designs utilize a ring configuration with a Sagnac Loop Mirror (SLM) [18], giving a low SNR and also questionable output stability. The system applied in this study used a low power EDFA as the gain medium to provide the amplification for the FWM process, thus increasing the efficiency of the system [20]. The system does not use any SLM in the cavity, which therefore produced higher SNR of more than 40 dB and a very stable output power with fluctuations of less than 0.1 dB for a test period of over one hour.

The following Figure 5.8 below shows the experimental setup of the HNLF based on a multiwavelength fibre laser in a ring cavity configuration. The main components of the ring cavity are a forward-pumped EDFA, a 100 m long HNLF, an optical circulator and also a 90/10 output coupler which is used to tap a portion of the output signal into the OSA with a resolution of 0.02 nm. The EDFA consisted of an 11 m Metrogain EDF (DF1500L, Fibrecore Ltd.) with an Erbium ion concentration of 900 ppm and signal and pump absorption coefficients of 18.06 dB m^{-1} and 8.3 dB m^{-1} at 1530 nm and 1490 nm respectively. The EDF is pumped by a 1490 nm laser diode at a pump power of 90 mW.

The HNLF is used to increase the nonlinear effect similar to nonlinear FWM effect between the closely spaced longitudinal modes.

For the FWM interaction, two sources of optical signals are designated as the Pump (P_I) and the Signal (P_S) and connected to the ring cavity through an optical circulator and a 3 dB coupler as shown in the Figure 4.8. P_I is generated from a TLS1 that is fixed at a wavelength of 1590 nm with an average output power of 12.8 dBm. P_S is generated from another TLS2 with an average power of 10.8 dBm and the signal is varied from 1570 nm to 1600 nm. The linewidths of these outputs are about 0.015 nm. These two outputs are then passed through into two PCs to alter its polarization state so that maximum power can be achieved and launched into the ring cavity. These two signals are combined using a 3 dB coupler that is then connected to Port 1 of the optical circulator. At this point, two wavelengths (P_I and P_S) are produced and injected into the ring cavity through Port 2 of the optical circulator, which are then reflected through the optical circulator in anti-clockwise direction. This process amplifies the dual wavelength optical signal in the EDFA, which then continues to travel towards the HNLF. The two wavelengths have therefore interacted in the non-linear gain medium to generate more wavelengths based on the FWM effect. This can be achieved with the condition that they are phase-matched. As in the case of the above ring configuration, the generated wavelengths from the FWM effect are initially low in power, but the power increases as they oscillates in the cavity several times. The output of the FWM spectrum is tapped out from the coupler with a larger portion of the light allowed to oscillate in the ring cavity.

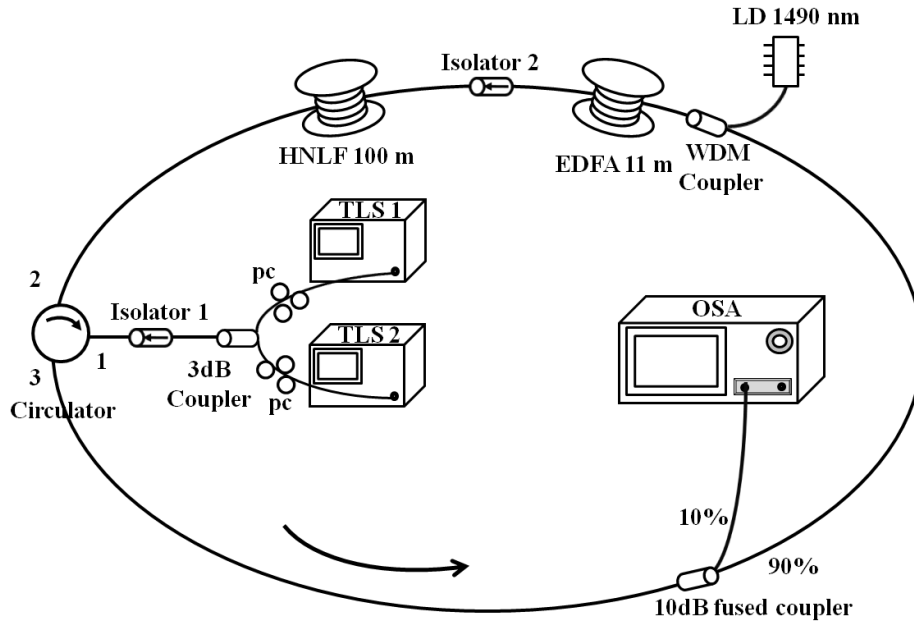


Figure 5.8 Experimental setup of HLNF based multiwavelength fibre laser in a ring Cavity configuration [20].

Since the EDF is a homogeneously broadened gain medium, there will be mode competition between the different oscillating wavelengths. Therefore, tunable lasers are used to generate the dual-wavelength output so as to lock-in the dual-wavelength oscillations in the ring cavity. Figure 5.9 shows a free-running EDF laser output that is taken without the dual wavelength input from TLS1 and TLS2. The EDF is pumped at 1490 nm laser diode using a pumping power of 90 mW. In this spectrum, it can be seen that only a few peaks in the L-band region of 1570 to 1600 nm are present. This is due to the long length of the highly-doped EDF that was used, whereby a Conventional (C-) Band ASE is used to pump the end portion of the EDF, thus generating operation in the Long-Wavelength (L-) band region. By reducing the length of this fibre, the same observation can be made for the C-band region. In this thesis, the demonstration has been done in the L-

band region mainly to utilize the uniform gain that is achievable in the L-band region, giving the same gain for wavelengths in this region. In this regard, the chosen wavelength of operation for the FWM effect should be within the region of the free-running condition of the EDF laser which exhibits a peak power of about -40 dBm and a bandwidth of approximately 4 nm centered at 1591.8 nm.

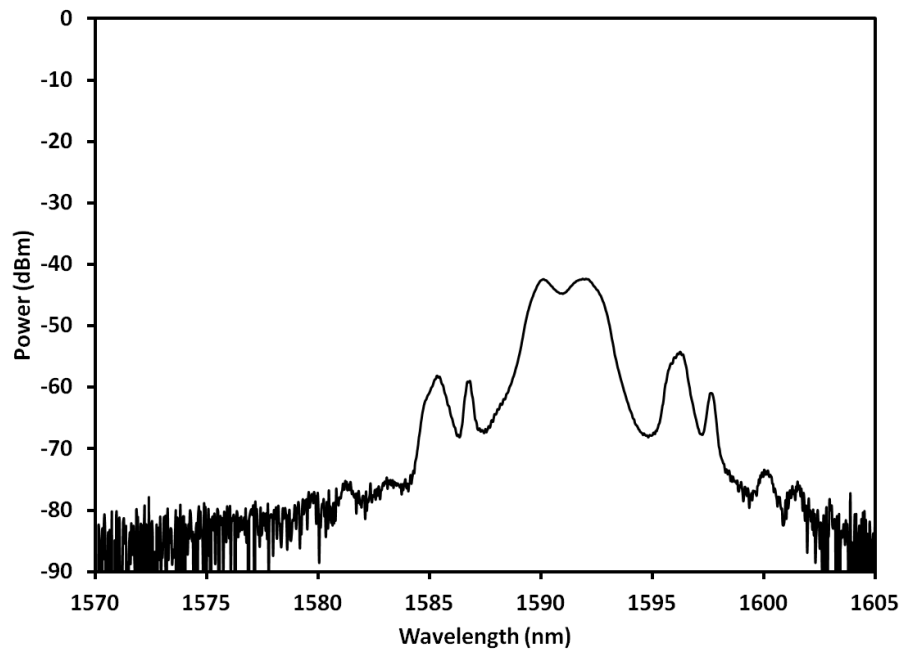


Figure 5.9 Free-Running Spectrum of the FWM (without pump and signal wavelengths) [20].

The dual-wavelength fibre laser is initially amplified by the EDFA and then launched into the HNLF and will generate a multi-wavelength output as shown in Figure 5.10. The occurrence of the FWM effect in the HNLF is due to the incidence of the dual-wavelength lasers (for instance λ_1 and λ_2) where it produces a moving refractive index grating which is

temporally modulated at the wavelength detuning of $\Delta\lambda = \lambda_1 - \lambda_2$. Therefore, any signal at a wavelength of λ that propagates in the HNLF will experience inelastic diffraction by a grating which then has the effect of generating a new wavelength of $\lambda \pm \Delta\lambda$ as these signals travel in the HNLF it will continue to generate wavelengths by the general formula of $\lambda \pm n\Delta\lambda$ ($n = \pm 1, \pm 2, \dots \pm n$). In particular, the incident lasing wavelengths will be self-diffracted and the output spectrum will exhibit a number of sidebands at $\pm n\Delta\lambda$ on each side of the incident wavelengths, thus generating a multi-wavelength output. This can be seen in Figure 5.10 of the generated wavelengths due to the dual wavelength fibre lasers at λ_{P1} and λ_S . These generated wavelengths, λ_{C1} and λ_{C2} , based on the degenerate case of FWM and meeting the phase matching conditions are fulfilled by equations 5.5 and 5.6 [19]:

$$\lambda_{C1} = \lambda_{P1} - (\lambda_S - \lambda_{P1}), \text{ and} \quad 5.5$$

$$\lambda_{C2} = \lambda_S - (\lambda_S - \lambda_{P1}). \quad 5.6$$

These converted wavelengths will also oscillate in the cavity and therefore increase in power, and will continue to generate further wavelengths such as λ_{D1} and λ_{D2} , where λ_{D1} is the side-band generated as a result of the interaction between λ_{C1} and λ_{P1} (the interaction between λ_{C1} and λ_{P1} also generates a signal at λ_S which in this case serves to enhance the power level of the original λ_S signal). In a similar manner, λ_{D2} is the side-band generated as a result of the interaction between λ_{C2} and λ_S (the interaction between λ_{C2} and λ_S also generates a signal at λ_{P1} which in this case serves to enhance the power level of the original λ_{P1} signal). This process is repeated for λ_{E1} and λ_{E2} and other wavelengths as shown in Figure 5.10. This figure also shows that the number of generated wavelengths is measured

against the pump powers of the EDFA as well as the measured SNR, which is found to be 43 dB. As the figure is super-imposed, it is difficult to differentiate the number of lines generated at different pump powers and this is presented in Figure 5.11 for different pump powers of the EDFA and also for different values of the signal wavelength, λ_s .

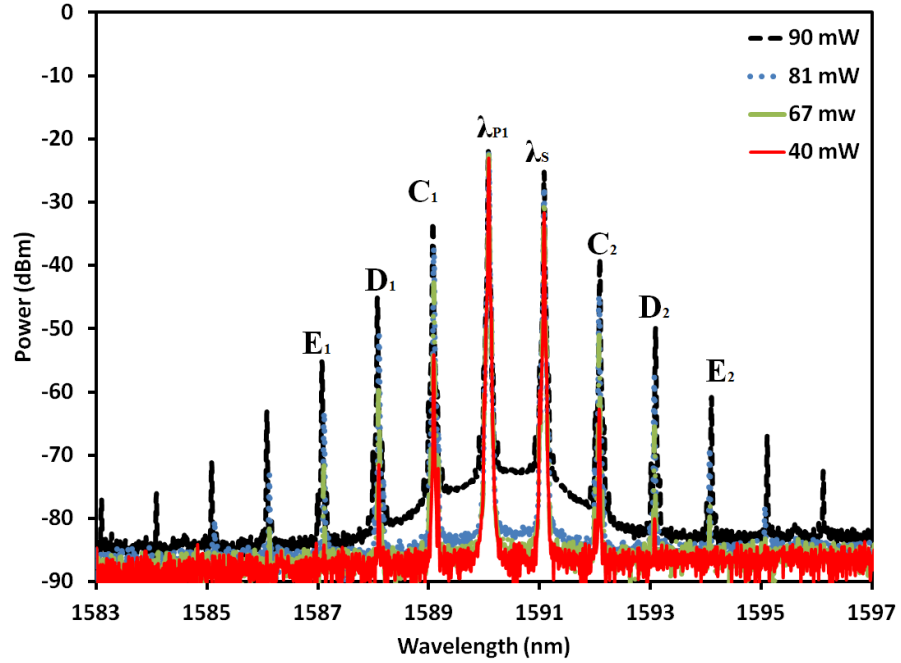


Figure 5.10 Power spectra at the output of the fibre [20].

It can be seen that at a maximum pump power of 90 mW, 11 lines are observed when λ_s is tuned from 1582 nm to 1600 nm, and λ_p is fixed at 1590 nm. The number of lines generated is constant at 11 lines between the signal wavelengths of 1582 nm to 1600 nm at a pump power of 90 mW. At shorter signal wavelengths, the number of lines generated is reduced, with only 7 lines generated at 1573 nm, 9 lines generated at 1576 nm and 10 lines generated at 1578 nm. This could be due to the gain profile of the EDF, where the gain profile is more consistent between 1582 nm to 1600 nm. At a pump power of 80 mW, 9 lines are

generated. As the pump power is reduced further to 67 mW, 8 lines are generated, whilst at 40 mW, 4 lines generated. The reduced number of lines at lower pump powers is due to the lower gain of the EDFA. One of the most important observations is that most of the generated lines at different EDF pump powers give a constant number of lines for different input signal wavelengths.

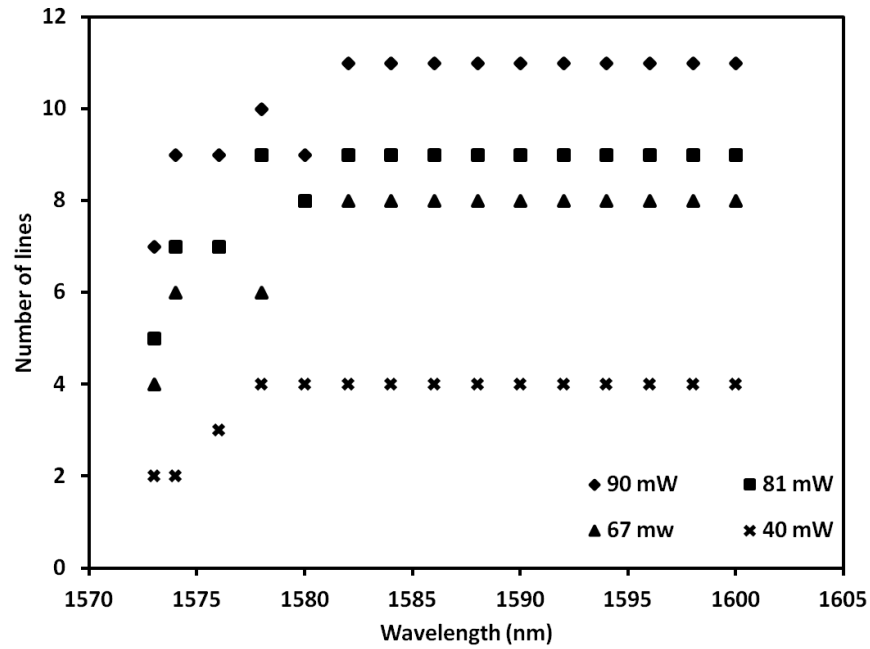


Figure 5.11 Number of generated wavelengths (lines) based on FWM in HNLf with different EDFA pump powers against the signal wavelength, λ_s [20].

The other important measurement is the stability of the output, presented in Figure 5.12. From this figure, it can be seen that the output power of the generated wavelengths are very stable with time. Unlike in the case of multi-wavelength generation in the EDFA, which suffers from mode competition due to the homogeneous line broadening and also instability due to cross-saturation gain for signals with different wavelengths, the multi-wavelength output that is generated based on the FWM effect in the HNLf ensures self-stability as

shown in this experiment. Figure 5.12 also shows the spectral evolutions of the proposed multi-wavelength with HNLF in terms of time. This was taken using repeated scans of the OSA at intervals of 5 minutes to 1 hour. The multi-wavelength output is seen to be stable with peak fluctuations of only 0.1 dB (the points in the graph are actually 13 times taken over the 1 hour span) at room temperature.

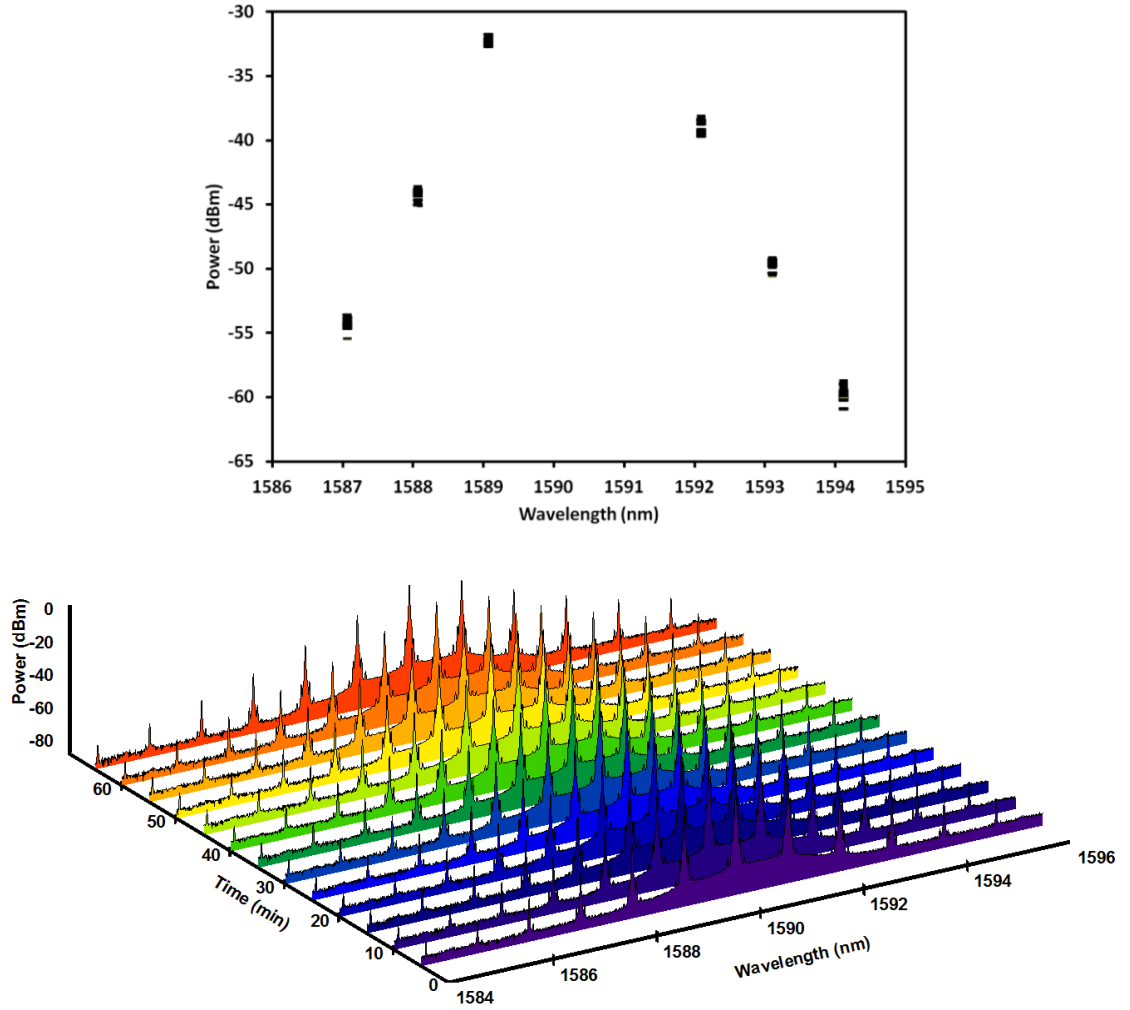


Figure 5.12 Output Power Stability of the Generated Wavelengths based on FWM. Points in the Graph Indicate the Output Power of the Various Generated Wavelengths such as E_1 , D_1 , C_1 , C_2 , D_2 and E_2 of Figure 4 [20].

The advantage of this setup is that it has the ability to generate multi-wavelength outputs based on the FWM effect with a detuning spacing of 1 nm or larger and using a low-gain amplifier with a saturation power of 9 dBm as compared to other setups which uses a much higher saturation power [18]. The other important advantage of this setup is that the length of the HLNf used is much shorter as compared to those used in previous works [18] with similar output power for the generated multi-wavelengths. In addition, the measured SNR is about 43 dB and is higher and better than those typically obtained in similar system, which typically obtain values of roughly 30 dB [20]. In short, the proposed configuration is suitable for wavelength conversion application based on the FWM effect in HLNfs, with very stable outputs that can find applications in optical communication networks.

5.4 Summary

The FOPA and multiwavelength fibre laser produced via the FWM effect are discussed in this chapter. In the first part, the basic principle and equations of FOPA are explained. The successful configuration of a low power single-pump FOPA is achieved with the 28 dB gain and 22 nm wavelength tuning. The compact ring configuration multiwavelength fibre laser utilizing the FWM effect in a short length HNLf is then discussed in the second part.

Reference

- [1] G. P. Agrawal, "Nonlinear Fibre Optics 2nd," Academic Press, San Diego, 2001.
- [2] J. Hansryd, P. A. Andrekson, M. Westlund, J. Li, and P. O. Hedekvist, "Fibre-based optical parametric amplifiers and their applications," IEEE J. Sel. Top. Quantum Electron., vol. 8, pp. 506-520, 2002.
- [3] M. N. Islam and O. Boyraz, "Fibre parametric amplifiers for wavelength band conversion," IEEE J. Sel. Top. Quantum Electron., vol. 8, pp. 527-537, 2002.
- [4] C. J. McKinstrie, S. Radic and A. R. Chraplyvy, "Parametric amplifiers driven by two pump waves," IEEE J. Sel. Top. Quantum Electron., vol. 8, pp. 538-547, 2002.
- [5] S. Radic, C. J. McKinstrie, A. R. Chraplyvy, G. Raybon, J. C. Centanni, C. G. Jorgensen, K. Brar and C. Headley, "Continuous-wave parametric gain synthesis using nondegenerate pump four-wave mixing," IEEE Photon. Technol. Lett., vol. 14, pp. 1406-1408, 2002.
- [6] S. Radic and C. J. McKinstrie, "Two-pump fibre parametric amplifiers," Opt. Fibre. Technol., vol. 9, pp. 7-23, 2003.
- [7] G. A. Nowak, Y. Hao, T. J. Xia, M. N. Islam and D. Nolan, "Low-power high-efficiency wavelength conversion based on modulational instability in high-nonlinearity fibre," Opt. Lett., vol. 23, pp. 936-938, 1998.
- [8] S. Watanabe and M. Shirasaki, "Exact compensation for both chromatic dispersion and Kerr effect in a transmission fibre using optical phase conjugation," J. Lightwave Technol., vol. 14, pp. 243-248, 1996.
- [9] J. A. Levenson, I. Abram, T. Rivera, and P. Grangier, "Reduction of quantum noise in optical parametric amplification," J. Opt. Soc. Am. B., vol. 10, pp. 2233-2238, 1993.

- [10] I. H. Deutsch and I. Abram, "Reduction of quantum noise in soliton propagation by phase-sensitive amplification," *J. Opt. Soc. Am. B*, vol. 11, pp. 2303-2313, 1994.
- [11] T. Yamamoto and M. Nakazawam, "Active optical pulse compression with a gain of 29 dB by using four wave mixing in an optical fibre," *IEEE Photon. Technol. Lett.*, vol. 9, pp. 1595-1597, 1997.
- [12] T. Torounidis, P. A. Andrekson and B. Olsson, "Fibre optical parametric amplifier with 70 dB gain," *IEEE Photon. Technol. Lett.*, vol. 18, pp. 1194-1196, 2006.
- [13] J. Hansryd and P. A. Andrekson, "Broadband continuous wave pumped fibre optical parametric amplifier with 49 dB gain and wavelength conversion efficiency," *IEEE Photon. Technol. Lett.*, vol. 13, pp. 194-196, 2001.
- [14] H. Ahmad, N. A. Awang and S. W. Harun, "Fibre optical based parametric amplifier in a highly nonlinear fibre (HNLF) by using a ring configuration," *Journal of Modern Optics*, vol. 58, pp. 1065-1069, 2011.
- [15] N. Park and P. F. Wysocki, "24 lines multi-wavelength operation of erbium doped fibre laser," *IEEE Photon. Technol. Lett.*, vol. 8, pp. 1459 -1461, 1996.
- [16] A. Zhang, H. Liu, M. S. Demokan and H. Y. Tam, "Stable and broad bandwidth multiwavelength fibre ring laser incorporating a highly nonlinear photonics crystal fibre," *IEEE Photon. Technol. Lett.*, vol. 178, pp. 2535-2537, 2005.
- [17] Y. G. Han, T.V. A. Tran and S. B. Lee, "Wavelength spacing tunable multiwavelength erbium doped fibre laser based on four wave mixing of dispersion shifted fibre," *Opt. Lett.* vol. 31, pp. 697-699, 2006.
- [18] D. S. Moon, U. C. Paek, Y. Chung, "Multiwavelength lasing oscillations in an erbium doped fibre laser using a few mode fibre Bragg grating," *Opt. Expr.*, vol. 12, pp. 6147-6152, 2004.

- [19] K. K. Qureshi, H. Y. Tam, W. H. Chung, P. K. Wai, "Multiwavelength laser source using linear optical amplifier," IEEE Photon. Technol. Lett., vol. 17, pp. 1611-1613, 2005.
- [20] N. A. Awang, M. Z. Zulkifli, A. A. Latif, S. W. Harun and H. Ahmad, "Stable power multiwavelength fibre laser based on four wave mixing in a short length of highly nonlinear fibre," J. Opt., vol. 13, pp. 1-5, 2011.

CHAPTER 6

CONCLUSION AND FUTURE WORKS

6.1 Conclusion

In conclusion, we have achieved all objectives set in this work. The conclusion of this thesis can be divided into the following subsections,

- 6.1.1 Nonlinear characterization,
- 6.1.2 Wavelength conversion based on FWM, and
- 6.1.3 Development of FOPA and multiwavelength fibre laser.

6.1.1 Nonlinear characterization.

The first objective of our work is to characterise nonlinear parameters in HNLF and SOA such as the ZDW, CD, nonlinear coefficient, FWM power and FWM efficiency. To this purpose, we employed a procedure based on the FWM effect, a non-interferometric method which is preferred over conventional interferometric methods due to its simplicity, high sensitivity and accuracy, as well as suitability in all currently commercially available fibre types and SOAs. To

accomplish this, three FWM techniques, namely, varying of pump and signal wavelengths, varying the pump while keeping the wavelength constant and keeping the pump constant and varying the wavelength, are investigated. We found that the best technique is the third technique whereby the signal is kept constant while the pump is varied. The third technique was achieved by varying the signal wavelength from 1500 nm to 1600 nm at the variety of pump wavelength. A pump power of 5.5 mW and signal power of 4.25 mW was used for this technique. From this experiment, the ZDW was taken as the meeting point between FWM spectrum powers and was found to be located at 1531 nm. The nonlinear parameters that were obtained from the experiments were then compared to the manufacture's HNLF specification and were found to be similar to the manufacturer's values as in the datasheet (e.g the dispersion slope @ 1550 nm of $0.007 \text{ ps.nm}^{-2}\text{km}^{-1}$, ZDW of 1531 nm and nonlinear coefficient of $10.7 \text{ W}^{-1}\text{km}^{-1}$) with an error of 0.93%.

We then employed this technique for the measurement of the FWM power and FWM efficiency in a SOA, in addition to the gain performance, which is measured using conventional methods. The gain performance is key in determining other nonlinear parameters in an SOA, where in this thesis; the ultra-wide SOA operates at a current of 390 mA. The gain at the lowest input signal power (-35 dBm) in the S-, C- and L-band regions are 23.7 dB, 17.4 dB and 10.2 dB respectively, with output saturation powers of -10 dBm, -5 dBm and 0 dBm, respectively. Using the above values, the highest achievable FWM power, FWM efficiency and SNR are -8 dBm, -14.7 dB and 38.3 dB, respectively, with detailed explanation given in chapter 3.

6.1.2 Wavelength conversion based on FWM

The next objective in this thesis is to study the various configurations in achieving wavelength conversion based on the FWM effect in nonlinear gain media such as HNLF and SOA.

In the case of HNLF as the gain media, two configurations utilising different pump sources for wavelength conversion were studied, namely, dual-wavelength fibre laser and two independent laser sources from two TLS. The nonlinear parameters obtained from these two configurations are summarised as follows in Table 6.1,

Table 6.1 Comparison of two different pump sources for wavelength conversion configuration.

Nonlinear parameter	Dual Wavelength Fibre Laser	Two TLS
Conversion efficiency	-20 dB	-4 dB
Tuning range	180 nm (1460 nm to 1640 nm)	27 nm (1573 nm to 1600 nm)
SNR	30 dB	43 dB
Remarks	<ul style="list-style-type: none">- Low conversion efficiency and SNR- More cost effective and inexpensive- Smooth and wide range tuning of the wavelength	<ul style="list-style-type: none">- High conversion efficiency and SNR- Higher cost- Smaller wavelength tuning

Subsequently, further experimentation is done using SOA as the nonlinear gain medium. In this experiment, the downward wavelength conversion from 1310 nm to 1550 nm was successfully achieved. The dual-wavelength fibre laser is used to generate the FWM effect inside the SOA which acts as both the nonlinear medium as well as the amplifier. This design has the advantage of being compact in size, simple and compatible with current telecommunications system. The experimental setup uses an AWG as a mechanism to generate multiple outputs at 1310 nm, and the required wavelengths can be selected using optical switch selectors. The two outputs at 1310 nm is then combined and interact with another CW wavelength source at 1550 nm to generate the downward conversion. In this configuration, the wavelength conversion from 1316.75 nm to 1542.93 nm with wavelength tuning of 226 nm is obtained with the FWM conversion efficiency reaching -64.42 dB and SNR of 3.5 dB. This second objective is successfully achieve and has been explained in detail in chapter 4.

6.1.3 Development of FOPA and multiwavelength fibre laser

The last objective of this thesis is to construct the FOPA and also multiwavelength fibre laser based on HNLF with the capability to act as an amplifier as well as multiwavelength optical sources. A linear FOPA system with a relatively low pump power (500 mW) was successfully constructed. However, due to the limitations of the availability of certain components in the laboratory, the operation of the linear FOPA cannot provide the required gain owing to insufficient pump power. This mooted an improved design based on a ring cavity configuration, which gave an efficient parametric gain of 28 dB with a tuning range of 30 nm and a fluctuation of only 3 dB. The resulting converted wavelength (from 1564 nm to 1600 nm) is observed to have a wavelength conversion efficiency of -4 dB with a fluctuation of 2 dB within a tuning

range of 20 nm (1570 nm to 1600 nm). The high gain is primarily due to the efficient SBS suppression of the pump and amplified signals.

In the case of the multiwavelength fibre laser system, a length of 100 m of HNLF is used as a nonlinear gain medium in a ring configuration. This system also consists of an EDFA with a 11 m of highly doped EDF and is pumped at 1490 nm with a pump power of 90 mW as to provide the necessary amplification required for the FWM process (refer to section 5.3). With this configuration, the number of lines generated is about 11 lines stretching from 1582 nm to 1600 nm with a SNR of 43 dB. The measured power fluctuates within 0.1 dB over a test period of one hour. The generated multi-wavelength output is very stable which can find many applications as optical sources in DWDM systems, optical instrument testing, optical sensors, and spectroscopy. Therefore, we have successfully met the objective, which have been described in detail in chapter 5.

6.2 Future Work

The nonlinear phenomenon of FWM can be employed for making FOPA. In the simplest implementation of a FOPA, a weak optical signal is amplified by injecting a pump whose wavelength is detuned from the signal by 10 nm or so and falls close to the ZDW of the fibre. In this situation, the phase-matching condition can be satisfied if the pump experiences a relatively small amount of anomalous dispersion. For future work, the proposed configuration can be used for different nonlinear fibres such as photonics crystal (PCF), microstructure and normal dispersion fibres which can have a tuning range of over several hundred nanometres.

Additionally, work can also be done to improve the distortion of a signal pulse in a dual-wavelength fibre laser which is due to the generation of a new wavelength pulse via the FWM effect in the nonlinear media. This system is required for modern WDM systems where it acts as a device that can convert the wavelength of a channel without affecting its bit pattern (or information content).

Another potential future research direction for FWM is for dispersion compensation in WDM systems. This application rests on the important property of phase conjugation during the FWM process. If the pump phase stays constant during the FWM process, the idler represents the phase conjugate of the signal field. As a result, the sign of the accumulated dispersion is effectively reversed for the idler wave.

One final idea for future work might be the production of a source of entangled photon pairs by using FWM in optical fibres. This source is useful for application related to quantum communication, quantum cryptography and quantum computing. Since the signal and idlers photons are generated from the pump photons at the same instant, FWM provides a simple way to generate correlated photon pairs within a single spatial mode. Quantum noise acts as the seed for initiating the so-called spontaneous FWM and generates the correlated signal and idler photons.

APPENDIX A

Selected papers related to this work.

Tunable High Power Fiber Laser Using an AWG as the Tuning Element¹

A. A. Latif^a, H. Ahmad^a, N. A. Awang^a, M. Z. Zulkifli^{a,*}, C. H. Pua^a,
Z. A. Ghani^b, and S. W. Harun^c

^a *Photonics Laboratory, Department of Physics, University of Malaya, 50603 Kuala Lumpur, Malaysia*

^b *Faculty of Applied Sciences, MARA University of Technology, 40450 Shah Alam, Selangor, Malaysia*

^c *Department of Electrical Engineering, Faculty of Engineering, University of Malaya, 50603 Kuala Lumpur, Malaysia*

*e-mail: mohdzamani82@yahoo.com

Received October 27, 2010; in final form November 4, 2010; published online March 4, 2011

Abstract—In this paper, a design of a High Power Tunable Fiber Laser (HP-TFL) in C-band region from 1536.7 to 1548.6 nm is set forth with Erbium Doped Fibers (EDFs) being used as a seeding signal and a booster amplifier. With a 1×16 channels Arrayed Waveguide Grating (AWG), this setup is capable of generating 16 different wavelengths with an average output power of 20.7 dBm.

DOI: 10.1134/S1054660X11070152

INTRODUCTION

High power fiber lasers have attracted much attention due to their applications in Dense Wavelength Division Multiplexing System (DWDM), cutting, drilling and welding [1, 2] for material processing, gravitational wave detection [3, 4] and also marking. Even though applications in the communication systems involve high power fiber lasers, they are however, not as high powered and are just enough for signal transfers of less than several watts. Several different methods have been used to generate high power fiber lasers such as by using a cladding pumping in Ytterbium, but even though they produced a few hundred until thousands of milliwatts of output power which are quite high, the amplification range is only in the 1060 nm region [5–7]. To shift this gain region to a higher wavelength of about 1550 nm region, which is the region that is gaining a lot of interests due to the infrared eye-safe wavelength laser source with high manipulation for use in the communication systems, co-doped fibers called Ytterbium–Erbium doped fibers are used [8–11] with Ytterbium as a pump absorber that transfers energy non-radiatively to Erbium ion. Here the amplification in 1550 nm range is improved by having higher inversion in this region [12]. Due to problems faced in normal silica-based Erbium-doped fibers, high output power fiber lasers cannot be realized. However, there has been a remarkable growth in the use of optical fiber for communication systems especially in providing more efficient laser diode pumps for use in Erbium-doped Fiber Amplifier (EDFA). There are also more devices to provide higher efficiency in amplification including high pump power laser diodes [13, 14] (more specifically for 980 and 1480 nm laser diode pumps) and effi-

ciently coupled pump combiner of certain particular wavelength. Due to this significant improvement, the use of a normal EDF for high power application can now be realized.

A switchable high power fiber laser also has an added advantage due to the selectable wavelength choices. Even though there have been a lot of researches done in tunable fiber lasers [15–20], most of them operate within a low power regime with just a few providing high power switchable fiber lasers [21]. In this paper, we propose a new design of a high power switchable fiber laser using a seeding signal and booster amplifier to provide 20–21 dBm output power by using an AWG and Optical Switch (OS) as a selective element.

EXPERIMENTAL SETUP

Figure 1 illustrates the experimental setup of the high power tunable fiber laser (HP-TFL). It consists of two sections, Sections 1 and 2. Section 1 acts as the seeding signal which serves as an input power for further amplification at booster amplifier in Section 2. The seeding signal uses a 5 m Metrogain Erbium-doped Fiber (EDF) with absorption coefficients of 11.9 dB/m at 979 nm and 16.4 dB/m at 1531 nm as a gain medium. A 980 nm laser diode with 110 mW pump power is connected to the EDF via a 1550/980 wavelength division multiplexer (WDM) coupler. The propagation of 980 nm pump light through WDM coupler to the EDF creates an Amplified Spontaneous Emission (ASE) which then circulates inside the cavity in a clockwise direction. This ASE is then filtered when it enters an Arrayed Waveguide Grating (AWG) which works as a multiplexer that slices the ASE source into 16 different channels in the C-band region. The AWG has been optimized for use in the C-

¹ The article is published in the original.

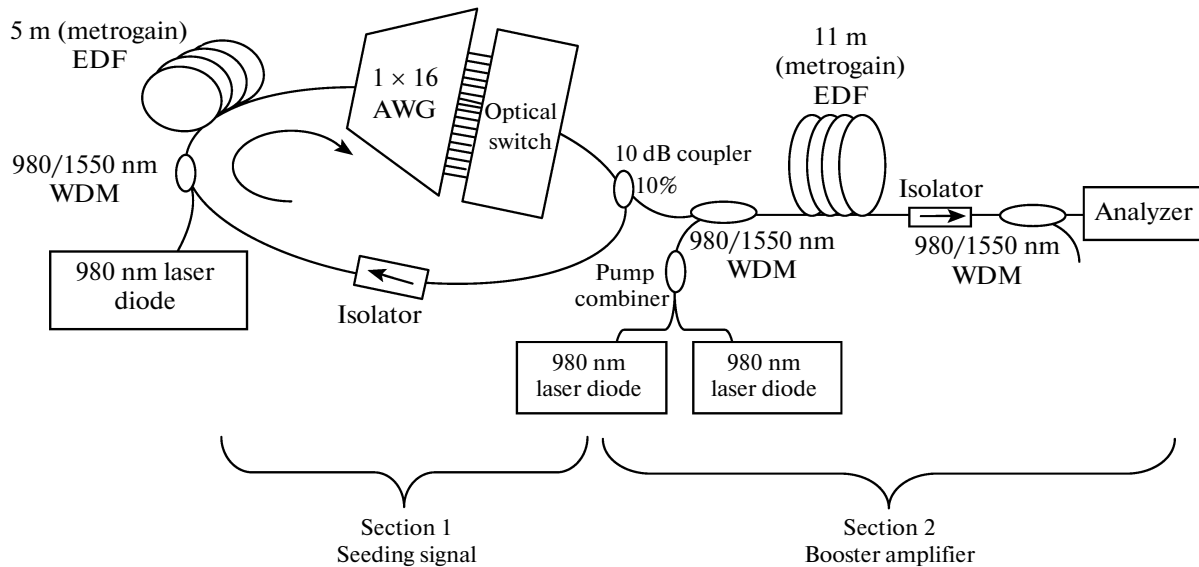


Fig. 1. Experimental setup.

band region with 100 GHz narrow band transmission that equals 0.8 nm of interval spacing (from two adjacent channels). There are 16 lasing wavelengths that begin from channel 1 (1536.7 nm) and end at channel 16 (1548.6 nm). The 16 ports of the AWG are connected to the 2×16 OS which is used to select only one wavelength at a time. This optical switch is a commercial unit for switching in the 1550 nm region with 500 ms switching time between two adjacent channels. As such, the AWG and the OS work together as a wavelength selector inside the cavity. The output of the OS is then connected to the 10 dB coupler with 10% being connected to the output port and 90% of its port works to provide feedback for the laser by connecting it to the 1550 nm input port of the WDM coupler. An isolator is inserted between the 10 dB coupler and the WDM coupler to ensure a unidirectional propagation of the laser inside the cavity and also to enhance the Side Mode Suppression Ratio (SMSR) by compressing the backward ASE for full optimization of the seeding signal output power.

Section 2 of the setup acts as a booster amplifier and it comprises of the 980/1550 nm WDM couplers, an EDF and an isolator. In this section, the 980 nm laser diode is combined by using a pump combiner with a total pump power of 430 mW. This pump is connected to the second EDF via the WDM coupler. 11 m Metrogain EDF is connected to the isolator to optimize the amplification. At the end of this section, 980/1550 nm WDM coupler is inserted to ensure only C-band light source comes out from the output before being connected to the analyzer without the excess pump from the 980 nm source.

RESULTS AND DISCUSSION

Figure 2 shows the ASE of the booster amplifier with 430 mW of pump power that is pumped longitudinally to 11 m of EDF through the WDM when the seeding signal is unconnected from it. As seen in previous studies carried out during the year 2000 [22, 23], the longer the length of EDF used, the peak power of the ASE shifts towards longer wavelength. Based on this fact and the ASE spectrum result that we have, the most suitable high power fiber laser is in the 1560 nm region. And also, due to the high ASE level when using OSA measurement that is higher than -20 dBm at 1560 nm and -35 dBm at 1530 nm, this amplifier is capable of generating an output power fiber laser also in the 1550 nm region. The 3 dB bandwidth of this amplifier is about 11.4 nm which is quite broad. However, due to the AWG used in this setup which is fabricated to be used for the C-band region, that is from 1536.7 to 1548.6 nm, only 16 different wavelengths can be produced with 12 nm of tuning range as depicted in Fig. 3a. Conversely, if a wide tuning range of AWG, such as a 1×40 channels is used, a broader tuning range that includes the C and L regions can be realized, provided the seeding signal also has to produce the output fiber lasers at this particular wavelength.

To observe the output spectrum, measurement is first taken using an optical spectrum analyzer (OSA) and the result is as depicted in Fig. 3a. 16 different wavelengths are obtained by using the proposed setup with an almost flat output power from 1536.7 to 1548.6 nm (12 nm of tuning range). There is 0.8 nm of equal space difference of the AWG that equals 100 GHz tuning step with no distortion on the spec-

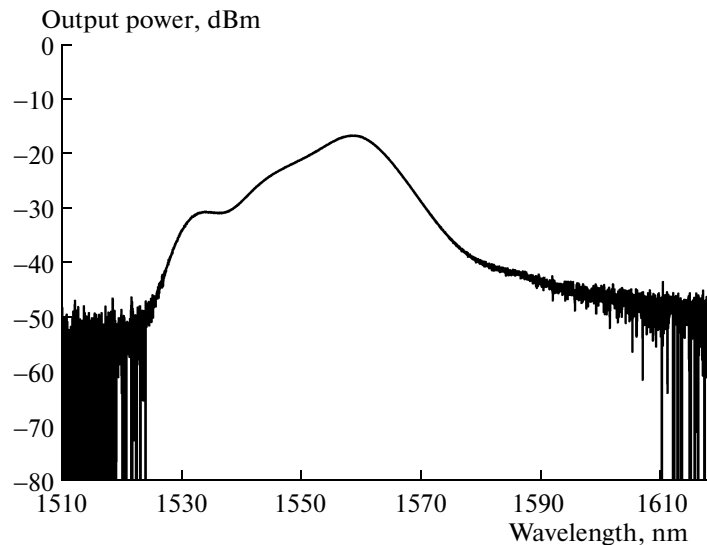


Fig. 2. ASE output power from booster amplifier (Section 2).

trum. As can be seen in the figure, the ASE level is low compared to the output, and this is due to the high compression in the seeding signal. However, the ASE still appears because this type of emission still present in a booster optical amplifier (Section 2) and this can be seen from the measurement using an OSA. As 11 m of EDF is used with a high pump power the results are expected to have the ASE centered at the 1560 nm region. Due to this, it can be seen that the shorter the wavelength the higher the ASE level that is created. This contributes to a smaller difference between the peak power and the noise level.

Figure 3b shows measurements taken using an optical power meter (OPM). The average output power is 20.74 dBm with 0.64 dB maximum difference. The output power increases slightly with an increase in wavelengths and this is due to the power variation which is inherent in wavelength-dependence gain of the EDF. As can be seen, the output power measured by using an OPM is slightly different compared to the one measured by using an OSA due to the different measurement methods of these two devices and it is well accepted that the value given by the OPM is more precise since measurement using OSA is influenced by its resolution and span at the moment the measurement is taken. This fact is confirmed by the measurement taken with the same input power of the OSA that is 5.5 dBm from a small laser source with different wavelengths of 10, 30, and 100 nm. As in the graph, the lower the span range the more accurate is the data obtained as results show a drop of about 2.5 dB for measurements with 30 and 100 nm compared to 10 nm of span as in Fig. 3c.

Figure 4 shows the SMSR measurements taken of the 16 wavelengths with an average value of 59.25 dB. The maximum difference is 2.82 dB, with the highest

value obtained at channel 15 with 60.78 dB of SMSR and the smallest comes from channel 6 with 57.96 dB of SMSR. As is shown in the graph, the laser is stable in terms of SMSR due to the large difference between the output peak power and the ASE level of the laser with the SMSR being higher than 55 dB for each of the laser outputs. By moving towards longer wavelengths, the SMSR gets higher due to the output power gain dependence which is higher at longer wavelengths. As a matter of fact, longer lengths of EDF will shift the ASE towards longer wavelengths. The output power in *L*-band region can also be produced by using an AWG that is fabricated to select the wavelengths in this band.

Figure 5 shows the gain of the booster amplifier with the average input signal power of -3.65 dBm. The average gain of the booster amplifier is 25 dBm. The gain variance is ± 0.6 dB with large decrement comes from channel 8 (1542.3 nm) with 23.75 dB gain, which is 1.25 dB drops from the average value. This lower gain is due to a higher connection loss at this channel port compares to the others. High value of SMSR as depicted in Fig. 4 is due to a high compression of ASE from the booster amplifier with 24.9 dB gain.

Figure 6 shows the stability performance of two wavelengths taken of the shortest and the longest wavelengths from channel 1 and channel 16 respectively, over 60 min operation time. As can be seen, the output powers for these two wavelengths are stable with 20.19 and 20.83 dBm average output powers at channel 1 and channel 16, respectively. The maximum differences of these two channels are 0.18 dB for channel 1 and 0.12 dB for channel 16. The graph also shows that the output power of channel 16 is a little bit higher than that of channel 1 which is due to the wavelength-dependence gain coming from the booster amplifier which has a higher gain spectrum at a longer wave-

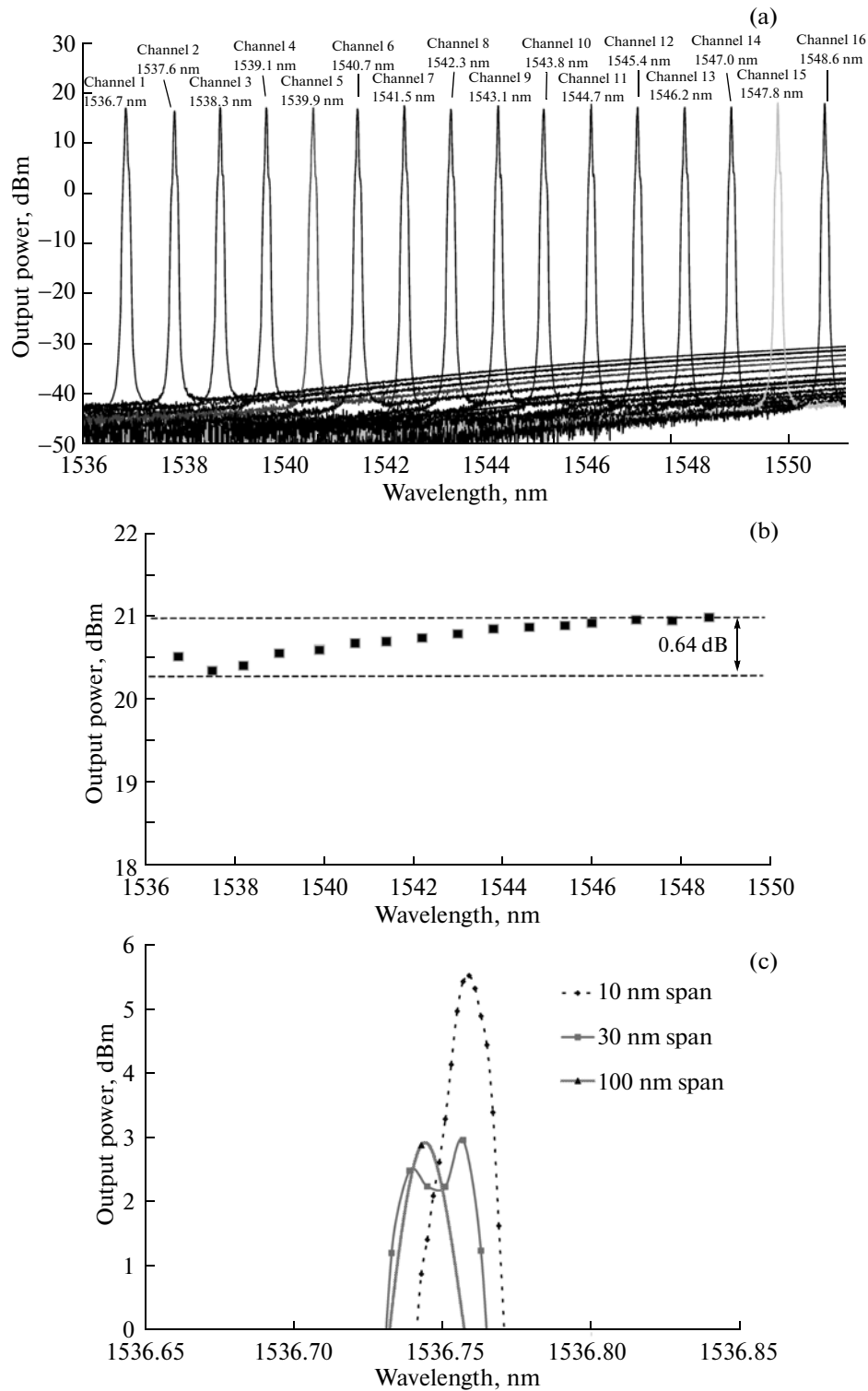


Fig. 3. (a) Superimposed output spectra of 16 different wavelengths. (b) Output powers against wavelengths using an optical power meter. (c) Results obtained using different OSA's span range with the same 5.5 dBm input power.

length. The maximum differences of the output powers are 0.18 and 0.12 dB for channels 1 and 16, respectively. The output power variances are ± 0.09 dB (channel 1) and ± 0.06 dB (channel 16) which are less than

0.1 dB. The proposed setup thus provides a stable and a reliable mechanism that is capable of producing stable output power with very small variation over the one hour period.

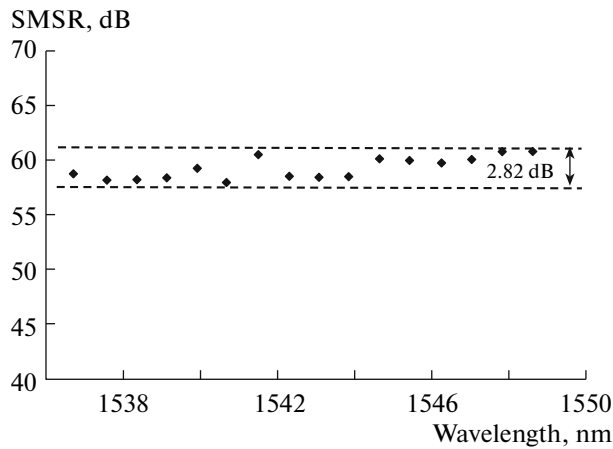


Fig. 4. SMSR of tunable high power laser.

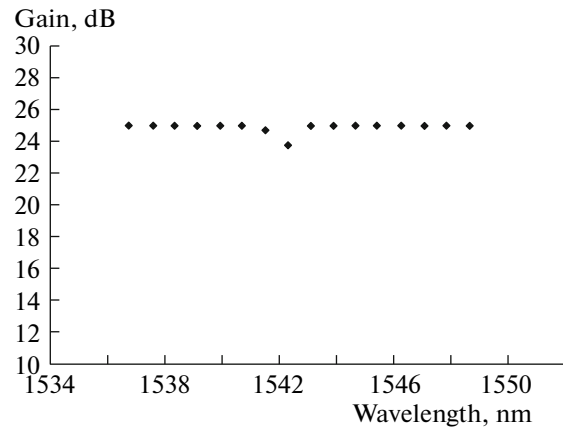


Fig. 5. Gain measurements of the booster amplifier.

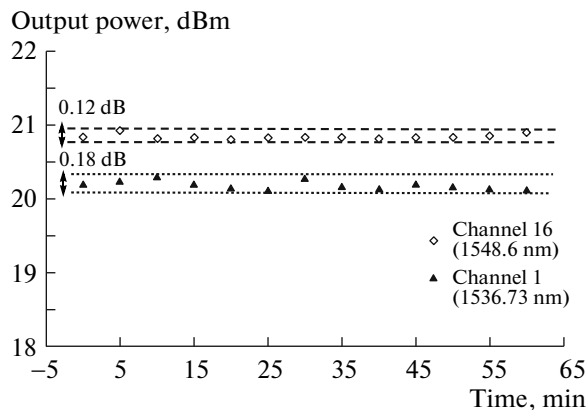


Fig. 6. Stability performance taken in an hour of operation.

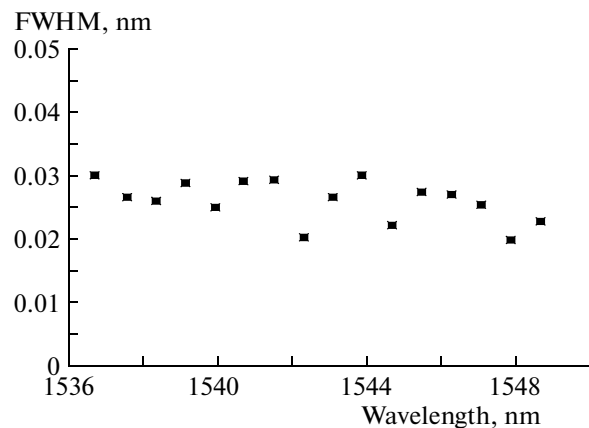


Fig. 7. FWHM output spectra of 16 different wavelengths.

Figure 7 shows the value of the Full Width at Half Maximum (FWHM) of each output laser with an average value of 0.026 nm. The variance FWHM is ± 0.01 nm indicating that the FWHM is quite constant and stable. The FWHM of this output laser is also very small, suitable for use in the 0.8 nm interchannel spacing of DWDM systems. With efficient and consistent value of FWHM locked by the 0.8 nm bandwidth of AWG, and with sufficient pump power, the system is capable of producing a stable and a constant HP-TFL.

CONCLUSIONS

A tunable high output power fiber laser is demonstrated with an average output power of 20.74 dBm. The selectable output wavelength element consists of AWG and OS with 16 different wavelength choices starting from 1536.7 to 1548.6 nm with 12 nm of wavelength tuning which qualified the ITU grid standard. This tunable high power fiber laser is achievable due to its high stability over an hour of operation time with output power variances of ± 0.06 dB taken from chan-

nel 16 and ± 0.09 dB taken from channel 1. The SMSR versus wavelengths curve also shows good quality results with an average value of 59.25 dB with all of them having SMSR values higher than 56 dB which is the required value for a stable output power fiber laser.

REFERENCES

1. L. Quintino, A. Costa, R. Miranda, D. Yapp, V. Kumar, and C. J. Kong, *Mater. Design* **28**, 1231 (2007).
2. Y. Jeong, J. Nilsson, J. K. Sahu, D. B. S. Son, C. Alegria, P. Dupriez, C. A. Codemard, D. N. Payne, R. Horley, L. M. B. Hickey, L. Wanzcyk, C. E. Chrysosou, J. A. Alvarez-Chavez, and P. W. Turner, *Opt. Lett.* **30**, 459 (2005).
3. K. Ueda and A. Liu, *Laser Phys.* **8**, 774 (1998).
4. M. Frede, R. Wilhelm, R. Gau, M. Brendel, I. Zawischa, C. Fallnich, F. Seifert, and B. Willke, *Class. Quantum Gravity* **21**, 895 (2004).
5. C. J. Mackechnie, W. L. Barnes, D. C. Hanna, and J. E. Townsend, *Electron. Lett.* **29**, 52 (1993).

6. C. Kangkang, S.-U. Alam, D. Lin, A. Malinowski, and D. J. Richardson, in *Proceedings of the Lasers and Electro-Optics, 2009 and 2009 Conference on Quantum Electronics and Laser Science Conference. CLEO/QELS 2009*.
7. S. Huang, Y. Feng, J. Dong, A. Shirakawa, M. Musha, and K. Ueda, *Laser Phys. Lett.* **2**, 498 (2005).
8. M. Hofer, M. E. Fermann, and L. Goldberg, *IEEE Photon. Technol. Lett.* **10**, 1247 (1998).
9. J. S. Kim, C. Codemard, J. Nilsson, and J. K. Sahu, *Electron. Lett.* **42**, 515 (2006).
10. M. R. A. Moghaddam, S. W. Harun, M. R. Tamjis, and H. Ahmad, *Laser Phys. Lett.* **6**, 586 (2009).
11. X. H. Li, X. M. Liu, Y. K. Gong, H. B. Sun, L. R. Wang, and K. Q. Lu, *Laser Phys. Lett.* **7**, 55 (2010).
12. J. E. Townsend, W. L. Barnes, K. P. Jedrzejewski, and S. G. Grubb, *Electron. Lett.* **27**, 1958 (1991).
13. C. R. Giles, C. A. Burrus, D. J. DiGiovanni, N. K. Dutta, and G. Raybon, *IEEE Photon. Technol. Lett.* **3**, 363 (1991).
14. B. Sverdlov, B. Schmidt, S. Pawlik, B. Mayer, and C. Harder, in *Proceedings of the 28th European Conference on Optical Communication* (2002), vol. 5, p. 1.
15. M. Z. Zulkifli, N. Tamchek, A. A. Latif, S. W. Harun, and H. Ahmad, *Opt. Commun.* **282**, 2576 (2009).
16. Y. W. Song, S. A. Havstad, D. Starodubov, Y. Xie, A. E. Willner, and J. Feinberg, *IEEE Photon. Technol. Lett.* **13**, 1167 (2001).
17. H. Ahmad, M. Z. Zulkifli, K. Thambiratnam, A. A. Latif, and S. W. Harun, *Laser Phys. Lett.* **6**, 539 (2009).
18. A. A. Latif, M. Z. Zulkifli, N. A. Hassan, S. W. Harun, Z. A. Ghani, and H. Ahmad, *Laser Phys. Lett.* **7**, 597 (2010).
19. H. Ahmad, M. Z. Zulkifli, A. A. Latif, and S. W. Harun, *Laser Phys. Lett.* **7**, 164 (2010).
20. A. A. Latif, M. Z. Zulkifli, N. A. Awang, S. W. Harun, and H. Ahmad, *Laser Phys.* **20**, 2006 (2010).
21. X. Dong, H. Y. Tarn, B. O. Guan, C. Zhao, and X. Dong, *Opt. Commun.* **224**, 295 (2003).
22. M. Yamada, H. Ono, T. Kanamori, S. Sudo, and Y. Ohishi, *Electron. Lett.* **33**, 1477 (1997).
23. S. W. Harun, N. Tamchek, P. Proopalan, and H. Ahmad, *Jpn. J. Appl. Phys.* **42**, L173 (2003).

A Simple Linear Cavity Dual-Wavelength Fiber Laser Using AWG as Wavelength Selective Mechanism¹

A. A. Latif^a, M. Z. Zulkifli^a, N. A. Awang^a, S. W. Harun^b, and H. Ahmad^a

^a Photonics Laboratory, Department of Physics, University of Malaya,
Kuala Lumpur, 50603 Malaysia

^b Department of Electrical Engineering, Faculty of Engineering,
University of Malaya, Kuala Lumpur, 50603 Malaysia
e-mail: mohdzamani82@yahoo.com

Received June 8, 2010; in final form, June 22, 2010; published online October 3, 2010

Abstract—In this paper, a simple design of linear cavity dual-wavelength fiber laser (DWFL) is proposed. Operating in the C-band region stretching from 1538.3 nm to 1548.6 nm, an arrayed waveguide grating (AWG) is used to generate the dual-wavelengths output together with a broadband fiber Bragg grating as a back reflector and an optical circulator with a 10% output coupling ratio which acts as a front mirror. The measured average output power of the DWFL is about -5.66 dBm and with a side mode suppression ratio (SMSR) of 53.1 dB. The spacing between the two output wavelengths can be varied from 0.8 nm to 10.3 nm with a stable output and minimum power fluctuations.

DOI: 10.1134/S1054660X10210061

INTRODUCTION

Multiwavelength fiber lasers have attracted numerous interests especially for possible application as alternative laser sources for wavelength division-multiplexing (network), for terahertz generation and also in high resolution spectroscopy. Generally, these lasers are operated with erbium doped fiber (EDF) as an active gain medium. Interest in the erbium doped fiber is primarily due to its compatibility, compact size and simplicity. There is an issue in generating multiwavelength outputs from EDF which is largely due to the homogeneous broadening exhibited by this material. This inhibits operation of more than one wavelength due to the gain competition. To overcome this, many methods have been used such as cooling the EDF in liquid nitrogen [1, 2], using hybrid gain medium and sagnac loop mirror [3–7], elliptical EDF [8, 9], cavity loss controlled [10, 11] and self-injected laser diode [12, 13] among others [14–17]. These methods are commonly applied to ring resonators, but due to the long length of the cavity they lead to many longitudinal modes oscillating around the central oscillating mode. Many techniques have been utilized to limit these possible large number of modes by incorporating ultra-narrow band fiber Bragg grating (FBG) filter or unpumped erbium doped fiber based saturable absorber [18–22]. As opposed to ring configuration [23–25], a linear cavity will be an attractive approach due to its short length which can limit the number of longitudinal modes [26]. As an example, using an all-polarization maintaining linear cavity which comprises of polarization maintaining fiber Bragg grating

and polarization maintaining linearly chirped fiber Bragg grating is able to generate a dual-wavelength output which can be tuned from 0.22 to 0.05 nm [27]. Another approach is to use FBG based Fabry–Perot filter in a ring configuration which is then connected linearly to a section of unpumped erbium doped fiber which is terminated by a narrow band FBG. Wavelength selection and switching are achieved by tuning the FBG to provide a variable spacing between the two wavelengths from 0.20 to 0.54 nm [28, 29]. These two methods have limited tuning range and the system designs are complex and involved.

In this paper, a simple method in generating dual-wavelength output from a linear cavity by using an AWG as a wavelength selector, a broadband FBG and loop back optical as cavity reflectors, is proposed. This design is capable of generating 14 different wavelengths to provide seven ways of dual-wavelength output that can have spacings between them from 0.8 nm to 10.3 nm, which is largely set upon by 100 GHz interchannel spacing of the AWG.

EXPERIMENTAL SETUP

The experimental setup is shown in Fig. 1 which comprises a short length of 5 m erbium doped fiber with a dopant concentration of 900 ppm (absorption 11.9 dB/m at 979 nm) as a gain medium. This erbium doped fiber is pumped by a 980 nm laser diode operating at 110 mW through a 980/1550 nm Wavelength Division Multiplexer (WDM) fused biconical coupler. The front reflector is a composition of a 3-port optical circulator (OC) at 1550 nm with port 1 connected to a 90/10 fused coupler and the other end looping back to

¹ The article is published in the original.

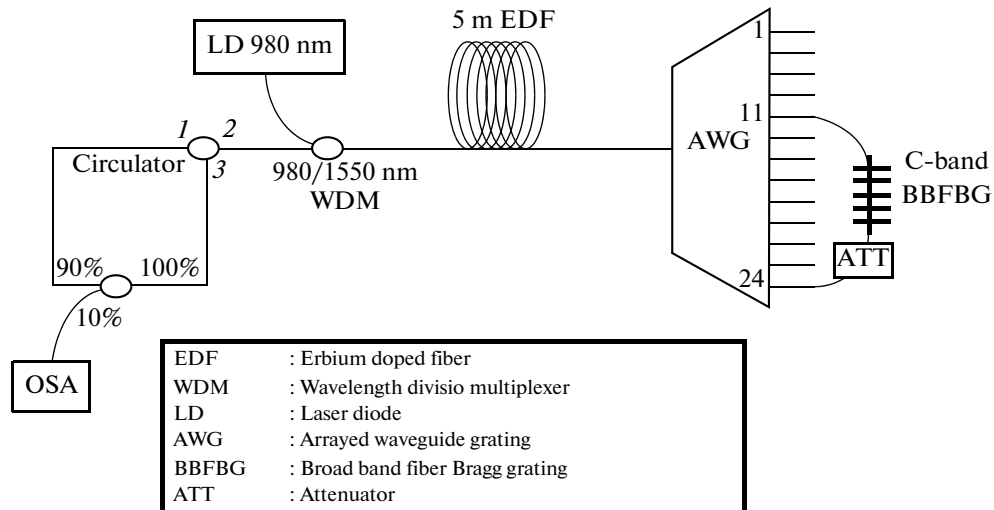


Fig. 1. Experimental setup of DWFL in a linear cavity configuration.

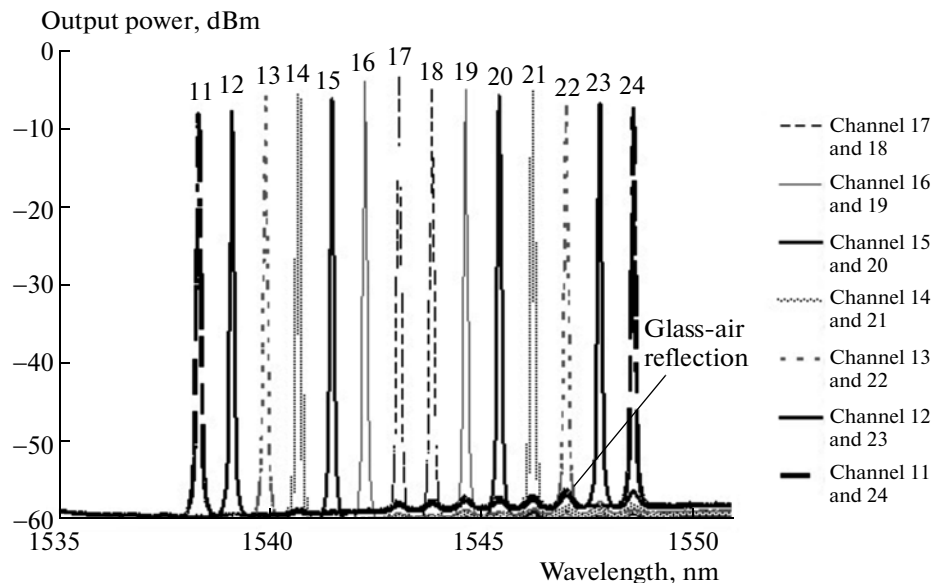


Fig. 2. Spectrum of DWFL from the narrowest spacing of 0.8 nm spacing (channels 17 and 18) to the widest spacing of 10.3 nm (channels 11 and 24).

the optical circulator. The 10% port of the fused coupler is connected to an ANDO AQ6317C optical spectrum analyzer with a resolution of 0.02 nm which also acts as the output coupler. Port 2 of the OC is connected to the input port of the WDM coupler. The back reflector consists of a 1×24 AWG at 100 GHz interchannel spacing with its output port at two different channels connected to a C-band broadband fiber Bragg grating (B-BFBG). The Amplified Spontaneous Emission (ASE) from the gain medium will be emitted at both ends of the erbium doped fiber (EDF). The portion of ASE that travels to the 1×24 AWG will be sliced into 24 different outputs with interchannel spacings of 0.8 nm (100 GHz) which ranges from

1530.4 to 1548.6 nm. For generating the dual wavelength outputs, two output channels of the AWG are connected to a broadband FBG reflector which will reflect back into the gain medium and travel towards the optical circulator. For instance, if we choose channel 11 and 24 of the AWG, the two wavelengths that will be reflected into the gain medium will be 1538.3 and 1548.6 nm.

These two wavelengths will then be amplified by the EDF gain medium and again will be reflected back by the optical circulator. The dual wavelength outputs are taken out at the 10% port of the fused coupler. This process repeats and the spacing between the two wave-

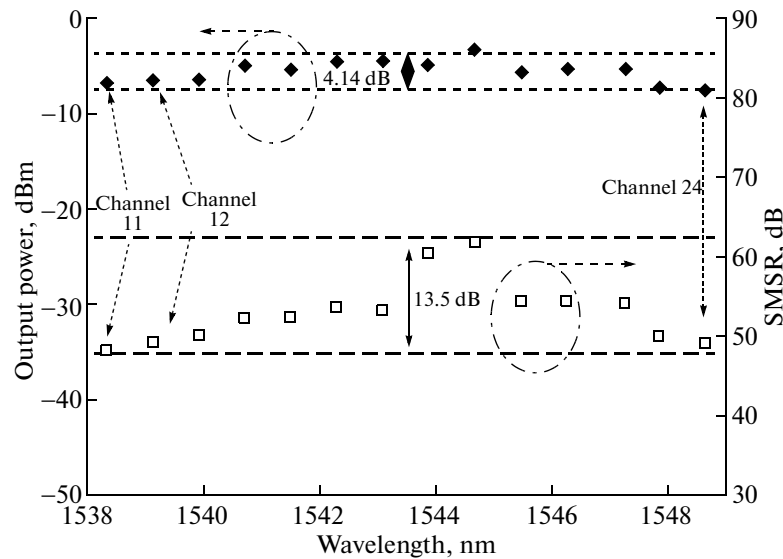


Fig. 3. Output power and SMSR of linear cavity DWFL.

lengths can be adjusted by taking outputs at different channels. This can be automated by using an optical switch selector to provide a switchable dual wavelength output.

As a result of the homogeneous broadening in the EDF, a stable operation of dual-wavelengths can be a daunting task; therefore an optical attenuator is placed at the output end of the high numbered channels. This is largely due to the longer wavelength. The energy required to support oscillation will be smaller as compared to those at shorter wavelength. At channels 13 to 24, the output wavelengths are shorter as compared to channels 1 to 12. In the case of channels 11 and 24, ($\lambda_{11} = 1538.3$ nm and $\lambda_{24} = 1548.6$ nm) the attenuator is placed directly at the output end of channel 24. The attenuator will provide the balance of power for the longer wavelengths such that the generation of dual-wavelength can be made possible by using this cavity

loss method, similar demonstrations can be done for other paired channels and the results are shown in Fig. 2.

RESULTS AND DISCUSSION

Figure 2 shows the different channel combinations such as 12 and 23, 13 and 22 until towards channel 17 and 18 giving the narrowest tunable spacing of about 0.8 nm (channels 17 and 18) to the widest spacing of 10.3 nm (channels 11 and 24). Since this design is specifically for C-band region, lasing can only be observed from channels 11 to 24, that is at wavelengths 1538.3 to 1548.6 nm. By operating the gain medium at longer and higher pump power, a wider tuning range can be achieved. From the same figure, small “bumps” or small peaks can be observed at the baseline which is due to the 4% Fresnel reflection of glass air interface at the end of the AWG ports. This can be avoided by applying a thin layer of index matching gel at the end of the ports.

The measurements on the output power of the dual-wavelength fiber lasers and its SMSR is shown in Fig. 3. They are taken in pairs, such as channels 11 and 24, channels 12 and 23, channels 13 and 22 and subsequently channels 17 and 18. The average output power is about -5.66 dBm and has a power variation among the channels of less than 4 dB. This can be further improved by fine tuning the optical attenuator and a nearly equal amplitude of dual-wavelengths peaks can be achieved. On the other hand, the average value of the SMSR is about 53.1 dB and this gives an indication that the signals are of good optical quality. Although the SMSR has a large variation of 13.5 dB between the channel peaks, this is due to the large variation between channels 18 and 19. The rest has peak to peak

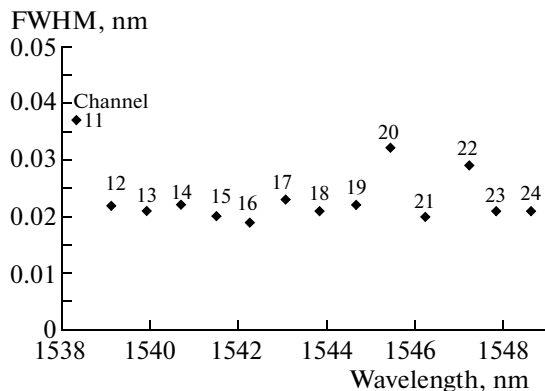


Fig. 4. The full width half maximum (FWHM) of DWFL from channel 11 until 24.

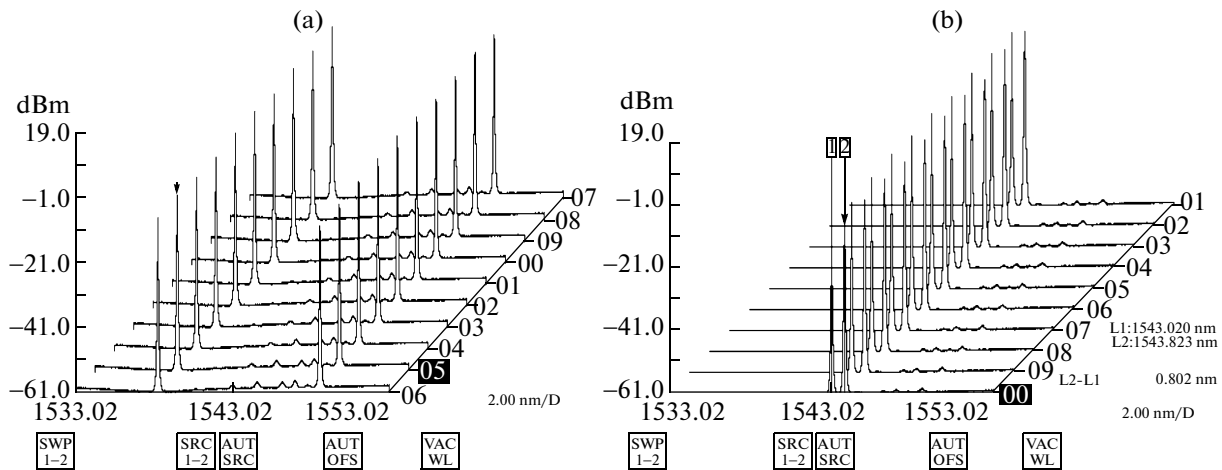


Fig. 5. Stability performance of DWFL with (a) the widest spacing and (b) the narrowest spacing.

variations of less than 4 dB. This high value at channels 18 and 19 could be due to the higher loss (insertion loss) at these ports, which is between the connectors and the adaptors. This is a quality issue of the AWG connectors.

Figure 4 shows the linewidth measurement of the various output channels of the dual-wavelengths fiber laser with an average value of 0.024 nm at full width half maximum (FWHM). Channels 11, 20, and 22 have a slightly higher value of 0.037, 0.033, and 0.028 nm, respectively. These higher values are due to the transmission characteristics of the AWG which may have a higher linewidth behavior of these channels. The rest of the channels have a linewidth hovering around 0.02 nm which is actually the resolution of the optical spectrum analyzer. Due to limited facility, accurate measurements on linewidth cannot be performed presently.

The stability measurements on the dual-wavelengths output of this laser were performed over a long period exceeding 24 h. Figure 5 shows the stability performance of the DWFL with 5 min time interval taken for half an hour on superimposed traces. As depicted in the 3D graph, the DWFL is reasonably stable with fluctuations of less than 3 dB. Figures 5a and 5b show the case for widest spacing of 10.3 nm and narrowest spacing of 0.8 nm.

On the whole, the proposed design provides a simple configuration in achieving a dual-wavelengths output with a minimum of components used in the cavity.

CONCLUSIONS

As a conclusion, this work demonstrates a simple design in generating a dual-wavelengths output from a homogeneous gain medium such as erbium doped fiber. The design is compact and only minimum number of components are used to generate the dual wave-

lengths output. The generated DWFL can be tuned from a narrowest spacing of 0.8 nm to the widest spacing of 10.3 nm. This is due to the AWG that is available in the laboratory which has an interchannel spacing of 100 GHz (0.08 nm). Smaller spacing is achievable having an AWG of interchannel spacing of 25 GHz (0.2 nm). The output power measured has an average value of -5.66 dBm and SMSR of 51.3 dB. The measured linewidth is about 0.02 nm, limited by resolving power of the optical spectrum analyzer. The long term operation of the DWFL is stable with minimum power fluctuations.

REFERENCES

1. S. Yamashita and K. Hotate, *Electron. Lett.* **32**, 1298 (1996).
2. N. Park and P. F. Wysocki, *IEEE Photon. Technol. Lett.* **8**, 1459 (1996).
3. S. L. Pan, X. F. Zhao, and C. Y. Lou, *Opt. Lett.* **33**, 764 (2008).
4. S. Qin, D. Chen, Y. Tang, and S. He, *Opt. Express* **14**, 10522 (2006).
5. H. Ahmad, M. Z. Zulkifli, K. Thambiratnam, S. F. Latif, and S. W. Harun, *Laser Phys. Lett.* **6**, 380 (2009).
6. D. N. Wang, F. W. Tong, Xiaohui Fang, W. Jin, P. K. A. Wai, and J. M. Gong, *Opt. Commun.* **228**, 295 (2003).
7. D. Chen, S. Qin, and S. He, *Opt. Express* **15**, 930 (2007).
8. G. Das and J. W. Y. Lit, *IEEE Photon. Technol. Lett.* **14**, 606 (2002).
9. G. Sun, Y. Chung, and D. S. Moon, *Laser Phys.* **18**, 1196 (2008).
10. M. Durán-Sánchez, A. Flores-Rosas, R. I. Álvarez-Tamayo, E. A. Kuzin, O. Pottiez, M. Bello-Jimenez, and B. Ibarra-Escamilla, *Laser Phys.* **20**, 1270 (2010).

11. A. W. Al-Alimi, M. H. Al-Mansoori, A. F. Abas, M. A. Mahdi, and M. Ajiya, *Laser Phys. Lett.* **6**, 727 (2009).
12. C. H. Yeh, F. Y. Shih, C. H. Wang, Y. F. Wu, and S. Chi, *IEEE Photon. Technol. Lett.* **21**, 125 (2009).
13. C.-H. Yeh, F.-Y. Shin, C.-T. Chen, C.-N. Lee, and S. Ch, *Laser Phys. Lett.* **5**, 210 (2008).
14. P. S. Liang, Z. X. Zhang, Q. Q. Kuang, and M. H. Sang, *Laser Phys.* **19**, 2124 (2009).
15. X. M. Liu, *Laser Phys.* **20**, 842 (2010).
16. Z. Y. Liu, Y. G. Liu, J. B. Du, S. Z. Yuan, and X. Y. Dong, *Laser Phys. Lett.* **5**, 122 (2008).
17. S. W. Harun, M. Z. Zulkifli, and H. Ahmad, *Laser Phys. Lett.* **3**, 369 (2006).
18. X. Liu, *Opt. Commun.* **280**, 147 (2007).
19. D. Chen, H. Fu, and W. Liu, *Laser Phys.* **17**, 1246 (2007).
20. J. Liu, J. P. Yao, J. Yao, and T. H. Yeap, *IEEE Photon. Technol. Lett.* **16**, 1020 (2004).
21. K. Zhang and J. U. Kang, *Opt. Express* **16**, 14173 (2008).
22. J. Sun, X. Yuan, X. Zhang, and D. Huang, *Opt. Commun.* **267**, 177 (2006).
23. H. B. Sun, X. M. Liu, Y. K. Gong, X. H. Li, and L. R. Wang, *Laser Phys.* **20**, 522 (2010).
24. A. W. Al-Alimi, M. H. Al-Mansoori, A. F. Abas, M. A. Mahdi, F. R. M. Adikan, and M. Ajiya, *Laser Phys.* **19**, 1850 (2009).
25. Y. Wei and B. Sun, *Laser Phys.* **19**, 1252 (2009).
26. H. Wang, Y. G. Li, X. D. Chen, B. Huang, F. Y. Lu, and K. C. Lu, *Laser Phys.* **19**, 1257 (2009).
27. D. Liu, N. Q. Ngo, X. Y. Dong, S. C. Tjin, and P. Schum, *Appl. Phys. B* **81**, 807 (2005).
28. X. He, X. Fang, C. Liao, D. N. Wang, and J. Sun, *Opt. Express* **17**, 21773 (2009).
29. S. Feng, O. Xu, S. Lu, T. Ning, and S. Jian, *Opt. Commun.* **282**, 2165 (2009).

High power dual-wavelength tunable fiber laser in linear and ring cavity configurations

H. Ahmad^{1*}, A. A. Latif¹, M. Z. Zulkifli¹, N. A. Awang¹, and S. W. Harun²

¹Photonics Laboratory, Department of Physics, University of Malaya, 50603 Kuala Lumpur, Malaysia

²Department of Electrical Engineering, Faculty of Engineering, University of Malaya, 50603 Kuala Lumpur, Malaysia

*Corresponding author: harith@um.edu.my

Received May 3, 2011; accepted June 10, 2011; posted online August 30, 2011

We describe and compare the performances of two crucial configurations for a tunable dual-wavelength fiber laser, namely, the linear and ring configurations. The performances of these two cavities and the tunability in the dual-wavelength output varied from 0.8 to 11.9 nm are characterized. The ring cavity provides a better performance, achieving an average output power of 0.5 dBm, with a power fluctuation of only 1.1 dB and a signal-to-noise ratio (SNR) of 66 dB. Moreover, the ring cavity has minimal or no background amplified spontaneous emission (ASE).

OCIS codes: 060.2320, 060.2410, 060.3510.

doi: 10.3788/COL201210.010603.

Dual-wavelength tunable fiber lasers (DWTFs) are relevant to the provision of a stable and tunable dual wavelength output that can be used in many applications, such as the study of high-bit-rate soliton pulses^[1], differential absorption measurement of trace gases^[2], photonic generation of microwave carriers^[3], and microwave photonic filters^[4].

Initial research into the development of dual-wavelength fiber lasers has been limited by the inability to generate a high power lasing output. This limitation was caused by the effect of mode competition between the closely spaced wavelengths; resulting in the domination of the longer wavelength over the shorter wavelength. The mode competition itself is largely caused by the homogenous broadening effect in erbium-doped fibers (EDFs), which are normally used as the gain media for fiber-based dual-wavelength sources. To overcome the effect of the homogenous broadening in EDF-based dual-wavelength fiber laser sources, various methods have been proposed, including the cooling of the EDF in liquid nitrogen^[5,6] by using elliptical EDFs^[7] or by incorporating polarization maintaining fiber Bragg gratings (FBGs) for wavelength selection^[8], utilizing frequency shifter in the cavity^[9], and many other methods^[10–13].

The key ability which is sought after in the development of a DWFTL is repeatability. Generally, multi-wavelength output generated using FBGs as filters to select specific wavelengths provide tunability by adjusting the strain or compression that the FBG contends with because of the repeatability issue. The reason is the difficulty to revert to the original position to produce the previous wavelength once the FBG has been modified to select a new wavelength. This problem can be overcome using a filter mechanism with a series of pre-determined wavelengths, such as an arrayed waveguide grating (AWG), as proposed in this letter.

In addition, the cavity configuration plays an important role in the generation of a high-powered output with a good signal-to-noise ratio (SNR). Numerous configurations have been proposed to generate DWFLs, such as linear cavities^[14,15], ring cavities^[16,17], and sigma

cavity configuration^[18]. This is in line with the growing research interest in the generation of high-powered DWFLs for applications such as wavelength conversion using four wave mixing (FWM)^[19], generation of microwave signals^[20], and generation of terahertz waves^[21].

We propose the use of AWG as a tuning element because of its repeatability and also compare the two main configurations of DWTFs, namely, the linear and ring configurations, to determine which can provide a better SNR performance.

Figure 1(a) shows the experimental setup for the linear cavity DWTF, whereas Fig. 1(b) shows the ring configuration. The linear cavity configuration, as shown in Fig. 1(a), consists of a 5-m MetroGain (fibrecore) erbium-doped fiber with absorption coefficients of 980 and 1550 nm at 11 and at approximately 13 dB/m, respectively. The length is chosen to meet the requirement of the pumping power of the 980-nm laser diode operating at 110 mW. The EDF is subsequently connected to a 980/1550-nm wavelength division multiplexer (WDM). The MetroGain EDF acts both as a source for the amplified spontaneous emission (ASE) and as an amplifying medium for the DWTF. The output ASE will travel in both directions, and the ASE on the right-hand side will be sliced by the 1×16 AWG with an interchannel spacing of 100 GHz (0.8 nm).

To generate the dual wavelength output, any two channels of the AWG can be combined into a broad-band fiber Bragg grating (BB-FBG) that also acts as a “mirror” on the right-hand side of the experimental setup. The ASE will be sliced into 16 different wavelengths, ranging from 1536.7 (channel 1) to 1548.6 nm (channel 16). Channel 1 and channel 16 can be connected to the input ports of the BB-FBG that will subsequently reflect these two wavelengths back into the AWG. The broadband reflection spectrum is shown in Fig. 1(c). The tunable wavelength range is approximately 11.9 nm.

Consequently, the combined output will travel to the 5-m EDF for amplification and will be emitted at the 1550-nm port of the WDM toward port 2 of the optical

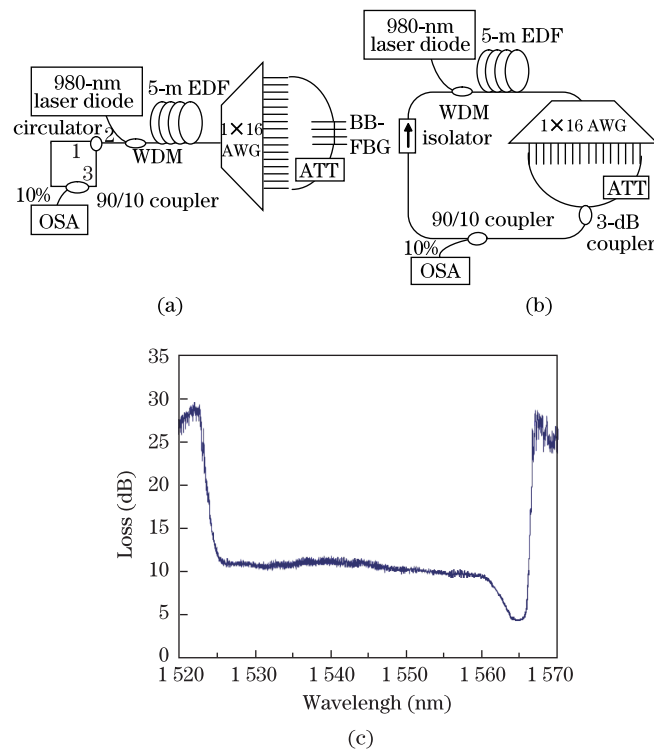


Fig. 1. (a) Linear cavity configuration; (b) ring cavity configuration; and (c) the BB-FBG transmission spectrum with the region of loss (dB) against wavelength, which indicates the reflection.

circulator (OC). Port 2 is connected to port 3 which facilitates the travel of the dual-wavelength output toward the 90:10 couplers with the 10% port connected to the optical spectrum analyzer (OSA). The dual wavelength will continue to travel to port 1 and will be emitted to port 2 again. This serves as the signal for the wavelength to travel to the amplifying medium for further amplification and to move onwards to the 1×16 AWG, where the whole process repeats until two lasing wavelengths of the desired power are obtained.

The tunability of these two wavelengths is accomplished by proper selection of the combinations of the channels. Erbium-doped fiber amplifiers (EDFA) exhibit homogenous broadening characteristic. Thus, mode competition can occur. The probability of the longer wavelength to lase is higher than that of the shorter wavelength.

An optical attenuator (ATT) is placed at the longer wavelength output to balance the dual wavelength output power (known as the cavity loss control method) and to create two lasing wavelengths of equal power. A similar approach is implemented on the ring configuration, as shown in Fig. 1(b).

In the ring configuration, reflecting “mirrors” are not required. Instead, the ASE generated on the right hand side of the EDF travels to the 1×16 AWG, where it will be sliced into 16 different wavelengths (channels), similar to the case of the linear cavity. For dual-wavelength output, two of the channels can be combined using a 3-dB fused coupler, which is subsequently connected to a 90:10 fused coupler in the ring cavity. Similar to the linear cavity configuration, the 10% port is connected to an OSA, whereas the 90% port is connected to an

isolator to ensure unidirectional and onward travel to the 1550-nm port of the WDM.

The common port of the WDM is connected to the EDF, which provides amplification and completes the ring cavity. Similar to the linear cavity, an attenuator is placed at the longer wavelength channel. The reason is similar as that of the previous case.

Both configurations are analyzed for their output spectra, output power, SNR, and stability to determine which of the two designs can provide the higher output power with the better SNR. The largest channel spacing available in the current experiment is 11.9 nm (channels 1 and 16), and the narrowest spacing is 0.8 nm (channels 8 and 9). These are not restricted to these channels; because various channel pair configurations can be created to provide nearly continuous channel spacing.

Figure 2 shows the spectra of the DWTFM for the linear and ring cavity configurations, whereas Fig. 2(a) presents the dual wavelength output taken in pairs from the largest to the smallest channel spacing, i.e., channels 1 and 16 (the largest), channels 2 and 15, and so on until channels 8 and 9 (the smallest), which are superimposed on the same trace. The peaks ride on the ASE background where the floor is approximately -45 dBm. The inset indicates the ASE spectra of the 5-m MetroGain fiber.

The maximum power of the dual wavelength output is approximately 0 dBm with a 3-dB bandwidth of approximately 0.025 nm for each channel. For the ring cavity, the maximum power of the dual wavelength

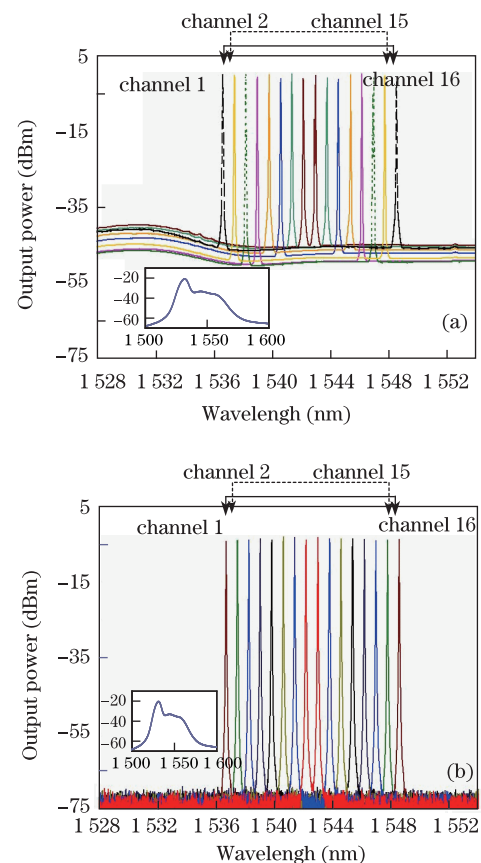


Fig. 2. DWFL spectra obtained for the (a) linear configuration; (b) ring configuration. Inset shows the ASE spectra of the 5-m MetroGain EDF.

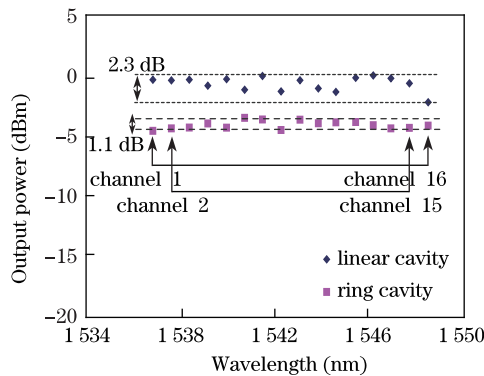


Fig. 3. DWFL output power for the ring and linear cavity configurations.

output is approximately -5 dBm. The ring cavity has a constant value throughout the process of obtaining different dual wavelength pairs. As shown in the graph, the dual wavelength pairs do not ride onto the ASE spectrum, thus producing a better SNR. The tunability of the wavelength spacing can be determined using various output channel combinations in addition to the pair scheme proposed in this letter.

The absence of the ASE background in the ring cavity is largely due to the filtering process of the cavity. In Fig. 1, the output ASE of the 5-m EDF directly travels to the 1×16 AWG that is consequently split into the various wavelengths without any ASE background. These wavelength pairs travel into the ring cavity and back to the AWG and undergo the same splitting process without having the ASE background. This is not the case with the linear cavity, where the reflected output of the 16 channels from the AWG undergoes amplification in the 5-m EDF prior to its travel toward the OC port 2. At this instance, the output consists of the multiple channels riding on top of the background ASE, which is subsequently tapped out at the 90:10 coupler.

The output powers are measured for different pair combinations, as shown in Fig. 3. The wavelengths of the pair are given as the abscissa of the graph and the ordinate is the output power. In Fig. 3, the linear cavity has an average power of approximately 0 dBm with a power variation of 2.3 dB. In the case of the ring cavity, the average power is approximately -5 dBm with a power variation of 1.1 dB. Although the linear cavity has a higher output power compared with the ring cavity, it fares poorly in terms of the SNR, as shown in Fig. 4. The slight variation in the power output in Fig. 3 can be further improved by properly cleaning the port channels of the AWG.

In Fig. 4, the SNR of the ring cavity is superior to that of the linear cavity, with an average SNR value of 66 dB compared with the value of 44 dB for the linear cavity. The SNR variation between the pair channels is approximately 2.5 dB for the ring cavity, whereas for the linear cavity, the variation is approximately 10.7 dB. This implies that the output power of the dual-wavelength output from the ring cavity is more consistent compared with the various combinations of the pair channels. In the linear cavity, the large variation of the SNR in the pair channels makes it unsuitable for applications that require a tunable dual-wavelength output with constant power. Based on this measurement, the ring cavity is

an important source for a dual-wavelength with a stable and constant power.

The other important parameter in characterizing the dual-wavelength source is the stability measurement of the output power against time. This is shown in Fig. 5 for two extreme cases; one with the widest spacing (channels 1 and 16) and the second with the narrowest spacing (channels 8 and 9), as shown in Figs. 5(a) and (b), respectively. The fluctuations of the linear and the ring cavity have almost similar patterns, with variations of 1.61 and 1.22 dB, respectively, for channel 1. As for channel 16, the variation is 1.61 dB for the linear configuration, whereas the ring cavity configuration shows a variation of 1.69 dB.

Figure 5(b) shows the variation for channels 8 and 9, which are the narrowest channel spacings for the dual-wavelength laser output, with variations of 1.65

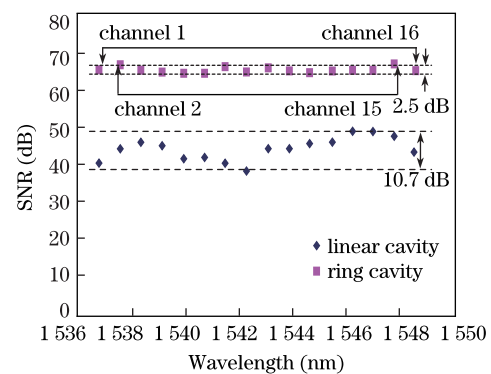


Fig. 4. SNR of DWFL output for the ring and linear cavity configurations.

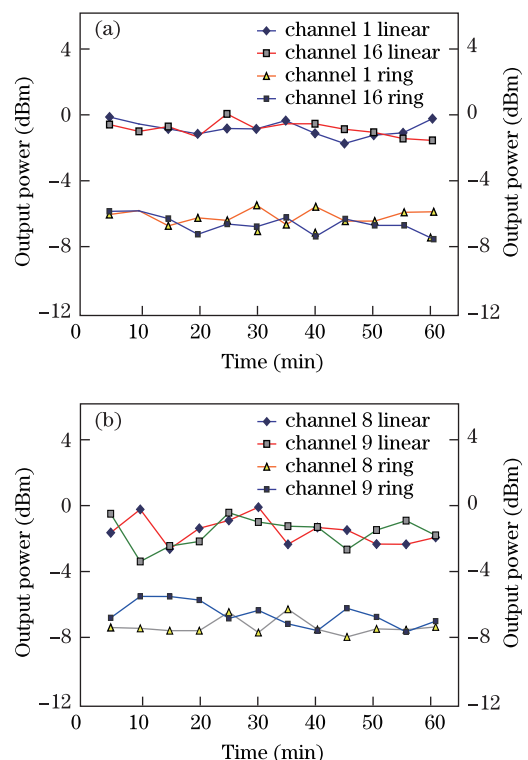


Fig. 5. Stability of the DWFL for the ring cavity and linear cavity configurations for (a) the widest spacing (channels 1 and 16) and (b) the narrowest spacing (channels 8 and 9).

and 2.49 dB, as well as 2.12 and 2.91 dB, for the ring and linear cavity configurations, respectively. Although there are slight variations in the output power stability, this can be further improved by refining the attenuation, minimizing the insertion losses, and properly cleaning the connectors.

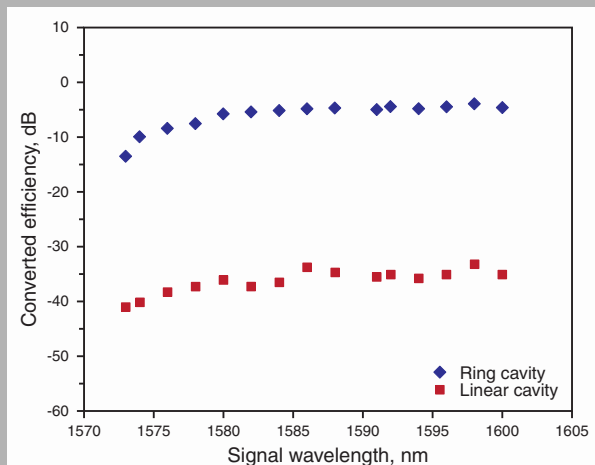
For practical applications of tunable dual-wavelength fiber lasers, the ring cavity configuration is the best choice because it can provide a constant output power for various wavelength combinations.

In conclusion, we describe and compare the performance of two important configurations, namely, the linear and ring cavity configurations, for tunable dual-wavelength output fiber lasers. The tunability can vary from 0.8 to a maximum of 11.9 nm by selecting the various output channels from the AWG. The performance of the ring cavity is superior to that of the linear cavity, achieving a power variation of only 1.1 dB and average output power of -5 dBm. Although the linear cavity has a higher average output power of 0 dBm, the power variation between paired channels is large, with a value of 2.3 dB. Another advantage of the ring cavity is the higher SNR of 66 dB, with a fluctuation of only 2.5 dB compared with the linear cavity SNR of 44 dB, with a higher fluctuation of 10.7 dB. Therefore, the ring cavity is a suitable candidate as a tunable dual-wavelength fiber laser source.

References

1. M. Tadakuma, O. Aso, and S. Namiki, in *Proceedings of OFC'2000* 178 (2000).
2. A. J. Ruggiero, M. W. Bowers, and R. A. Young, in *Proceedings of CLEO'99* 523 (1999).
3. L. Xia, P. Shum, and T. H. Cheng, *Appl. Phys. B* **86**, 61 (2007).
4. D. Liu, N. Q. Ngo, G. Ning, P. Shum, and S. C. Tjin, *Opt. Commun.* **266**, 240 (2006).
5. S. Yamashita and K. Hotate, *IEEE Photon. Technol. Lett.* **32**, 1298 (1996).
6. N. Park and P. F. Wysoncki, *IEEE Photon. Technol. Lett.* **8**, 1459 (1996).
7. G. Das and J. W. Y. Lit, *IEEE Photon. Technol. Lett.* **14**, 606 (2002).
8. S. Feng, O. Xu, S. Lu, T. Ning, and S. Jian, *Opt. Commun.* **282**, 825 (2009).
9. A. Bellemare, M. Karasek, M. Rochette, S. L. Rochelle, and M. Tetu, *J. Lightwave Technol.* **18**, 825 (2000).
10. J. Sun, Y. Dai, X. Feng, Y. Zhang, and S. Xie, *IEEE Photon. Technol. Lett.* **18**, 2587 (2006).
11. M. P. Fok and C. Shu, *Opt. Express* **15**, 5925 (2007).
12. C. H. Yeh, C. W. Chow, F. Y. Shih, C. H. Wang, Y. F. Wu, and S. Chi, *IEEE Photon. Technol. Lett.* **21** (2009).
13. C. H. Yeh, *Opt. Express* **15**, 13844 (2007).
14. D. Liu, N. Q. Ngo, X. Y. Dong, S. C. Tjin, and P. Shum, *Appl. Phys. B* **81**, 807 (2005).
15. X. He, X. Fang, C. Liao, D. N. Wang, and J. Sun, *Opt. Express* **17**, 21773 (2009).
16. J. Nilsson, Y. W. Lee, and S. J. Kim, *IEEE Photon. Technol. Lett.* **8**, 1630 (1996).
17. X. Chen, Z. Deng, and J. Yao, *IEEE Transact. on Microwave Theory and Techniques* **54**, 804 (2006).
18. S. Pan and J. Yao, *Opt. Express* **17**, 12167 (2009).
19. D. Z. Hsu, S. L. Lee, P. M. Gong, Y. M. Lin, S. S. W. Lee, and M. C. Yuang, *IEEE Photonics Tech. Lett.* **16**, 1903 (2004).
20. Y. Yao, X. Chen, Y. Dai, and S. Xie, *IEEE Photon. Technol. Lett.* **18**, 187 (2006).
21. I. Park, I. Fisher, and W. Elsaber, in *Proceedings of CLEO/Europe'2003* (2003).

Abstract: An efficient system for generating the four-wave mixing (FWM) effect in a short length of a highly nonlinear fiber (HNLF) is demonstrated using a ring configuration, which to our knowledge is the first of its kind to be reported. The conversion efficiency obtained is -4 dB for a HNLF length of 100 m when pumped with a 90 mW diode pump laser at 1490 nm in ring configuration which is the highest ever reported. The signal-to-noise (SNR) ratio is 43 dB. The conversion efficiency and SNR are flat over a span of 20 nm and can provide an effective means of wavelength conversion for telecommunication applications.



OSNR against signal wavelength, P_s , keeping pump wavelength, P_p , fixed at 1590 nm in HNLF by using ring and linear cavity

© 2011 by Astro Ltd.

Published exclusively by WILEY-VCH Verlag GmbH & Co. KGaA

Wavelength conversion based on four-wave mixing in a highly nonlinear fiber in ring configuration

H. Ahmad,^{1,*} N.A. Awang,^{1,2} A.A. Latif,¹ M.Z. Zulkifli,¹ Z.A. Ghani,³ and S.W. Harun⁴

¹ Photonics Laboratory, Department of Physics, University of Malaya, 50603 Kuala Lumpur, Malaysia

² Faculty of Science, Art and Heritage, Universiti Tun Hussein Onn Malaysia, 86400 Batu Pahat, Johor, Malaysia

³ Faculty of Applied Sciences, MARA University of Technology, 40450 Shah Alam, Malaysia

⁴ Department of Electrical Engineering, Faculty of Engineering, University of Malaya, 50603 Kuala Lumpur, Malaysia

Received: 15 April 2011, Revised: 26 April 2011, Accepted: 29 April 2011

Published online: 28 July 2011

Key words: Four-wave mixing; highly nonlinear fiber; conversion efficiency; optical signal-to-noise ratio

1. Introduction

Nonlinear optical phenomenon has become an important technique in the generation of new frequencies that finds many applications in the area of parametric oscillation, multiwavelength fiber lasers [1–4], and wavelength converters. Of interest lately is the ability to develop an all-optical network system whereby the current electrical wavelength converters will be replaced by an all-optical wavelength converter. This will definitely improve the network accessibility and also promote flexibility [5–7].

The function of a wavelength converter is to convert one or more of incoming wavelengths from a wavelength division multiplexing (WDM) network into a desired wavelength or group of wavelengths without significant distortion in the output signals. There are many optical wavelength conversion techniques that have been reported such as the use of the nonlinear behavior in a semiconductor optical amplifier (SOA) and also the use of highly nonlinear fiber (HNLF) as a nonlinear medium to name a few. The common approach in achieving wavelength conver-

* Corresponding author: e-mail: harith@um.edu.my

© 2011 by Astro Ltd.

Published exclusively by WILEY-VCH Verlag GmbH & Co. KGaA

sion is through cross phase modulation (XPM) [8,9], cross gain modulation (XGM) [10,11] and through four-wave-mixing (FWM) [12–15]. Among these methods, FWM provides an interesting approach due to its simplicity and unique characteristics of providing the preservation of amplitude and phase, data format and bit rate transparencies. Another advantage is that wavelength conversion based on FWM in HNLF, photonic crystal fiber (PCF) [16,17], bismuth oxide fiber (BiF) [18] and dispersion shifted fiber (DSF) that allows for operation at higher bit rates as reported in reference [13]. This is an advantage over using an SOA as the nonlinear medium, which can only accommodate low bit rate due to the long response time of the carriers.

In the FWM phenomenon, the fourth wavelength is generated from three different input wavelengths. The efficiency of this nonlinear interaction depends largely on the nonlinear phase matching, and chromatic dispersion is a key parameter that determines this value. For the degenerate case, the same phenomena can be observed whereby only two wavelengths are needed to generate the third wavelength. In most instances the degenerate case is frequently utilized for FWM. As such, a dual-wavelength laser will be an interesting approach to generate FWM in a nonlinear medium. This has been demonstrated for the case of the SOA acting as the nonlinear medium [14,19].

One of the key issues in FWM is the conversion efficiency, whereby a recent work by S. Petit et. al. [20] uses a high power laser operating at 28 dBm to generate FWM effect in a highly nonlinear fiber. The conversion efficiency achieved is only -5 dB in a 120 m length of HNLF with nonlinear coefficient of $\gamma = 12 \text{ W}^{-1}\text{km}^{-1}$. Similarly, work by D. Dahan et. al. [21] also obtained a conversion efficiency of -5 dB while using a high power pump and signal laser operating at 22 dBm in 1000 m HNLF (nonlinear coefficient $\gamma = 10.5 \text{ W}^{-1}\text{km}^{-1}$).

As discussed above these methods require high power lasers together with a long length of HNLF. In this paper, we propose an effective method whereby a lower pump power and signal are used in 100 m HNLF (nonlinear coefficient $\gamma = 10.8 \text{ W}^{-1}\text{km}^{-1}$) giving higher conversion efficiency of -4 dB and also a better signal-to-noise (SNR) ratio of 43 dB. The other interesting point of this work is that the conversion efficiency is as broad as 20 nm of the 3 dB bandwidth where the pump and signal interact.

2. Experimental setup

Fig. 1 shows a schematic structure of the FWM in a highly nonlinear fiber (HNLF) in a ring configuration. The main components are an erbium-doped fiber (EDF), which acts as an optical amplifier (EDFA), a 100 m long HNLF, an optical circulator and an output coupler. The EDFA consists of 11 m of Metrogain erbium doped fiber (DF1500L, Fibercore Ltd.) with erbium ion concentration of 900 ppm and absorption coefficient of 18.06 and 11.3 dB/m at

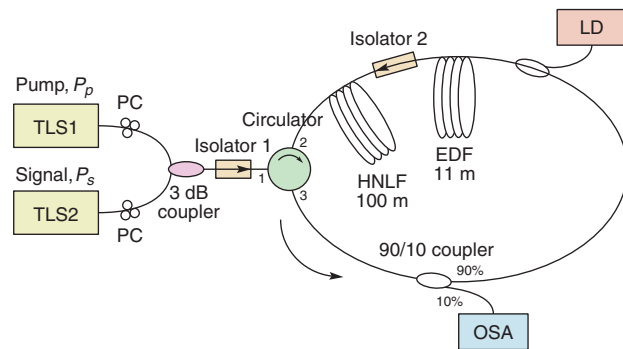


Figure 1 (online color at www.lphys.org) Schematic diagram for generating FWM effect in a ring configuration

1530 and 980 nm, respectively. The EDF is pumped by a laser diode with pump power of 90 mW at 1490 nm. The HNLF is used as the nonlinear medium to generate FWM when two closely spaced signals (pump, P_p and signal, P_s) travel in this fiber. The HNLF used in this experiment is from OFS (Furukawa) with specifications of the nominal zero dispersion wavelength (ZDW), loss coefficient, dispersion slope and nonlinear parameter of the HNLF being 1531 nm, 0.73 dB/km, 0.007 ps/nm² km and $10.8 \text{ W}^{-1}\text{km}^{-1}$, respectively. The other components are an isolator 2, which forces the oscillation in a counter-clockwise direction, an optical circulator that provides a means of injecting the dual wavelength input into the ring cavity and a 90/10 coupler to extract the signal into the optical spectrum analyzer (OSA).

The input signal for the FWM in the HNLF is taken from two tunable laser sources (TLS) (YOKOGAWA AQ2200) with pump wavelength, P_p , at 1590 nm and output power of 12.8 dBm. The other signal, which is referred to as the input signal, P_s , is from another TLS with an output power of 10.8 dBm and the input signal wavelength tuned from 1570 to 1600 nm. The output linewidth of these TLSs is about 0.015 nm. Both of these signals are made to pass into a polarization state as to synchronize the two signals to satisfy the phase matching in HNLF. These two signals then combine with a 3 dB coupler where the output port is connected to port 1 of the optical circulator via the isolator 1. This combination signal of dual wavelength (P_p and P_s) will be emitted into port 3 of the circulator in the ring cavity. This setup takes advantage of the low isolation loss of the circulator from port 1 to port 3, however, in a real scenario; the isolation is just about 45 dB, which lead to the signal leakage from port 1 to port 3. The combined signal will travel to the EDFA to be amplified and then travels to the HNLF to generate the FWM in this nonlinear medium. Careful adjustments of the polarization controllers (PCs) are required so as to provide the phase matching to generate the new wavelength output based on FWM. The output sig-

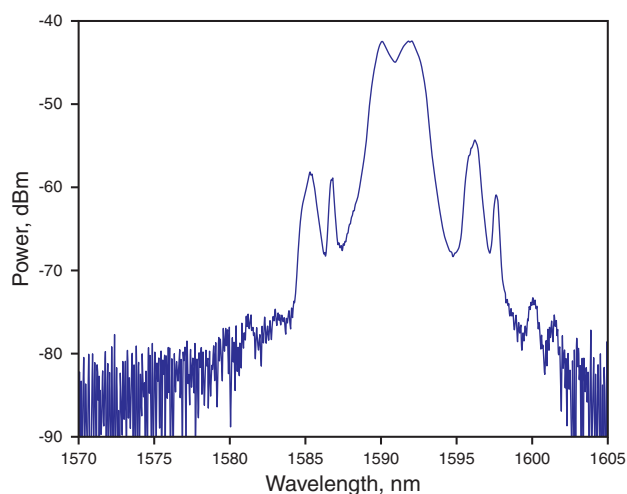


Figure 2 (online color at www.lphys.org) Free-running spectrum (without pump and signal wavelength) at the LD pump power of 90 mW

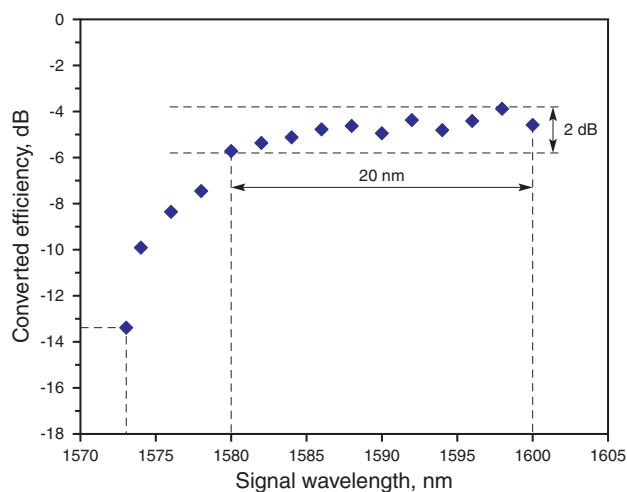


Figure 4 (online color at www.lphys.org) FWM conversion efficiency versus the signal wavelength, P_s , with HNLF fitting pump wavelength, P_p , at 1590 nm

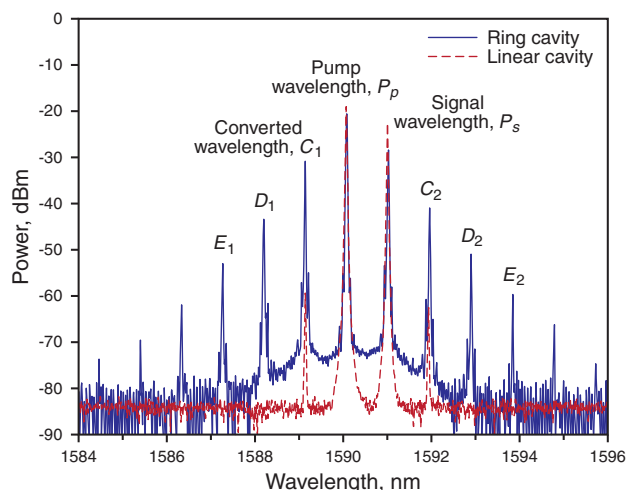


Figure 3 (online color at www.lphys.org) Power spectra at the output of the fiber

nal is detected using an optical spectrum analyzer (OSA) (YOKOGAWA AQ6370B), which is connected to the 10% port of the 90/10 coupler.

3. Results and discussion

In Fig. 2, a “free-running” spectrum, which is taken without having any dual wavelength input into the ring cavity is shown. This is taken at a low diode pumping power of 90 mW at 1490 nm. The spectrum shows a few peaks in the L-band region (1573–1600 nm) where the gain is

most prominent. This is basically due to the long length of highly doped fiber used which results in amplification shifting towards the L-band. A shorter length of this fiber will give a similar gain spectrum in the C-band region. Normally, having the EDF as a gain medium will exhibit mode competition due to the homogeneously broadened gain. This is of little significance in the case of the above experiment whereby the dual wavelength input comes from two independent sources as shown in Fig. 1. The chosen input wavelength is set closer to the L-band region of the gain medium such that it can extract the required energy for amplifications. The region of interest in this experiment is centered at 1591.8 nm, which coincides with “free-running” spectrum in the ring cavity.

The dual-wavelength input into the ring cavity are set at 1590 and 1591 nm for the pump wavelength, P_p , and signal wavelength, P_s , respectively, which is launched into the ring cavity via the optical circulator and moves in a counter-clockwise direction. This dual-wavelength signal will experience amplification at the EDF gain medium and then travels toward the HNLF. In this nonlinear medium, FWM takes place and generates the multiple outputs as in Fig. 3 when phase matching condition is satisfied. From the figure, the P_p and P_s generate the C_1 and C_2 signals due to the FWM phenomenon. As a result of the high intensity between the converted wavelengths, C_1 and P_p , it can also generate new wavelengths D_1 and P_s (which in this case will enhance the signal level of P_s). Then subsequently the signals at C_2 and P_s will generate new wavelengths at D_2 and also at P_p . Similarly, signals at C_1 and D_1 will generate E_1 and also signals at C_2 and D_2 will generate E_2 . This process will repeat depending on signal power levels of the interacting waves. The interest in converted signals will depend largely on the power levels

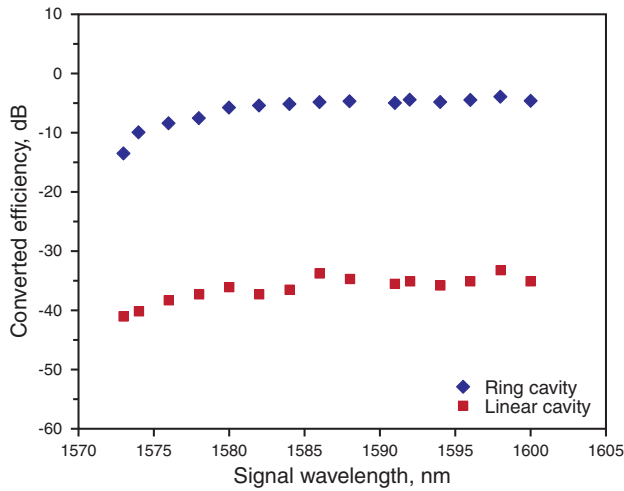


Figure 5 (online color at www.lphys.org) FWM conversion efficiency versus the signal wavelength, P_s , with HNLFF fitting pump wavelength, P_p , at 1590 nm by using ring and linear cavity

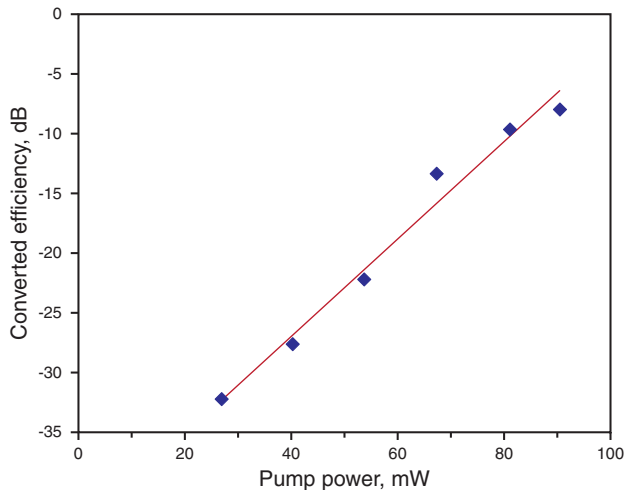


Figure 6 (online color at www.lphys.org) FWM conversion efficiency versus 1490 nm LD pump power

of the “free-running” spectrum, where the power of FWM increases when the pump wavelength is located near its peak. The novelty of the ring cavity, which is giving the highest peak of converted wavelength rather than the linear cavity (same HNLFF and pump power level), which is shown in Fig. 3.

An important parameter for FWM is the conversion efficiency which is shown in Fig. 4 whereby the signal wavelength is varied from 1573 to 1600 nm while keeping the pumping wavelength fixed at 1590 nm for the case of the first converted signal, C_1 . Measurement of the conversion efficiency from the spectrum obtained using OSA, where the FWM conversion efficiency $\eta(\text{dB}) = P_s(\text{dBm}) -$

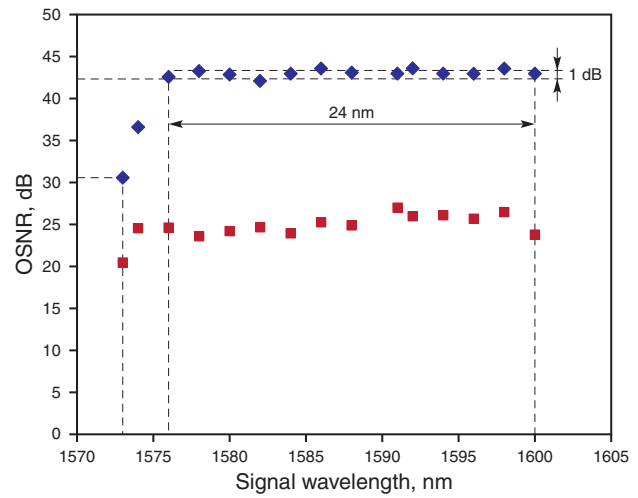


Figure 7 (online color at www.lphys.org) OSNR against signal wavelength, P_s , keeping pump wavelength, P_p , fixed at 1590 nm in HNLFF

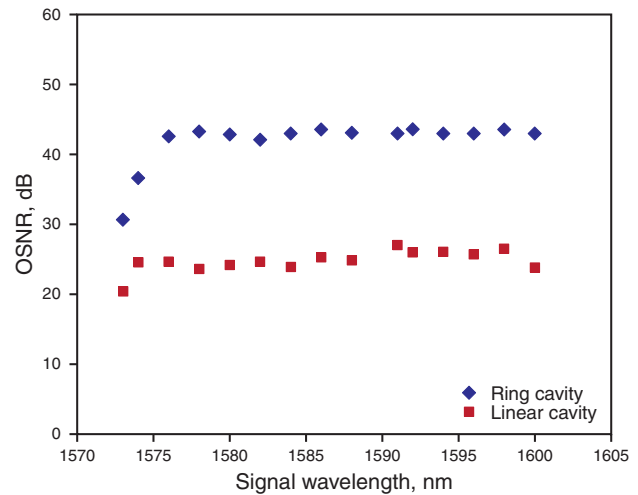


Figure 8 (online color at www.lphys.org) OSNR against signal wavelength, P_s , keeping pump wavelength, P_p , fixed at 1590 nm in HNLFF by using ring and linear cavity

$P_{C1}(\text{dBm})$. As the detuning of P_s increases the conversion efficiency also increases from -13.42 to -5.69 dB when the wavelength is changed from 1573 to 1580 nm. The conversion efficiency plateaus off at 1580 until 1600 nm with a value of -4 dB. The fluctuation is only about 2 dB within a region of 20 nm as shown in Fig. 4. This measurement can be extended into the C-band region if a shorter length of EDF is used.

In Fig. 6, the conversion efficiency versus the laser diode pump is shown with the conversion starting at 27 mW and increasing as the pump power is increased. The novelty of this experiment is that higher conversion

efficiency can be achieved at a lower laser pump power as compared to linear cavity by using the same HNLF and laser pump power. The proposed design leads to a higher amplification by the EDF caused by the circulation inside the ring cavity. The other important parameter in the FWM experiment is the optical signal-to-noise (SNR) ratio, which is shown in Fig. 7. The definition of the optical signal to noise ratio (OSNR) [dB] is the measure of the ratio of signal power to noise power in an optical channel. Measurements are taken by varying the signal wavelength, P_s , and keeping the pump wavelength, P_p , fixed at 1590 nm, as in the case in Fig. 4. As the signal increases from 1573 to 1576 nm, the SNR improves from 30 to 43 dB. Further increase of the P_s does not change the SNR very much as it plateaus off after 1576 nm. The peak at peak variation within a region of 24 nm is only about 1 dB. Besides the conversion efficiency, we also compared the SNR in linear and ring cavity that is illustrated in Fig. 8, whereby the SNR of the ring cavity is obtained higher than linear cavity in the range of 20 dB.

4. Conclusion

The proposed experiment demonstrates an efficient system for generating FWM in a 100 m HNLF using a ring configuration which to our knowledge is the first of its kind to be reported. The measured conversion efficiency is about -4 dB, which is the highest conversion efficiency using a 90 mW pump power laser at 1490 nm and OSNR of 43 dB for the case of the first converted signal, C_1 . This experimental setup exhibits a flat conversion efficiency as well as OSNR over a span of 20 nm. In short, the proposed technique will be of suitable application for wavelength conversion in many practical communication systems.

References

- [1] A.K. Zamzuri, U.S. Ismail, M.H. Al-Mansoori, M.S. Islam, and M.A. Mahdi, *Laser Phys. Lett.* **8**, 62 (2011).
- [2] M.Z. Zulkifli, N.A. Hassan, N.A. Awang, Z.A. Ghani, S.W. Harun, and H. Ahmad, *Laser Phys. Lett.* **7**, 673 (2010).
- [3] S. Shahi, S.W. Harun, and H. Ahmad, *Laser Phys. Lett.* **6**, 454 (2009).
- [4] B.O. Guan, H.Y. Tam, S.Y. Liu, P.K.A. Wai, and N. Sugimoto, *IEEE Photon. Technol. Lett.* **15**, 1525 (2003).
- [5] S.L. Danielsen, P.B. Hansen, and K.E. Stubkjaer, *J. Lightwave Technol.* **16**, 2095 (1998).
- [6] M. Kovacevic and A. Acampora, *IEEE J. Sel. Areas Commun.* **14**, 868 (1996).
- [7] S.J.B. Yoo, *J. Lightwave Technol.* **14**, 955 (1996).
- [8] W. Wang, H.N. Poulsen, L. Rau, H.-F. Chou, J.E. Bowers, and D.J. Blumenthal, *J. Lightwave Technol.* **23**, 1105 (2005).
- [9] J.J. Yu, X.Y. Zheng, C. Peucheret, A.T. Clausen, H.N. Poulsen, and P. Jeppesen, *J. Lightwave Technol.* **18**, 1007 (2000).
- [10] A. Hamie, A. Sharaiha, M. Guegan, and J. Le Bihan, *IEEE Photon. Technol. Lett.* **17**, 1229 (2005).
- [11] Y. Liu, M.T. Hill, E. Tangdiongga, H. de Waardt, N. Calabretta, G.D. Khoe, and H.J.S. Dorren, *IEEE Photon. Technol. Lett.* **15**, 90 (2003).
- [12] J. Yu, Z. Jia, Y.K. Yeo, and G.K. Chang, in: *Proc. of the 25th European Conference on Optical Communication, Glasgow, UK, September 25–29, 2005 (ECOC 2005)*, p. 32.
- [13] J.X. Ma, J.J. Yu, C.X. Yu, and Z. Zhou, *Opt. Commun.* **260**, 522 (2006).
- [14] A.E. Kelly, D.D. Marcenac, and D. Nasset, *Electron. Lett.* **33**, 2123 (1997).
- [15] D. Chen, B. Sun, and Y. Wei, *Laser Phys.* **20**, 1733 (2010).
- [16] X.M. Liu, *Laser Phys.* **20**, 842 (2010).
- [17] H.B. Sun, X.M. Liu, L.R. Wang, X.H. Li, and D. Mao, *Laser Phys.* **20**, 1994 (2010).
- [18] S.W. Harun, R. Parvizi, S. Shahi, and H. Ahmad, *Laser Phys. Lett.* **6**, 813 (2009).
- [19] C. Porzi, A. Bogoni, L. Poti, and G. Contestabile, *IEEE Photon. Technol. Lett.* **17**, 633 (2005).
- [20] S. Petit, T. Kurosu, M. Takahashi, T. Yagi, and S. Namiki, *Electron. Lett.* **45**, 1084 (2009).
- [21] D. Dahan, E. Shumakher, and G. Eisenstein, *IEEE Photon. Technol. Lett.* **18**, 592 (2006).



Four-wave mixing in dual wavelength fiber laser utilizing SOA for wavelength conversion

N.A. Awang^a, H. Ahmad^{a,*}, A.A. Latif^a, M.Z. Zulkifli^a, S.W. Harun^b

^a Photonics Laboratory, Department of Physics, University of Malaya, 50603 Kuala Lumpur, Malaysia

^b Department of Electrical Engineering, Faculty of Engineering, University of Malaya, 50603 Kuala Lumpur, Malaysia

ARTICLE INFO

Article history:

Received 4 November 2009

Accepted 27 May 2010

Keywords:

Four-wave mixing

Dual wavelength fiber laser

Semiconductor optical amplifier

Bi-EDF doped fiber

ABSTRACT

In this paper, a novel configuration of a wavelength converter is set forth by utilizing a semiconductor optical amplifier (SOA) as a nonlinear gain medium to generate a four-wave mixing (FWM) effect by using a dual wavelength bi-erbium-doped fiber laser that uses an Arrayed Waveguide Grating (AWG) together with two optical channel selector (OSC) as selective elements to function as a dual wavelength switchable pump power. The four-wave mixing (FWM) is produced with a wavelength detuning of 7 nm from the pump and signal which used is as the converted signal at wavelength 1532.8 nm or 1534.5 nm for transferring data from the input signal at wavelength 1547.0 nm. Thus, even though the conversion efficiency is as low as -43 dB, it is still possible for applications as a wavelength converter.

© 2010 Elsevier GmbH. All rights reserved.

1. Introduction

Four-wave mixing (FWM) in semiconductor optical amplifiers (SOA) is useful depending on the application such as wavelength converter [1], supercontinuum generation [2], fast optical switching [3] and sub-carrier multiplexed radio over fiber [4]. The generation of the FWM effect is associated with the nonlinearity of the SOA. It is principally caused by carrier density pulsation, carrier heating and spectra hole burning changes induced by the amplifier input signal [1]. The mechanism of generating FWM is based on wavelength detuning where in the detuning above a few nm; the mechanism called a carrier density modulation happens [4]. Such a mechanism falls within the category of interband effects that change the carrier density due to the depletion caused by stimulated emission. For wavelength detuning below a few nm, the FWM generated is based off the intraband effect where it is associated with two phenomenon; spectra hole burning (SHB) and carrier heating (CH). In the SHB mechanism, an optical input signal create holes and changes the intraband carrier distribution producing modulation of the occupation probability of carriers within the energy band. The CH phenomena on the other hand is caused when free carriers at low energy levels are removed by stimulated emission or transferred to a higher level due to free carrier absorption [4].

Recently, the FWM effect in SOAs has become a promising technique with regards to wavelength converters. Wavelength

converters are important tool in future WDM-based high speed optical networks because it provides simultaneous conversion of a single data channel into different channels without the necessity of multiple optical–electronic–optical transponders. Basically the wavelength converter utilizing the FWM technique has two schemes, the co-polarized pump scheme and orthogonal polarized pump scheme [5]. A typical dual wavelength laser source is injected to the nonlinear medium by incorporating two external laser sources such as a tunable laser source (TLS) as a pump source for the wavelength conversion. Recently, we have reported a simple configuration dual wavelength fiber laser by utilizing 24 Channel Arrayed Waveguide Gratings (AWG) as a wavelength selector in a two-cavity configuration that produces dual wavelength outputs by controlling both of the cavity losses to cope with the homogeneous broadening effect that comes from the Erbium-doped fiber, by now an infamously well known obstacle in producing dual and/or multiwavelength laser sources by using EDF as an active medium [6]. In this paper, we propose and demonstrate the conversion of wavelengths by the FWM effect by using an orthogonal polarized pump scheme in a dual wavelength fiber laser. This scheme represents a larger wavelength detuning range of input signal, pump signal and converted signal.

2. Experimental setup

The proposed experimental setup is shown in Fig. 1 below:

This experimental setup consists of two ring cavities that shares the same gain medium, a 14 m long Erbium-doped fiber (EDF), a 48 cm Bismuth-Erbium-doped fiber (Bi-EDF) and a 1550 nm SOA

* Corresponding author. Tel.: +60 3 79674290; fax: +60 3 79676770.
E-mail address: harith@um.edu.my (H. Ahmad).

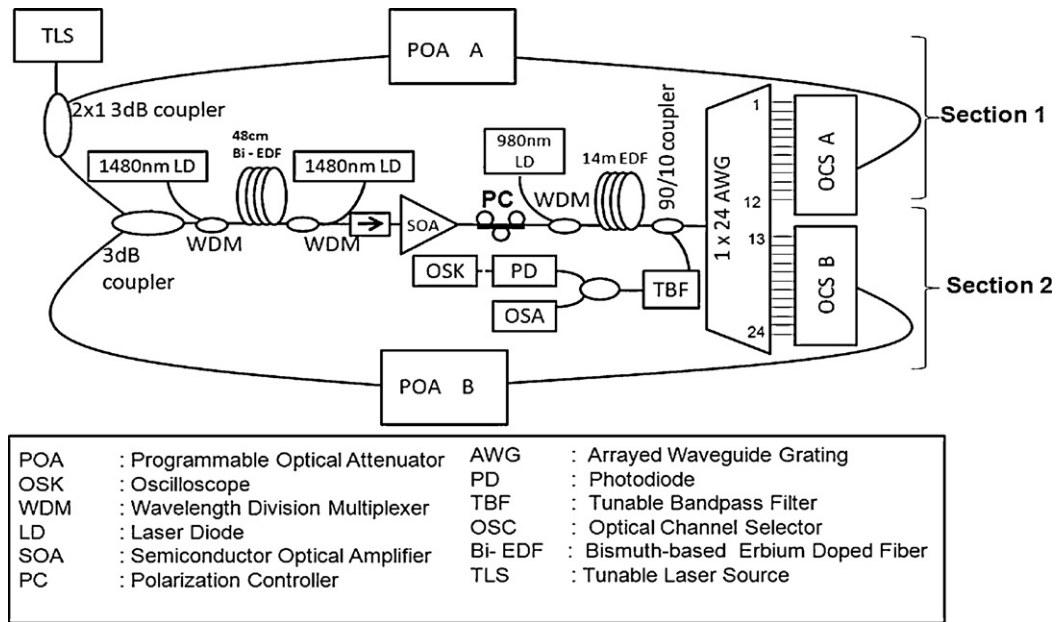


Fig. 1. Setup on wavelength conversion using orthogonal polarized pump four-wave mixing in SOA.

that contributes to the production of dual wavelengths and the FWM effect simultaneously. The Bi-EDF is pumped bi-directionally with two 1480 nm laser diodes with a power of 180 mW each via 1480/1550 nm wavelength division multiplexers (WDM) with a built in isolator inside the input WDM. The Bi-EDF plays two important roles here. First of which is to act as a gain medium for generating dual wavelengths and secondly, as a pre-amplifier for the four-wave mixing effect output enhancement in the SOA. The isolator that is placed next to the Bi-EDF is used to avoid the back scattering effect inside the cavity which can improve the amplified spontaneous emission (ASE) significantly. The 1550 nm SOA is used as a nonlinear medium for producing the FWM effect. The SOA is biased with 300 mA current that equals to a 5 dBm output power. A polarization controller (PC) is placed between the SOA and EDFA to control the polarization state of the two pumps to make it orthogonally polarized. The 14 m long EDF has an absorption rate of approximately 4.5 dB/m at 980 nm and is pumped with a 980 nm laser diode at 80 mW via a 980/1550 nm wavelength division multiplexer (WDM). The output end of the EDF is connected to a 90/10 coupler in which the 90% ratio goes to the single input of a 1×24 Arrayed Waveguide Grating (AWG) while the 10% ratio goes to a tunable bandpass filter (TBF) which is further connected to a 50/50 optical coupler. The 50/50 optical coupler splits the optical signal into an Optical Spectrum Analyzer (OSA) and into a photodetector (PD) which is then connected to an oscilloscope (OSK). In the configuration, there are two sections of the AWG as to create a dual-cavity configuration. Section 1 consists of outputs 1 until 12 that are connected to an optical channel selector (OCS), designated as OCS A whereas output channels 13–24 are connected to another OCS, designated as OCS B, as per the diagram in Fig. 1. The OCS used in this configuration setup is a 2×16 motor driven optical switch with a maximum switching time of 500 ms between each subsequent channel. The outputs of both OCS units are then connected to Programmable Optical Attenuator (POAs), with the output of OCS A connected to POA A and the output of OCS B connected to POA B. The POA functions as a means to control the loss for each cavity. The output end of POA A is then connected to the 50% leg of a 3 dB coupler while the other 50% leg is connected to a tunable laser source (TLS). The TLS is modulated by an internal modulator which allows the TLS to act as the input signal for

this experiment. The 100% leg is then connected to another 50% leg of a second 3 dB coupler. The other 50% leg of the second 3 dB coupler is connected to POA B while the 100% leg completes the ring cavity configuration via connection to the Bi-EDF through a WDM.

The process of generating the spectra of FWM is based on the dual wavelength fiber laser. First, a balanced dual wavelength fiber laser has to be produced by controlling both of the cavity losses by using a VOA with a certain attenuation value to reduce the incoming power before it is looped back into the cavity. When the output powers of both wavelengths are almost similar, the nonlinear medium (the SOA) is inserted into the cavity to generate the

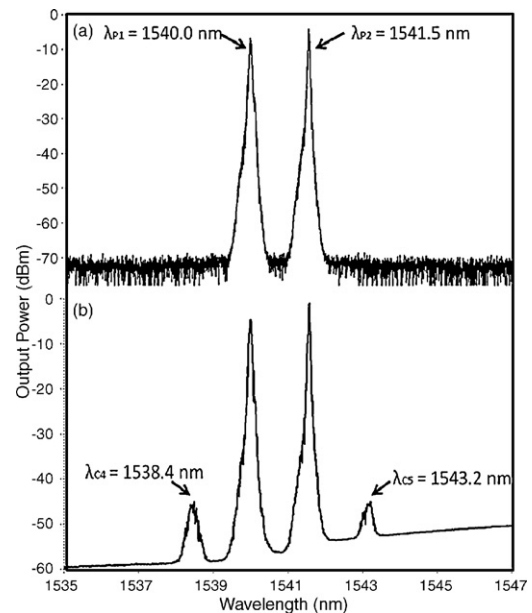


Fig. 2. Output spectra without inserted modulated input signal (a) dual wavelength output of Bi-EDF ring cavity showing the oscillating at λ_{p1} of 1540.0 nm and λ_{p2} of 1541.5 nm (b) an insertion of SOA, four-wave mixing is generated whereby λ_{c4} of 1538.4 nm and λ_{c5} of 1543.2 nm is due to four-wave mixing.

four-wave mixing effect with a 14 m long EDF as a booster amplifier in order to optimize the efficiency of the FWM. Fig. 2(a) shows the output spectrum of the dual wavelength fiber laser before the SOA and 14 m EDF are inserted in the cavity. Meanwhile Fig. 2(b) shows the generation of FWM in the SOA with λ_{C4} and λ_{C5} are generated by FWM effect from dual wavelength fiber laser λ_{P1} and λ_{P2} . In order to be compliant with future network WDM systems, the modulated input signal has to be inserted to make it function as a wavelength converter system. The proposed experiment used an internal modulator with a frequency modulation of 2 kHz, 1.5 kHz and 0.25 kHz from the TLS.

3. Results and discussion

Fig. 3 illustrates the spectra of signals that are observed when the two polarized pumps (λ_{P1} and λ_{P2}) and the modulated signal (λ_S) is launched into the setup. Due to the interactions between the three input waves, numbers of conjugates are generated. There are the two conjugate FWMs (λ_{C4} and λ_{C5}) of the λ_{P1} and λ_{P2} , two replicas (λ_{C6} and λ_{C7}) of the signal with wavelength spacing from the signal equal to the spacing of the two pumps and the three others conjugates which are λ_{C1} , λ_{C2} and λ_{C3} . The components in the spectra have different optical wavelengths that can be expressed as [4,7].

$$\begin{aligned}\lambda_{C1} &= 2 \times \lambda_{P1} - \lambda_S \\ \lambda_{C2} &= 2 \times \lambda_{P2} - \lambda_S \\ \lambda_{C3} &= \lambda_{P1} + \lambda_{P2} - \lambda_S \\ \lambda_{C4} &= \lambda_{P1} - (\lambda_{P2} - \lambda_{P1}) \\ \lambda_{C5} &= \lambda_{P2} - (\lambda_{P2} - \lambda_{P1}) \\ \lambda_{C6} &= \lambda_S - (\lambda_{P2} - \lambda_{P1}) \\ \lambda_{C7} &= \lambda_S + (\lambda_{P2} - \lambda_{P1})\end{aligned}\quad (1)$$

A conjugate signals (λ_{C1} and λ_{C2} with 1532.8 nm and 1534.6 nm, respectively) that is generated by mixing the optical signal of λ_S (1547 nm) with one of the pumps each is called a converted

FWMs. Therefore, the novelty of this paper is, the optical signal of 1547.0 nm can be converted the pulse signal at wavelength 1532.8 nm and 1534.6 nm. Fig. 1(a) and (b) shows that the power of the converted signal (λ_{C1}) increases when increasing the power of pump 1 (λ_{P1}) and vice versa. The conjugate signal (λ_{C3}) generated by mixing the optical signal with both pump signals is called a non-converted FWM. This reaction can be called a converted signal when the conjugate signal is λ_{C6} (1545.6 nm). Most reference for instance [3,7–9], used λ_{C6} as their converted signal but in this experiment λ_{C1} and λ_{C2} are utilized instead, due to the power of λ_{C1} being higher than λ_{C6} . Besides that, λ_{C1} and λ_{C2} also have a wider wavelength detuning of 7 nm, so, the other components can be filtered out for measuring the converted signal. We must note however that the conversion efficiency of λ_{C1} and λ_{C2} are –43 dB and –47 dB, respectively, which is quite low for signal conversion. However in this experiment, the signal of λ_{C1} and λ_{C2} still can be converted and detected. The lower conversion efficiency can be attributed to the increment in ASE noise of the amplifier.

The optical bandpass filter is used to selectively pick out λ_{C1} (1532.9 nm) or λ_{C2} (1534.5 nm) by removing the pump signal, the input signal and the other conjugated signals generated by FWM. Fig. 4 shows the spectra of λ_{C1} and λ_{C2} . The disparity in spectra is due to the difference in polarization of the optical signals, which indicates a special measure for optimization of the system performance against the polarization dependence.

This spectrum is also observed through an oscilloscope and the non-inverting pulse is obtained as shown in Fig. 5. Based on the time domain, the input signal, λ_S (1547.0 nm) converts the pulse signal to the converted signal, λ_{C1} (1532.8 nm) or λ_{C2} (1534.5 nm) similar to the frequency modulator. But the converted signal will have a finite rise time and fall time due to the non-zero carrier lifetime. In the case of negligible waveguide losses, the conversion bandwidth is inversely proportional to the spontaneous carrier lifetime but enhanced by the amplifier gain. This bandwidth enhancement is due to propagation effect in the amplifier gain. The slow carrier response at the start of the amplifier leads to a distortion of the

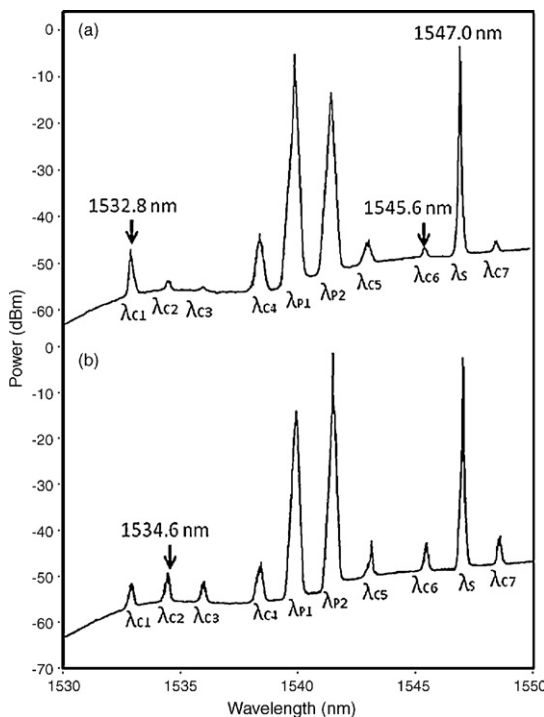


Fig. 3. The spectra signal of orthogonal polarized pump scheme before connected with optical bandpass filter (a) $\lambda_{P1} \geq \lambda_{P2}$ (b) $\lambda_{P1} \leq \lambda_{P2}$.

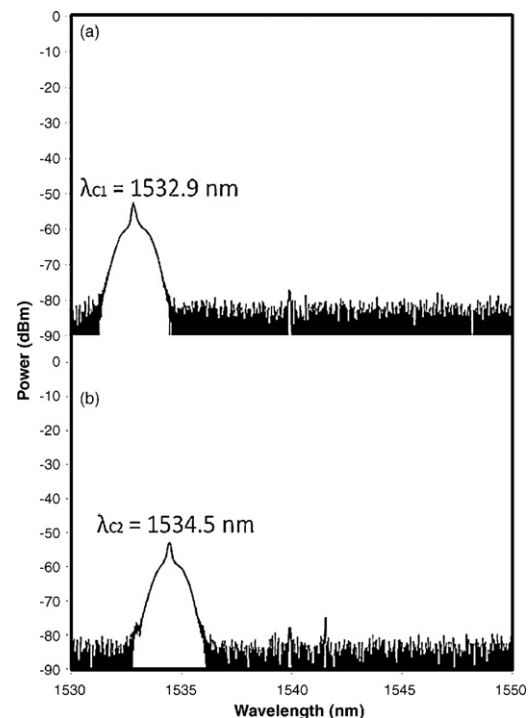


Fig. 4. The output signal after the optical bandpass filter (a) λ_{C1} (b) λ_{C2} .

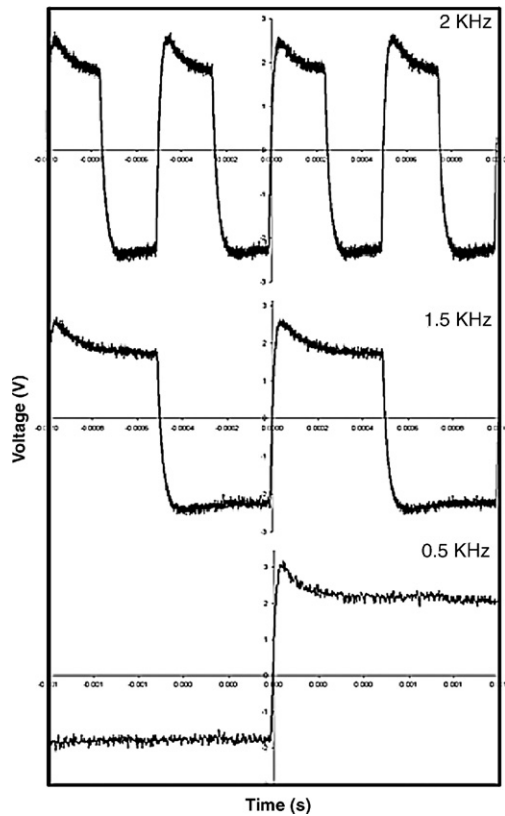


Fig. 5. The converted signal at wavelength 1532.8 nm and 1534.5 from input signal at wavelength 1547.0 nm after passing through the SOA.

optical pulses at the middle of the amplifier. The distorted pulse with strong leading edges then saturates the carrier more rapidly in the last parts of the device leading to an enhanced bandwidth.

4. Conclusion

As a conclusion, a converted signal with wide wavelength detuning is observed in a dual wavelength fiber laser setup by utilizing the FWM effect in an SOA. The modulated signal is transferred from wavelength 1547.0 nm into a converted signal at wavelength 1532.8 nm or 1534.5 nm in the lowest conversion efficiency of -43 dB and -47 dB for the input signal power of 1 dBm. This converted signal is useful for low-power wavelength converter applications.

References

- [1] A. D'Ottavi, A. D'Ottavi, L. Francois Girardin, F. Graziani, P. Martelli, A. Spano, S. Mecozzi, R. Scotti, J. Dall'Ara, G. Eckner, Guekos, Four-wave mixing in semiconductor optical amplifiers: a practical tool for wavelength conversion, *IEEE J. Sel. Top. Quantum Electron.* 3 (April) (1997).
- [2] K. Morioka, K. Mori, S. Kawanishi, M. Saruwatari, Pulse-width tunable, self-frequency conversion of short optical pulses over 200 nm based on super-continuum generation, *Electron. Lett.* 30 (1994) 1960–1962.
- [3] S. Diez, C. Schmidt, R. Ludwig, H.G. Weber, K. Obermann, S. Kindt, I. Koltchanov, K. Petermann, Four-wave mixing in semiconductor optical amplifiers for frequency conversion and fast optical switching, *IEEE J. Sel. Top. Quantum Electron.* 3 (October) (1997).
- [4] H.J. Kim, J.I. Song, An all-optical frequency up-converter utilizing four-wave mixing in a semiconductor optical amplifier for sub-carrier multiplexed radio-overfiber applications, *Opt. Expr.* 15 (March) (2007).
- [5] M.J. Connelly, *Semiconductor Optical Amplifier*, Kluwer Academic Publishers, 2004.
- [6] M.Z. Zulkifli, H. Ahmad, A.A. Latif, S.W. Harun, Tunable dual wavelength incorporating AWG and optical channel selector by controlling the cavity loss, *Opt. Commun.* (2009).
- [7] K.K. Chow, C. Shu, M.W.K. Mak, H.K. Tsang, Widely tunable wavelength converter using a double-ring fiber laser with a semiconductor optical amplifier, *IEEE Photon. Technol. Lett.* 14 (10, October) (2002).
- [8] C.M. Greco, F. Martelli, A. D'Ottavi, A. Mecozzi, P. Spano, R. Dall'Ara, Frequency-conversion efficiency independent of signal-polarization and conversion-interval using four-wave mixing in semiconductor optical amplifiers, *IEEE Photon. Technol. Lett.* 11 (June (6)) (1999).
- [9] J. Lu, Z. Dong, L. Chen, J. Yu, Polarization insensitive wavelength conversion based on four-wave mixing for polarization multiplexing signal in high-nonlinear fiber, *Opt. Commun.* 282 (2009) 1274–1280.

Enhancement of Four Wave Mixing Characteristic in Semiconductor Optical Amplifier Using Fiber Loop Mirror

Y. S. Hussein and S. W. Harun
Dept. of Electrical Engineering
University of Malaya
50603 Kuala Lumpur, Malaysia.

N. A. Awang and H. Ahmad
Photonics Research Center.
University of Malaya
50603 Kuala Lumpur, Malaysia.

Abstract—We investigate the effect of the input wave power, wavelength detunes between the two source waves and the conjugate wave power to conversion efficiency. The essential part of the investigation is about suppression ratio of pump power and conjugated wave power. The proposed setup success for suppress the pump power and increase the conjugate signal in wavelength detuning of 1.4 nm. It is due to loop mirror that act as a reflector where depend to the high birefringence of the Polarization Maintaining Fiber (PMF) and the polarization controller.

I. INTRODUCTION

Besides the optical amplification characteristics, the most attractive application of Semiconductor Optical Amplifiers (SOAs) are also associated with their nonlinear optical properties. The injection of light into SOA varies the carrier density and carrier distribution within the energy bands which results in a modulation of gain and refractive index in the active region of the amplifier [1]. When two optical wave (pump power and signal power) launched into the SOA with the state of the polarization [2], the beating of both waves modulates the carrier density and carrier distribution in the active medium, thereby generating dynamics index and gain grating. The interaction of the launched waves with these gratings lead to new wavelength components, the four wave mixing signals, that can be observed in the SOA output spectrum. The new wavelength is called the conjugate because its phase is the opposite of the signal phase. This means that the spectrum of the conjugate signal is shifted and inverted replica of the input signal [3]. The relationship between the conjugate, pump and signal waves can be explained by the equation;

$$f_c = 2f_p - f_s \quad (1)$$

Where: f_p is the pump frequency, and f_s is the signal frequency.

The generated of four wave mixing is based on inter and intra-band effects.

In this paper, some experimental studies are implemented on the effect of Four Wave Mixing (FWM) in SOA. The loop mirror is used to obtain the highest of conjugated signal. It is shown that input waves power, wavelength detunes between the two source waves and the biased current of the SOA have significant influences in the conversion efficiency.

II. EXPERIMENT

The schematic diagram for the experimental set-up is shown in Fig. 1. The FWM effect in SOA is observed for the set-up configured with and without the Fiber Loop Mirror (FLM) as shown in Figs. 1(a) and 1(b), respectively.

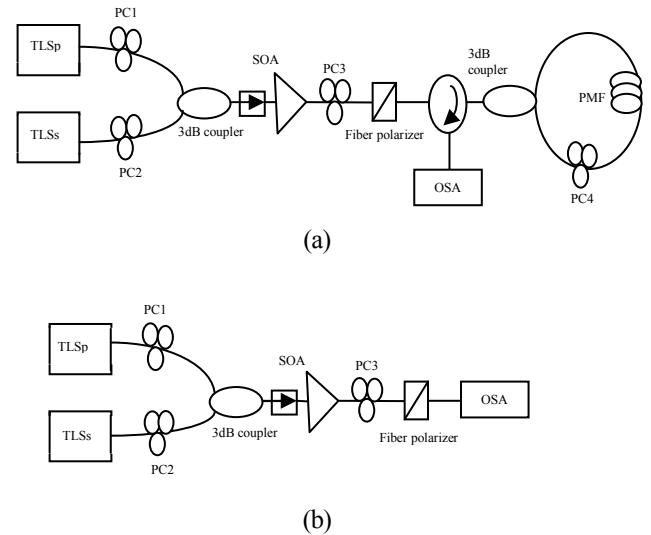


Figure 1. The experimental setup to investigate the FWM effect in SOA (a) with FLM (b) without FLM.

Two beams from the Tunable Laser Sources (TLS) are coupled by a 3dB optical coupler before launched into an SOA. In between, an optical isolator is used to prevent backscattered wave from the SOA back to the laser sources. Polarization Controllers (PC1 and PC2) are used to adjust the state of polarization of each beam in order to achieve optimum effect of FWM in the SOA. PC3 and fiber polarizer are used to control the state of polarizations of the output waves of the SOA before entering into the fiber loop mirror which consists of a 2.8 meter long Polarization Maintaining Fiber (PMF) and a PC. The wavelength spacing of the FLM is depending on the length of the fiber and is approximately 2.6nm in our experiment. In order to achieve optimum contrast in the reflection spectrum of the loop mirror, PC4 which is placed in the loop is used to rotate the beams that propagate from both directions in such a way that one of them is rotated 90° in relative to another beam in

the loop. A fiber circulator is used to extract the reflection from the loop mirror, which is then analyzed using an Optical Spectrum Analyzer (OSA). On the other hand, the wavelength for the input signal is fixed at 1550.8 nm and the pump signal is varied from 1449.4 nm to 1441.4 nm. The input signal and pump powers are fixed at -8dBm and 8dBm, respectively. The SOA is electrically pumped with a bias current of 350mA. The output spectrum of the system is compared and investigated for both set-ups with and without the FLM.

III. RESULTS AND DISCUSSION

The experiment was implemented to observe the FWM effect in the SOA with and without the loop mirror. The signal wavelength is fixed at 1550.8 nm. In general, the pump and signal waves have higher power compared to the generated conjugate power as shown in Fig. 2 for the setup without loop mirror. On the other hand, it is observed that there is an increment of 5 dB in the conjugate wave power while the pump wave power is suppressed by 16dB if loop mirror is involved. This is attributed to the FLM, which acts as a filter/reflector to suppress the pump signal and allow the input signal and the conjugate signal to propagate. The FLM uses a piece of PMF as high birefringence. Birefringence causes a variation of optical path length with polarization angle. This output spectrum from the FLM is depending to the PC4, when the polarization angle in line with the light and the pump power is generated at the dip of the PMF segments. So, the pump wave power is suppressed. In general, if the pump power decreased, the conjugated also decreased. Therefore, loop mirror is the one technique for suppressing the pump without suppressed the conjugate based on the polarization angle in the fiber. In other research, the high power of pump should be used for obtain the higher conjugate by suppressing the pump power, but in this research, the low power of pump is used.

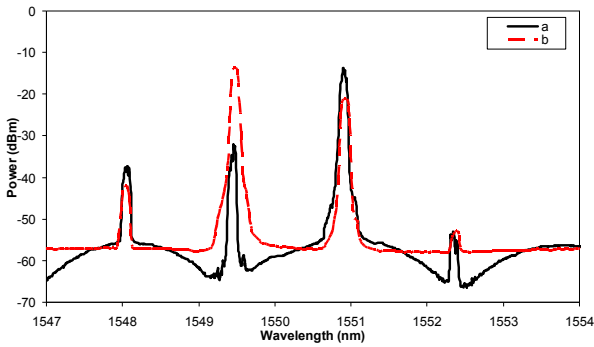


Figure 2. The spectrum of four wave mixing with and without FLM.

Fig. 3 shows the output spectrum with different detuning. Besides the pump is suppressed, the loop mirror also could generate the conjugated signal of four wave mixing in longer detuning rather than without loop. Using this setup, the four wave mixing in SOA can be observed until the detuning around 20 nm. In Fig. 3, the four wave mixing conjugate signal is observed at about -38dBm with input signal power of -11.8dBm and pump power of 8dBm. As

shown in Fig. 3, the FWM signal power will reduce and disappear as wavelength detuning increases. This is due to limited region in amplified spontaneous emission (ASE) power at SOA.

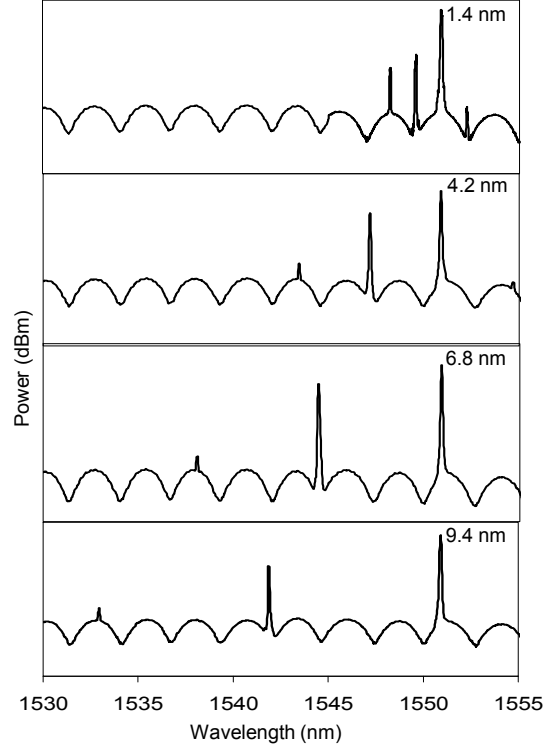


Figure 3. Four wave mixing spectrum for different detuning.

Fig. 4 shows the FWM conversion efficiency for different wavelength detuning. The FWM conversion efficiency, η is given by:

$$\eta = \frac{P_{c,out}}{P_{s,in}} \quad (2)$$

Where: $P_{c,out}$ is output conjugate power, and $P_{s,in}$ is input signal power.

It is observed that with decrement in the input signal power, the conversion efficiency increases. As shown in this figure, conversion efficiency decreased as the wavelength detuning increases wherever at conversion for input power of -11.8dBm. The maximum conversion efficiencies achieved for down conversion and up conversion are -25.44dB and -31.4dB respectively. It is due to the limitations of the driving current of SOA for thermal dissipation reasons.

Fig. 5 shows the conjugate wave power over the pump wave power suppression ratios at different wavelength detuning observed in two different setups, where the circular point (a) refer to the full setup with fiber loop mirror and the square point (b) refer to setup without fiber loop mirror. Based on this figure, the circular point achieves the highest suppression ratio compared to the square point. The maximum suppression ratio is -5dB for the wavelength detuning of 1.4nm. This is attributed to the use of FLM, which can suppress the pump wave power and at the same time increases the conjugate wave power as shown in Fig. 3.

The suppression ratio is decreased as the wavelength detuning increased and caused a weaker four wave mixing.

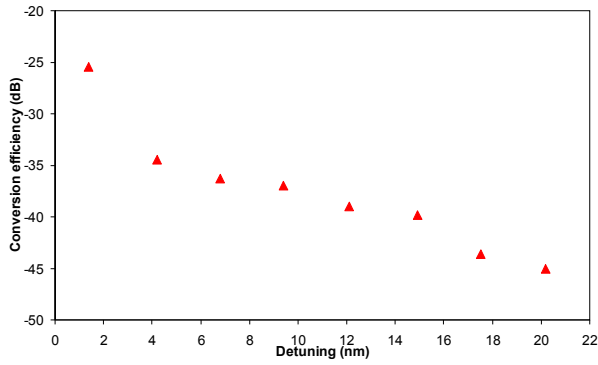


Figure 4. FWM conversion efficiency, $P_{s,in} = -11.8$ dBm.

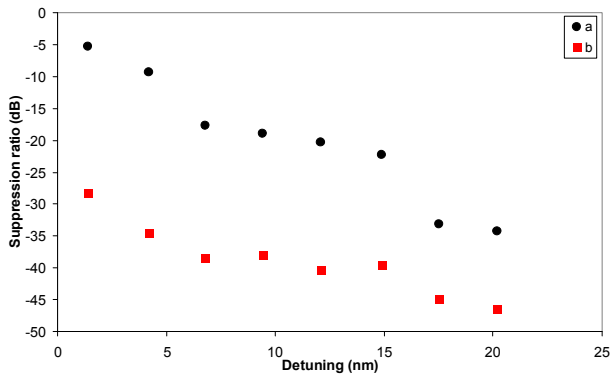


Figure 5. Suppression ratio at different wavelength detunes.

IV. CONCLUSION

We have investigated the effect of the input wave power, wavelength detunes between the two source waves and the conjugate wave power to conversion efficiency. The essential part of the investigation is about suppression ratio of pump power and conjugated wave power. This setup success for suppress the pump power and increase the conjugate signal in wavelength detuning of 1.4 nm. It is due to loop mirror that act as a reflector where depend to the high birefringence of the PMF and the polarization controller.

REFERENCES

- [1] D. K. Mynbaev and L. L. Scheiner, "Fibre-Optic Communications Technology", Prentice Hall, New Jersey, 2001.
- [2] S. Diez, C. Schmidt, R. Ludwig, H. G. Weber, K. Obermann, S. Kindt, I. Koltchanov, K. Petermann, "Four-Wave Mixing in Semiconductor Optical Amplifiers for Frequency Conversion and Fast Optical Switching", IEEE Journal of Selected Topics in Quantum Electronics, Vol. 3, No. 5, October 1997.
- [3] J. Hashimoto, K. Koyama, T. Katsuyama, Y. Tsuji, K. Fujii, K. Yamazaki and A. Ishida, "1.3 μ m GaInNAs Bandgap Difference Confinement Semiconductor Optical Amplifiers", Jpn. J. Appl. Phys., Vol. 45, pp. 1635-1639, 2006.

Stable power multi-wavelength fibre laser based on four-wave mixing in a short length of highly non-linear fibre

This article has been downloaded from IOPscience. Please scroll down to see the full text article.

2011 J. Opt. 13 075401

(<http://iopscience.iop.org/2040-8986/13/7/075401>)

View [the table of contents for this issue](#), or go to the [journal homepage](#) for more

Download details:

IP Address: 161.142.24.130

The article was downloaded on 23/05/2012 at 02:48

Please note that [terms and conditions apply](#).

Stable power multi-wavelength fibre laser based on four-wave mixing in a short length of highly non-linear fibre

N A Awang^{1,3}, M Z Zulkifli¹, A A Latif¹, S W Harun³ and H Ahmad¹

¹ Photonics Laboratory, Department of Physics, University of Malaya, 50603 Kuala Lumpur, Malaysia

² Department of Electrical Engineering, Faculty of Engineering, University of Malaya, 50603 Kuala Lumpur, Malaysia

³ Faculty of Science, Art and Heritage, Universiti Tun Hussein Onn Malaysia, 86400 Batu Pahat, Johor, Malaysia

E-mail: harith@um.edu.my (H Ahmad)

Received 21 January 2011, accepted for publication 24 March 2011

Published 28 April 2011

Online at stacks.iop.org/JOpt/13/075401

Abstract

A multi-wavelength fibre laser utilizing the four-wave mixing (FWM) effect in a 100 m long highly non-linear fibre (HNLF) is proposed and demonstrated. The multi-wavelength fibre laser is configured in a ring cavity and only needs a low power erbium doped fibre amplifier (EDFA) as the gain medium to generate 11 lines in the range of 1582–1600 nm with a signal-to-noise ratio (SNR) of 43 dB. The proposed system is very stable, with only minor fluctuations of 0.1 dB in the output power of the generated multi-wavelengths observed for a test period of more than an hour. The multi-wavelength fibre laser has many potential applications in optical communications and optical sensing systems.

Keywords: four-wave mixing (FWM), highly non-linear fibre (HNLF), multi-wavelength fibre laser

1. Introduction

Multi-wavelength fibre lasers have recently become the focus of increasing research and development efforts due to their enormous potential as optical sources for a multitude of applications. Multi-wavelength fibre lasers are particularly advantageous due to their output stability, low cost and high compatibility with existing systems, thus making them highly suited for applications such as wavelength division multiplexing and wavelength conversion in optical communications [1–3] and also as transmission sources for optical fibre based sensors. Previous works on multi-wavelength sources have been reported using erbium doped fibres (EDFs) [1, 4] as the gain medium, and more recently with semiconductor optical amplifiers (SOAs) [5] as the gain medium. The EDF is an excellent candidate as the gain medium in a multi-wavelength source due to its inherent

advantages such as low threshold power and high power conversion efficiencies [6]. However, it is still a challenge to generate an EDF based multi-wavelength fibre laser with a stable output due to the mode competition arising from the homogeneous line broadening effect in the EDF. The mode competition causes the dominant wavelength to suppress other wavelengths, thus preventing a multi-wavelength output as well as causing significant fluctuations in the output power stability, making them unsuitable for practical applications. While it is possible to overcome the effect of homogeneous broadening in the EDF by cooling it with liquid nitrogen, this approach is far from easy and not suitable for practical applications. Therefore, research efforts have now focused on alternative approaches towards developing multi-wavelength fibre lasers, including utilizing non-linear phenomena such as stimulated Brillouin scattering (SBS) and the four-wave mixing (FWM) [7] effect to generate the desired multi-wavelength output.

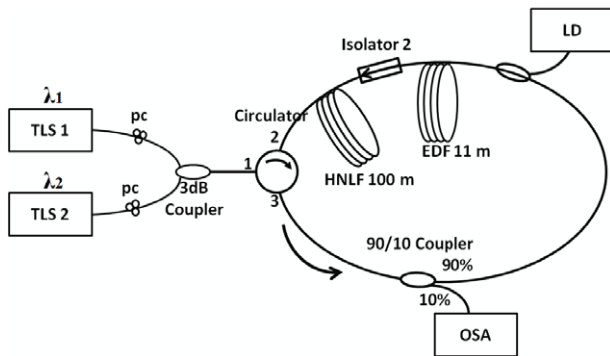


Figure 1. Experimental setup of the HNLF based multi-wavelength fibre laser in a ring cavity configuration.

The FWM effect, in particular, has shown significant promise in the development of a stable multi-wavelength fibre laser. The FWM effect occurs when two or more optical signals at different frequencies propagate simultaneously through a non-linear medium. When the phase matching conditions are satisfied, new optical signals are generated at new frequencies through the conversion of the optical power from the original signal wavelengths [8, 9] (in quantum mechanical terms, photons from one or more waves are annihilated and new photons are created at different frequencies but still conserving the net energy and momentum of the system). By using a non-linear gain medium such as a highly non-linear fibre (HNLF) [10], the FWM effect can be utilized to create a stable multi-wavelength output with up to five stable lasing wavelengths and a signal-to-noise ratio (SNR) of 20 dB, as demonstrated in earlier works [11, 12]. However, the requirement for a long HNLF to generate the FWM effect and the need for a very high-gain amplifier with a saturated output power of around 30 dBm [13] represents a drawback in developing an FWM based multi-wavelength fibre laser for practical applications. Furthermore, most multi-wavelength fibre laser designs that take advantage of the HNLF to generate the FWM effect utilize a Sagnac loop mirror (SLM) [13] in the fibre laser configuration, thus giving a low SNR and also affecting the output stability.

In this paper, a compact ring cavity multi-wavelength fibre laser utilizing the FWM effect in a short length HNLF is proposed and demonstrated. The system also uses a low power erbium doped fibre amplifier (EDFA) to provide the amplification during the FWM process, thus increasing the efficiency of the system. Furthermore, the proposed setup does not incorporate an SLM as in other works and therefore has an SNR of more than 40 dB and a highly stable output power.

2. Experimental setup

Figure 1 shows the experimental setup of the HNLF based multi-wavelength fibre laser in a ring cavity configuration.

The main components of the ring cavity are the forward-pumped EDFA, a 100 m long HNLF, an optical circulator and also a 90:10 output coupler which is used to tap a portion of the output signal into the optical spectrum analyser

(OSA) with a resolution of 0.02 nm. The EDFA consists of an 11 m long Metrogain EDF (DF1500L, Fibercore Ltd) with an erbium ion concentration of 900 ppm and signal and pump absorption coefficients of 18.06 dB m⁻¹ and 8.3 dB m⁻¹ at 1530 nm and 1490 nm respectively and is pumped by a 1490 nm laser diode at a pump power of 90 mW. The HNLF (OFS, A Furukawa Company) used has nominal zero dispersion wavelength (ZDW), loss coefficient, dispersion slope and non-linear parameter of 1531 nm, 0.73 dB km⁻¹, 0.007 ps nm⁻² km⁻¹ and 10.8 (W km)⁻¹, respectively.

For FWM interaction, two sources of optical signals are required, which are designated as λ_1 and λ_2 in figure 1 and connected to the ring cavity through an optical circulator and a 3 dB coupler. λ_1 is generated from a tunable laser source (TLS1) that is fixed at a wavelength of 1590 nm with an average output power of 12.8 dBm, whilst λ_2 is generated from another tunable laser source (TLS2) with an average power of 10.8 dBm and a wavelength varied between 1570 and 1600 nm. The linewidths of these two outputs are about 0.015 nm and are made to individually pass through two polarization controllers (PCs) so as to optimize their polarization states before being launched into the ring cavity. These two signals are combined using a 2 × 1 3 dB coupler that is then connected to Port 1 of the optical circulator. At this juncture, two wavelengths (λ_1 and λ_2) are produced and injected into the ring cavity through Port 2 of the optical circulator, and subsequently reflected back by the optical circulator and made to travel in an anti-clockwise direction. This dual-wavelength optical signal will experience amplification in the EDFA and continue travelling towards the HNLF where the two wavelengths will now interact in the non-linear gain medium to generate more wavelengths based on the FWM effect, on the condition that they are phase-matched. As in the case of the above ring configuration, the generated wavelengths from the FWM effect are initially low in power, but the power increases as it oscillates in the cavity several times. The output of the FWM spectrum is tapped out from the coupler with a larger portion of the light allowed to oscillate in the ring cavity.

3. Results and discussion

As the EDF is a homogeneously broadened gain medium, mode competition occurs between the different oscillating wavelengths. As such, the two tunable lasers function to generate the dual-wavelength input so as to lock-in the dual-wavelength oscillation in the ring cavity. Figure 2 shows a free-running EDF laser output that is taken without the dual-wavelength input from TLS1 and TLS2 and the EDF pumped by the 1490 nm laser diode at a pumping power of 90 mW. In this spectrum, it can be seen that only a few peaks in the L-band region of 1570–1600 nm are present. This is due to the long length of the highly doped EDF that was used, whereby the conventional (C-) band amplifier spontaneous emission (ASE) is used to pump the end portion of the EDF, thus generating operation in the long-wavelength (L-) band region. By having a shorter length of this fibre, the same observation can be made for the C-band region. In this paper, the demonstration has been done in the L-band region mainly to utilize the uniform

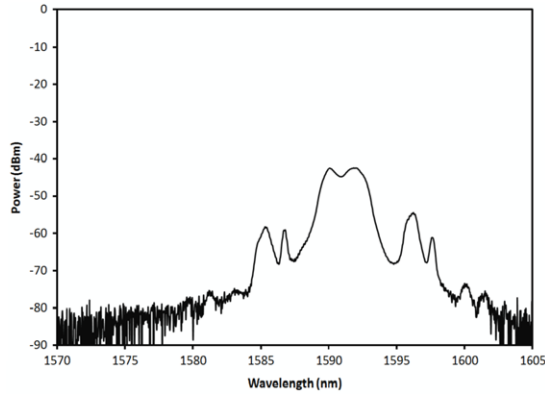


Figure 2. Free-running spectrum of the FWM (without pump and signal wavelengths).

gain that is achievable in the L-band region, giving the same gain for wavelengths in this region. In this regard, the chosen wavelength of operation for the FWM effect should be within the region of the free-running condition of the EDF laser which exhibits a peak power of about -40 dBm and a bandwidth of approximately 4 nm centred at 1591.8 nm.

The dual-wavelength laser that was initially amplified by the EDFA and then launched into the HNLF will generate a multi-wavelength output as shown in figure 3.

The occurrence of the FWM effect in the HNLF is due to the incidence of λ_1 and λ_2 (corresponding to frequencies ω_1 and ω_2) where it produces a moving refractive index grating which is temporally modulated at the frequency detuning of $\Delta\omega = \omega_1 - \omega_2$. Therefore, any signal at a frequency of ω that propagates in the HNLF will experience inelastic diffraction by a grating to generate a new frequency of $\omega \pm \Delta\omega$ and as these signals travel in the HNLF it will continue to generate frequencies by the general formula of $\omega \pm n\Delta\omega$ ($n = \pm 1, \pm 2, \dots, \pm n$). In particular, the incident lasing frequencies will be self-diffracted and the output spectrum will exhibit a number of sidebands at $\pm n\Delta\omega$ on each side of the incident frequencies, thus generating a multi-wavelength output. This can be seen in figure 3 of the generated frequencies due to the dual-wavelength fibre lasers at ω_1 and ω_2 . These generated frequencies, ω_{C1} and ω_{C2} , based on the degenerate case of FWM and meeting the phase matching conditions are fulfilled by [14]:

$$\omega_{C1} = 2\omega_1 - \omega_2 \quad (1)$$

$$\omega_{C2} = 2\omega_2 - \omega_1. \quad (2)$$

These converted wavelengths will also oscillate in the cavity and increase in power, and will continue to generate further wavelengths such as ω_{D1} and ω_{D2} , where ω_{D1} is the side-band generated as a result of the interaction between ω_{C1} and ω_1

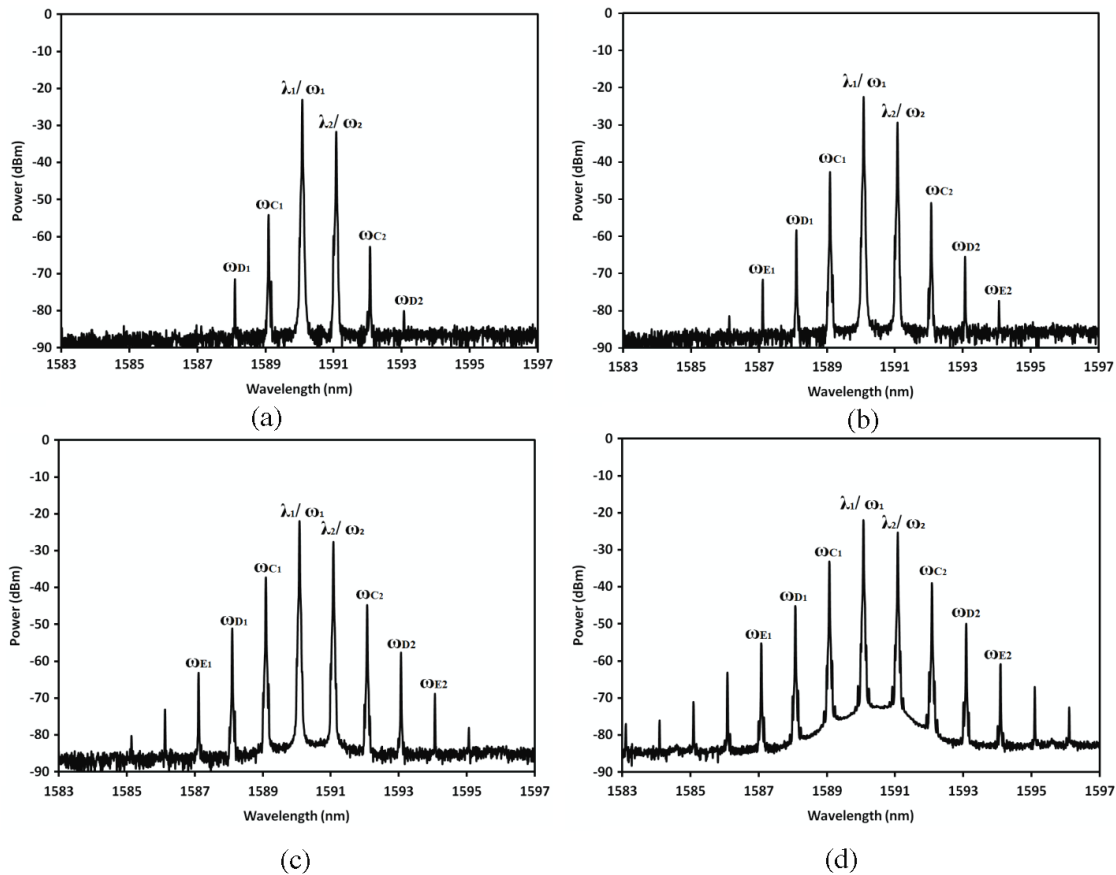


Figure 3. Power spectra at the output of the fibre at pump power of (a) 40 mW, (b) 67 mW, (c) 81 mW and (d) 90 mW.

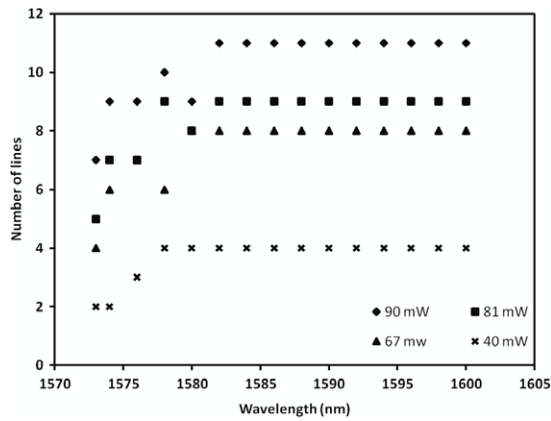


Figure 4. Number of generated wavelengths (lines) based on FWM in HNLf against different EDFA pump powers and also the variation of the signal wavelength, λ_s .

(the interaction between ω_{C1} and ω_1 also generates a signal at ω_2 which in this case serves to enhance the power level of the original ω_2 signal). In a similar manner, ω_{D2} is the side-band generated as a result of the interaction between ω_{C2} and ω_2 (the interaction between ω_{C2} and ω_2 also generates a signal at ω_1 which in this case serves to enhance the power level of the original ω_1 signal). This process repeats for ω_{E1} and ω_{E2} and other wavelengths, as shown in figure 3.

Also in this figure, the number of generated wavelengths is measured against the pump powers of the EDFA and the measured SNR is 43 dB. As the figure is superimposed, it is difficult to differentiate the number of lines generated at different pump powers and this is presented in figure 4 for different pump powers of the EDFA and also for different values of the signal wavelength, ω_2 .

It can be seen that at a maximum pump power of 90 mW, 11 lines are observed when λ_s is tuned from 1582 to 1600 nm, whilst λ_p is fixed at 1590 nm. The number of lines generated is constant at 11 lines between signal wavelengths of 1582–1600 nm at the pump power of 90 mW. At shorter wavelengths of the signal fewer lines are generated, with only seven lines generated at 1573 nm, nine lines generated at 1576 nm and ten lines generated at 1578 nm. This could be due to the gain

profile of the EDF which is more consistent between 1582 and 1600 nm. At a pump power of 80 mW, nine lines are generated. As the pump power is reduced further to 67 mW, eight lines are generated, whilst at 40 mW only four are lines generated. The reduced number of lines at lower pump powers is due to the lower gain of the EDFA. One of the most important observations is that most of the generated lines at different EDF pump powers give a constant number of lines for different input signal wavelengths.

The other important measurement is the stability of the output, and this is presented in figures 5(a) and (b). From this figure, it can be seen that the output power of the generated wavelengths is very stable with time. Unlike in the case of multi-wavelength generation in the EDFA, which suffers from low output power due to mode competition and also unstable outputs due to cross-saturation gain for signals at different wavelengths, the multi-wavelength output generated by the FWM effect in the HNLf is highly stable [7], as shown in this experiment.

Figure 5(a) also shows the spectral evolutions of the proposed multi-wavelength with HNLf in terms of time. This was taken using repeated scans in the OSA at intervals of 5 min for 1 h. The multi-wavelength output is seen to be stable with fluctuations of only 0.1 dB at room temperature. Figure 5(b) shows the output power stability for each wavelength generated against time.

The advantage of this setup is that it has the ability to generate multi-wavelength outputs based on the FWM effect with a detuning spacing of 1 nm or larger and using a low-gain amplifier with a saturation power of 9 dBm as compared to other works which use a much higher saturation power [13]. The other important advantage of this setup is that the length of the HNLf used is so much shorter than other previous works with about the same output power of the generated multi-wavelengths. In addition, the measured SNR is about 43 dB, which is higher and better than those typically obtained in other similar systems of about 30 dB only [11]. In short, the proposed configuration is suitable for multi-wavelength generation application based on the FWM effect in HNLfs, with very stable outputs that can find applications in optical communication networks.

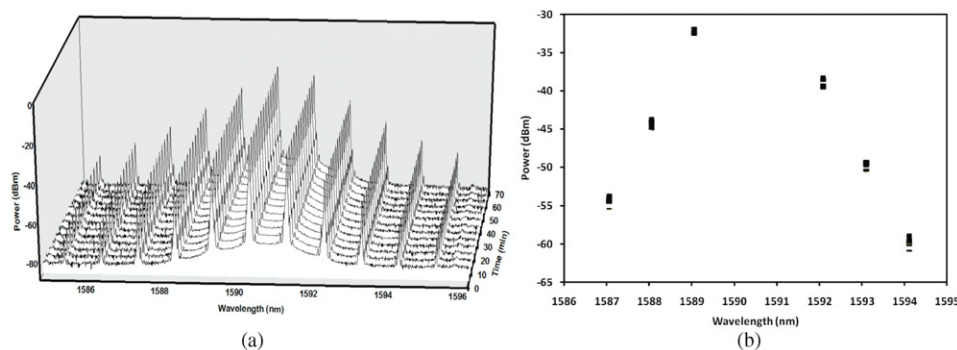


Figure 5. Peak power of generated wavelengths given in (a) a three-dimensional (3D) representation against time as well as (b) the peak power of the output wavelengths (the points in (b) indicate the output power of the various generated wavelengths such as E_1 , D_1 , C_1 , C_2 , D_2 and E_2 of figure 4).

4. Conclusion

In summary, multi-wavelength generation based on the FWM effect in a 100 m HNLF utilizing the ring configuration is demonstrated. The system uses a laser diode pump power of only 90 mW at 1490 nm with a saturated output power of 9 dBm to act as the gain medium for the multi-wavelength generation. The highest number of generated lines is about 11 lines with tuned signal wavelengths from 1582 to 1600 nm, keeping λ_1 fixed at 1590 nm and an SNR of 43 dB. The measured stability of the detected powers fluctuates by only 0.1 dB over the 1 h test period. The generated multi-wavelength output is very stable and with proper amplification can be used as a viable multi-wavelength source for many applications.

References

- [1] Park N and Wysocki P F 1996 *IEEE Photon. Technol. Lett.* **8** 1459–61
- [2] Zhang A, Liu H, Demokan M S and Tam H Y 2005 *IEEE Photon. Technol. Lett.* **17** 2535–7
- [3] Han Y G, Tran T V A and Lee S B 2006 *Opt. Lett.* **31** 697–9
- [4] Moon D S, Paek U C and Chung Y 2004 *Opt. Express* **12** 6147–52
- [5] Qureshi K K, Tam H Y, Chung W H and Wai P K 2005 *IEEE Photon. Technol. Lett.* **17** 1611–3
- [6] Zhang Z, Kuang Q, Sang M, Ye Z and Nie Y 2010 *Opt. Commun.* **283** 254–7
- [7] Liu X, Yang X, Lu F, Ng J, Zhou X and Lu C 2004 *Opt. Express* **13** 142–7
- [8] Agrawal G P 2001 *Nonlinear Fiber Optics* (New York: Academic Press)
- [9] Inoue K and Toba H 1992 *IEEE Photon. Technol. Lett.* **4** 69–72
- [10] Liu X M 2008 *Phys. Rev. A* **043818**
- [11] Parvizi R, Harun S W, Shahabuddin N S, Yusoff Z and Ahmad H 2010 *Opt. Laser Technol.* **42** 1250–2
- [12] Chen D 2007 *Laser Phys. Lett.* **4** 437–9
- [13] Yamashita S and Inoue Y 2005 *Japan. J. Appl. Phys.* **44** L1080–1
- [14] Liu X, Zhou X, Tang X, Ng J, Hao J, Choi T Y, Leong E and Lu C 2005 *IEEE Photon. Technol. Lett.* **17** 1626–8

APPENDIX B

Selected paper based on the study of nonlinear parameter from this thesis.

Highly Efficient and High Output Power of Erbium Doped Fiber Laser in a Linear Cavity Configuration¹

N. A. Awang^{a, b}, M. Z. Zulkifli^{a, *}, S. F. Norizan^a, S. W. Harun^c, Z. A. Ghani^d, and H. Ahmad^a

^a Photonics Laboratory, Department of Physics, University of Malaya, 50603 Kuala Lumpur, Malaysia

^b Department of Physics, Faculty of Science, Art and Heritage, University Tun Hussein Onn,
86400 Parit Raja, Batu Pahat, Johor, Malaysia

^c Department of Electrical Engineering, Faculty of Engineering, University of Malaya, 50603 Kuala Lumpur, Malaysia

^d Faculty of Applied Sciences, MARA University of Technology, 40450, Shah Alam, Selangor, Malaysia

*e-mail: mohdzamani82@yahoo.com

Received April 9, 2010; in final form, April 23, 2010; published online September 2, 2010

Abstract—A simple Erbium Doped Fiber Laser (EDFL) in linear cavity configuration is reported. The cavity design is based on an FBG as a back reflector, and a loop back optical circulator with an output coupler as the front reflector. Different coupling ratios of the coupler are tested and 50 : 50 provides the highest coupling output power of 22.06 dBm (160.7 mW). The pump power conversion efficiency is about 95% when pumping with two pump lasers at 1460 and 1490 nm with combined pumping power of 545 mW. The laser output has a measured linewidth of 0.0179 nm.

DOI: 10.1134/S1054660X10190011

INTRODUCTION

Erbium Doped Fiber (EDF) has revolutionized optical communication especially as an active medium in an optical amplifier. The development of Erbium Doped Fiber Amplifier (EDFA) has spurred numerous progresses in the area of optical communication. Besides as an amplifier, EDF can be used to generate laser output at 1550 nm. Of late, the interest is in the area of tunable switchable fiber laser [1–6] and also the development of dual-wavelength output that is switchable and can be tuned [7–11]. One of the important applications of this dual wavelength switchable output is in the area of microwave photonics although there are many other applications such as in the area of Wavelength Division Multiplexing (WDM) communication, fiber optic sensors [12] and modern instrumentation. One of the limitations in this system is the power output from fiber laser system which is generally low being in the region of –20 dBm to a few dBm [13–15]. For practical applications in the area of microwave photonics [16], the output power needs to be higher and this can open up new applications. There are recent reports on high power output from EDFL [17, 18] such as that based on the idea of Master Oscillator and Power amplifier (MOPA) [19] which is entirely based on EDF.

A simple approach to generate high output power in a linear cavity with a short length of highly doped EDF is proposed in this report. The design provides an output power of 27.16 dBm (520.1 mW) with pump power conversion efficiency as high as 95%.

EXPERIMENTAL SETUP

The experimental setup for high power output in the region of 26 dBm with high conversion efficiency is shown in Fig. 1. The length of EDF fiber which is highly doped is investigated to determine the optimum length to achieve a high power output. The length is varied from 5 to 15 m in a linear cavity [20, 21]. The fiber has absorption coefficients of 6.33 and 8.01 dB/m at pump wavelengths of 1460 and 1490 nm as measured in this experiment. The signal absorption coefficient at 1530 nm is about 18.06 dB/m (Fibercore Ltd.). The optimum optical length is chosen from an experiment to measure the Amplified Spontaneous Emission (ASE) at different lengths to find the highest ASE output at different pump powers. This setup is shown in Fig. 1a. The measurement of ASE output is taken using ILX Lightwave integrating sphere photo detection system (ILX OMH6727).

Figure 1b provides the second experimental setup which is the cavity design for generating the high optical output power laser at 1550 nm by using Fiber Bragg Grating (FBG) [22]. A FBG is used as the back reflector to reflect back the traveling wave onto itself. The FBG reflectivity wavelengths are varied to find the best wavelengths for reflection and to provide high output power with good conversion efficiency. The wavelengths tested are 1552, 1557, and 1560 nm, with a reflectivity of more than 90%. These wavelengths are chosen due to the ability of the FBG. In this design, the other end of the cavity is cleaved into a single mode fiber which is exposed to the air giving a 4% Fresnel reflection and measured by ILX OMH6727, labeled as Cavity 1.

¹ The article is published in the original.

Experimental setup

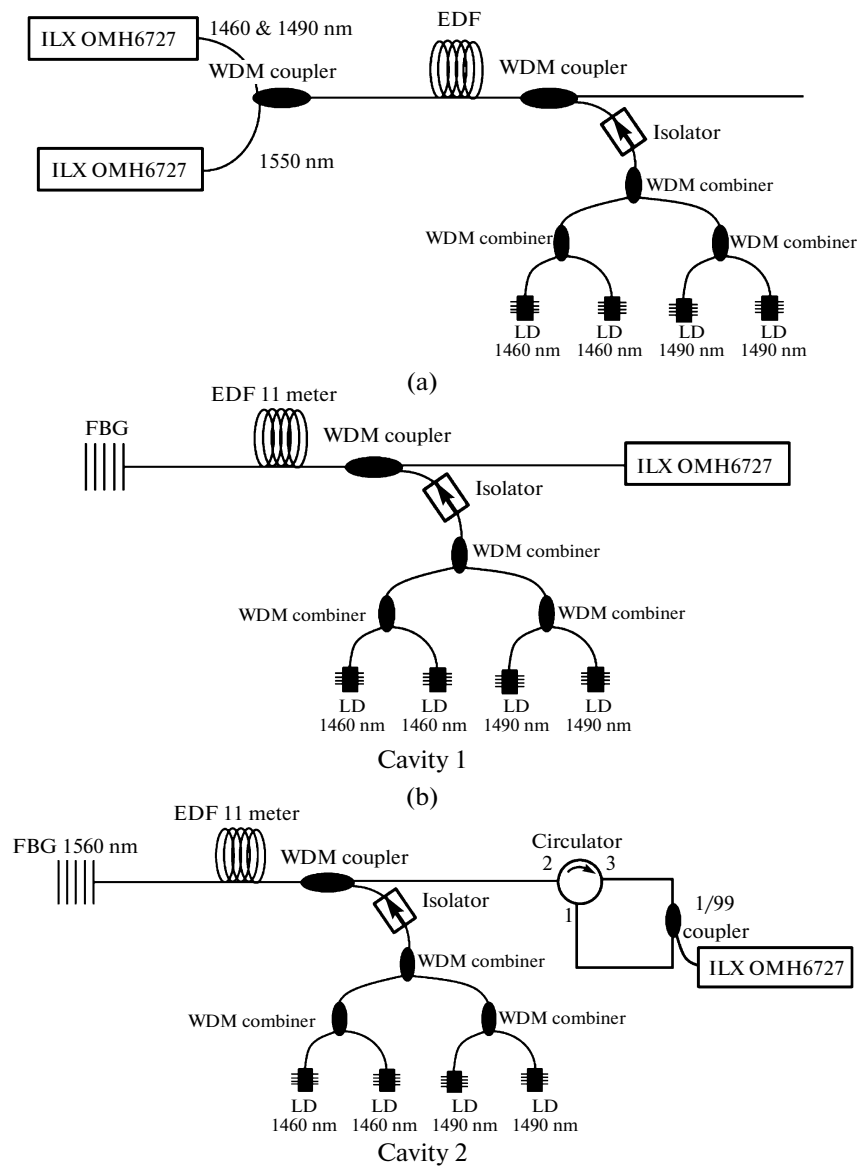


Fig. 1. (a) Experimental setup to measure the ASE output for different fiber lengths at different pump powers. (b) Proposed setup for high power EDFL.

For the third experimental setup which is labeled as Cavity 2, it comprises an optimum EDF length of 11 m, an FBG with 95% reflectivity at 1560 nm at the end, and a 3-port optical circulator at the other end, which is looped back to form the linear cavity. An optical coupler of different coupling ratios such as 1/99, 20/80, 30/70, and 50/50 is inserted between port 3 and port 1 of the optical circulator. The coupler leg with the smallest coupling output is taken as the output which is connected to the power meter. The highly

doped EDF with dopant concentration of 900 ppm is pumped by two laser diodes of pump wavelengths 1460 and 1490 nm, as in Fig. 1a. The ASE output at both ends will be reflected back into the cavity and the FBG provides the selection of output wavelength for the fiber laser. The output power of the fiber laser is detected by using a high powered photodetector via a fused coupler. This experimental setup is designed to measure the high power output from a highly doped EDF and also the conversion efficiency.

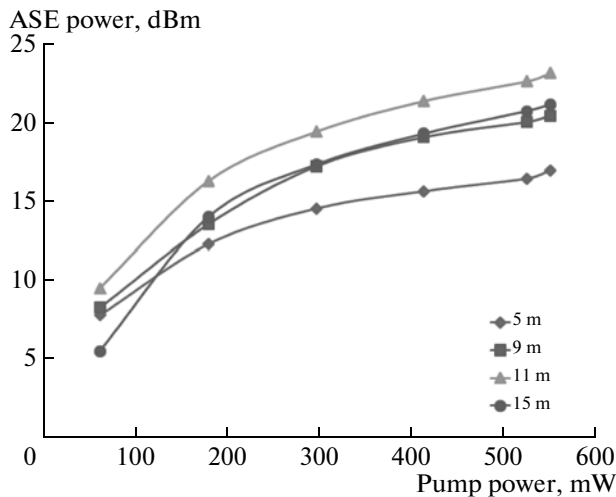


Fig. 2. The ASE powers with different pump powers.

RESULTS AND DISCUSSION

The experimental results on the ASE output power at different lengths of EDF is shown in Fig. 2. The lengths of EDF are changed to find the best length than can give maximum ASE output with combined pump power of 545 mW. The ASE is a maximum for EDF length of 11 m. For a length of 15 m the ASE output drops to 21 dBm. The ASE output characteristics are measured by varying the pump power from 100 to 550 mW. For shorter lengths of the fiber such as 5 and 9 m, the measured ASEs are 16 and 20 dBm, respectively. The lower ASE is primarily due to the lower number of the Er^{3+} ions available to absorb the excess pump power. A wavelength division demultiplexer fused coupler is placed at the output end to measure

the excess pump power. From these measurements, 11 m of EDF is the optimum length for pump power of 550 mW.

In Fig. 3, the output powers of a simple cavity using an FBG as a reflector at three different wavelengths (Cavity 1), 1552, 1557, and 1560 nm, are shown with reflectivity of 95%. The other end is an exposed single mode fiber giving a 4% Fresnel reflection. These measurements are performed to find the wavelength, among these three FBGs, that gives the highest output power. As from the results, there is only a marginal difference of the output power at these three wavelengths, with 1560 nm giving a slightly better output power when compared to the others. The measured output powers are 25.0 dBm (316.2 mW), 25.8 dBm (380 mW), and 26.1 dBm (407.4 mW) for 1552, 1557, and 1560 nm, respectively.

The Pump Power Conversion Efficiency (PCE) of these three FBG wavelengths for the 1460 and 1490 nm pump power is shown in Fig. 4. From the results, the PCE for 1560 nm is the best among these three wavelengths that were investigated, giving a value of 73.5% for combined pump power of 545 mW. The output power of the EDFL in a linear configuration is shown in Fig. 5 for two cases; one with a 4% output end (Cavity 1), and the other is connected to 1550 nm 3-port optical circulator that loop back the signal into the cavity (Cavity 2). For the case of Cavity 2, a 1/99 fused coupler is used to extract the output power with the 1% leg connected to the power meter. The measured output powers are 26.7 and 27.16 dBm for the 4% reflector (Fresnel reflection) and Cavity 2, respectively. As a point to note, in the case of Cavity 2, the output power is measured based on the optical circulating power in the linear cavity.

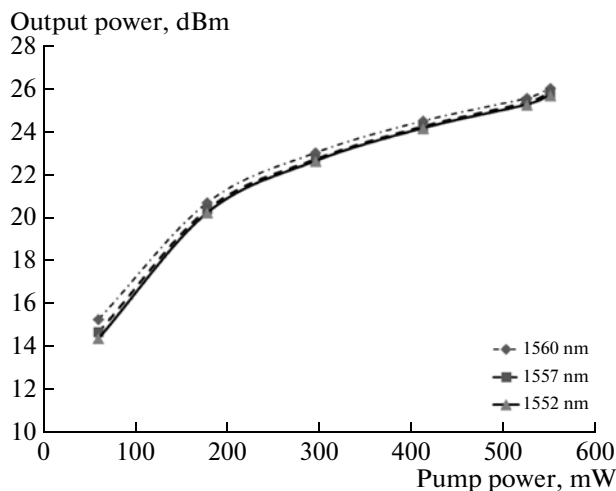


Fig. 3. Output powers for wavelengths of 1552, 1557, and 1560 nm with different pump powers.

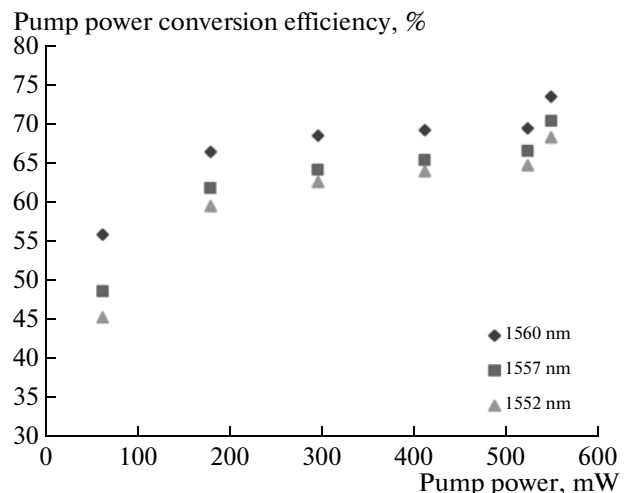


Fig. 4. PCE for wavelengths of 1552, 1557, and 1560 nm with different pump powers.

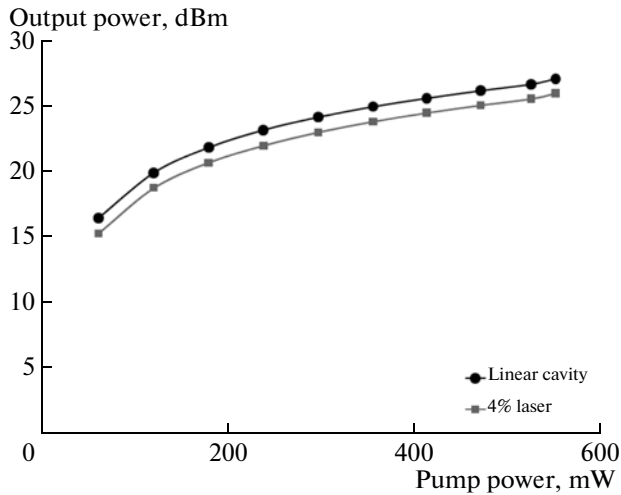


Fig. 5. The output powers of the different pump powers.

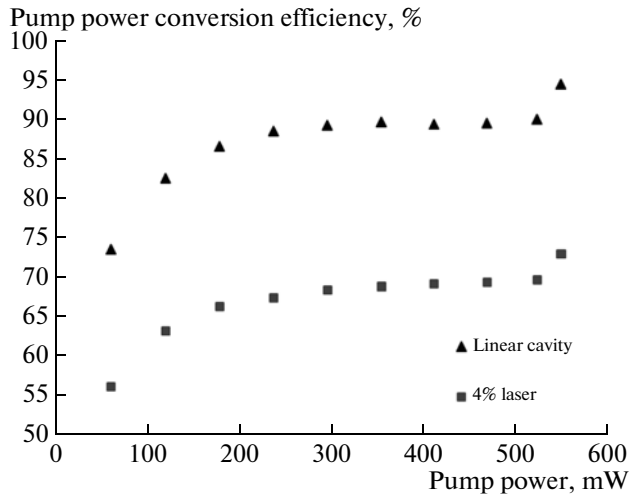


Fig. 6. PCE of linear cavity laser and 4% laser at different pump powers.

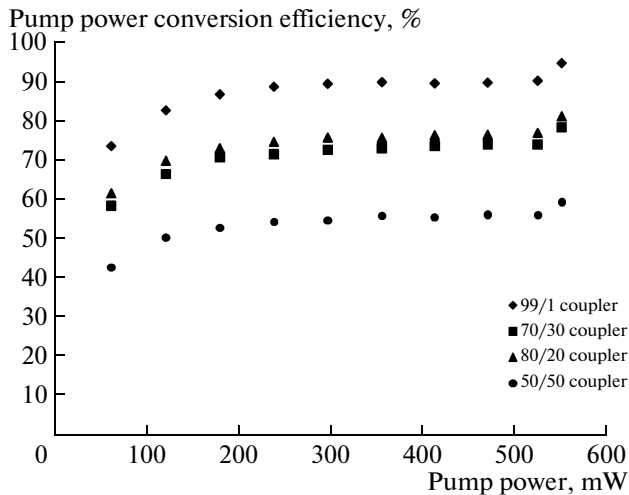


Fig. 7. PCE of different coupling ratio pump powers.

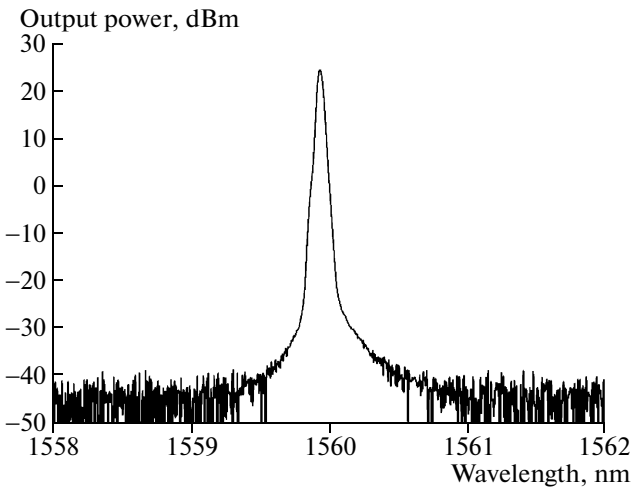


Fig. 8. The output spectrum of 1560 nm wavelength.

The conversion efficiency of the system is depicted in Fig. 6. This was done for the two cavity designs, and Cavity 2 gives higher conversion efficiency with a value of 90% for pump power of between 200 and 450 mW and 95% for pump power of 545 mW. These results are taken with 1/99 fused coupler and the calculated values are the oscillating powers in the cavity. The PCE for Cavity 2 is 25% higher than that of Cavity 1. The maximum PCE is 95% for Cavity 2, and 75% for Cavity 1.

In Fig. 7, the performance of Cavity 2 is shown for different coupling ratios. The pump conversion efficiency is calculated based on the internal circulating power of the linear cavity. From the above figure, the 1/99 gives the best power conversion efficiency, and the 50/50 gives the highest output power measured

directly from the output leg of the fused coupler which is 22.06 dBm (160.7 mW). Similarly, the output power leg of 1/99, 20/80, and 30/70 are 7.16 dBm (5.2 mW), 20.7 dBm (117.5 mW), and 21.1 dBm (128.8 mW), respectively.

The output power spectrum of the laser is shown in Fig. 8 at 1560 nm with a linewidth of 0.0179 nm. As in the spectrum, the laser emission has a sharp and clean profile which can be further processed to generate a high power dual wavelength output for terahertz applications.

CONCLUSIONS

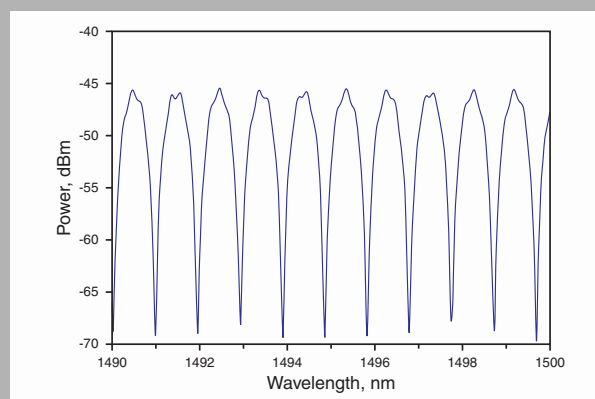
Generally, many of the reported output powers from an EDFL are in the range of -10 dBm to a few

dBm [17, 19, 23]. This research paper reports a relatively high output power in the range of 27.16 dBm (520.1 mW) with pump power conversion efficiency of about 95%. This value is taken for an EDF length of 11 m. Optimization of the linear cavity is done for different output coupling ratios and the one with 50 : 50 provides the best coupling output power with output power of 22.06 dBm (160.7 mW). The spectral output of the laser emission at 1560 nm has a linewidth of 0.0179 nm and trace shows a smooth output with little background noise.

REFERENCES

1. W. G. Chen, S. Q. Lou, S. C. Feng, L. W. Wang, H. L. Li, T. Y. Guo, and S. S. Jian, *Laser Phys.* **19**, 2115 (2009).
2. A. González-García, O. Pottiez, R. Grajales-Coutiño, B. Ibarra-Escamilla, and E. A. Kuzin, *Laser Phys.* **20**, 720 (2010).
3. A. P. Luo, Z. C. Luo, and W. C. Xu, *Laser Phys. Lett.* **6**, 598 (2009).
4. H. Ahmad, M. Z. Zulkifli, K. Thambiratnam, A. A. Latif, and S. W. Harun, *Laser Phys. Lett.* **6**, 539 (2009).
5. M. Z. Zulkifli, N. Tamchek, A. A. Latif, S. W. Harun, and H. Ahmad, *Opt. Commun.* **282**, 2576 (2009).
6. Q. Mao and J. W. Y. Lit, *IEEE Photon. Tech. Lett.* **14**, 612 (2002).
7. D. Liu, N. Q. Ngo, X. Y. Dong, S. C. Tjin, and P. Shum, *Appl. Phys. B: Lasers Opt.* **81**, 807 (2005).
8. X. Liu, X. Yang, F. Lu, J. Ng, X. Zhou, and C. Lu, *Opt. Express* **13**, 142 (2005).
9. H. Ahmad, M. Z. Zulkifli, A. A. Latif, and S. W. Harun, *Opt. Commun.* **282**, 4771 (2009).
10. S. Feng, O. Xua, S. Lu, X. Mao, T. Ning, and S. Jian, *Opt. Laser Technol.* **41**, 264 (2009).
11. H. Ahmad, M. Z. Zulkifli, A. A. Latif, K. Thambiratnam, and S. W. Harun, *J. Mod. Opt.* **56**, 1768 (2009).
12. Z. H. Fu, Y. X. Wang, D. Z. Yang, and Y. H. Shen, *Laser Phys. Lett.* **6**, 594 (2009).
13. T. Kashiwada, M. Shigematsu, T. Kougo, H. Kanamori, and M. Nishimura, *IEEE Photon. Technol. Lett.* **3**, 721 (1991).
14. J. F. Massicott, R. Wyatt, B. J. Ainslie, and S. P. Craig-Ryan, *Electron. Lett.* **26**, 1038 (1990).
15. J. C. Livas, S. R. Chinn, E. S. Kintzer, and D. J. DiGiovanni, in *Proc. of the Conf. on Lasers and Electro Opt.* **15** (1995).
16. D. Chen, H. Fu, and S. He, *Laser Phys. Lett.* **4**, 597 (2007).
17. Y. Tashiro, H. Tachibana, A. Fujisaki, and H. Ogoshi, *Opt. Fiber Commun. (OFC'97) Technical Digest* (1997), pp. 107–108.
18. S. W. Harun, M. R. A. Moghaddam, K. Dimyati, and H. Ahmad, *Laser Phys. Lett.* **6**, 458 (2009).
19. Y. J. Chiang, C. S. Hsiao, and Likarn Wang, *Opt. Commun.* **283**, 1055 (2010).
20. M. Zhang, L. L. Chen, C. Zhou, Y. Cai, L. Ren, and Z. G. Zhang, *Laser Phys. Lett.* **6**, 657 (2009).
21. D. F. Liu and C. H. Wang, *Laser Phys. Lett.* **7**, 153 (2010).
22. M. R. A. Moghaddam, S. W. Harun, M. R. Tamjis, and H. Ahmad, *Laser Phys. Lett.* **6**, 586 (2009).
23. X. Dong, H. Tarn, B. Guan, C. Zhao, and X. Dong, *Opt. Commun.* **224**, 295 (2003).

Abstract: A simple design of multi-wavelength generation in the S-band region of the optical network transmission is proposed. The design consists of broad-band fiber Bragg grating (BB-FBG), which acts as a filter to enhance operation in the S-band region. A Sagnac loop mirror (SLM) is used to generate multiple wavelength oscillations in the ring cavity. The output consists of 60 lasing wavelengths oscillating simultaneously between 1464 nm and 1521 nm with a spacing of 0.92 nm and an output linewidth of 0.66 nm.



The wider span of the multi-wavelength laser spectrum

© 2010 by Astro Ltd.

Published exclusively by WILEY-VCH Verlag GmbH & Co. KGaA

Multi-wavelength fiber laser in the S-band region using a Sagnac loop mirror as a comb generator in an SOA gain medium

M.Z. Zulkifli,¹ N.A. Hassan,¹ N.A. Awang,¹ Z.A. Ghani,² S.W. Harun,³ and H. Ahmad^{1,*}

¹ Photonics Laboratory, Department of Physics, University of Malaya, 50603 Kuala Lumpur, Malaysia

² Faculty of Applied Sciences, MARA University of Technology, 40450 Shah Alam, Selangor, Malaysia

³ Department of Electrical Engineering, Faculty of Engineering, University of Malaya, 50603 Kuala Lumpur, Malaysia

Received: 5 May 2010, Revised: 10 May 2010, Accepted: 13 May 2010

Published online: 30 June 2010

Key words: fiber laser; Sagnac loop mirror; semiconductor optical amplifier

1. Introduction

Multi-wavelength fiber lasers (MFL) have made tremendous advances in the last 10 years. The advantages of fiber lasers are primarily due to their simple structure, ease of operation, low cost and minimal insertion loss. The interest in multi-wavelength fiber laser is in its application as a laser source in a dense wavelength division multiplexing network (DWDM), a source for optical fiber sensors, optical instrument testing, spectroscopy and others [1–4]. In the DWDM network, as a result of increased traffic, there is a need to extend the transmission bands from C- to L-bands and lately towards the S-band. There have been earlier reports of multi-wavelength investigation in

erbium doped fiber (EDF) [5]. Due to the homogeneous gain in EDF, multi-wavelength operation can be difficult to achieve. Many techniques have been put forward to overcome this problem, including as cooling of the fiber, using a phase modulator and an in-line comb filter, frequency shifted feedback, photonics crystal fiber and by controlling the cavity loss [6–18].

As an alternative to EDF, semiconductor optical amplifier (SOA) provides an interesting alternative approach whereby due to its inhomogeneous gain profile, multiple oscillating wavelengths can be generated. Earlier works on SOA focused on the generation of multi-wavelength in the C- and L-bands using Fabry-Perot filter in the cav-

* Corresponding author: e-mail: harith@um.edu.my

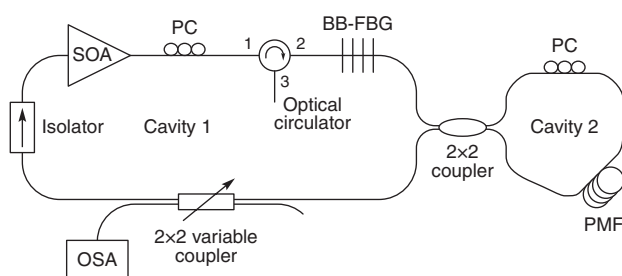


Figure 1 The experimental setup for flat output S band multi-wavelength fiber laser

ity as the comb generator [18–20]. Another approach is to use a Lyot filter to generate multiple outputs in a standing wave cavity [21] and in-fiber Mach-Zehnder interferometer incorporated into the ring cavity serving as wavelength-selective filter [22]. The problem with these devices is the peak to peak output variation which can be very large, exceeding 3 dB. A recent work in this area [23–27] uses a fiber based Sagnac loop mirror (SLM) to generate about 17 lasing lines with interchannel spacing of 100 GHz (0.8 nm) in 1550 nm band (C-band). The peak amplitude has a peak power variation of about 3 dB. As it stands, there are no reports of multiple wavelength output in the S-band region, which will be useful for current and future needs.

In this paper, a simple design based on two ring cavities is proposed and the multiple wavelength generation is based on SLM. The gain medium used is a wide band SOA that covers an amplification bandwidth that stretches from 1400 nm to 1600 nm. The emitted multiple wavelength output covers the S-band region of 1480 nm to 1520 nm.

2. Experimental setup

The experimental setup for generating multi-wavelengths output in the S-band region is shown in Fig. 1. It consists of two ring cavities joined together with a 2×2 fused coupler. The main cavity consists of SOA from Alphion, a polarization controller 1 (PC1), a broadband fiber Bragg grating (BB-FBG), an isolator, a 3 port optical circulator and a variable 2×2 fused coupler. The first ring, ring 1, is closed by connecting the 2×2 fused coupler using the two input legs. Ring 2 consists of another polarization controller (PC2), a short length of 5 m of polarization maintaining fiber (PMF) and the ring is closed by connecting the output legs (3 and 4) of the 2×2 fused coupler having a wideband transmission from 1450 nm to 1600 nm. The SOA in ring 1, which is driven at 450 mA provides the gain medium, which also emits an amplified spontaneous emission (ASE) that ranges from 1400 nm to 1600 nm. The output is fed into port 1 of the optical circulator which is then emitted at port 2 and travels to the BB-FBG which has 90% reflectivity, for wavelengths ranging from 1530 nm

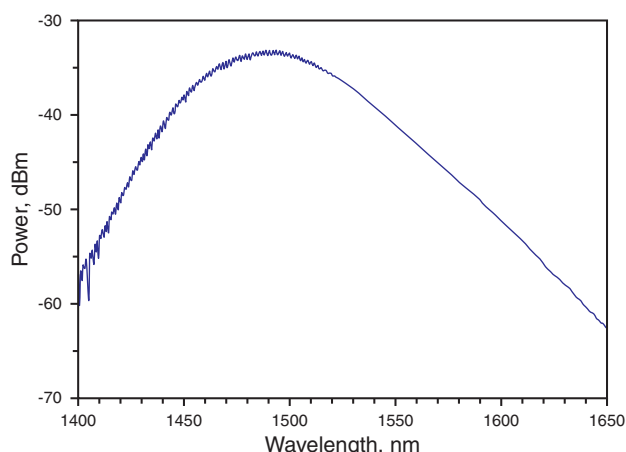


Figure 2 (online color at www.lphys.org) The ASE spectrum of wideband SOA

to 1560 nm (C-band). This reflected light in the C-band region will then be emitted at port 3 of the optical circulator which is removed from oscillating in the ring cavity. The transmitted signal, which will be largely in the S-band region will then travel to port 1 of 2×2 fused coupler into ring 2, which splits into two equal portions traveling in opposite directions. One of the ports is connected to the 5 m PMF and another one is connected to the PC2. The birefringence of the PMF generates a wavelength-dependent phase difference between the fast and slow components of the light waves propagating in the fiber loop. This condition is achieved by adjusting the PC2 in the loop so that the two counter-propagating light waves travel along different axes of the PM fiber. The other port of PC2 is connected back to the 2×2 coupler to complete the circle of SLM.

The two will recombine at the fused coupler and will travel back into ring 1 towards the 2×2 variable coupler with one of the output legs connected to an optical spectrum analyzer (OSA) (Yokogawa AQ6370B) with a resolution of 0.02 nm. The other leg is connected to the optical isolator to force the signal to propagate in the clockwise direction. The SOA provides the necessary amplification for the multi-wavelengths output generated by the SLM. A variable coupler provides the necessary coupling ratio for optimum operation.

3. Results and discussion

The output ASE spectrum of the SOA is shown in Fig. 2, which has an ultra-wide gain bandwidth that is based on quantum dot technology. The output spans from 1400 nm to 1650 nm, taking the case for emission output power above −60 dBm. In fact the output spectrum covers the S-, C-, and L-bands region of an optical network. It will be of interest to generate multi-wavelength output in the S-band, since the C- and L-bands are already well studied.

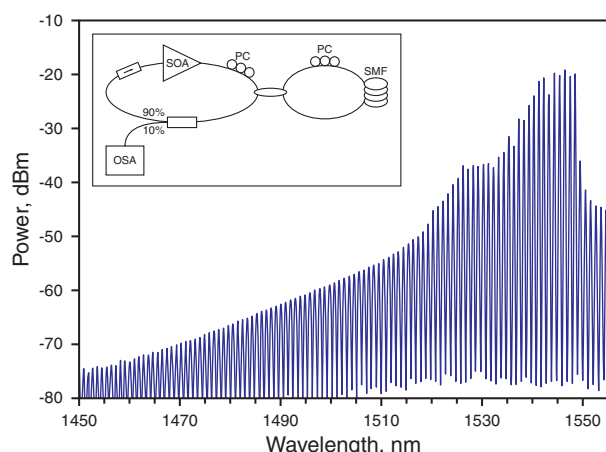


Figure 3 (online color at www.lphys.org) The spectrum of multi-wavelength fiber laser without BB-FBG

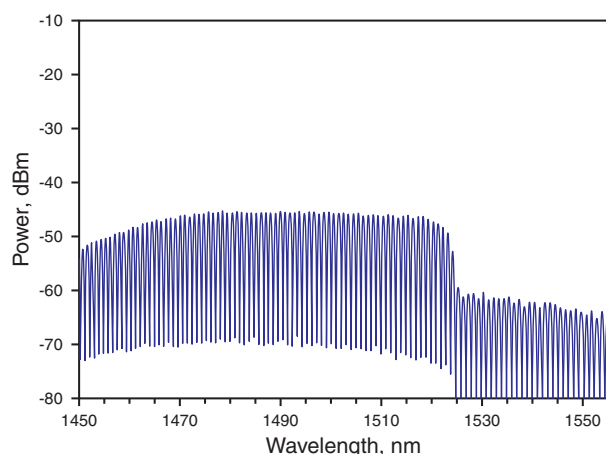


Figure 4 (online color at www.lphys.org) The spectrum for S-band multi-wavelength fiber laser with BB-FBG

In Fig. 3, the multi-wavelength output spectrum of the ring fiber laser without the BB-FBG is shown. It ranges from 1450 nm to 1600 nm with a peak occurring in the region of 1540 nm. Strong lasing action in this region deprives the available energy for amplification of signal output of the S-band. The measured output power is about -20 dBm for output in the region of 1540 nm to 1550 nm. From experiment, the output spectrum is unstable and fluctuates from peak to peak.

By having the BB-FBG in ring cavity 1, the output spectrum is more stable with dominant output in the S-band as in Fig. 4. From the figure, the peak to peak variations are minimal and show a certain flatness in the output. The BB-FBG filters out the oscillations in the C-band providing the necessary gain in the S-band region. The average peak to peak power is about -48 dBm, which is 20 dB

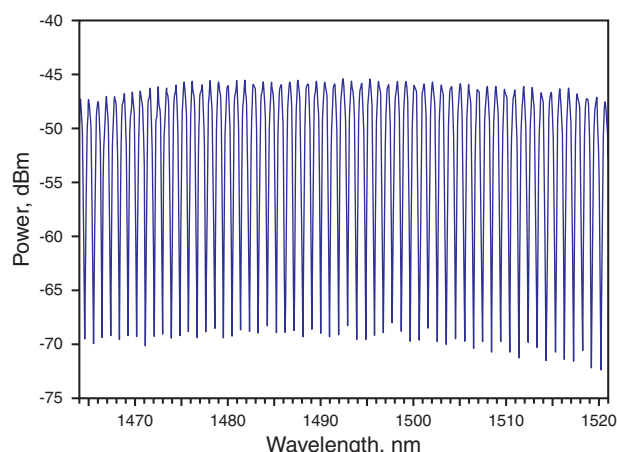


Figure 5 (online color at www.lphys.org) The flat output spectrum of 60 wavelength channels

higher than that without the BB-FBG. The output spectrum is stable and provides repeatable output over long operating hours. The peak power flatness and the optical signal to noise ratio (OSNR) improve considerably for wavelength regions stretching from 1450 nm to 1520 nm. The OSNR increases from about 10 dB and 20 dB for the case without and with BB-FBG, respectively. Although there are still some oscillations within the C-band as a result of the BB-FBG reflectivity of only 90%, this portion can be readily removed using a S/C demux fused coupler.

As a point to note, the coupling ratio of the variable coupler plays a crucial role in obtaining the best result for the multi-wavelength laser output. By optimizing the coupling ratio to 90/10 with 10% on the useful output, the output power can be maximized to generate a stable and flat output as shown in Fig. 5. The figure shows about 60 different lasing wavelengths that can be achieved from 1464 nm to 1521 nm with a spacing of 0.92 nm between them. The measured spacing is similar to the calculated spacing using the equation

$$\Delta\lambda = \frac{\lambda^2}{BL},$$

where λ is the operation wavelength, B is the modal birefringence of PMF fiber, which is 4.9×10^{-4} , and L is the length of the PMF fiber. The measured peak-to-peak variation, which is from the maximum peak to the minimum peak, is less than 3 dB.

Fig. 6 shows the spectrum on an expanded scan providing a measured linewidth of 0.66 nm at full width and half-maximum (FWHM). The stability and performance behavior tests of the output spectrum are performed over a period of 1 hour as shown in Fig. 7 to indicate long term stability with 10 minutes interval time. A stable operation is observed over long periods when the system is left to operate for 24 hours. This measurement provides the important indication that the proposed design is very stable over long

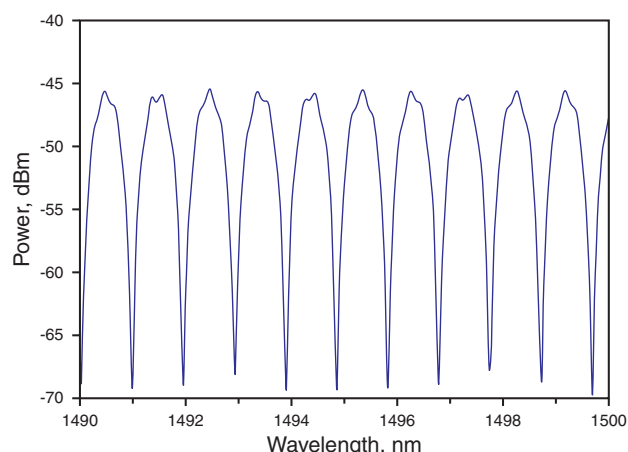


Figure 6 (online color at www.lphys.org) The wider span of the multi-wavelength laser spectrum

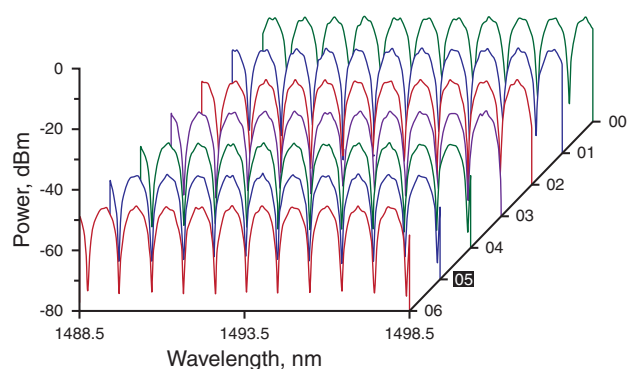


Figure 7 (online color at www.lphys.org) Stability performance of the MFL during 1-hour duration test

periods which is an important criterion for laser source in the dense wavelength division multiplexing (DWDM) optical system.

4. Conclusion

The proposed design provides a stable MFL output in the S-band region for application in a DWDM network system. The wavelength ranges from 1450 nm to 1520 nm. The output is flat with peak power variation of less than 3 dB. The laser operates better with stable output power by having a BB-FBG in the ring cavity. The OSNR increases from about 10 dB to 20 dB by having the BB-FBG, and the outputs are stable over many hours of operation with an average peak power of about -48 dBm. In the proposed design, about 60 different lasing wavelengths can be achieved from 1464 nm to 1521 nm with a spacing of 0.92 nm between them and linewidth of 0.66 nm.

References

- [1] S. Yamashita and T. Baba, *Electron. Lett.* **37**, 1015–1017 (2001).
- [2] D.N. Wang, F.W. Tong, X.H. Fang, W. Jin, P.K.A. Wai, and J.M. Gong, *Opt. Commun.* **228**, 295–301 (2003).
- [3] C.-S. Kim and J.U. Kang, *Appl. Opt.* **43**, 3151–3157 (2004).
- [4] Y.-G. Han, C.-S. Kim, J.U. Kang, U.-C. Paek, and Y. Chung, *IEEE Photon. Technol. Lett.* **15**, 383–385 (2003).
- [5] N. Park and P.F. Wysocki, *IEEE Photon. Technol. Lett.* **8**, 1459–1461 (1996).
- [6] Y.-G. Han, G. Kim, J.H. Lee, S.H. Kim, and S.B. Lee, *IEEE Photon. Technol. Lett.* **17**, 989–991 (2005).
- [7] H. Ahmad, M.Z. Zulkifli, A.A. Latif, and S.W. Harun, *Opt. Commun.* **282**, 4771–4775 (2009).
- [8] M.R. Shirazi, N.S. Shahabuddin, S.N. Aziz, K. Thambirathan, S.W. Harun, and H. Ahmad, *Laser Phys. Lett.* **5**, 361–363 (2008).
- [9] S.W. Harun, M.R. Shirazi, and H. Ahmad, *Laser Phys. Lett.* **4**, 678–680 (2007).
- [10] S.W. Harun, M.R. Shirazi, and H. Ahmad, *Laser Phys. Lett.* **5**, 48–50 (2008).
- [11] H. Ahmad, A.H. Sulaiman, S. Shahi, and S.W. Harun, *Laser Phys.* **19**, 1002–1005 (2009).
- [12] S.W. Harun, R. Parvizi, S. Shahi, and H. Ahmad, *Laser Phys. Lett.* **6**, 813–815 (2009).
- [13] H. Ahmad, S.F. Norizan, M.Z. Zulkifli, and S.W. Harun, *Fiber Integr. Opt.* **28**, 430–439 (2009).
- [14] S. Shahi, S.W. Harun, and H. Ahmad, *Laser Phys. Lett.* **6**, 737–739 (2009).
- [15] M.R.A. Moghaddam, S.W. Harun, M.C. Paul, M. Pal, A. Dhar, R. Sen, S. Das, S.K. Bhadra, and H. Ahmad, *Microwave Opt. Technol. Lett.* **51**, 2511–2512 (2009).
- [16] Z.C. Luo, A.P. Luo, and W.C. Xu, *Laser Phys.* **19**, 2120–2123 (2009).
- [17] M.N. Mohd Nasir, Z. Yusoff, M.H. Al-Mansoori, H.A. Abdul Rashid, and P.K. Choudhury, *Laser Phys.* **19**, 2027–2030 (2009).
- [18] N. Pleros, C. Bintjas, M. Kalyvas, G. Theophilopoulos, K. Yiannopoulos, S. Sygletos, and H. Avramopoulos, *IEEE Photon. Technol. Lett.* **14**, 693–695 (2002).
- [19] S.W. Harun and H. Ahmad, *Jpn. J. Appl. Phys.* **41**, L1234–L1236 (2002).
- [20] H. Ahmad, N.S. Shahabuddin, and S.W. Harun, *Optoelectron. Adv. Mater. Rapid Commun.* **3**, 1–3 (2009).
- [21] N. Pleros, T. Houbavlis, G. Theophilopoulos, K. Vlachos, C. Bintjas, and H. Avramopoulos, *Fiber Integr. Opt.* **23**, 263–274 (2004).
- [22] W.G. Chen, S.Q. Lou, S.C. Feng, L.W. Wang, H.L. Li, T.Y. Guo, and S.S. Jian, *Laser Phys.* **19**, 2115–2119 (2009).
- [23] D. Liu, N.Q. Ngo, H. Liu, and D. Liu, *Opt. Commun.* **282**, 1598–1601 (2009).
- [24] L. Zhan, J.H. Ji, J. Xia, S.Y. Luo, and Y.X. Xia, *Opt. Express* **14**, 10233–10238 (2006).
- [25] K.S. Lim, C.H. Pua, N.A. Awang, S.W. Harun, and H. Ahmad, *Prog. Electromagnet. Res. C* **9**, 101–108 (2009).
- [26] D.S. Moon, B.H. Kim, A.X. Lin, G.Y. Sun, W.-T. Han, Y.-G. Han, and Y.J. Chung, *Opt. Express* **15**, 8371–8376 (2007).
- [27] X.W. Shu, S. Jiang, and D.X. Huang, *IEEE Photonics Technol. Lett.* **12**, 980–982 (2000).



All fiber passively mode locked zirconium-based erbium-doped fiber laser

H. Ahmad^{a,*}, N.A. Awang^{a,b}, M.C. Paul^c, M. Pal^c, A.A. Latif^a, S.W. Harun^d

^a Photonics Laboratory, Department of Physics, University of Malaya, 50603 Kuala Lumpur, Malaysia

^b Faculty of Science, Technology and Human Development, Universiti Tun Hussein Onn Malaysia, Batu Pahat, 86400 Johor, Malaysia

^c Fiber Optics and Photonics Division, Central Glass & Ceramic Research Institute—CSIR, 700 032 Kolkata, India

^d Department of Electrical Engineering, Faculty of Engineering, University of Malaya, 50603 Kuala Lumpur Malaysia

ARTICLE INFO

Article history:

Received 27 June 2011

Received in revised form

28 July 2011

Accepted 23 August 2011

Available online 5 October 2011

Keywords:

Zirconium-erbium doped fiber laser

Mode-locking

Non-Linear Polarization Rotation technique

ABSTRACT

All passively mode locked erbium-doped fiber laser with a zirconium host is demonstrated. The fiber laser utilizes the Non-Linear Polarization Rotation (NPR) technique with an inexpensive fiber-based Polarization Beam Splitter (PBS) as the mode-locking element. A 2 m crystalline Zirconia–Yttria–Alumino-silicate fiber doped with erbium ions (Zr–Y–Al-EDF) acts as the gain medium and generates an Amplified Spontaneous Emission (ASE) spectrum from 1500 nm to 1650 nm. The generated mode-locked pulses have a spectrum ranging from 1548 nm to more than 1605 nm, as well as a 3-dB bandwidth of 12 nm. The mode-locked pulse train has an average output power level of 17 mW with a calculated peak power of 1.24 kW and energy per pulse of approximately 730 pJ. The spectrum also exhibits a Signal-to-Noise Ratio (SNR) of 50 dB as well as a repetition rate of 23.2 MHz. The system is very stable and shows little power fluctuation, in addition to being repeatable.

© 2011 Elsevier Ltd. All rights reserved.

1. Introduction

Mode-locked fiber lasers have recently garnered increasing focus as an effective approach towards the generation of ultra-short pulses and multi-wavelength outputs for optical communications systems [1–5]. Passively mode-locked fiber lasers are of particular interest as they are able to produce highly stable pulses with sub-picosecond durations while at the same time maintaining cost effectiveness. Furthermore, mode-locked fiber lasers are robust and have a good beam quality as well as efficient heat distribution. They are also highly reliable, while at the same time maintaining a significantly smaller footprint as compared to bulkier conventional solid-state systems. These characteristics give mode-locked fiber lasers significant potential for use in various commercial applications, such as materials processing, super-continuum generation, optical frequency metrology, and biomedical applications.

Various techniques have been explored for generating passively mode-locked fiber lasers, such as the use of semiconductor saturable absorbers [6], nonlinear optical loop mirrors [7], nonlinear amplified loop mirrors [8], and the Nonlinear Polarization Rotation (NPR) technique [9,10]. Of these, the NPR technique can be conveniently implemented as it is a passive technique and does not require external modulation. The underlying principle of the NPR technique is the non-linear change that occurs in the

polarization state of an intense optical pulse as it propagates through a non-polarization maintaining fiber. The physical cause of these effects is related to self-phase and cross-phase modulation, and to some extent the uncontrolled birefringence in the fiber. It has a similar behavior to that of a saturable absorber, giving an intensity dependent loss. Typically, in the NPR technique, a Polarization Dependent Isolator (PDI) is sandwiched between two fiber based Polarization Controllers (PCs).

In this paper, a novel method of employing the NPR technique using an inexpensive Polarization Beam Splitter (PBS) is proposed, in conjunction with the use of a new type of erbium-doped fiber to generate mode-locked pulses. The fiber used is a ternary glass host, Zirconia–Yttria–Aluminum codoped in erbium silica fiber (Zr–Y–Al-EDF) giving an opportunity for extremely low waveguide losses as well as a wider gain bandwidth spectrum [11,12]. This paper is the first report of mode-locked behavior in this particular type of fiber.

2. Experimental setup

Fig. 1 shows the experimental setup for the generation of all passively mode-locked Zr-EDF fiber laser based on the NPR technique, which is typically implemented using a PDI sandwiched in between two fiber based PCs. The approach presented in this paper is a simplified version that uses an inexpensive fiber-based PBS. The active medium here is formed by erbium ions doped in the non-crystalline Zr–Y–Al-EDF [11,12], which is fabricated in a ternary glass host, Zirconia–Yttria–Alumino codoped silica fiber, through the

* Corresponding author. Tel.: +60 3 79677133; fax: +60 3 79674290.
E-mail address: harith@um.edu.my (H. Ahmad).

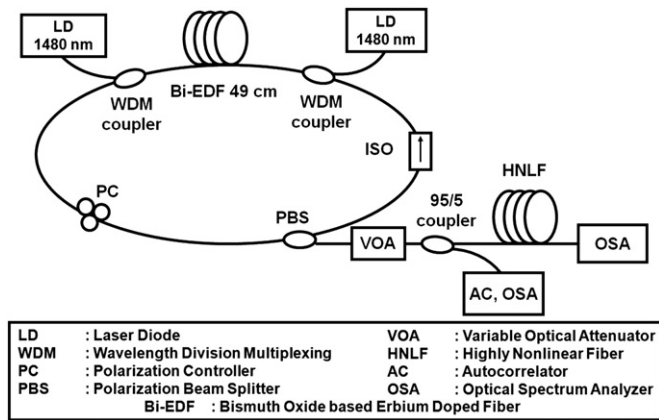


Fig. 1. Schematic diagram for the mode locked Zr-Y-Al-EDF laser.

solution doping technique, along with Modified Chemical Vapor Deposition (MCVD). Zr and Al are added to achieve a high erbium doping concentration of about 3000 ppm in the glass host, without any clustering of the rare-earth ions. Doping of Er_2O_3 into Zirconia–Yttria–Alumina silicate based glass was performed using a solution doping process. Small amounts of Y_2O_3 and P_2O_5 ions serve as the nucleating agents to increase the phase separation leading to the generation of Er_2O_3 ion-doped micro-crystallites in the core matrix of the optical fiber preform, which is then drawn into a fiber in a standard process. The advantage of the Zirconia-based host is that it provides a wide-band characteristic that will be useful for generating ultra-short pulses.

The Zr-Y-Al-EDF of length 2 m, with a pump absorption rate of about 13.5 dB/m at 1480 nm, is then connected to two 1480/1550 nm Wavelength Division Multiplexing (WDM) fiber based couplers. The Zr-Y-Al-EDF is then pumped bi-directionally by two 1480 nm Diode Pump Lasers (LDs) at pump power levels of 154 mW and 152 mW, giving a total pump power of about 300 mW. The 1550 nm output of the WDM coupler, Port 1, is connected to a fiber-based PC, which is then connected to a fiber-based 50:50 PBS, with one of the ports of the PBS (the slow axis) connecting to a polarization insensitive isolator and then connected back to Port 2 of the second WDM coupler so as to close the ring cavity. The second port of the PBS (the fast axis) is connected to the auto-correlator (Alnair) and also to an Optical Spectrum Analyzer (OSA) (Yokogawa AQ6371B). This arrangement allows for operation in the stretched-pulse regime as explained in Ref. [13]. The total length of the cavity is about 5.5 m. In this setup, the PC placed before the PBS acts as the mode-locking element in a similar manner to those reported in Refs. [9,14]. Although the use of a PBS typically implies a 50:50 ratio, other ratios are also possible. In this work, due to the components that were available, a 50:50 ratio PBS has been used. The slow axis is used in this ring configuration, to provide self-starting mode-locking by adjusting the PC and observing the spectrum from the OSA. The underlying principle of the generation of the mode-locked pulses is based on the NPR technique, whereby an intense optical pulse propagating in a non-polarization maintaining optical fiber can experience non-linear changes in the polarization state. The primary cause of these effects is likely to be the self-phase and cross-phase modulation, as well as some uncontrolled birefringence in the fiber. This behavior is similar to that of saturable absorbers.

The inclusion of the optical isolator greatly reduces the back-scatter from various reflecting surfaces and promotes traveling wave oscillation. With a total pump power of 300 mW, the average output power of the mode-locked pulses is about 17 mW. The threshold pump power level for mode-locked

operation was found to be a total of 180 mW. Experimental observation shows that the generated mode-locked pulse train is very stable and the mode-locked laser operates for several hours without breaking up and is also immune to external vibrations. The experimental results are presented in the following Section 3.

3. Results

Fig. 2 shows the measured Amplified Spontaneous Emission (ASE) spectrum obtained from the 2 m long Zr-Y-Al-EDF. The ASE output exhibits a spectrum that stretches from 1500 nm to 1650 nm as compared to the normal ASE spectrum of erbium in a silica fiber, which typically has a spectrum ranging from 1520 nm to 1580 nm. The rather wide-spectrum obtained from the Zr-Y-Al-EDF will assist in generating a much narrower pulse.

Fig. 3 provides the spectrum of the generated mode-locked pulses as obtained from the OSA, taken using the 5 percent port of a 95:5 fused optical fiber coupler. The mode-locked pulses are generated by carefully rotating the three loops of the Lefevre PC so as to initiate mode-locking in the ring cavity. The spectrum obtained spans from 1548 nm to more than 1605 nm, and the 3 dB bandwidth (Full-Width at Half Maximum, FWHM) is about 12 nm. The Signal-to-Noise Ratio (SNR) is approximately 50 dB, with an average output power of 17 mW. The repetition rate

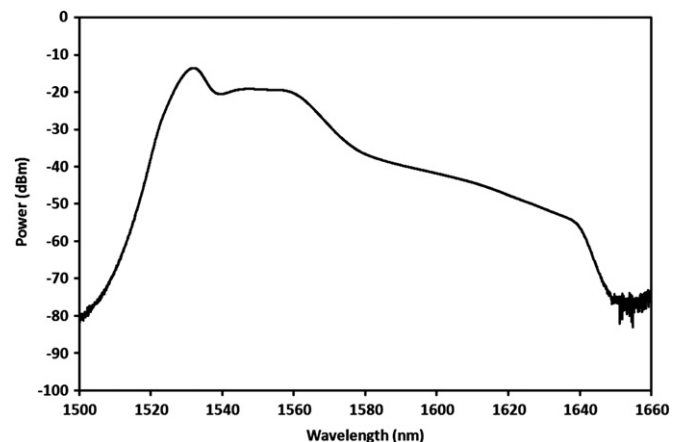


Fig. 2. ASE spectrum of Zr-Y-Al-EDF.

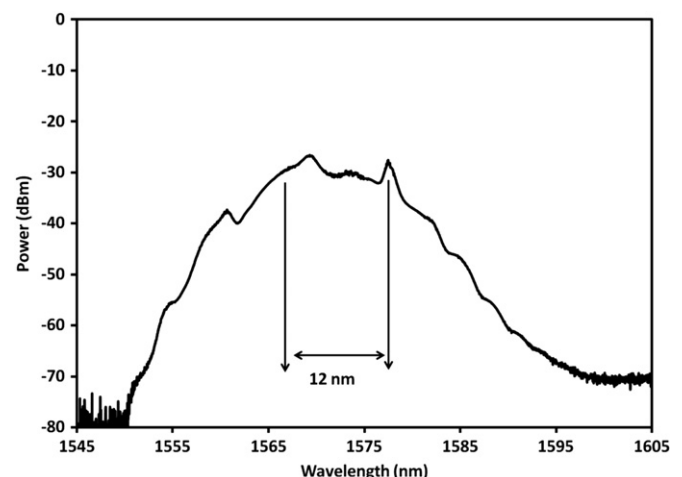


Fig. 3. Optical spectrum of the generated mode-locked pulses from the Zr-Y-Al-EDF.

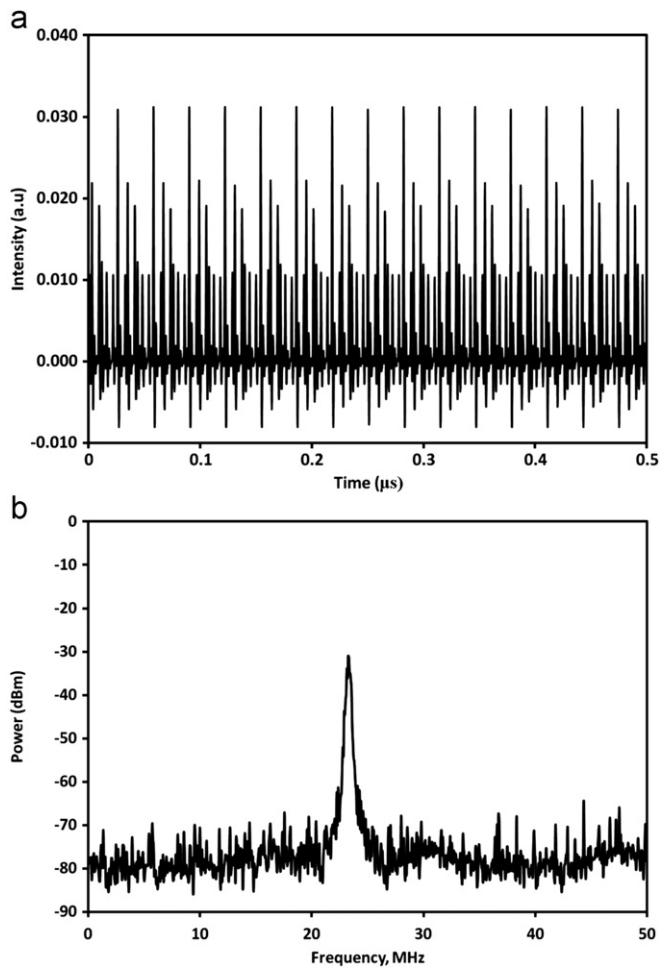


Fig. 4. (a) Sampling oscilloscope traces of the photodetected output laser pulses (b) the RF spectrum of the photodetected output laser pulse train.

measured is 23.2 MHz, with a calculated peak power of 1.24 kW. The spectrum shown in Fig. 3 is continuous over a wavelength range of approximately 1555–1595 nm. The nature of this spectrum implies that the birefringence-induced comb-filtering behavior observed by Luo et al. [15] is not present in our setup. In consequence, our fiber laser is not suitable for wavelength tunability in its present form.

The time trace of the mode locked pulse train is measured using a photodetector with a bandwidth of 6 GHz that is connected to an oscilloscope and also to a Radio Frequency (RF) spectrum analyzer. The measurement is taken at the 5 percent port of the fused coupler, as shown in Fig. 4. Fig. 4(a) shows the trace from a sampling oscilloscope, while Fig. 4(b) gives the RF spectrum of the output laser pulse. The repetition frequency is measured from the top-most peaks of the traces. There are also sidebands or multi-pulses observable in the traces. These sidebands can be removed by a shorter cavity length, which at the same time also increases the pulse repetition rate. Alternatively, if the pulse repetition rate is to be maintained, the sidebands can be reduced by decreasing the pump power to the near threshold value of the mode-locked fiber laser as well as properly optimizing the PC. The occurrence of sidebands is common in passive mode-locking techniques using saturable absorbers. Fig. 4(b) shows the RF spectrum of the output laser pulse and confirms the pulse repetition frequency of around 23.2 MHz.

On top of this, the pulse-width of the mode-locked pulses has been measured using an auto-correlator. The pulse-width depends on the net dispersion of the ring cavity as well as the presence of the fiber placed between the output of the ring-configuration and the

auto-correlator. The ring configuration and the output of this fiber laser consisted of a piece of Zr–Y–Al-EDF (length about 2 m) with negative dispersion and several types of optical fibers (total length 5.48 m) with positive dispersion, D through estimated via modulation instability (MI) using the technique described in Ref. [16] and is determined to be approximately 1.03 ps/nm km at a wavelength of 1566 nm. From this result, the net dispersion will be positive, thereby giving a stretched pulse fiber laser [13]. Mode-locked pulses as short as 0.59 ps (obtained using a hyperbolic secant squared (sech^2) pulse shape) have been generated with proper optimization, as shown in Fig. 5. With a spectral spread of 12 nm, the time-bandwidth product for this pulse length (0.59 ps) is estimated to be approximately 0.9, i.e. significantly larger than its transform limited value and indicates that there is significant chirping. The resolution of the autocorrelator was estimated to be ± 25 fs. The peak power of these mode-locked pulses is about 1.24 kW, giving an energy per pulse of about 730 pJ.

Besides the above measurements, a stability measurement was also taken to provide information on the repeatability of the system and is given in Fig. 6, which indicates the spectrum of the mode-locked pulses, which can be correlated with the pulse

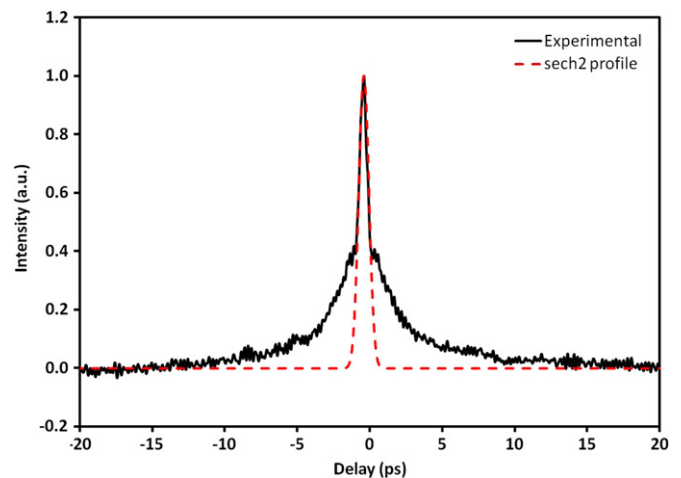


Fig. 5. The spectra of femtosecond pulse trains Zr–Y–Al-EDF mode locking.

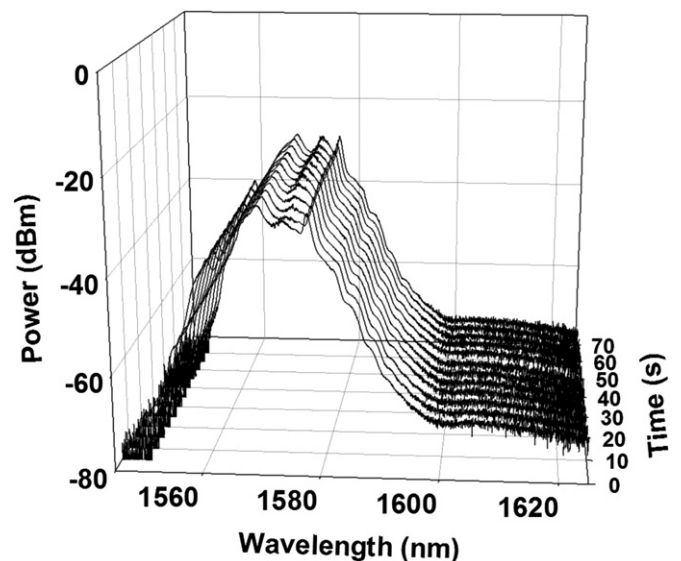


Fig. 6. Output spectra of the proposed Zr–Y–Al-EDF mode-locked fiber laser taken at 5 min intervals over a 1 h period of continuous operation.

width. The measurements were taken every 5 min for a period of 1 h, and from the figure, the trace reproduces itself indicates that the system is very stable, with minimum power fluctuations.

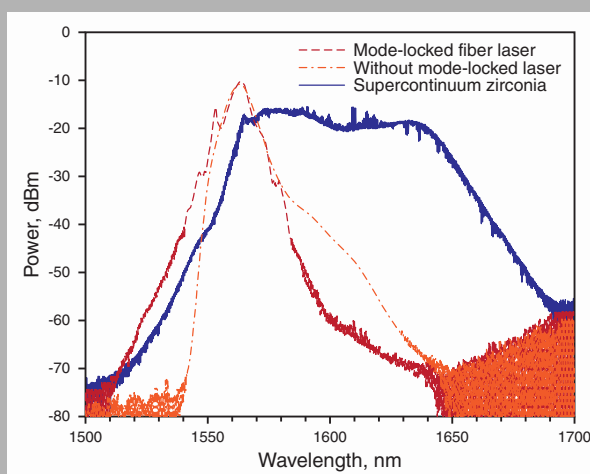
4. Conclusion

In this work, an all-fiber passively mode-locked zirconium-based erbium-doped fiber laser has been proposed and demonstrated. The mode-locked operation is based on the NPR technique, using an inexpensive all-fiber PBS, as well as a 2 m long Zr–Y–Al-EDF pumped at 1480 nm, which acts as the gain medium. The system generates a wide ASE spectrum that ranges from 1500 nm to 1650 nm, which better assists in generating narrower pulses as compared to those obtained from silica based EDFs. The generated mode-locked pulse spectrum spans from 1548 nm to more than 1605 nm, with a 3 dB bandwidth (FWHM) of approximately 12 nm and an SNR of 50 dB. The average output power of the mode-locked pulse train is 17 mW, with a calculated peak power of 1.24 kW and energy per pulse of about 730 pJ, as well as a repetition rate of 23.2 MHz. The system is highly stable and exhibits only minimal power fluctuations.

References

- [1] Tamura K, Doerr CR, Nelson LE, Haus HA, Ippen EP. Technique for obtaining high-energy ultrashort pulses from an additive-pulse mode-locked erbium-doped fiber ring laser. *Optics Letters* 1994;19:46.
- [2] Luo ZC, Luo AP, Xu WC. Tunable and switchable multiwavelength passively mode-locked fiber laser based on SESAM and inline birefringence comb filter. *Photonics Journal, IEEE* 2011;3:64.
- [3] Aia F, Caoa Z, Zhanga X, Zhanga C, Zhanga B, Yu B. Passively mode-locked fiber laser with kilohertz magnitude repetition rate and tunable pulse width. *Journal of Optics and Laser Technology* 2001;43:3.
- [4] Pan S, Zhao X, Yu W, Lou C. Dispersion-tuned multiwavelength actively mode-locked fiber laser using a hybrid gain medium. *Journal of Optics and Laser Technology* 2008;40:854.
- [5] Gong YD, Shum P, Tang DY, Lu C, Guo X, Paulose V, et al. Regimes of operation states in passively mode-locked fiber soliton ring laser. *Journal of Optics and Laser Technology* 2004;36:299.
- [6] DeSouza EA, Soccolich CE, Pleibel W, Stolen RH, Simpson JR, DiGiovanni DJ. Saturable absorber modelocked polarisation maintaining erbium-doped fiber laser. *Electronics Letters* 1993;29:447.
- [7] Richardson DJ, Laming RJ, Payne DN, Phillips MW, Matsas VJ. 320 fs soliton generation with passively mode-locked erbium fibre laser. *Electronics Letters* 1991;27:730.
- [8] Seong NH, Kim DY. Experimental observation of stable bound solitons in a figure-eight fiber laser. *Optics Letters* 2002;27:1321.
- [9] Matsas VJ, Newson TP, Richardson DJ, Payne DN. Selfstarting passively mode-locked fibre ring soliton laser exploiting nonlinear polarisation rotation. *Electronics Letters* 1992;28:1391.
- [10] Wang F, Zhang X-L, Dong J-J, Huang X. A fiber ring laser incorporating dual-mode locking mechanism. *Journal of Optics and Laser Technology* 2009;41:85.
- [11] Paul MC, Harun SW, Huri NAD, Hamzah A, Das S, Pal M, et al. Wideband EDFA based on erbium doped crystalline zirconia yttria aluminium silicate fiber. *Journal of Lightwave Technology* 2010;28:2919.
- [12] Paul MC, Harun SW, Huri NAD, Hamzah A, Das S, Pal M, et al. Performance comparison of Zr-based and bi-based erbium-doped fiber amplifiers. *Optics Letters* 2010;35:2882.
- [13] Haus HA, Tamura K, Nelson LE, Ippen E. Stretched-pulse additive pulse mode-locking in fiber ring lasers: theory and experiment. *IEEE Journal of Quantum Electronics* 1995;31:591.
- [14] Nikodem M, Abramski K. 169 MHz repetition frequency all-fiber passively mode-locked erbium doped fiber laser. *Optics Communications* 2010;283:109.
- [15] Luo Z-C, Luo A-P, Xu W-C, Yin H-S, Liu J-R, Ye Q, et al. Tunable multi-wavelength passively mode-locked fiber ring laser using intracavity birefringence-induced comb filter. *IEEE Photonics Journal* 2010;2:571.
- [16] Fatome J, Pitois S, Millot G. Measurement of nonlinear and chromatic dispersion parameters of optical fibers using modulation instability. *Optical Fiber Technology* 2006;12:243.

Abstract: We propose and demonstrate the generation of a supercontinuum (SC) spectrum from a 10 m long silica fiber co-doped with zirconia-yttria-alumino and erbium (Zr-EDF) as a non-linear medium. The proposed system utilizes a 2 m long Zr-EDF in a ring laser configuration to generate mode-locked pulses at 1560 nm based on the non-polarization rotation (NPR) technique. The fiber laser generates a mode-locking spectrum from 1526 to 1640 nm with a peak power of -10 dBm at approximately 1565 nm as well as a 6.1 nm bandwidth at the 3 dB level. The generated mode-locked pulses have average and peak powers of 15 mW and 1 kW respectively with a repetition rate of 23.2 MHz. These pulses are subsequently used to generate the SC spectrum from the 10 m Zr-EDF, with the SC spectrum obtained having a 200 nm bandwidth from 1500 nm as well as a large 3-dB bandwidth of 68.2 nm. The SC pulse width is 0.59 ps with a symmetrical shape at about 1600 nm and a 3-dB bandwidth of approximately 0.12 ps. This is the first report of a zirconia host employed as a non-linear medium for SC generation.



The spectra from the mode-locked fiber laser, ASE, and SC

© 2012 by Astro Ltd.

Published exclusively by WILEY-VCH Verlag GmbH & Co. KGaA

Supercontinuum from Zr-EDF using Zr-EDF mode-locked fiber laser

H. Ahmad,^{1,*} N.A. Awang,^{1,2} M.Z. Zulkifli,¹ K. Thambiratnam,¹ M.C. Paul,³ S. Das,³ and S.W. Harun⁴

¹ Photonics Laboratory, Department of Physics, University of Malaya, 50603 Kuala Lumpur, Malaysia

² Faculty of Science, Technology, and Human Development, Universiti Tun Hussein Onn Malaysia, 86400 Batu Pahat, Johor, Malaysia

³ Fiber Optics and Photonics Division, Central Glass & Ceramic Research Institute-CSIR, Kolkata-32, India

⁴ Department of Electrical Engineering, Faculty of Engineering, University of Malaya, 50603 Kuala Lumpur, Malaysia

Received: 22 June 2011, Revised: 4 July 2011, Accepted: 7 July 2011

Published online: 2 November 2011

Key words: supercontinuum; zirconia-based erbium-doped fiber; mode-locked fiber laser

1. Introduction

Since its demonstration in the early 1970s by R.R. Alfano and S.L. Shapiro [1,2], supercontinuum (SC) generation and the spectral broadening of partially or fully coherent light signals in optical waveguides has been the focus of significant research efforts. SC generation in particular has attracted much attention owing to the enormous spectral broadening experienced by laser pulses, which have many useful applications in telecommunications [3], spectroscopy [4], frequency metrology [5], optical coherence tomography [6], and device characterization [7].

SC generation is a complex physical phenomenon involving the interaction of classical nonlinear optical effects such as self-phase modulation (SPM), cross phase modulation (CPM), four wave mixing (FWM), and stimulated Raman scattering (SRS) [8]. R.R. Alfano and S.L. Shapiro first reported the generation of an SC output using 5 mJ/ps pulses at 530 nm in BK7 bulk glass to obtain a white light spectrum covering the entire visible range from 400 to 700 nm. However, this approach is highly complex and requires the intricate alignment and coupling of various optical components as well as the use of high energy ultra-short pulses. Instead, a more practi-

* Corresponding author: e-mail: harith@um.edu.my

cal approach would be to use the tight spatial confinement of lower energy pulses within a suitably nonlinear waveguide, as the higher nonlinearity of the material lowers the power levels required for SC generation. J.K. Ranka et al. [9] demonstrated SC generation in a photonic crystal fiber (PCF) with an extremely small solid-core, generating an SC spanning over 550 THz in spectral width. Since then, there has been growing interest in SC generation using optical fibers and microstructured optical fibers fabricated from highly nonlinear glasses such as PCFs and highly nonlinear dispersion shifted fibers (HNLFs) [10–18] and in dual-core microstructured fibers [19]. On top of these, there are also reports on all fiber SC generation [20] and also SCs with high power outputs [21,22]. There have been investigations of SC generation in the UV region from 509 to 640 nm using tapered PCFs [23] and also numerical simulations of mid-infrared SC generation of up to 5 μm in a single-mode fluoride fiber [24]. However, there are very limited reports on the use of standard optical fibers as a medium for SC generation. It will be of interest to have SC generation in standard silica fibers that can be conveniently spliced into standard single-mode fibers (SMFs) as this approach is inexpensive. There is a need to investigate new types of optical fibers that can provide SC generation which also have a high non-linear coefficient and based on standard silica hosts as well as its variations.

In this paper, the generation of an SC spectrum is proposed and demonstrated using a new type of optical fiber; a zirconia-erbium-doped fiber (Zr-EDF). The Zr-EDF is fabricated using a ternary glass host, zirconia-yttria-aluminum (Zr-Al-Y) co-doped silica fiber. The combination of both Zr and Al allows for a higher erbium doping concentration, thus allowing the fabrication of a short-length erbium-doped fiber amplifier (EDFA). Besides its usage as an amplifying medium, the Zr-EDF also exhibits high non-linearity characteristics as demonstrated in this paper, as a medium for SC generation. The Zr-EDF is pumped with a passively mode-locked Zr-EDF fiber laser generating ultra-short pulses.

2. Experimental setup

The experimental setup for SC generation from a Zr-EDF is shown in Fig. 1. In this work, two Zr-EDF lengths are used; first, a 2 m long Zr-EDF is used to create a passively mode-locked fiber laser, and its output is then propagated through a 10 m long Zr-EDF in order to generate the SC spectrum. The Zr-EDFs are fabricated from a silica fiber co-doped with zirconia-yttria-alumino using the modified chemical vapor deposition (MCVD) technique as well as erbium ions using a solution doping approach. The addition of zirconia and aluminum ions into the glass host allows for a high erbium doping concentration of about 1500 ppm to be obtained without any clustering of the rare-earths ions, while small amounts of Y_2O_3 and P_2O_5 ions serve as the nucleating agents to increase the phase separation between the erbium ion-doped micro crystallites in

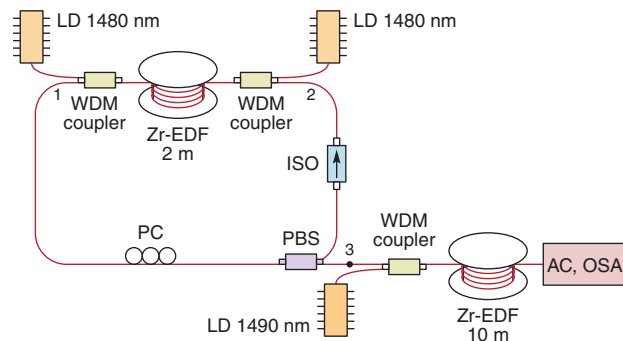


Figure 1 (online color at www.lphys.org) Schematic diagram for generating mode-locked fiber laser and SC in a Zr-EDF. LD – laser diode, WDM – wavelength division multiplexor, PBS – polarization beam splitter, AC – autocorrelator, OSA – optical spectrum analyzer, PC – polarization controller, and Zr-EDF – zirconia based erbium-doped fiber

the core matrix of optical fiber preform [25,26]. The advantage of the zirconia-based host is that it is useful in generating ultra-short pulses as a result of its wide-band characteristic.

The mode-locked fiber is based on the non-linear polarization rotation (NPR) technique and uses an inexpensive fiber-based polarization beam splitter (PBS) as opposed to the typical approach of a polarization dependent isolator (PDI) sandwiched in between two fiber-based polarization controllers (PCs). The 2 m long Zr-EDF has a pump absorption rate of about 13.5 dB/m at 1480 nm and is connected to the common ports of two 1480/1550 nm wavelength division multiplexers (WDMs). The 1480 nm ports of the WDMs are connected to two 1480 nm pump laser diodes (LDs) that are set to operate at 150 mW and configured in a bi-directional pumping scheme to provide a total pump power of about 300 mW. The 1550 nm output of the first WDM, Port 1 is connected to a fiber-based PC, which is then connected to a fiber-based 50:50 PBS. The slow axis port of the PBS is connected to a polarization insensitive isolator and then connected back to Port 2 of the second WDM as to complete the ring cavity of the mode-locked fiber laser, with a total cavity length of approximately 5.5 m. The PC acts as the mode-locking element [27,28] and is used to adjust the polarization of the signal that travels in the slow-axis in order to provide self-start mode-locking. The generation of the mode-locked pulses is based on the NPR technique, where an intense optical pulse propagating in a non-polarization maintaining optical fiber can experience non-linear changes in the polarization state due to the self-phase and cross-phase modulation as well as some uncontrolled birefringence in the fiber. This behavior is similar to that of saturable absorbers, giving an intensity dependent loss.

The short-pulses generated from the fiber laser have an average power of 15 mW with a repetition rate of

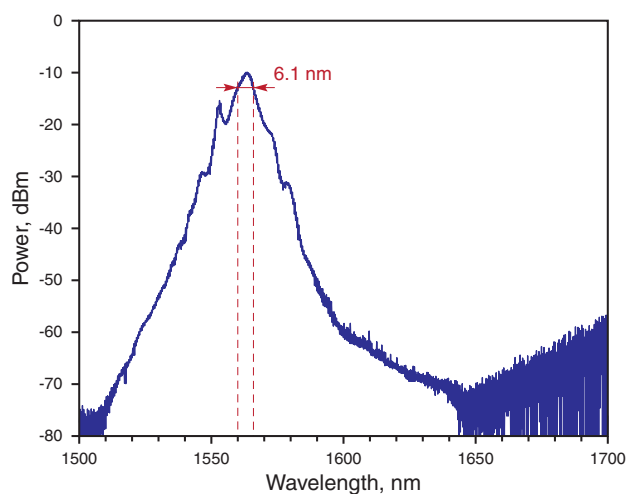


Figure 2 (online color at www.lphys.org) Optical spectra of the output laser pulse

23.2 MHz, giving a peak power of about 1 kW, which is extracted through the fast axis output of the PBS. This output is then connected to the 1550 nm port of a third WDM, which is joined to a 10 m long Zr-EDF which acts as the medium for SC generation. The 1490 nm LD is used to pump the erbium ions in the Zr-EDF as to make it transparent, thus allowing the input mode-locked pulses to pass through without being absorbed and therefore able to interact with the glass host of the Zr-EDF to generate the SC output. The output of the Zr-EDF is then connected to a Yokogawa AQ6370B optical spectrum analyzer (OSA) with a resolution of 0.02 nm and an Alnair auto-correlator. The mode-locked pulses are very stable and can operate for several hours without breaking up as well as being immune to external vibrations. This translates the generation of an SC spectrum with a similar degree of high stability. The experimental results are presented in the following section.

3. Results and discussions

The generation of the mode-locked pulses from the Zr-EDF laser can be achieved by adjusting the PC, with self-starting mode-locked pulse at 1560 nm being obtained at a LD power of 130 mW and above. With appropriate adjustments of the PC, the mode-locked pulses are generated based on the NPR technique, which is largely due to SPM and CPM occurring in the fiber, along with some uncontrolled birefringence. This effect is similar to the behavior of saturable absorbers, which gives intensity dependent loss [29]. The mode-locking spectrum that is generated by the Zr-EDF is shown in Fig. 2, giving a span from 1525 to 1640 nm with a bandwidth of 6.1 nm at the 3 dB level. It has a peak power of about -10 dBm at a wavelength of 1560 nm.

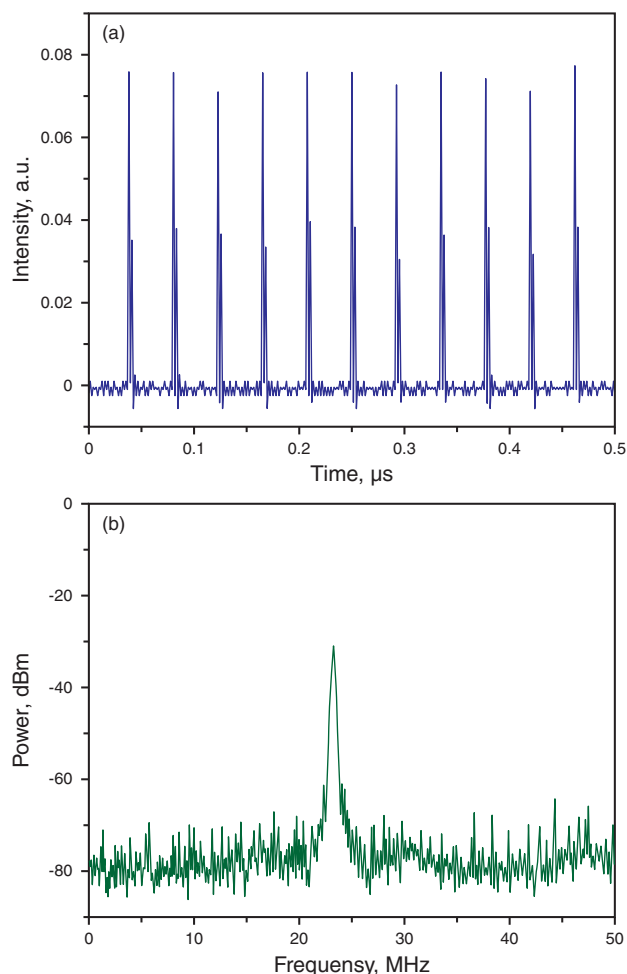


Figure 3 (online color at www.lphys.org) Spectrum of the output laser pulses at (a) – sampling oscilloscope and (b) – RF spectrum analyzer

The generated mode-locked pulses are shown in Fig. 3. Fig. 3a shows the sampling oscilloscope trace with a repetition rate of 23.2 MHz. From the trace, there are also side-pulses that are a consequence of the technique based on saturable absorbers and these can be removed by the proper adjustment of the PC. From Fig. 3b, the repetition rate as obtained using a radio frequency (RF) spectrum analyzer together with a 6 GHz bandwidth photo-detector, which is taken from the 5% port of a 95:5 fused bi-conical coupler. The measured frequency is about 23.2 MHz, similar to that calculated value using Fig. 3a. The repetition rate of the mode-locked fiber laser depends on the fiber cavity length and in this setup the length is about 5.5 m. A shorter cavity length will increase the repetition rate. The present cavity length gives a positive dispersion near the 1560 nm region [27] thus providing operation in the normal dispersion regime, which is normally referred to as a stretched pulse mode-locked fiber laser.

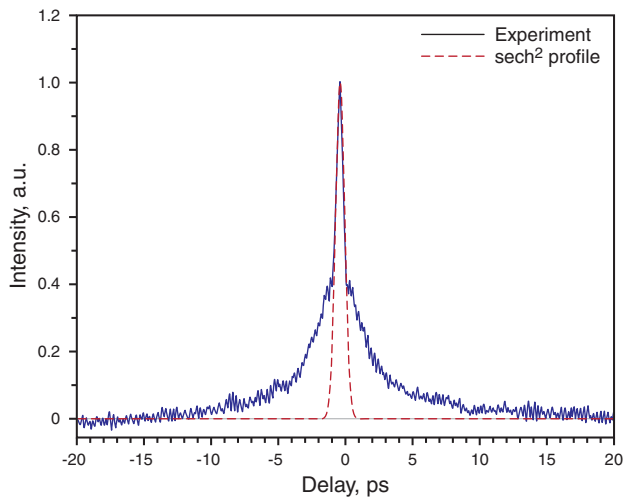


Figure 4 (online color at www.lphys.org) The spectra of femtosecond pulses obtained experimentally (from the Alnair auto-correlator output) and using a hyperbolic secant squared (sech^2) profile, giving a pulse width of 0.59 ps

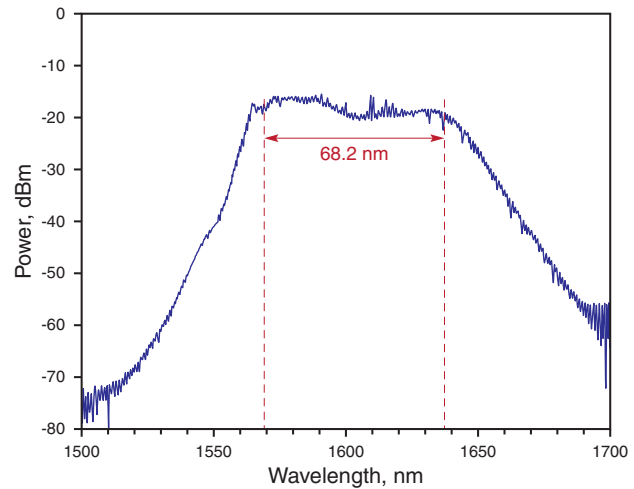


Figure 6 (online color at www.lphys.org) SC output generated from the 10 m long Zr-EDF

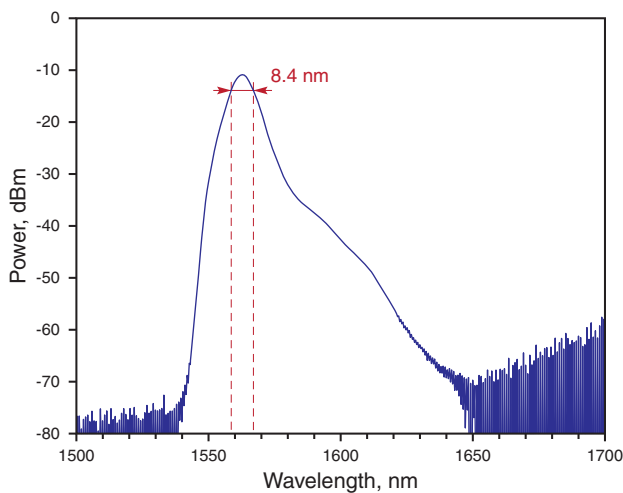


Figure 5 (online color at www.lphys.org) The ASE spectrum of Zr-EDF with Port 3 disconnected

The duration of the mode-locked pulses from the Zr-EDF laser is obtained using the Alnair auto-correlator and is shown in Fig. 4. Using a hyperbolic secant squared (sech^2) profile; a pulse duration of 0.59 ps is measured when the system is optimally configured.

The average power measured is 15 mW with a peak power of 1 kW. The energy per pulse is about 0.6 nJ. These mode-locked pulses are then connected to a 10 m Zr-EDF as in Fig. 1 for SC generation.

Another measurement of interest would be the amplified spontaneous emission (ASE) spectrum from the 10 m long Zr-EDF, which is taken by disconnecting Port 3 in

Fig. 1 such that it is measured at the output end that is connected to the OSA. The spectrum is shown in Fig. 5 when it is pumped at 170 mW from the LD at 1490 nm, which is connected to the third WDM. The purpose of this ASE spectrum is to provide a comparison with the SC spectrum generated.

The generated ASE spectrum spans from about 1540 to 1650 nm, with a peak power of approximately -11 dBm at 1565 nm. The measured 3 dB bandwidth or full-width at half-maximum (FWHM) of the ASE spectrum is about 8.4 nm.

The SC spectrum is generated by connecting the output of the mode-locked ring fiber laser to Port 3 of the third WDM, which is connected to the 10 m long Zr-EDF and the LD pump power is adjusted such that the doped fiber becomes transparent with gain factor of only 1. This is to allow the usage of the ternary glass host, zirconia-yttria-aluminum co-doped silica fiber as a non-linear medium of interest. The mode-locked pulses are made to travel into the Zr-EDF and the SC output generated is shown in Fig. 6. The SC spectrum wavelength spans from 1500 to 1700 nm, with a bandwidth as large as 68.2 nm at 3-dB level when excited by mode-locked pulses at 1560 nm with a pulse width of 0.59 ps. The SC spectrum shifted towards the longer wavelength as similarly observed in most case [30]. From the Fig. 6, it has a symmetrical shape of around 1600 nm.

The pulse width of the SC is characterized using a similar autocorrelator and the measurement is taken using the 5% port of the 95:5 fused bi-conical coupler as to limit the input power to less than 1 mW. The pulse width has a FWHM of about 0.12 ps using the hyperbolic secant squared (sech^2) technique, as a result of pulse compression. This normally occurs when for the case of opera-

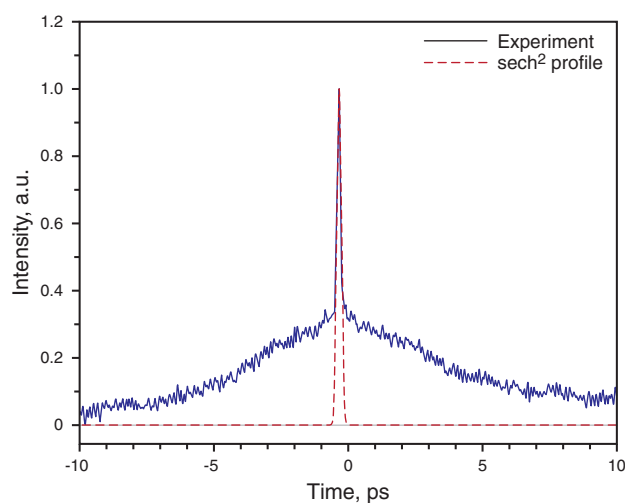


Figure 7 (online color at www.lphys.org) The SC pulse width obtained experimentally and using a hyperbolic secant squared (sech^2) profile, giving a pulse-width of 0.12 ps

tion in the anomalous dispersion region. This is shown in Fig. 7.

Fig. 8 shows the comparison of the spectrum from the mode-locked fiber laser, the ASE spectrum as taken from the 10 m Zr-EDF, which is disconnected from the mode-locked ring fiber laser system and the SC spectrum of the zirconia host when mode-locked pulses is injected into the medium. This clearly indicates that the measured SC spectrum is due to the non-linear behavior of the zirconia host and not from the ASE of the Zr-EDF or the wavelength spectrum of the mode-locked pulses.

In this paper, the Zr-EDF is capable of generating an SC output when mode-locked pulses are injected into the medium. This indicates that the zirconia host acts as a non-linear medium. Typically, for SC generation, highly non-linear fibers, dispersion shifted fibers and photonic crystal fibers are used as the medium. This is the first report whereby a zirconia host; Zr-EDF is shown to have a non-linear behavior and able to generate SC. The system can be configured as a compact SC generator using short lengths of the Zr-EDF. The current fiber has a zero dispersion wavelength at around the 1300 nm region. By proper design, and shifting the zero-dispersion wavelength into the shorter region, will be able to generate a wider SC spanning from the visible to infrared.

4. Conclusion

In this work, SC generation from a silica based zirconia host is proposed and demonstrated. The proposed system utilizes a 2 m long Zr-EDF based laser in a ring cavity to generate self-starting mode-locked pulses at 1560 nm, which are then used to generate the SC spectrum from a

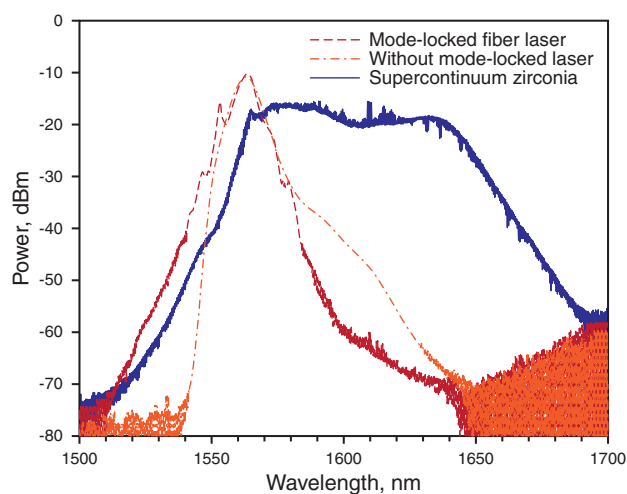


Figure 8 (online color at www.lphys.org) The spectra from the mode-locked fiber laser, ASE, and SC

10 m long Zr-EDF. The fiber laser is based on the NPR technique and generates a mode-locking spectrum from 1526 to 1640 nm with a 6.1 nm bandwidth at 3-dB level and a peak power of -10 dBm at about 1560 nm. The mode-locked pulses generated have an average power of 15 mW with a peak power of 1 kW as well as 0.6 nJ energy per pulse at a repetition rate of 23.2 MHz. The SC spectrum obtained ranges from 1500 to 1700 nm, with a large 3-dB bandwidth of 68.2 nm. The SC has a pulse width of 0.59 ps with a symmetrical shape at about 1600 nm as well as a 3-dB bandwidth of approximately 0.12 ps. This is the first report of a silica-based zirconia host used as a non-linear medium for SC generation.

Acknowledgements The authors would like to express their gratitude to the University of Malaya, Malaysia for providing the funding for this work and the Central Glass & Ceramic Research Institute, India for the optical fiber.

References

- [1] R.R. Alfano and S.L. Shapiro, *Phys. Rev. Lett.* **24**, 584 (1970).
- [2] R.R. Alfano and S.L. Shapiro, *Phys. Rev. Lett.* **24**, 592 (1970).
- [3] J.M. Dudley, G. Genty, and S. Coen, *Rev. Mod. Phys.* **78**, 1135 (2006).
- [4] J. Shah, *Ultrafast Spectroscopy of Semiconductors and Semiconductor Nanostructures*, 2nd ed., Springer Series in Solid-State Sciences, vol. 115 (Springer, 1999).
- [5] B.R. Washburn, S.A. Diddams, N.R. Newbury, J.W. Nicholson, M.F. Yan, and C.G. Jørgensen, *Opt. Lett.* **29**, 250 (2004).
- [6] W. Drexler, U. Morgner, F.X. Kärtner, C. Pitris, S.A. Boppart, X.D. Li, E.P. Ippen, and J.G. Fujimoto, *Opt. Lett.* **24**, 1221 (1999).

- [7] R.T. Neal, M.D.C. Charlton, G.J. Parker, C.E. Finlayson, M.C. Netti, and J.J. Baumberg, *Appl. Phys. Lett.* **83**, 4598 (2003).
- [8] G. Brambilla, F. Koizumi, V. Finazzi, and D.J. Richardson, *Electron. Lett.* **41**, 795 (2005).
- [9] J.K. Ranka, R.S. Windeler, and A.J. Stentz, *Opt. Lett.* **25**, 25 (2000).
- [10] A.K. Abeeluck, S. Radic, K. Brar, J.-C. Bouteiller, and C. Headley, in: *Proc. of the Optical Fiber Communication Conference, Atlanta, GA, USA, March 22–28, 2003 (OFC 2003)*, paper ThT1.
- [11] J.W. Nicholson, A.K. Abeeluck, C. Headley, M.F. Yan, and C.G. Jørgensen, *Appl. Phys. B* **77**, 211 (2003).
- [12] A.K. Abeeluck, C. Headley, and C.G. Jørgensen, *Opt. Lett.* **29**, 2163 (2004).
- [13] R. Buczynski, D. Pysz, R. Stepień, A.J. Waddie, I. Kujawa, R. Kasztelan, M. Franczyk, and M.R. Taghizadeh, *Laser Phys. Lett.* **8**, 443 (2011).
- [14] M.R.A. Moghaddam, S.W. Harun, R. Akbari, and H. Ahmad, *Laser Phys. Lett.* **8**, 369 (2011).
- [15] R. Buczynski, H.T. Bookey, D. Pysz, R. Stepień, I. Kujawa, J.E. McCarthy, A.J. Waddie, A.K. Kar, and M.R. Taghizadeh, *Laser Phys. Lett.* **7**, 666 (2010).
- [16] D.A. Sidorov-Biryukov, K.A. Kudinov, A.A. Podshivalov, and A.M. Zheltikov, *Laser Phys. Lett.* **7**, 355 (2010).
- [17] S.-P. Chen, J.-H. Wang, H.-W. Chen, Z.-L. Chen, J. Hou, X.-J. Xu, J.-B. Chen, and Z.-J. Liu, *Laser Phys.* **21**, 519 (2011).
- [18] Y. Gu, L. Zhan, D.-D. Deng, Y.-X. Wang and Y.-X. Xia, *Laser Phys.* **20**, 1459 (2010).
- [19] R. Buczynski, D. Pysz, T. Martynkien, D. Lorenc, I. Kujawa, T. Nasilowski, F. Berghmans, H. Thienpont, and R. Stepień, *Laser Phys. Lett.* **6**, 575 (2009).
- [20] S.M. Kobtsev and S.V. Kukarin, *Laser Phys.* **20**, 372 (2010).
- [21] H.W. Chen, S.P. Chen, and J. Hou, *Laser Phys.* **21**, 191 (2011).
- [22] S.M. Kobtsev, S.V. Kukarin, and S.V. Smirnov, *Laser Phys.* **20**, 375 (2010).
- [23] S.P. Stark, A. Podlipensky, N.Y. Joly, and P.St.J. Russell, *J. Opt. Soc. Am. B* **27**, 592 (2010).
- [24] L. Liu, G.S. Qin, Q.J. Tian, D. Zhao, and W.P. Qin, *Opt. Express* **19**, 10041 (2011).
- [25] M.C. Paul, S.W. Harun, N.A.D. Huri, A. Hamzah, S. Das, M. Pal, S.K. Bhadra, H. Ahmad, S. Yoo, M.P. Kalita, A.J. Boyland, and J.K. Sahu, *J. Lightwave Technol.* **28**, 2919 (2010).
- [26] M.C. Paul, S.W. Harun, N.A.D. Huri, A. Hamzah, S. Das, M. Pal, S.K. Bhadra, H. Ahmad, S. Yoo, M.P. Kalita, A.J. Boyland, and J.K. Sahu, *Opt. Lett.* **35**, 2882 (2010).
- [27] H.A. Haus, K. Tamura, L.E. Nelson, and E.P. Ippen, *IEEE J. Quantum Electron.* **31**, 591 (1995).
- [28] Z.C. Luo, A.P. Luo, W.C. Xu, C.X. Song, Y.X. Gao, and W.C. Chen, *Laser Phys. Lett.* **6**, 582 (2009).
- [29] V.J. Matsas, T.P. Newson, D.J. Richardson, and D.N. Payne, *Electron. Lett.* **28**, 1391 (1992).
- [30] X. Liu, C. Xu, W.H. Knox, J.K. Chandalia, B.J. Eggleston, S.G. Kosinski, and R.S. Windeler, *Opt. Lett.* **26**, 358 (2001).



Supercontinuum generation using a passive mode-locked stretched-pulse bismuth-based erbium-doped fiber laser

N.S. Shahabuddin^a, N.A. Awang^b, H. Ahmad^b, H. Arof^a, K. Dimyati^c, Z. Yusoff^d, S.W. Harun^{a,b,*}

^a Department of Electrical Engineering, University of Malaya, 50603 Kuala Lumpur, Malaysia

^b Photonics Research Center, University of Malaya, 50603 Kuala Lumpur, Malaysia

^c Department Electrical and Electronic Engineering, National Defense University of Malaysia, Kem Sungai Besi, 57000 Kuala Lumpur, Malaysia

^d Faculty of Engineering, Multimedia University 63100 Cyberjaya, Malaysia

ARTICLE INFO

Article history:

Received 17 August 2011

Received in revised form

22 November 2011

Accepted 23 November 2011

Available online 9 December 2011

Keywords:

Supercontinuum

Nonlinear polarization rotation

Passive mode-locking

ABSTRACT

A Supercontinuum (SC) generation in photonic crystal fiber (PCF) is demonstrated using an amplified picosecond stretched-pulses from a passive mode-locked Bismuth-based Erbium-doped fiber laser (Bi-EDFL). The Bi-EDFL employs of a piece of a highly nonlinear 49 cm long Bismuth-based Erbium-doped fiber (Bi-EDF), an optical isolator and a polarization controller in a cavity to generate a mode-locked stretched-pulse via a nonlinear polarization rotation technique. It operates at 1560 nm with a repetition rate of 42 MHz and a pulse width of 131 fs. The SC lights, which extends from 1250 nm to 1910 nm as well as in the visible green wavelength region are obtained with a 100 m long PCF and the amplified pump power of 30 dBm.

© 2011 Elsevier Ltd. All rights reserved.

1. Introduction

A Supercontinuum (SC) generation describes an extreme spectral broadening induced by the coupling of a high peak power sub picosecond pulse laser in an adequately long nonlinear optical fiber. It has been a hot topic in recent years due to its potential applications in a variety of areas such as optical coherent tomography [1], sensing [2] and optical communication [3]. Many works have been performed to understand the phenomenon as well as to implement the intended practical devices. Special fibers such as the photonic crystal fibers (PCFs) offer high nonlinearity with a manageable dispersion profile, and therefore can be used to generate SC light [4]. Most widely used types of PCFs consist of pure silica core surrounded by a periodic array of air holes. In this case, a genuine photonic band-gap guidance can occur, and PCFs of this type have attracted much interest due to their potentials for lossless and distortion-free transmission, particle trapping, optical sensing, and for novel applications in nonlinear optics [5–7].

An SC can be generated using a picosecond to nanosecond pulses, or even a continuous wave pump where spectral broadening is initiated in the so-called “long pulse” regime [8–10]. Research is now shifting towards an SC that uses a more robust and cheaper mode-locked laser, which can be achieved through some innovative design as well as a new understanding of the SC

process with picosecond or nanosecond pulsed lasers. In our earlier work, a supercontinuum generation is demonstrated in various nonlinear fibers using a 131 fs mode-locked Bismuth-based Erbium-doped fiber laser (Bi-EDFL), which is achieved using a semiconductor saturable absorber [11]. In this paper, we experimentally demonstrate a simpler optical fiber-based supercontinuum source using a mode-locked Bi-EDFL and a highly nonlinear PCF. The mode-locked Bi-EDFL is achieved using a simple ring cavity structure incorporating a Bismuth-based erbium-doped fiber (Bi-EDF), an isolator and a polarization controller. Since the gain medium is only a piece of 49 cm long Bi-EDF, the cavity length of the EDFL is considered short and therefore stable and clean pulses can be generated with an increase in the repetition frequency. The supermode noise can also be suppressed effectively because the Bi-EDF has a very high nonlinearity. To the best of the authors' knowledge, this is the first demonstration of a passively mode-locked fiber laser, which uses such a short length Bi-EDF in conjunction with a nonlinear polarization rotation (NPR) method. Compared to the previous work, the new Bi-EDFL does not require a saturable absorber and is capable of generating a supercontinuum in a visible green region as well. This method may also be extrapolated to generate supercontinuum in other optical regions, such as the visible spectral region and the THz regime, using suitable gain media [12–14].

2. Experimental setup

The experimental setup of the proposed system for supercontinuum generation is illustrated in Fig. 1, which consists of a

* Corresponding author at: Department of Electrical Engineering, University of Malaya, 50603 Kuala Lumpur, Malaysia.

E-mail addresses: swharun@um.edu.my, kaharudin@upnm.edu.my (S.W. Harun).

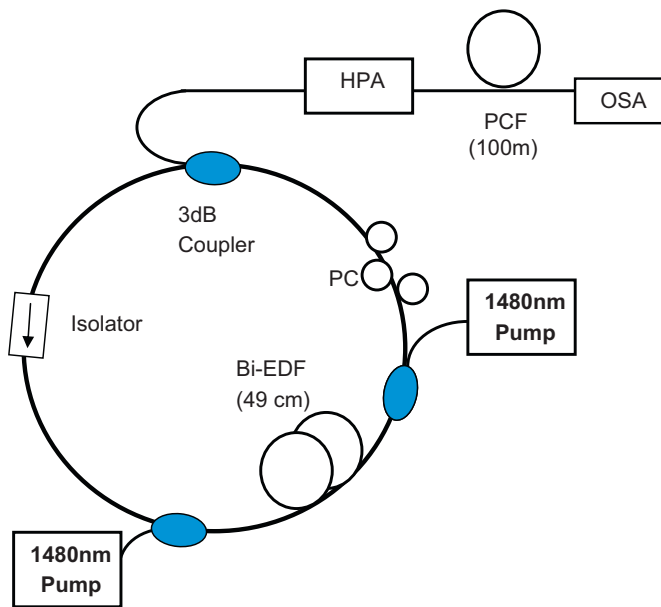


Fig. 1. Experimental setup of the supercontinuum generation showing the main three parts namely the mode locked Bi-EDFL, high power amplifier (HPA) and a piece of PCF.

mode-locked Bismuth-based Erbium-doped fiber laser (Bi-EDFL), a high power amplifier (HPA) and a 100 m long PCF. The Bi-EDFL resonator consists of a piece of Bi-EDF, a wavelength division multiplexing (WDM) coupler, an isolator, a polarization controller (PC) and a 3 dB output coupler. The total length of the cavity is about 2.5 m, which comprises a 49 cm long Bi-EDF and a 2.0 m long SMF-28 used in a coupler, polarization controller, isolator and 1480/1550 nm WDM coupler. The Bi-EDF has a nonlinear coefficient of $\sim 60 \text{ (W/km)}^{-1}$ at 1550 nm, an Erbium concentration of 3250 ppm, a cut-off wavelength of 1440 nm, a pump absorption rate of 130 dB/m at 1480 nm and a dispersion parameter of 130 ps/km.nm at $\lambda = 1550 \text{ nm}$. It is bi-directionally pumped using a 1480 nm laser diode via the WDM to provide an amplification in the C-band region. The other part of the ring cavity uses a standard single mode fiber (SMF-28) with a dispersion of 17 ps/nm.km at $\lambda = 1545 \text{ nm}$. A standard isolator is used to ensure a unidirectional operation of the laser and acts as a polarizer. A PC is used to rotate the polarization state and allows continuous adjustment of the birefringence within the cavity to balance the gain and loss for laser pulse generation.

A fraction of the stretched-pulse laser operating at 1560 nm is extracted through the 50% output of the coupler. The pulse width and repetition rate of the pulse laser are measured to be around 131 fs and 42 MHz, respectively. The pulse train is then amplified by the HPA before being launched into a piece of PCF for SC generation. The amplifier boosts the signal up to the output power of 30 dBm so that it can produce a desired spectral broadening. The PCF used in the experiment has a zero and -1.5 ps/(km nm) dispersion at wavelength of 1550 nm and 1580 nm, respectively. The PCF length is fixed at the optimized length of 100 m. The nonlinearity coefficient of the PCF is around $11 \text{ W}^{-1} \text{ km}^{-1}$. The output power and spectrum are measured by a power meter and an optical spectrum analyzer (OSA), respectively. The entire experimental setup is fusion-spliced together.

3. Result and discussion

To achieve a mode locking operation, a polarization state of light inside the cavity should be adjusted by the PC. By altering

the polarization state inside the cavity, the optical spectrum can be broadened to initiate Q-switching and then mode-locking operation. When a linearly polarized light is incident to a piece of weakly birefringent fiber such as a Bi-EDF, the polarization of the light will generally become elliptically polarized in the fiber. The orientation and ellipticity of the final light polarization is fully determined by the fiber length and its birefringence. However, if the intensity of the light is strong, the nonlinear optical Kerr effect in the fiber must be considered, which introduces extra changes to the light polarization. As the polarization change introduced by the optical Kerr effect depends on the light intensity, if a polarizer or isolator is put behind the fiber, the light intensity transmission through the polarizer will become light intensity dependent. By selecting the orientation of the polarizer appropriately, an artificial saturable absorber effect with ultra-fast response could then be achieved in such a system, where light of higher intensity experiences less absorption loss on the polarizer. The proposed laser makes use of this artificial saturable absorption to achieve the passive mode locking. Once a mode-locked pulse is formed, the nonlinearity of the fiber further shapes the pulse into the ultrashort stretched-pulse.

In the experiment, both 1480 nm pump powers were fixed at 125 mW. The output spectrum of the mode-locked EDFL obtained after the 3 dB coupler is shown in Fig. 2. A broad spectrum with a 3 dB bandwidth of 21.7 nm is obtained at the optimum polarization state, which indicates that the output laser has a stretched-pulse characteristic. The spectrum has a peak wavelength at 1560 nm. Q-switching operation mode is observed by an oscilloscope as an unstable pulse train with periodic variation in pulse amplitude. Further adjustment of polarization produces a more stable mode locked pulse train as shown in Fig. 3. The mode locked pulse train has a constant spacing of 24 ps, which translates to a repetition rate of 42 MHz. The high repetition rate pulse trains are produced from harmonically mode-locked laser, where multiple pulses circulate within the cavity. The multiple pulses are generated passively in a laser because of the phenomenon of soliton energy quantization. The pulse characteristic of the mode locked EDFL at the 3 dB coupler is also investigated by an auto-correlator. Fig. 4 shows the auto-correlator trace of the pulse, which shows the sech^2 pulse profile with a full width half maximum (FWHM) of 131 fs. The output of the femtosecond pulses is also observed to be very stable at room temperature. The operation of the Bi-EDFL can be tuned by incorporating a tunable band-pass filter in the ring cavity. By optimizing the length of the Bi-EDF, a wideband tunable operation is also expected to be achieved up to the extended L-band region.

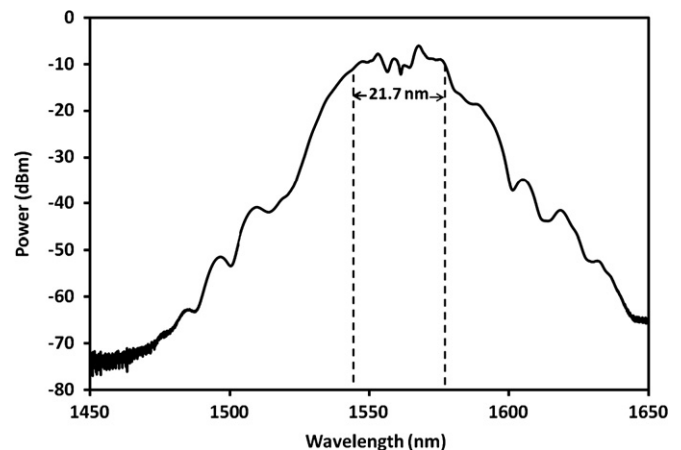


Fig. 2. Optical spectrum of the mode locked laser showing the 3 dB bandwidth of 21.7 nm.

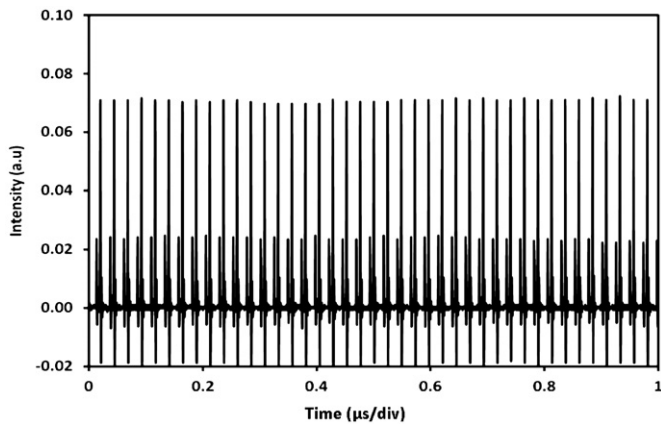


Fig. 3. Pulse train of the passive mode locked laser with a repetition rate of 42 MHz.

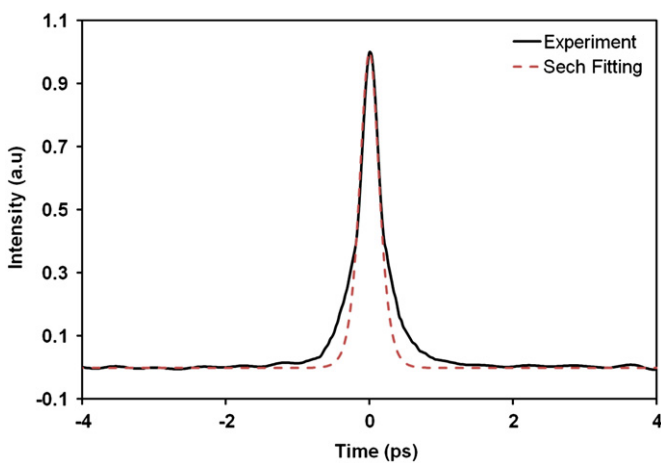


Fig. 4. Auto-correlator pulse trace with FWHM of 131 fs and Sech² pulse shape.

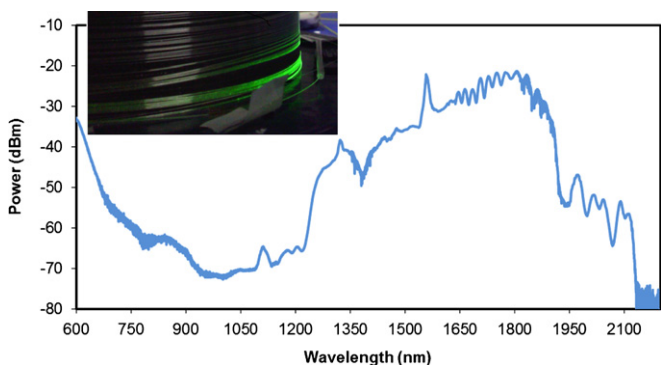


Fig. 5. SC generation with 100 m long PCF at fixed average pump power of 30 dBm. Inset shows the green emission from the PCF.

Fig. 5 shows an SC generation in a piece of 100 m long PCF, which is pumped by the amplified 1560 nm femtosecond fiber laser at different injected pulse laser power levels. As shown in Fig. 5, we observe an SC starting from 1250 nm up to 1910 nm at the maximum pump power of 30 dBm. The broadband light is also observed at visible green wavelength as shown in the inset of Fig. 5. The broad SC is obtained due to the injection of 1560 nm pulse laser in the anomalous-dispersion regime of the PCF. The pulse initially begins to self-Raman shift to longer wavelengths and this would have caused asymmetric SC spectrum. When these higher-order solitons break up, parametric four-wave mixing generates frequencies at wavelengths shorter than the zero-dispersion wavelength.

The spectrum widens and the flatness also improves as the pump power increases. The visible green spectral radiation is generated by a combination of Raman self-frequency shifting and third-harmonic generation [15–16]. As the power of femtosecond pulse increases, it splits temporally and is followed by Raman self-frequency shifting of the split pulse, with subsequent third-harmonic frequency conversion of both pulses. The use of a shorter pulse and higher output laser is expected to produce a flat supercontinuum spectrum covering the range of visible to 2 μm region.

4. Conclusion

An SC generation in a PCF has been demonstrated using a mode-locked Bi-EDFL, which employs of a piece of highly nonlinear 49 cm long Bi-EDF, an optical isolator and a polarization controller in the cavity. The Bi-EDFL generates a mode-locked stretched-pulse via a nonlinear polarization rotation technique, which operates at 1560 nm with a repetition rate of 42 MHz and a pulse width of 131 fs. By injecting the amplified pulse laser of 30 dBm output power into a 100 m long PCF, SC light extending from 1250 nm to 1910 nm as well as in visible green wavelength region are obtained.

Acknowledgment

This work is funded by the University of Malaya under High Impact Research Grant Scheme (Grant no.: D0000009-16001) and UMRG (Grant no.: RG108/11AET)

References

- [1] Hartl I, Li XD, Chudoba C, Ghanta RK, Ko TH, Fujimoto JG, et al. Ultrahigh-resolution optical coherence tomography using continuum generation in an air-silica microstructure optical fiber. *Optics Letters* 2001;26:608–10.
- [2] Kano H, Hamaguchi H. Characterization of a supercontinuum generated from a photonic crystal fiber and its application to coherent Raman spectroscopy. *Optics Letters* 2003;28:2360–2.
- [3] Mori K, Sato K, Takara H, Ohara T. Supercontinuum lightwave source generating 50 GHz spaced optical ITU grid seamlessly over S-, C- and L-bands. *Electronics Letters* 2003;39:544–6.
- [4] Parvizi R, Harun SW, Shahabuddin NS, Yusoff Z, Ahmad H. Multi-wavelength bismuth-based erbium-doped fiber laser based on four-wave mixing effect in photonic crystal fiber. *Optics and Laser Technology* 2010;44:1250–2.
- [5] Russell P. Photonic crystal fibers. *Science* 2003;299:358–62.
- [6] Wiederhecker GS, Cordeiro CMB, Couny F, Benabid F, Maier SA, Knight JC, et al. Field enhancement within an optical fibre with a subwavelength air core. *Nature Photonics* 2007;1:115–8.
- [7] Benabid F, Couny F, Knight JC, Birks TA, Russell PS. Compact, stable and efficient all-fibre gas cells using hollow-core photonic crystal fibres. *Nature* 2005;434:488–91.
- [8] Harun SW, Akbari R, Arof H, Ahmad H. Supercontinuum generation in photonic crystal fiber using femtosecond pulses. *Laser Physics* 2011;21:1215–8.
- [9] Wang Z, Wang CY, Han YK, Cao SY, Zhang ZG, Lai L. Octave-spanning spectrum generation in Ti : sapphire oscillator. *Optics and Laser Technology* 2006;38:641–4.
- [10] Gorbach AV, Skryabin DV. Light trapping in gravity-like potentials and expansion of supercontinuum spectra in photonic-crystal fibres. *Nature Photonics* 2007;1:653–7.
- [11] Moghaddam MRA, Harun SW, Akbari R, Ahmad H. Flatly broadened supercontinuum generation in nonlinear fibers using a mode-locked bismuth oxide based erbium-doped fiber laser. *Laser Physics Letters* 2011;8(5):369–75.
- [12] He X–Y. Numerical analysis of the propagation properties of subwavelength semiconductor slit in the terahertz region. *Optics Express* 2009;17:15359–71.
- [13] He X–Y. Investigation of terahertz Sommerfeld wave propagation along conical metal wire. *Journal of the Optical Society of America B* 2009;26: A23–8.
- [14] He X–Y. Investigation of terahertz surface waves of a metallic nanowire. *Journal of the Optical Society of America B* 2010;27:2298–303.
- [15] Omenetto FG, Taylor AJ, Moores MD, Arriaga J, Knight JC, Wadsworth WJ, et al. Simultaneous generation of spectrally distinct third harmonics in a photonic crystal fiber. *Optics Letters* 2001;26:1158–60.
- [16] Efimov A, Taylor AJ, Omenetto FG, Knight JC, Wadsworth WJ, Russell PStJ. Phase-matched third harmonic generation in microstructured fibers. *Optics Express* 2003;11:2567–76.